CHEMICAL
REVIEWS

Review

pubs.acs.org/CR

Atomically Precise Clusters of Noble Metals: Emerging Link between Atoms and Nanoparticles

Indranath Chakraborty[†] and Thalappil Pradeep*

DST Unit of Nanoscience (DST UNS) and Thematic Unit of Excellence, Department of Chemistry, Indian Institute of Technology Madras, Chennai 600036, India

Supporting Information

ABSTRACT: Atomically precise pieces of matter of nanometer dimensions composed of noble metals are new categories of materials with many unusual properties. Over 100 molecules of this kind with formulas such as $Au_{25}(SR)_{18}$, $Au_{38}(SR)_{24}$, and $Au_{102}(SR)_{44}$ as well as $Ag_{25}(SR)_{18}$, $Ag_{29}(S_2R)_{12}$, and $Ag_{44}(SR)_{30}$ (often with a few counterions to compensate charges) are known now. They can be made reproducibly with robust synthetic protocols, resulting in colored solutions, yielding powders or diffractable crystals. They are distinctly different from nanoparticles in their spectroscopic properties such as optical absorption and emission, showing well-defined features, just like molecules. They show isotopically resolved molecular ion peaks in mass spectra and provide diverse information when examined through multiple instrumental methods. Most important of these properties is luminescence, often in the visible−near-infrared window, useful in biological applications. Luminescence in the visible region, especially by clusters protected with proteins, with a large Stokes shift, has been used for various sensing applications, down to a few tens of molecules/ions, in air and water. Catalytic properties of clusters, especially oxidation of organic substrates, have been examined. Materials science of these systems presents numerous possibilities and is fast evolving. Computational insights have given reasons for their stability and unusual properties. The molecular nature of these materials is unequivocally manifested in a few recent studies such as intercluster reactions forming precise clusters. These systems manifest properties of the core, of the ligand shell, as well as that of the integrated system. They are better described as protected molecules or *aspicules*, where *aspis* means shield and *cules* refers to molecules, implying that they are "shielded molecules". In order to understand their diverse properties, a nomenclature has been introduced with which it is possible to draw their structures with positional labels on paper, with some training. Research in this area is captured here, based on the publications available up to December 2016.

CONTENTS

1. Introduction 8209
  1.1. Noble Metal Nanoparticles: From Alchemy to Today 8210
  1.2. Gas Phase Clusters 8211
  1.3. Early Monolayer Protected Clusters: Au_{13} and Others 8212
  1.4. Brust Synthesis and Beyond: Monolayer Protected Nanoparticles 8213
  1.5. Evolution of New Synthetic Methods at the Ultrasmall Regime 8213
2. Monolayer Protected Clusters 8214
  2.1. Entry of Mass Spectrometry to Noble Metal Nanoparticles and Identification of Clusters 8214
  2.2. Other Molecular Tools 8215
3. Toward Atomic Precision: Gold Clusters 8216
  3.1. Synthesis and Separation of $Au_{25}(SR)_{18}$ Cluster 8216
  3.2. Evolution of the Electronic Structure 8217
    3.2.1. Optical Spectroscopy 8217
    3.2.2. Photoluminescence 8218
  3.3. Understanding the Composition, Structure, and Properties 8218
    3.3.1. Advanced Mass Spectrometry 8219
    3.3.2. MS/MS and Related Studies 8220
    3.3.3. Single Crystal Studies 8222
    3.3.4. NMR Spectroscopy 8224
    3.3.5. Other Spectroscopies 8224
  3.4. Other Gold Clusters 8225
4. Atomically Precise Silver Clusters 8225
  4.1. Early Synthesis of Silver Clusters 8225
  4.2. New Routes for Silver Clusters 8226
  4.3. Well-Defined Mass Spectral Characterization 8226
  4.4. Single Crystal Studies 8228
  4.5. Thermal Stability of Silver Clusters 8230
  4.6. Emergence of Metallicity in Silver Clusters 8231
5. Chemistry of Clusters 8231
  5.1. Ligand Exchange 8231
  5.2. Ligand Conjugation 8233
  5.3. Intercluster Reactions 8233
6. Alloy Clusters 8233
7. Protein Protected Clusters 8234
8. Other Properties 8234

Received: November 12, 2016
Published: June 6, 2017

DOI: 10.1021/acs.chemrev.6b00769
Chem. Rev. 2017, 117, 8208−8271

8.1. Two-Photon Absorption 8234
8.2. Magnetism 8236
9. Applications 8236
9.1. Sensors 8236
9.2. Biological Applications 8238
9.2.1. Biolabels 8238
9.2.2. Biomedical Targeting 8239
9.2.3. Other Biological Applications 8239
9.3. SERS 8239
9.4. Catalysis 8240
9.5. Solar Cells 8240
10. New Materials 8242
10.1. Graphene Composites 8242
10.2. Other Composites 8242
11. Optical Chirality 8244
12. Similar Structures 8244
12.1. Hydride-Rich Silver Clusters 8244
12.2. Silver Sulfide Clusters 8246
13. Atomically Precise Pt and Pd Clusters 8246
13.1. Platinum Clusters 8246
13.2. Palladium Clusters 8247
14. Naming and Structural Understanding 8248
15. Future Prospects 8248
15.1. New Synthetic Methodologies 8248
15.2. Ligand Induced Properties 8248
15.3. Alloys 8248
15.4. Hydride-Rich Clusters 8249
15.5. Cluster Composites 8249
15.6. Computational Approaches 8249
15.7. Stabilizing Cluster Luminescence 8249
15.8. Crystallization 8249
15.9. Intercluster Reactions 8249
15.10. Cluster Assembled Solids 8249
15.11. Clusters as New Molecules 8249
Associated Content 8250
Supporting Information 8250
Author Information 8250
Corresponding Author 8250
ORCID 8250
Present Address 8250
Notes 8250
Biographies 8250
Acknowledgments 8250
Abbreviations 8250
References 8250
Note Added in Proof 8271

1. INTRODUCTION

Electronic confinement in nanoscale pieces of matter of noble metals has resulted in giant advances in science and technology.[1] Chemical synthesis of such materials,[2] manipulation of their properties, and utilization of emerging phenomena at this length scale have all contributed to this advancement.[3,4] As dimensions of such particles shrink further, novel molecular properties evolve in the cluster regime of materials, especially in metals. Such atomically precise entities are composed of a few to tens of atoms of metals with a definite ligand shell, forming molecules of definite composition.[5−7] For the purpose of this review, we considered only those particles with precise formulas possessing optical properties, which are different from corresponding plasmonic nanoparticles. Their stability in electronic terms has been explained by the superatom model[8−10] which is based on the "jellium" model of electrons confined within a spherically symmetric potential well of the metal core. If the number of free electrons falls in the "magic" number series of 2, 8, 18, 20, 34, 58, ..., the cluster shows high stability.[8−10] The number of free electrons of a metal cluster protected with ligands (such as thiolate) is calculated as $N_s = N\nu_A - L - q$, where N_s is the shell closing number (free electron count), N is the number of core metal atoms, ν_A is the effective valence electrons (for Au/Ag, $\nu_A = 1$), L is the number of one-electron withdrawing ligands, and q is the total charge ($+q$ or $-q$) on the cluster.[10] Ligands such as phosphine or amine do not withdraw electrons; rather they bond to a metal core through a dative bond and do not get counted in the way they are counted in N_s.

Assigning an appropriate name to these atomically precise pieces of matter has been a challenge, and they have been referred to variedly, such as nanoparticles, quantum dots, clusters, nanoclusters, quantum clusters (QCs), monolayer protected clusters (MPCs), nanomolecules, artificial atoms, superatoms, faradaurates, etc. However, this class of materials has molecule-like optical properties, so it is not appropriate to treat them as nanoparticles, which exhibit distinctly different optical features.[7] Many of the emerging chemical phenomena of these materials emphasize their molecular nature. "Nanoclusters" and "quantum clusters" are more suitable titles as such atomically precise pieces have quantized energy levels and, as a result, show multiple bands in their optical spectra, resembling molecules. Thus, naming them continues to be an issue. We will revisit this topic later in the text.

Tens of such nanoclusters are now known with detailed mass spectral data,[11,16,27−37] and among them a few have also been characterized with single crystal X-ray diffraction.[15,38−47] With new preparation methods[48] and adaptation of modern separation methodologies, synthesis of a large number of unique materials in the immediate future is highly possible. The possibility to create well-defined clusters with different ligands and associated variation in chemical properties has led to a plethora of applications ranging from chemistry to biology and also from materials science to devices.[49−53] An illustration of these clusters and their diverse possibilities is presented in Figure 1.

Combining properties of other nanosystems, such as graphene, with clusters has resulted in novel composites.[54] Creation of atomically precise clusters in proteins and biomolecular templates has given other directions in chemical research.[55] Utilizing the unique chemistry of these systems, new sensors have been developed and extension of this science has created new materials for contaminant removal from surface waters.[56] Modification of electronic structure in the cluster size regime has been used in catalysis, which has given rise to unusually large conversion efficiencies for several transformations. Modification of the metal core itself has produced novel alloys with precise composition and systematic variation in properties. Electronic structures of these systems can be controlled by ligands that can also induce chirality in the overall system. The cluster core itself can be chiral, and such chiral induction depends on various parameters. Studies in this area have greatly benefited by the use of advanced instrumentation, especially adaptation of soft ionization mass spectrometry. Understanding of these structures, reasons for their increased stability and chemical reactivity including catalysis, assignments of their electronic transitions, and predictions of their emerging properties have immensely benefited from the advances in

DOI: 10.1021/acs.chemrev.6b00769
Chem. Rev. 2017, 117, 8208−8271

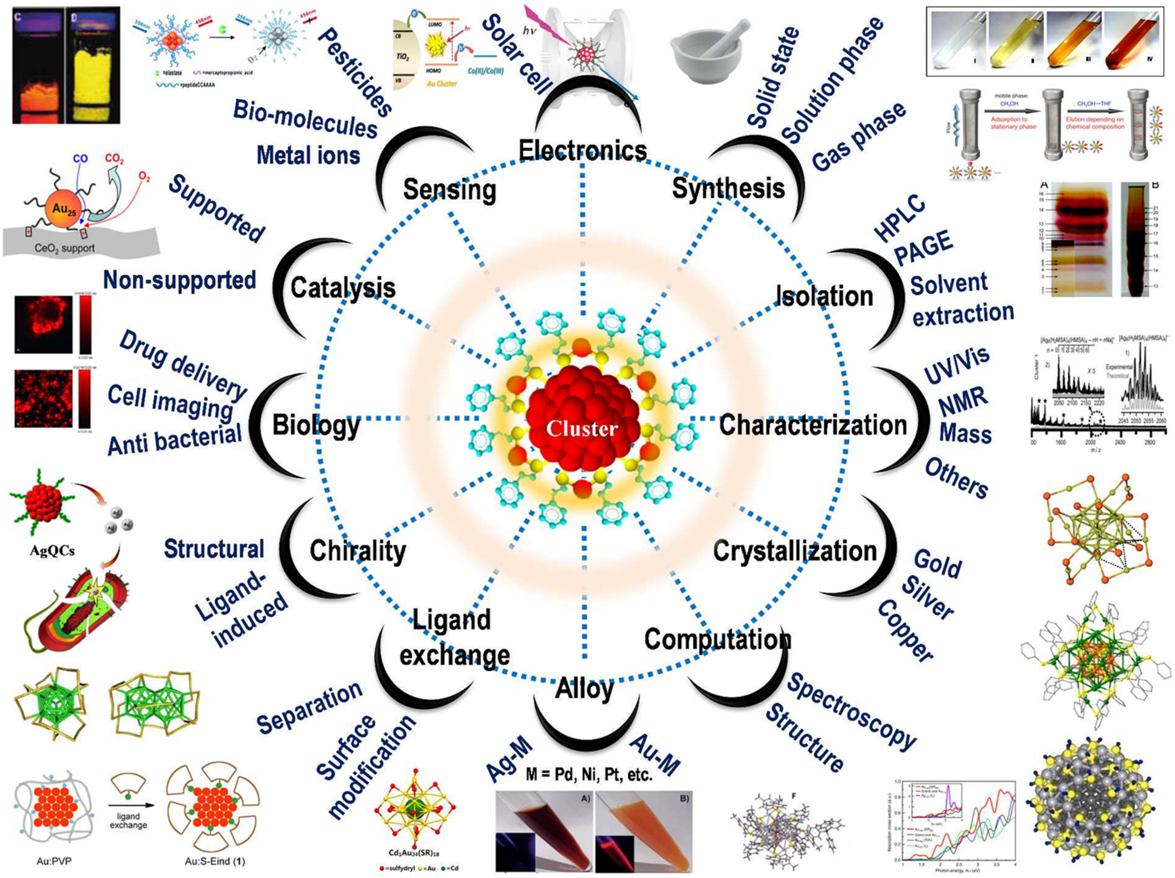

Figure 1. Illustration of monolayer protected clusters, their chemical diversity, and different studies performed using them. Parts of the images are from the literature.[11−26]

computational materials science. A schematic diagram of the evolution of such clusters over the years is provided in Figure 2. Research in this area extending over 5000 research publications (Figure 2, inset) suggests an explosion of activities in the near future, and a consolidated documentation is necessary at this stage. It is important to mention that since there was a recent review article[7] covering theoretical aspects of clusters, our focus is only on experimental research.

1.1. Noble Metal Nanoparticles: From Alchemy to Today

"Noble metals" refers to those metals that are resistant to processes such as oxidation under normal atmosphere. They are ruthenium, rhodium, osmium, iridium, palladium, platinum, silver, and gold. Because of their poor abundance, all of them are also precious, to varying degrees. Among the noble metal nanoparticles,[57−86] those of gold and silver have drawn tremendous interest from the scientific community because of their versatile applications.[87−90] Starting from historical times, gold and silver have been used extensively by mankind for several purposes including coloration of glass, as well as in esthetic and medicinal practices. A mixture of gold salts with molten glass was used to produce gold colloids of rich ruby color. In the medieval days, artisans exploited many such varieties for the coloration of ceramics and glasses. The oldest example of these is the fourth century A.D. Lycurgus Cup made by the Romans. Purple of Cassius, a pink pigment commonly used in the 17th century, was a combination of gold particles and tin dioxide.[91] Using metallic minerals including gold, the great alchemist and the founder of modern medicine, Paracelsus (1493−1541), developed many highly successful treatments.[92] Egyptians used gold for physical, mental, and spiritual purification.[92] In Ayurveda (an Indian medical system), gold has been used in several preparations; one such example is *Saraswatharishtam*, usually prescribed for memory enhancement. The chemical synthesis of colloidal gold particles was discovered by Michael Faraday in 1857.[93] He observed the formation of deep red colored colloidal gold when aqueous solution of $AuCl_4^-$ was reduced by phosphorus in carbon disulfide (CS_2).

Similar to gold, silver also has a historical background. The color of the Lycurgus Cup is due to Au−Ag nanoparticles. But the major use of silver in those days was in medicinal field, mainly as an antimicrobial agent. Silver vessels were used to keep water fresh by Greeks.[92] But they were not aware of the antibacterial properties of silver. The purpose of addition of silver was to increase the clarity, reduce odor, and improve the taste of water. The Greeks may have understood that disease-causing pathogens would not survive in the presence of silver, and perhaps for that reason silver was used in drinking vessels, dishware, and eating utensils, although microbes as disease-causing agents was suggested only in 1880.[94] Even in other medical therapies such as bone prostheses, ophthalmic surgery, etc., silver was used extensively. Silver colloids were made by Frens, Overbeek, and Lea in 1969 when they reduced silver nitrate using ferrous sulfate in the presence of citrate ion which acted as a protecting agent.[95] Scientists have shown huge interest thereafter in silver colloids and their antibacterial properties.[96−99] Until the last century, the use of gold and silver particles was restricted only for medicinal and antibacterial

DOI: 10.1021/acs.chemrev.6b00769
Chem. Rev. 2017, 117, 8208−8271

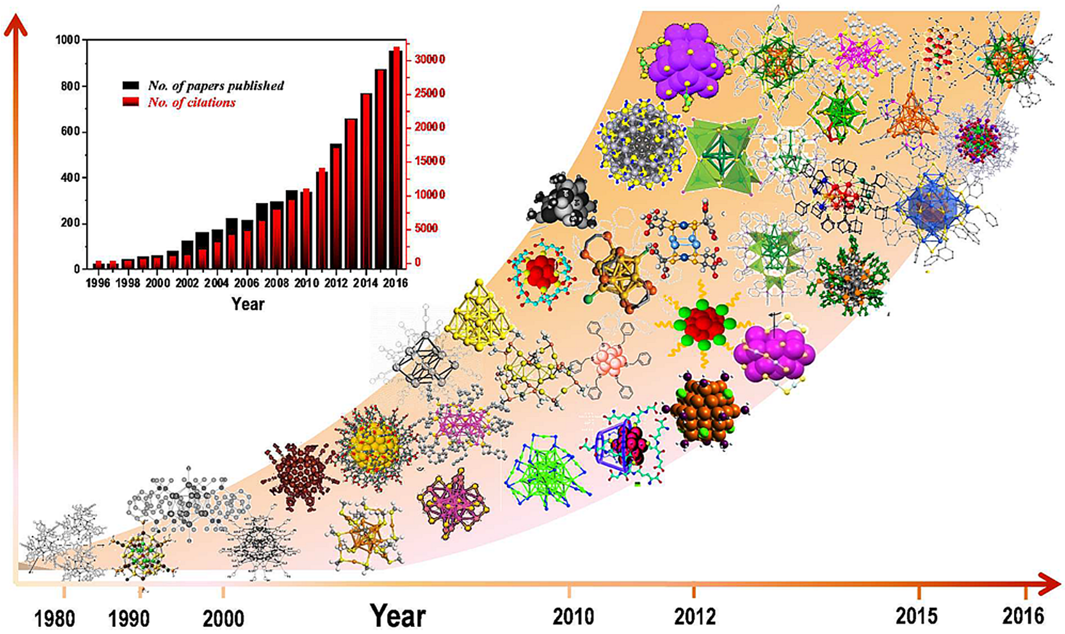

Figure 2. Evolution of clusters (of the type described here) with respect to time. Inset shows the number of papers published and citations in each year for metal nanoclusters (collected from Web of Science using "gold nanoclusters" or "silver nanoclusters" as keywords). The data were collected up to Dec 31, 2016.

activity, but now it is being explored intensely in catalysis, optics, and several other biological applications.[87,89,90,100,101] Even in the 15th and 16th centuries, people of Deruta used silver and copper nanoparticles to fabricate glazes. They mixed copper and silver salts with vinegar, ochre, and clay and applied them on the surface of already glazed pottery for fabrication.[92] Therefore, from alchemy to today, noble metals such as gold and silver have been used for a large number of applications in several directions because of their diverse properties. A historical account of the use of noble metals is provided in ref 92.

1.2. Gas Phase Clusters

Clusters made in the gas phase have drawn tremendous interest from the scientific community,[102] especially after the discovery of C_{60}.[103] For any material, the number of surface atoms is very important as it controls its properties. In a cluster (assumed to be spherically shaped), the fraction F of surface atoms is $F = 4/n^{1/3}$, where n is the total number of atoms. It can be seen that F is equal to 0.3, 0.2, and 0.04 when n is 1000, 10 000 and 1 000 000, respectively.[102] Normally, in gas phase clusters, valencies of the surface atoms are unsatisfied, because of which they are extremely reactive. For this reason, clusters cannot be kept in a free state and they should be made in situ, in experimental apparatuses where the properties are to be investigated. That is why practically all the studies of such clusters are carried out in a vacuum or in inert (noble) gases.[104] Gas phase clusters are usually made through a variety of cluster sources, such as laser vaporization source, laser ablation cluster source, pulsed arc cluster ion source, ion sputtering source, liquid metal ion source, etc.[102,104] The concepts of electron shell closing based on the jellium model[105] and superatoms[8] were established after the observation of such gas phase metal clusters.

Although there are numerous reports on gas phase clusters such as ionic, covalent, metallic, molecular, van der Waals, etc.,[9,106−114] in the present context, we will focus mainly on noble metal clusters.[102,104] The study of gas phase Au and Ag clusters was initiated in the 1960s.[106,110] Chemical sputtering of gold and silver metal targets by inert gas ions produced smaller naked clusters.[115] Coalescence of such clusters formed larger clusters.[116] Such studies have also been done with pulsed laser evaporation.[102] The clusters so formed exist as neutral or ionic (positive or negative) entities and have been detected by various mass spectrometric techniques such as Wien filter, time-of-flight (TOF) analyzer, quadrupole mass filter (QMF), ion cyclotron resonance (ICR) spectrometer, etc.[102] Katakuse et al. have investigated a series of copper $(Cu)_n^+$, silver $(Ag)_n^+$, and gold $(Au)_n^+$ clusters up to the size $n = 250$.[115] These clusters were generated by bombardment of 10 keV Xe ions and analyzed using a sector-type mass spectrometer. Details of several gas phase atomic and molecular clusters can be found in the book of R. L. Johnston.[117]

Baksi et al.[118] have shown the existence of clusters such as Au_{18}^+, Au_{25}^+, Au_{38}^+, and Au_{102}^+ with unprotected metal cores, having unusual stability in the gas phase. These clusters were prepared via laser desorption ionization of the precursor metal ions in protein templates. Nucleation occurred in the vicinity of the protein in the gas phase. In another report, using a similar approach, alloy clusters of the type $Au_{24}Pd^+$ were detected.[119] Even though over the years many efforts have been made to improve the synthesis techniques of these clusters and to understand them in great detail, isolation of such gas phase species continues to be a challenge and so far no reports exist in the literature. Deposition of such gas phase clusters on substrates[120−123] will open the field of cluster catalysis, as these systems are catalytically active.[124] Much of such supported cluster catalysis research is documented in two recent review articles.[125,126] Lu et al. have reported the effect of size-selected silver clusters on lithium peroxide batteries.[127] They have deposited ultrasmall atomically precise silver clusters on passivated carbon to study the discharge process in lithium−oxygen cells. Dramatically different morphologies of electrochemically grown lithium peroxide were seen depending on the size of the clusters. Therefore, by controlling the surface structure on cathodes, the performance of lithium−oxygen cells can be improved.

1.3. Early Monolayer Protected Clusters: Au_{13} and Others

Gas phase clusters cannot be isolated in the free form as they are not stable in ambient conditions. Using protecting ligands, it is possible to synthesize nanoparticles or nanoclusters in the solution phase. After the discovery of Faraday's colloidal particles, several efforts were made to synthesize colloids of noble metals, but most of them resulted in nanoparticles with a broad size distribution. Turkevich et al.[128] have discovered a simple way to synthesize colloidal gold in 1951 which was then refined by Frens[132] in the 1970s. In their method, gold chloride was reduced by sodium citrate in aqueous medium.

Creation of highly monodisperse nanoparticles was a great challenge in those early days. Phosphine type ligands were used at that time to protect the gold core. The very first report of $Au_{11}(SCN)_3(PPh_3)_7$[133] came in 1969, which was followed by the crystal structure of $Au_{11}I_3[P(C_6H_4\text{-}p\text{-}Cl)_3]_7$ in 1970.[129] The Au_{11} cluster can be best described in terms of an incomplete icosahedron, where the central gold atom [Au(1)] is surrounded by 10 other gold atoms as depicted in Figure 3a. Other derivatives of Au_{11} also exist in the literature.[134] Many clusters with lower nuclearity have also been reported.[135−140] Clusters of very small nuclearity,[135−138] such as Bertand's mono- and diatomic Au complexes[141] and Schmidbaur's tetraatomic Au complex,[142] suggest that this class of materials indeed bridges the gap between molecules and nanoparticles. The $Au_8(PPh_3)_7(NO_3)_2$[143] and $Au_9[P(C_6H_4\text{-}p\text{-}Me)_3]_8(PF_6)_3$[144] clusters exist as incomplete icosahedrons, whereas $Au_{10}Cl_3(PCy_2Ph)_6NO_3$[145] shows a D_{3h} symmetry (many more clusters are listed in Table S1). Several theoretical analyses predicted the existence of higher nuclearity gold clusters such as Au_{13}. In 1981, Briant et al. solved the crystal structure of the Au_{13} cluster which has a perfect icosahedral structure (Figure 3b) with a central gold atom.[130] Many groups have studied this cluster extensively.[146−151] $[Au_{20}(PP_3)_4]Cl_4$ (PP_3, tris[2-(diphenylphosphino)ethyl]phosphine)[152] and $[Au_{39}(PPh_3)_{14}Cl_6]Cl_2$ have also been reported with phosphine protection.[153] Some alloy clusters such as $[Au_9Ag_4Cl_4(PMePh)_2]_8{}^+$ (Figure 3c),[131] $[(p\text{-}Tol_3P)_{10}Au_{13}Ag_{12}Br_8](PF_6)$,[154] $[(p\text{-}Tol_3P)_{12}Au_{18}Ag_{20}Cl_{14}]$,[155] and $[Au_{12}Ag_{12}M(PR_3)_{10}Cl_7]^+$ (M = Pt, Ni)[156] have also been reported. The $[(p\text{-}Tol_3P)_{10}Au_{13}Ag_{12}Br_8](PF_6)$ cluster is constructed by two icosahedrons sharing a vortex atom (later, a similar structure was seen for a rod-shaped Au_{25} cluster with phosphine and thiol protection[47]). In 1981 Schmid et al.[157] reported a 55 atom cluster, $Au_{55}(PPh_3)_{12}Cl_6$, which has a high tendency to self-assemble forming one- (1D),[158,159] two- (2D),[160] and three-dimensional (3D)[161] organized structures. Because of this self-organization, Au_{55} cluster has been used in several applications.[162−168] Single crystal studies and proper mass spectral characterization of this particle have not been reported yet, which makes the existence of this species controversial. However, the formation of Au_{55} core has been proven by mass-spectrometric analysis of thiolated Au_{55} analogues.[34,169,170] Several microscopic studies have shown the structural details of Au_{55} and its monodispersity.[171−173] Recently, the Palmer group has probed the structure of Schmid's Au_{55} cluster, using direct atomic imaging techniques.[174,175] Based on aberration-corrected scanning transmission electron microscopy (STEM) combined with multislice simulation of STEM images, they predicted that 42% of the clusters present on the TEM grid possess a hybrid structure (composed of icosahedral, cuboctahedral, and ino-decahedral shapes) and the remaining 58% are amorphous in nature. These reports suggest that the Schmid synthetic route[176] does produce the $Au_{55}(PPh_3)_{12}Cl_6$ cluster along with a few other clusters, composed of 35−60 Au atoms.

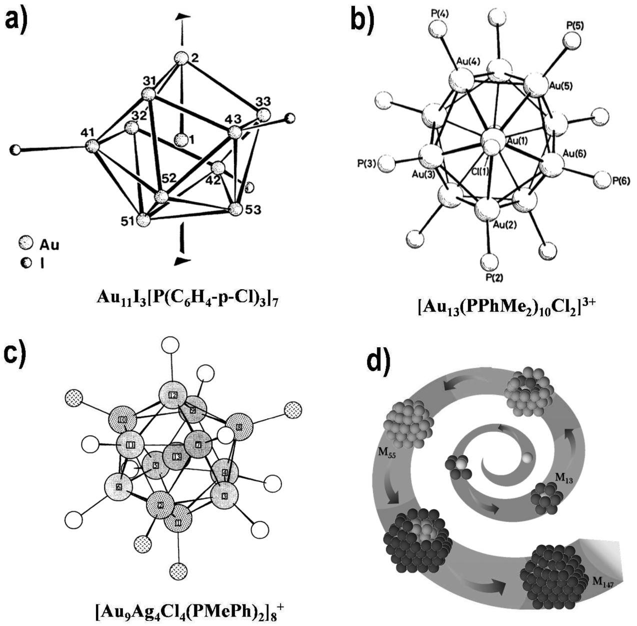

$Au_{11}I_3[P(C_6H_4\text{-}p\text{-}Cl)_3]_7$

$[Au_{13}(PPhMe_2)_{10}Cl_2]^{3+}$

$[Au_9Ag_4Cl_4(PMePh)_2]_8{}^+$

Figure 3. (a) Crystal structures of $Au_{11}I_3[P(C_6H_4\text{-}p\text{-}Cl)_3]_7$ cluster (phosphine groups have been omitted for clarity). Only gold atoms are numbered, although not sequentially as all the atoms in the cluster including ligands are counted. Reprinted with permission from ref 129. Copyright 1970 Royal Society of Chemistry. (b) Molecular structure of the $[Au_{13}(PPhMe_2)_{10}C1_2]^{3+}$ ion. For reasons of clarity, the carbon and hydrogen atoms on the phosphine ligands have been omitted. Reprinted with permission from ref 130. Copyright 1981 Royal Society of Chemistry (c) Perspective view of the $[Au_9Ag_4Cl_4(PMePh)_2]_8{}^+$ cluster ion. Phosphine substituents and bonds to the central atom are omitted for clarity. Key to atoms: gold, fine speckling; silver, course speckling; phosphorus, no pattern; chlorine, herringbone. Reprinted with permission from ref 131. Copyright 1996 Royal Society of Chemistry. (d) Schematic view of the growth of shell structure of clusters: Initially a single atom is surrounded by 12 other atoms to form a 13 atom core−shell M_{13} cluster. Then, 42 atoms can be densely packed on the surface of 12 atoms to produce a two-shell M_{55} cluster; in a similar fashion, a shell of 92 atoms can form over the second shell to generate a three-shell M_{147} cluster and this series may continue.

The most interesting aspect of clusters such as Au_{13} or Au_{55} is the unique full shell structures which explain their stability. The expression "full shell cluster" refers to a particle composed of a central atom that is surrounded by individual shells of atoms, eventually resulting in perfect geometries. The icosahedral geometry is a perfect example of this kind. The general rule for construction of such clusters is the number of atoms in the cluster = $1 + \sum(10n^2 + 2)$, where the summation runs over all the shell numbers (n = 1, 2, ...) in the cluster. A schematic is given in Figure 3d to understand the formation of such shells. Au_{13} cluster (n = 1) has been described as a one-shell cluster where a central atom is coordinated to the remaining 12 atoms which form the first shell. More details about the phosphinated gold clusters can be found in Table S1.

1.4. Brust Synthesis and Beyond: Monolayer Protected Nanoparticles

Two different approaches, namely bottom up and top down, have been followed to synthesize noble metal nanoclusters.

In the bottom-up approach, nanoclusters are synthesized from metal ion precursors by reducing them in the presence of suitable ligands. It is the most efficient way to nucleate clusters, and most importantly, nucleation can be controlled by varying the quantities of the ligands and reducing agents or by varying the solvents. Aqueous and organic soluble clusters can be produced using this approach. Synthesis of noble metal nanoclusters got a new direction after the easy and effective method developed by Brust et al.[177] in 1994. The Brust method is an example of the bottom-up approach to synthesize organic soluble metal nanoparticles as well as nanoclusters. The procedure followed a two-phase synthetic protocol in which water and an organic nonpolar solvent (mainly, toluene) were used as the two phases. The metal precursors were first dissolved in an aqueous solution and then phase transferred to the organic solvent using phase transfer reagents such as tetraoctylammonium bromide. Finally, organic protecting ligands and reducing agents were added to the mixture to obtain nanoclusters. Perala and Kumar[178] have tried to explain the mechanism of this method. According to them, phase transfer of chloroauric acid to the organic phase in the presence of the phase transfer catalyst (PTC) occurs through the following equation:

$$\begin{aligned} &H^+AuCl_4^-(aq) + (R_8)_4N^+Br^-(toluene) \\ &\quad = (R_8)_4N^+AuX_4^-(toluene) + HX(aq) \end{aligned} \tag{1}$$

Since the extent of substitution of Cl^- by Br^- is not known, X represents both Cl and Br. Then the reduction of Au(III) to Au(I) by thiol was believed to occur through the following equation:

$$\begin{aligned} &(R_8)_4N^+AuX_4^-(toluene) + 3RSH \rightarrow -(AuSR)_n- \\ &\quad + RSSR + (R_8)_4N^+ + 4X^- + 3H^+ \end{aligned} \tag{2}$$

At this stage, it was believed that the toluene phase contains PTC, dialkyl sulfide, Au(I)SR polymer (n is the number of AuSR monomers) and AuX_4^-, either complexed with PTC cation or excess RSH depending on the ratio of the ingredients. In the final step, the reduction of Au^{3+} or Au^+ to Au^0 happens by borohydride according to the following equation.

$$-(AuSR)_n- + BH_4^- + RSH + RSSR \rightarrow Au_x(SR)_y \tag{3}$$

$$(R_8)_4N^+AuX_4^- + BH_4^- + RSH + RSSR \rightarrow Au_x(SR)_y \tag{4}$$

Now, for the cluster case, depending on the ratio of Au, thiol, and sodium borohydride, the x and y values change (please note that reactions 2, 3, and 4 are not balanced reactions; impurities such as other clusters or some thiolates are also present in the final product for reactions 3 and 4, which were generally removed during the purification step). In most of the cases, some Au(SR) polymer remains as staple motifs such as $Au_2(SR)_3$ or $Au(SR)_2$ in the cluster structure, which suggests that they get restructured during the cluster growth and only the remaining gold species are reduced to the zero oxidation state.

Nanoclusters of different sizes and of different noble metals (Au, Ag, Pd, etc.) can be synthesized easily using this method.[170,179−182]

Among the monolayer protected metal nanoclusters, gold has been studied extensively because of its high stability under ambient conditions. From the early reports, it was believed that, in the Brust protocol, an $[Au(I)SR]_n$ polymeric compound is formed during the reduction of Au(III) to Au(I) in the presence of alkanethiol (RSH). But recently, Goulet and Lennox[183] have revised the view of the Brust method from an analysis of ^1H NMR data. According to their suggestion, in a one-phase method, Au(I)thiolate is likely to be the precursor, but for the two-phase Brust method, Au(I)−tetraoctylammonium halide complex $[TOA][MX_2]$ is the main precursor rather than the $[Au(I)SR]_n$ polymers before the reduction. The same was suggested by Li et al.[184] through their detailed Raman and NMR analyses. These revised views help understand the mechanism of this method.

In one-phase Brust−Schiffrin method, a polar solvent such as methanol or THF was used as solvent. Several modifications of this method have appeared, mainly by controlling different parameters such as temperature, solvents, concentration of each reactant, reducing agents, etc., to get highly monodispersed nanoclusters. Zhu et al. have synthesized $Au_{25}(SR)_{18}$ cluster just by tuning the stirring rate and controlling the temperature.[185] Wu et al. have introduced a facile single-phase (using THF) method to synthesize $Au_{25}(SR)_{18}$ cluster by "size focusing".[186] For water-soluble gold clusters, metal ions are first reduced to Au(I) complex by water-soluble ligands which is followed by reduction using suitable reducing agents. In most of the cases, sodium borohydride ($NaBH_4$) has been used as the reducing agent.[187]

In the top-down approach, the nanoclusters are synthesized from bigger nanoparticles by either core etching or size reduction. Initially, a metal nanoparticle is synthesized which is then treated with extra ligands or metal ions to form nanoclusters. Duan and Nie[188] in 2007 showed that polyethylenimine (PEI), a first generation dendrimer, could be used to synthesize nanoclusters from dodecylamine capped organic soluble metal nanoparticles. The synthesized cluster was identified as Au_8 from electrospray analysis, and the cluster was found to be highly luminescent. Qian et al.[189] in 2009 synthesized Au_{25} nanorods and nanospheres from polydispersed phosphine protected nanoparticles through a thiol etching procedure. As mentioned above, along with ligands, metal ions have also been used as etching agents. Lin et al.[190] have shown that, when didodecyldimethylammonium bromide (DDAB) stabilized nanoparticles were treated with Au precursors ($HAuCl_4$ or $AuCl_3$), a transparent solution was formed. A subsequent phase transfer and ligand exchange by dihydrolipoic acid (DHLA) resulted in the formation of red luminescent gold clusters.

1.5. Evolution of New Synthetic Methods at the Ultrasmall Regime

Apart from this traditional solution phase synthesis, several new protocols such as interfacial synthesis,[14,191] carbon monoxide (CO) directed method,[192] solid-state route,[16,36,37,193−196] etc., have been proposed lately as alternative approaches to synthesize atomically precise nanoclusters. A perspective article by Udayabhaskararao and Pradeep[48] summarizes the advancements in the synthesis of noble metal nanoclusters. A brief synopsis of all the synthetic routes is presented in Table 1.

Table 1. Different Routes Used for the Synthesis of Nanoclusters

method			example	ref
top down	alloying		(Cu$_n$Au$_{25-n}$)SR$_{18}$ (n = 1−5), Au$_{24}$Pd(SR)$_{18}$, Au$_{24}$Pt(SR)$_{18}$, Ag$_7$Au$_6$(H$_2$MSA)$_{10}$	17, 197−199
	etching	ligand induced	Au$_{25}$(SG)$_{18}$	200
		temperature induced	Ag@MSA and Au@DT	201, 202
		other	Ag$_7$(H$_2$MSA)$_7$ and Ag$_8$(H$_2$MSA)$_8$	14
	ligand exchange		Au$_{24}$Pd(DDT$_{18-n}$SBB$_n$), Au$_{25}$(DDT$_{18-n}$SBB$_n$)	12
bottom up	Brust method		Au$_{25}$(SC$_6$H$_{13}$)$_{18}$, Au$_{55}$(SC$_{18}$)$_{32}$	34, 180
	modified Brust method		Au$_{38}$(SC$_{12}$H$_{25}$)$_{24}$, Au$_{38}$(PET)$_{24}$	203, 204
	photoreduction		Ag@SG, Ag@PAMAM	21, 205
	microwave assisted		Ag@L-SG	206
	radiolytic approach		Ag$_3^{2+}$ and Ag$_4^{2+}$	207, 208
	microemulsion technique		Ag$_n$QCs	209
	sonochemical synthesis		Ag@PMAA	210
	electrochemical synthesis		Cu@TBAN	211
	template mediated	thiols and amines	Au$_{25}$SG$_{18}$, Ag$_{\sim 4,5}$@DHLA	200, 212
		proteins	Ag$_{15}$@BSA, Au$_{25}$@BSA, Au@NLF	32, 213, 214
		polymers	Ag@LA-PEG	215
		gels	Ag$_{25}$@SG	216
		DNA	Ag@DNA	217
		dendrimers	Ag@PAMAM	210
	solid state route		Ag$_9$, Ag$_{44}$, Ag$_{55}$, Ag$_{152}$, Pt$_{11}$, Cu@PET	16, 36, 37, 193, 195, 218
	high temperature route		~Ag$_{75}$(SG)$_{40}$	11
	slow reduction method		Au$_{18}$(SG)$_{14}$	219
	other solution phase		Ag$_{44}$(4-FTP)$_{30}$, Ag$_{44}$(MBA)$_{30}$, Ag$_{44}$(SePh)$_{30}$, Ag$_5$Pd$_4$(SePh)$_{12}$	30, 44, 196, 220−222

Box 1. Important Pointers in Monolayer Protected Nanoclusters

Some of the landmarks in the science of these materials are listed as follows: **1969−1981**: Synthesis of cluster compounds such as Au$_{11}$[133] and Au$_{13}$[130] occurred. **1994**: Brust−Schiffrin developed two-phase methods for the synthesis of monolayer protected gold nanoparticles.[177] **1996**: Whetten group explored the gold nanocrystal's core sizes by laser desorption mass spectrometry.[223] **1997**: Cleveland and Landman developed a structural model for gold clusters.[224−226] **1997−2000**: Whetten and Murray groups started exploring the gold cluster chemistry.[227,228] **2005**: Tsukuda group identified Au$_{25}$SG$_{18}$ through mass spectrometry.[229] **2005**: Kimura group made enantiomers of nanoclusters.[230] **2006**: Hakkinen developed the "divide and protect" concept.[231] **2007**: Jadzinsky et al. reported the first crystal structure of Au$_{102}$(SR)$_{40}$. **2008**:[45] Murray and Jin groups reported the crystal structure of Au$_{25}$(SR)$_{18}$.[15,41] **2009**: Ying group synthesized a highly fluorescent protein protected gold cluster.[213] **2009−2010**: Many synthetic routes were used to make clusters such as the "solid state route"[37] to synthesize silver clusters. **2013**: Bigioni and Zheng groups determined the crystal structure of Ag$_{44}$(SR)$_{30}$.[44,222] **2015**: Bakr group found the crystal structure of Ag$_{25}$(SR)$_{18}$.[46] **2015**: Pradeep group developed a nomenclature for clusters.[232] **2016**: Cluster chemistry was being developed; clusters react in solution between each other, conserving the structural motif, just like molecules.[233]

2. MONOLAYER PROTECTED CLUSTERS

Synthesis and characterization of monolayer protected gold clusters has become one of the prime interests of materials chemists. Although there have been several reports on phosphine protected gold clusters, very few reports existed with thiol protection in the early days of these materials (1990−2000s). In the following sections, we will mainly discuss the thiol protected clusters which have been synthesized and characterized during this period.

2.1. Entry of Mass Spectrometry to Noble Metal Nanoparticles and Identification of Clusters

Emergence of mass spectrometry (MS) as a principal tool of characterization of monolayer protected clusters is largely due to the versatility of soft ionization tools. Ionization of clusters directly from solution and from solid state by electrospray ionization and matrix assisted laser desorption ionization (LDI), respectively, have increased the power of mass spectrometry. Coupled with the capability to do analysis of extended mass ranges and additional capabilities such as fragmentation, mobility separation, and surface induced dissociation, MS can provide more information. Mass resolution has also changed tremendously in the recent past with new instrumentation touching numbers of the order of 50 000 ($m/\Delta m$). This makes it possible to assign mass peaks to unique products in view of the specific isotope patterns of various entities.

MS played an important role in identifying and understanding gas phase clusters. Fullerene family is the classic example here which includes C$_{60}$ and C$_{70}$.[103] Several metals such as alkali, alkaline earth, and transition metals have been studied in the gas phase.[234−236] In most of the cases, a discontinuous variation in intensity at N = 2, 8, 20, ..., 92 atoms

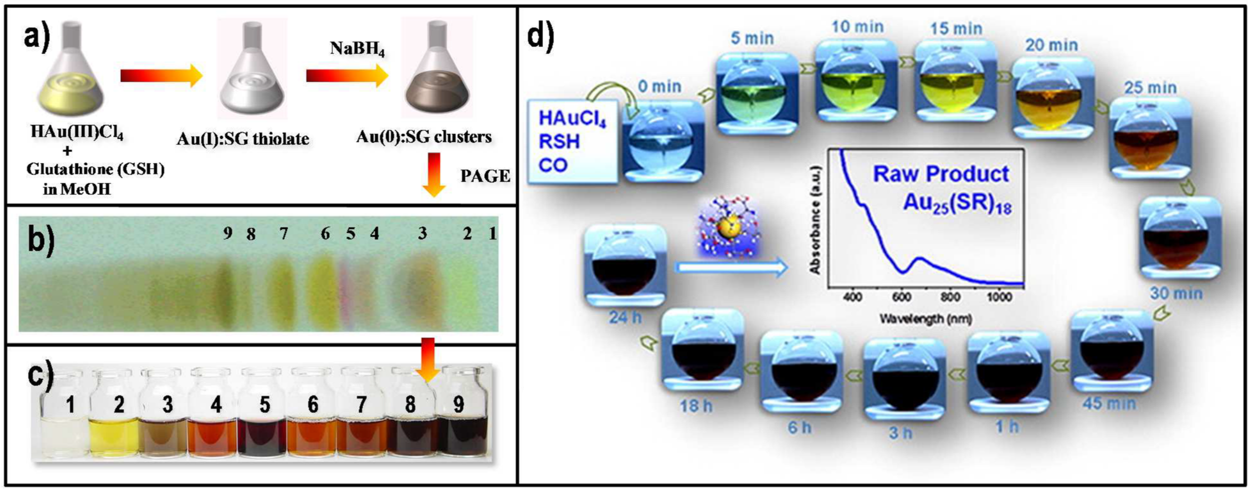

Figure 4. (a) Scheme of Au@SG cluster synthesis. (b) The PAGE shows nine isolated bands that were subsequently extracted in water. Corresponding photographs of all the cluster solutions are shown in (c). Reprinted from ref 229. Copyright 2005 American Chemical Society. (d) Photographs of the reaction mixture at different times during the synthesis of $Au_{25}(Cys)_{18}$ in the presence of CO. Inset shows the UV/vis spectrum of $Au_{25}(Cys)_{18}$ cluster. Reprinted from ref 192. Copyright 2012 American Chemical Society.

has been observed, which might be because of the high stability of these clusters.[235] Silver clusters with odd numbers of atoms are more intense as compared to clusters with even numbers of atoms. The former (2, 8, 20, ...) has an even number of valence electrons which results in spin pairing, and this enhances their stability as opposed to the latter which has an odd number of valence electrons.[115,237] Several molecular clusters have also been studied intensely by mass spectrometry.[238,239]

Along with gas phase clusters, mass spectrometry has given important directions to analyze noble metal cluster systems, prepared in solution.[240] The Whetten and Murray groups initiated early studies to identify such clusters using mass spectrometry and other characterization techniques.[223,227,241−243] Whetten et al.[223] showed a series of clusters with molecular mass starting from 27 to 93 kDa in thiol protected Au clusters. Based on the core size from TEM analysis and mass spectral characterization, they assigned clusters to be composed of 140−459 gold atoms. LDI MS was used mainly to identify the core mass. Clusters of core masses 5.6,[227] 14.0,[244] 22.0,[244] 28.0,[241] 29.0,[244] and 66.0 kDa[245] are known from their reports. In most of the cases, clusters were alkane (butane, hexane, octane, or dodecane) thiol protected. The effect of chain length on cluster properties was also studied extensively by Whetten and colleagues.[246] Some reports on gold clusters protected with glutathione,[244] functionalized alkenethiols,[228,247] or tiopronin[245] are also known. Among the clusters reported during those early years [1990s], only a few were tentatively assigned. The cluster of core mass 29.0 kDa was suggested to have a composition of $Au_{144-146}(SR)_{50-60}$.[248] Schaaff et al. assigned the 5.6 kDa (core mass) cluster as $Au_{28}(SG)_{18}$, and subsequently several reports came from the same group on the same cluster.[227,249] Later, Negishi et al.[229] reassigned the cluster as $Au_{25}(SG)_{18}$ in 2005 which is now one of the most studied clusters. Similarly, Murray's initial reports of $Au_{38}(SR)_{24}$ clusters[250−252] were later corrected as $Au_{25}(SR)_{18}$. Among the clusters reported so far, most of them have been assigned based on mass spectrometry, either by electrospray ionization (ESI) or matrix-assisted laser desorption/ionization (MALDI) MS (Table S1). Detailed discussion of these clusters is presented in section 3.3.1.

2.2. Other Molecular Tools

Other than mass spectrometry, several new molecular tools to characterize these clusters in more detail have been introduced by several research groups. Because of their distinct optical properties and photoluminescent nature, scientists started looking at these particles as molecules. Thus, optical spectroscopy became the immediate tool to understand the electronic structure of these clusters.[223,227,241,243,248] This investigation was also influenced by the fact that optical absorption spectroscopy is one of the most important methods for characterizing plasmonic nanoparticles. Distinct differences between these two categories of nanosystems are clear from such investigations. We will come back to this topic later in the text. Fluorescence spectroscopy has provided a new direction to the investigations which showed that these clusters can emit from the visible to the near-infrared (NIR) region, depending on their core size.[249,253] Energy gap between the highest occupied and lowest unoccupied molecular orbitals (HOMO and LUMO) and other features of the electronic structure have also been probed electrochemically using cyclic voltammetry (CV) or differential pulse voltammetry (DPV) experiments.[241,245−247] Along with characterization, isolation of such clusters is also important and polyacrylamide gel electrophoresis (PAGE) has been introduced for separating clusters of different sizes.[227,244,254] PAGE requires two kinds of gels: a stacking gel and a separating gel. Mostly acrylamide and bis(acrylamide) have been used in different weight percentages to create these gels. Normally, the sample solutions are loaded onto the stacking gel and then eluted for a long time at a constant voltage to get sufficient separation. The clusters are separated based on their size and aqueous soluble clusters; especially ligands with carboxylate functionality work well for PAGE separation. Separation can easily be observed by looking at the gels with different colors which are then cut and extracted in appropriate solvents to get the purified cluster. For organic soluble clusters, chromatographic techniques such as high performance liquid chromatography (HPLC),[12,255,256] gel permeation chromatography (GPC),[170] size exclusion chromatography (SEC),[257] and thin layer chromatography (TLC)[258] work well. More details about a few important techniques along with their recent advancement have been mentioned in section 3.

3. TOWARD ATOMIC PRECISION: GOLD CLUSTERS

Starting from Faraday's colloidal gold to particles synthesized through the Brust method, monodispersity has been improved tremendously. While several examples of such clusters are known today, it is not possible to discuss the synthesis of all of them in great detail in this review. To illustrate the case of gold clusters and highlight their essential characterization, $Au_{25}(SR)_{18}$ is considered as a representative system and a brief description is given below.

3.1. Synthesis and Separation of $Au_{25}(SR)_{18}$ Cluster

Monolayer protected gold quantum clusters and the evolution of their electronic, optical, and chemical properties as a function of the core size has led to new avenues in the field of cluster chemistry.[259] To develop the chemistry of these new nanosystems, there is indeed a need for novel procedures to synthesize such classes of materials with high purity. Several attempts have been made to create highly monodisperse particles of desired size (which are often treated as nanoclusters or nanomolecules) by optimizing the synthesis conditions such as solvent, gold-to-thiol ratio, temperature, reducing agent, etc.[260] Chemical reduction of Au(I) ions in the presence of thiols is the usual trend for synthesizing such clusters. The very first report of glutathione (SG) (a tripeptide composed of glycine, cysteine, and glutamic acid) protected stable gold cluster came from Schaaff et al.[227] in 1998. These authors prepared polymeric Au(I)SG in solution which was later reduced in a $MeOH/H_2O$ medium using $NaBH_4$ as the reducing agent. A mixture of solvents was used to control its size. They successfully isolated the 10.4 kDa cluster compound which was initially assigned as $Au_{28}(SG)_{16}$ based on ESI MS analysis. After that, Negishi et al.[261] in their procedure reduced the Au(I)−SG polymer in ice-cold condition which resulted in a mixture of glutathione protected gold clusters (a schematic of the process is illustrated in Figure 4a). Initially, six clusters were isolated and assigned with approximate compositions. Later in 2005,[229] nine such clusters were isolated through PAGE

Box 2. Synthesis of $Au_{25}(SR)_{18}$ Cluster

About 2 mL of 50 mM $HAuCl_4{\cdot}3H_2O$ in THF was diluted to 7.5 mL using THF. About 65 mg of TOAB was added to this solution and stirred at 1500 rpm for 30 min at room temperature. The initial yellow color of the solution turned deep red during stirring. About 0.5 mmol of pure thiol was added at a stretch while stirring at the same speed. The deep red color slowly turned to yellow and eventually became colorless after about 45 min. After stirring further for 2 h, 2.5 mL of ice-cold aqueous $NaBH_4$ (0.2 M) was added in one shot. The solution turned black immediately, and stirring was continued for 5−8 h depending on the ligands. A continuous monitoring of the UV/vis spectra is needed. Once the Au_{25} cluster has formed, all features will be prominent and optical spectra will not change over time. The solution was rotary evaporated and precipitated with methanol (~4 mL), washed repeatedly with the same, and dried (three times, until the smell of thiol was completely gone). This gives the purified and dried Au_{25} cluster which can be stored in a refrigerator (4 °C). With this methodology all alkanethiol and 2-PET protected Au_{25} cluster can be synthesized.

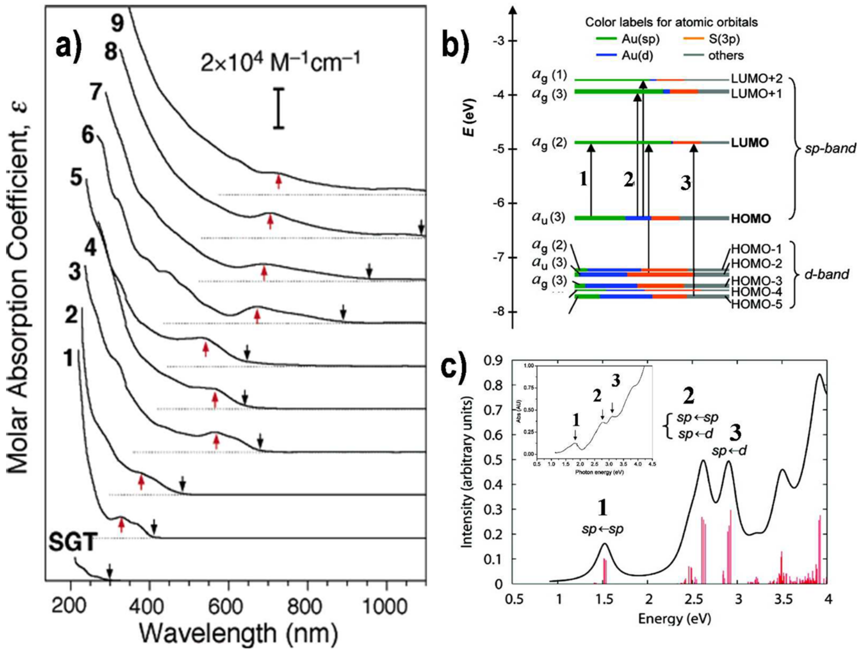

Figure 5. (a) Optical spectra of all nine isolated clusters in Figure 4b. Reprinted from ref 229. Copyright 2005 American Chemical Society. (b) Kohn−Sham (KS) orbital energy level diagram for the model cluster $Au_{25}(SH)_{18}^{-}$. Each KS orbital is drawn to indicate the relative contributions (line length with color labels) of the atomic orbitals of Au(6sp) in green, Au(5d) in blue, S(3p) in orange, and others in gray (those unspecified atomic orbitals, each with a <1% contribution). The left column of the KS orbitals shows the orbital symmetry (g, u) and degeneracy (in parentheses); the right column shows the HOMO and LUMO sets. (c) Theoretical absorption spectrum of $Au_{25}(SH)_{18}^{-}$. Inset shows the experimental absorption spectrum of $Au_{25}(PET)_{18}$ cluster. Peak assignments: peak 1 at1.8 eV, peak 2 at 2.75 eV, and peak 3 at 3.1 eV. Reprinted from ref 41. Copyright 2008 American Chemical Society.

separation (photograph provided in Figure 4b). After the separation, individual bands were cut and in the above study each one was extracted in water (photographs of the cluster solutions are given in Figure 4c). The corresponding clusters were assigned to $Au_{10}(SG)_{10}$, $Au_{15}(SG)_{13}$, $Au_{18}(SG)_{14}$, $Au_{22}(SG)_{16}$, $Au_{22}(SG)_{17}$, $Au_{25}(SG)_{18}$, $Au_{29}(SG)_{20}$, $Au_{33}(SG)_{22}$, and $Au_{39}(SG)_{24}$ using ESI MS. Interestingly, the $Au_{28}(SG)_{16}$ cluster reported by Schaaff et al.[227] was comparable and was reassigned here as $Au_{25}(SG)_{18}$. This first report of a precisely assigned and isolated $Au_{25}(SR)_{18}$ led to a revolution centered around this cluster. The main drawback of the above-mentioned two synthetic routes is the low yield of the product formed. Zhu et al.,[185] by using the Brust protocol with phenylethanethiol (PET), demonstrated that an increased yield is achievable by a kinetically controlled synthesis for $Au_{25}(SR)_{18}$. Since this report, several other methods have been discovered to obtain good yield and highly pure $Au_{25}(SR)_{18}$ clusters (see Table S1 for more details). Yu et al.[192] synthesized the $Au_{25}(Cys)_{18}$ cluster in large scale through a new CO-directed route, where CO has been used as the reducing agent. Photographs of the reacting solutions at different times are shown in Figure 4d. Several other clusters have also been synthesized using this methodology.[262] They have also developed the NaOH-mediated $NaBH_4$ reduction[263] and protection−deprotection method[264] for the synthesis of thiolated Au_{25} nanoclusters. Limited examples of $Au_{25}(SR)_{18}$ cluster synthesis have been discussed in this section, but it is important to note that there are several reports on this topic alone.

3.2. Evolution of the Electronic Structure

The distinct electronic structures of atomically precise clusters merge into the continuous bands of metallic particles. Absorption spectra resembling molecules have been seen in various well-defined clusters.[265] In order to observe such features, isolation studies of clusters have been performed from the very early period of cluster science. An expanding array of materials has confirmed the convergence of molecular bands to plasmonic features in a size dependent fashion, the threshold of which varies with the metal. While the changes have largely been seen in optical absorption, very few studies have observed a similar trend in photoluminescence. In many such studies, optical peak shifts tending to the NIR are seen, yet the disappearance of emission and shift into infrared are not observed.

3.2.1. Optical Spectroscopy. A usual characteristic of monolayer protected ultrasmall metal clusters (with diameter <2.2 nm) is an exhibition of prominent quantum confinement.[223,227,242,243,266,267] Therefore, optical spectroscopy is the best tool to identify nanoclusters. The appearance of step-like features (there may not be distinct steps all the time; rather they may look like peaks) with spectral broadening in their absorption profiles due to a molecule-like HOMO−LUMO transition and absence of the plasmon resonance confirms the formation of such species. Conversion of the electronic band structure to distinct energy levels leads to well-defined optical bands,[242,243,268] which can be seen in the optical spectra shown in Figure 5a of the PAGE separated bands shown in Figure 4b. Clear absorption onsets appear in the 400−1000 nm range for these nine clusters, which are marked by downward arrows in Figure 5a. The onsets are followed by humps (upward arrows in Figure 5a) that show a gradual blue shift with a decrease in size. A series of peaks with composition corresponding to $[Au_n(SG)_m{-}xH]^{x-}$ were observed in negative ion ESI MS.[229] The optical spectrum of $Au_{25}(SG)_{18}$ cluster (number 6 in Figure 5a) shows multiple features. The Aikens group has explained the origin of the optical spectrum through time-dependent density functional theory (TDDFT) calculations considering $Au_{25}(SH)_{18}^{-}$ as a model system.[41] The corresponding Kohn−Sham molecular orbitals (MO) and atomic orbital (AO) contributions are presented in Figure 5b. All the characteristic transitions are marked.

The calculated optical spectrum (Figure 5c) matches with the corresponding experimental one (inset of Figure 5c), especially in the spectral shape. The first excited state at 1.52 eV (peak 1) corresponds to a HOMO to LUMO transition (Figure 5b) which is essentially an intraband (sp to sp) transition. The nature of the electronic energy levels is understood from the calculations. The peak at 2.63 eV (marked as “2” in Figure 5c) arises from mixed intraband (sp to sp) and interband (d to sp) transitions (Figure 5b). The peak at 2.91 eV (marked as “3” in Figure 5c) arises principally from an interband transition (d to sp). Several other techniques also help in understanding the optical confinement of nanoclusters. The existence of gold-core and semi-ring gold state (see below) has been demonstrated through ultrafast optical measurements.[269−273] Miles et al.[274] have reported temperature dependent electrochemical properties of quantum-sized clusters, from which they claim that the HOMO−LUMO energy gap increases with decrease in temperature. Shibu et al.[275] have shown the temperature dependency of photoluminescence of $Au_{25}(SR)_{18}$ cluster (discussed in detail in section 3.2.2). Although many research groups have tried to investigate the origin of the optical properties of metal nanoclusters, some questions regarding the electron−phonon interactions, coupling of gold core states with the semi-ring states, nature of excitation states, etc., still remain unanswered. Devadas et al.[276] have tried to answer these questions from temperature dependent optical measurements of $Au_{25}(SR)_{18}$ and $Au_{38}(SR)_{24}$ clusters. For most of the nanocluster report, wavelength is converted to energy while plotting. These nanoclusters show bands over a broad spectral window which appear like a hump. Thus, it is difficult to distinguish between two humps or peaks, which makes the above transformation useful. It simply uses[277]

$$E = hc/\lambda \tag{5}$$

However, it is not enough to make a proper plot in energy units. It must be noted that the signal values recorded by a spectrometer are really values per unit wavelength or per unit energy. As wavelength and energy are inversely related, the intervals in terms of wavelength are not evenly sized across the energy spectrum. If the recorded signal is represented as a function $f(\lambda)$, then the energy conversion yields

$$f(\mathrm{E})\,\mathrm{d}E = f(\lambda)\,\mathrm{d}\lambda \tag{6}$$

Combining eqs 5 and 6, we get

$$\begin{aligned} f(E) &= f(\lambda)(\mathrm{d}\lambda/\mathrm{d}E) = f(\lambda)(\mathrm{d}/\mathrm{d}E)(hc/E) \\ &= -f(\lambda)(hc/E^2) \end{aligned} \tag{7}$$

The factor (hc/E^2), known as the Jacobian factor, is used to scale the signal values along with wavelength conversion [wavelength (in nm) = 1239.8/(energy (eV)]. Normally, it is plotted by multiplying the absorbance value with the factor $1/W^2$, where W is the value in electronvolts corresponding to the wavelength in nanometers.

DOI: 10.1021/acs.chemrev.6b00769
Chem. Rev. 2017, 117, 8208−8271

Coming back to the absorption spectrum of the $Au_{25}(SR)_{18}$ cluster,[276] the peak maximum at 1.81 eV is shifted to 1.90 eV as temperature decreases from 323 to 78 K. A new vibronic feature is also noticeable: the single peak at 1.81 eV (at 323 K), which corresponds to the HOMO−LUMO transition for the $Au_{25}(SR)_{18}$ cluster, resolves into two peaks with peak maxima at ∼1.67 and ∼1.90 eV at lower temperatures. Three main points could be confirmed from this study: (i) the absorption maxima shifted to higher energies, (ii) the absorption feature became sharper and new peaks emerged, and (iii) the oscillator strength increased significantly with a decrease in temperature. Experimental results fitted with models suggested that the nanocluster had significantly larger phonon energy due to the semi-ring gold, one of the structural units of the cluster (more details about the semi-ring have been explained in section 3.2.2).

An important difference among the three classes of noble metal nanoparticles is their difference in optical absorption spectra. In fact, this is an immediate aspect of comparison, as the spectra are easily measurable in any laboratory. This is illustrated with Figure 6, where the optical absorption spectra of three different particles are compared. The first one is the standard citrate protected gold nanoparticles in water. The other is MPC of 3 nm diameter, protected with DDT. The last is $Au_{25}(PET)_{18}$. While the first one has a sharp absorption attributed to plasmon resonance, the second one shows the same with significant broadening. The last one shows optical absorption features just like a dye molecule, but completely different from a nanoparticle. This difference holds good for a majority of gold clusters, while for silver, some clusters also show one prominent feature, slightly distorted with shoulders, but quite different from the plasmon excitation.

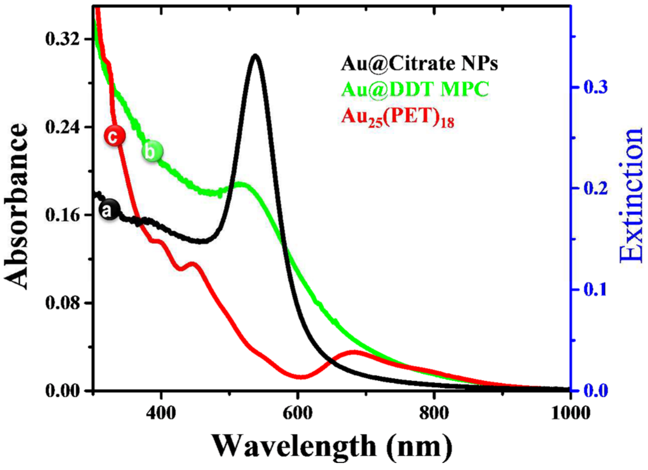

Figure 6. UV/vis spectra of three different kinds of particles: (a) 25 nm Au@citrate particles, (b) 3 nm Au@DDT MPC, and (c) $Au_{25}(PET)_{18}$ clusters, respectively. Several differences are seen between clusters and nanoparticles (and MPCs). Extinction (label on the right) is applicable for (a) and (b).

3.2.2. Photoluminescence. Photoluminescence, another distinct property of nanoclusters,[278,279] arises because of the transition between the HOMO and LUMO of the clusters.[249,280] The luminescence from the bulk metals or metallic particles is very inefficient because of the fast nonradiative relaxation due to their continuous band structure. However, it is possible to increase the quantum yield by decreasing the particle size, as the density of states decreases with the number of atoms in the cluster and this results in a larger gap between the adjacent energy levels for electrons and holes. Photoluminescence of nanoclusters also depends on local environments such as the protecting ligands and solvents.

Even though some of the gold clusters do not show visible luminescence under UV light exposure, they can show emission in the NIR region. Bigioni et al.[253] in 2000 have shown the emission of $Au_{25}(SR)_{18}$ clusters whose quantum yield (QY= $(4.4 \pm 1.5) \times 10^{-5}$) was found to be 5 orders of magnitude more than that of bulk gold. This exceptionally large QY was attributed to intraband (sp to sp) transitions. Different possible excitations and emissions for $Au_{25}(SR)_{18}$ are depicted in Figure 7a.[273] The cluster shows two distinct features (see Figure 7b): a strong emission (QY = $\sim 1 \times 10^{-3}$) in the NIR region and a weaker emission (QY = $\sim 10^{-6}$–10^{-7}) in the visible region which was further supported by steady state luminescence experiments.[249] The origin of fluorescence of $Au_{25}(SR)_{18}$ cluster can be explained from its structure. The $Au_{25}(SR)_{18}$ cluster can be viewed as a core−shell structure where the core consists of 13 gold atoms (Figure 7a) and the shell is the semi-ring made of $Au_2(SR)_3$ staples (detailed structure will be explained under section 3.3). This semi-ring is responsible for the fluorescence properties of $Au_{25}(SR)_{18}$ clusters. Wu and Jin have shown the effect of different ligands on the fluorescence properties of $Au_{25}(SR)_{18}$ clusters.[281] According to their report, the surface ligands can influence the fluorescence of clusters, in two different ways: (i) ligands to the metal cluster core charge transfer (i.e., LMCCCT) through the Au−S bonds, and (ii) direct donation of delocalized electrons of electron-rich atoms or groups of the ligands to the metal core. The high QY of glutathione protected cluster compared to organic thiol protected cluster is attributed to the presence of more electron-rich atoms (O, N, etc.) or groups (−COOH, $-NH_2$) which facilitate the LMCCCT. A report of Wang et al. also supports the role of ligands in the origin of fluorescence of $Au_{25}(SR)_{18}$ clusters.[282] Along with a solution phase study, Shibu et al.[275,283] have examined the solid state emission of the $Au_{25}(SG)_{18}$ cluster in a range of temperatures of 80−300 K (Figure 7c). The emission (a broad peak around 670 nm) intensity gradually increases with increase in temperature, and a strong enhancement occurs after 160 K. No change in the peak position confirms that the structure of $Au_{25}(SG)_{18}$ cluster is intact. In contrast to the $Au_{25}(SR)_{18}$ cluster, $Au_{38}(SR)_{24}$ exhibits a different behavior at very low temperatures. van Wijngaarden et al. have performed a solution phase temperature dependent study of $Au_{38}(SR)_{24}$ clusters.[284] At 4 K, multiple bands exist as fine structures, which overlap at higher temperatures and form a broad peak. At higher temperature, the energy difference between the emission bands is decreasing which increases the overlapping possibility to form a broad peak. Such broad emission features are normally seen for metal quantum clusters.[31,150,187,285−302]

3.3. Understanding the Composition, Structure, and Properties

A molecular system is understood entirely using several complementary tools. Mass spectrometry is one of the ways of understanding such a system, although this has been the single most important technique in this category of materials. The ligand shell required molecular techniques to characterize the functional groups, intercluster interactions, solvation shells, and changes in the media. These studies have revealed a wealth of information.

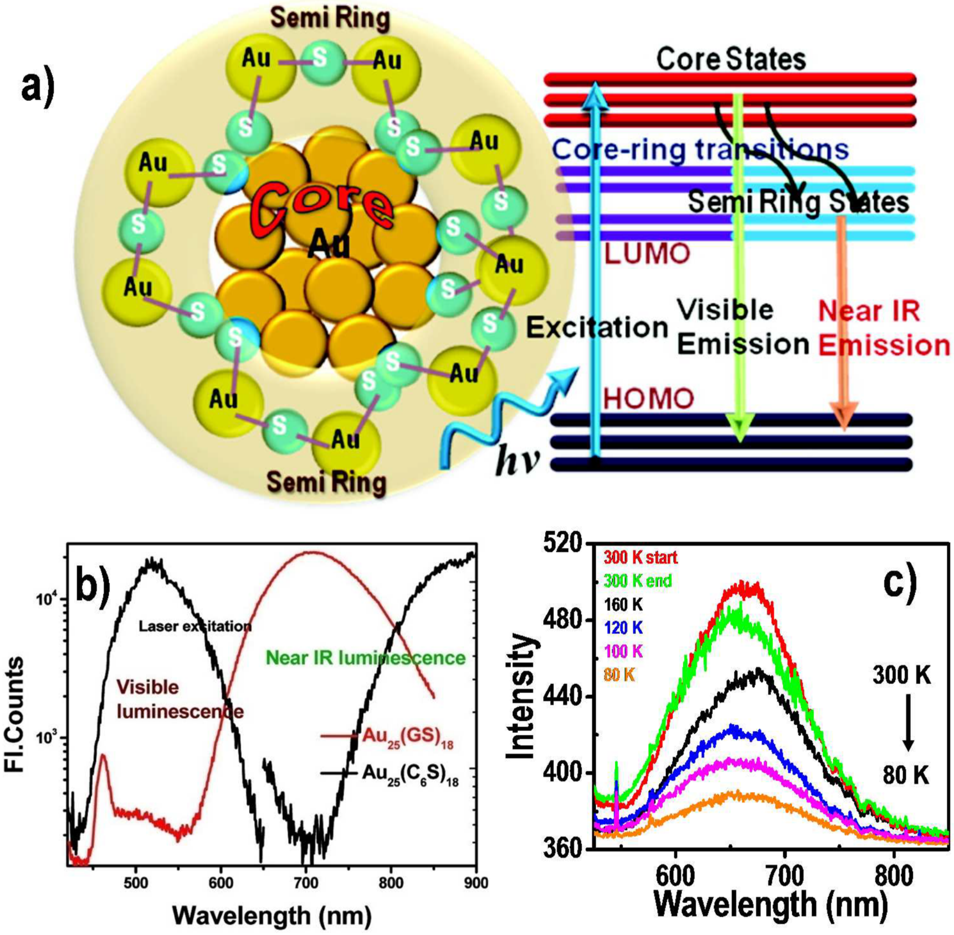

Figure 7. (a) Schematic of the Au_{25} cluster and the energy diagrams which show the corresponding excitations and emissions. Reprinted from ref 273. Copyright 2010 American Chemical Society. (b) Excitation and emission spectra of $Au_{25}(SR)_{18}$ cluster protected with glutathione (red trace) and hexanethiol (black trace), respectively. Reprinted from ref 249. Copyright 2002 American Chemical Society. (c) Temperature-dependent solid-state emission of $Au_{25}(SG)_{18}$. Reprinted with permission from ref 275. Copyright 2009 World Scientific Publishing.

3.3.1. Advanced Mass Spectrometry. Researchers have shown the effectiveness of mass spectrometry to characterize clusters.[29] It can give information about the core size as well as the ligand composition. Various advanced mass spectrometric techniques (e.g., MALDI TOF MS and HRESI MS) have been used to understand the molecular formulas of purified clusters. The earliest example of MALDI MS analysis of $Au_{25}(SR)_{18}$ cluster was by Schaaff et al.[227] A molecular peak around 10.4 kDa was assigned to an isolated glutathione protected gold cluster, though an accurate composition was not established. The exact composition was later found by Negishi et al.[229] via ESI MS measurements. They identified all nine isolated clusters based on their peak positions (Figure 8a) and isotopic distributions (Figure 8a, right panel). The clusters (1−9) were assigned as $Au_{10}(SG)_{10}$, $Au_{15}(SG)_{13}$, $Au_{18}(SG)_{14}$, $Au_{22}(SG)_{16}$, $Au_{22}(SG)_{17}$, $Au_{25}(SG)_{18}$, $Au_{29}(SG)_{20}$, $Au_{33}(SG)_{22}$, and $Au_{39}(SG)_{24}$, respectively. The calculated spectrum of $Au_{28}(SG)_{16}$ has also been plotted for band 6 in Figure 8a to illustrate that the assignment done by Schaaff et al.[227] was incorrect. This work by Negishi et al.[229] was the first report of a complete ESI MS assignment of a series of glutathione protected clusters. As depicted in Figure 8a, the negative-ion ESI mass spectra of 1−9 have a series of peaks corresponding to the formula, $[Au_n(SG)_m{-}xH]^{x-}$, where n, m, and x represent the numbers of gold atoms, GS ligands, and dissociated protons, respectively. The right panel of Figure 8a shows the deconvoluted mass spectra of $Au_n(SG)_m$ derived from a series of multiply charged peaks. Among 1−9, fractions 2−7 are single clusters with precise size as can be seen from the mass spectral data. Compound 6 with corresponding mass of 10 437 Da has been assigned as $Au_{25}(SG)_{18}$, which was previously assigned as $Au_{28}(SG)_{16}$ (10 415 Da).

In general, ESI MS works well with aqueous soluble gold clusters as they are easily ionizable, but for organic soluble clusters, this technique is not well-suited. In the recent past, several new methodologies have been implemented to overcome these problems. Researchers have shown that ionization efficiency can be improved by adding external ionizing agents such as cesium acetate (CsOAc).[33] Ligand exchange with an ionizable ligand is another way to obtain good mass spectral features.[303,304] Negishi et al.[305] introduced an oxidation (by $Ce(SO_4)_2$) or a reduction (by $NaBH_4$) process to improve the ionizing capacity by enhancing the charge state of the $Au_{25}(SR)_{18}$ cluster (see Figure 8b). The origin of magic stability of $Au_{25}(SR)_{18}$ cluster came out of the mass spectral study. The spectra were measured for monopositive and mononegative ions generated from neutral $Au_{25}(SR)_{18}$ cluster (Figure 8c). It can be noticed that ESI MS in the negative mode shows a single peak corresponding to $[Au_{25}(SC_6H_{13})_{18}]^-$ and, interestingly, the positive mode also shows the

DOI: 10.1021/acs.chemrev.6b00769
Chem. Rev. 2017, 117, 8208−8271

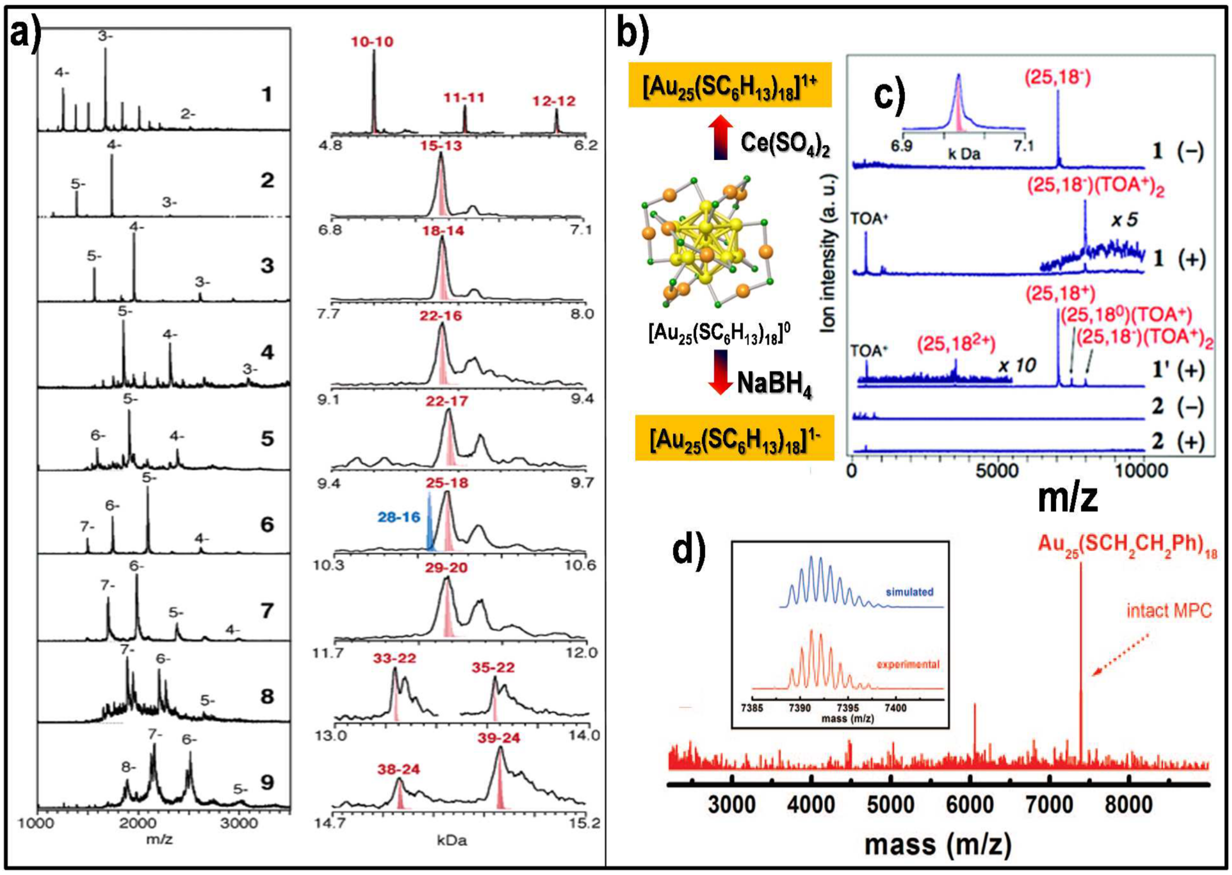

Figure 8. (a) ESI mass spectra of isolated clusters, 1−9, prepared in a synthesis. Left and right panels are the parent and deconvoluted spectra of the same, respectively. Red trace shows the corresponding calculated spectra for $Au_n(SG)_m$ clusters with the corresponding $n-m$ values. Reprinted from ref 229. Copyright 2005 American Chemical Society. (b) Scheme of positively and negatively charged $Au_{25}(SR)_{18}$ cluster synthesis from neutral $Au_{25}(SR)_{18}$ cluster. (c) Positive and negative mode ESI mass spectra of $[Au_{25}(SC_6H_{13})_{18}]^-$, $[Au_{25}(SC_6H_{13})_{18}]^+$, and $[Au_{25}(SC_6H_{13})_{18}]$ (1, 1′, and 2, respectively). The notation (n, m−/+) represents $[Au_n(SC_6H_{13})_m]^{-/+}$. Reprinted from ref 305. Copyright 2007 American Chemical Society. (d) Positive mode MALDI MS data of $Au_{25}(PET)_{18}$ cluster. Inset shows the expanded spectrum plotted with the calculated one (blue trace). Reprinted from ref 306. Copyright 2008 American Chemical Society.

$[Au_{25}(SC_6H_{13})_{18}]^-$ peak (marked by "+" sign to refer to the positive mode) with the counterion, TOA$^+$. The positive mode mass spectrum of the $[Au_{25}(SC_6H_{13})_{18}]^-$ cluster shows the corresponding composition along with a possible dication, while the neutral species does not show any prominent feature in either of the two modes as expected from its charged state. Even after implementation of all the methodologies to improve the ionizing efficiency, all clusters do not ionize by electrospray. For such cases, MALDI MS is a good option but it requires a suitable matrix to get mass spectra at good resolution. Weak organic acids such as sinapinic acid, cinnamic acid, etc., were usually used as matrixes, but they were unable to prevent fragmentation of clusters.

In 2008, Dass et al.[306] illustrated the suitability of *trans*-2-[3-(4-*tert*-butylphenyl)-2-methyl-2-propenylidene] malononitrile (DCTB) as a matrix, particularly for $Au_{25}(PET)_{18}$ clusters (Figure 8d). A comparison of the mass spectral quality of $Au_{25}(PET)_{18}$ clusters using a range of matrixes showed that a much better resolution was achieved with this DCTB matrix. DCTB ionizes the molecule by electron transfer, whereas other organic acids do the same with proton transfer, which is the main reason for its high effectiveness for Au clusters. Following these reports, several groups have shown the extreme capability of MALDI MS using DCTB as the matrix.[27,303,306−309]

Mass spectrometry of clusters has advanced tremendously in the recent past. Precise mass assignment is possible for almost any cluster system now. Excellent ways of ionization without fragmentation, enhanced resolution at high masses, extremely high transmission, and high sensitivity have all contributed to the advancements. Coupled with ion mobility analysis and MS/MS, new properties of these clusters are being discovered today. To appreciate the power of new mass spectrometry, we are presenting the ESI MS of $Au_{25}(PET)_{18}$ (a) and $Ag_{25}(DMBT)_{18}$ (b) in Figure 9. The spectra are remarkably clean with no additional peaks except that of the molecular ions. The molecular ions show well-defined isotopically resolved peaks, fully in agreement with the theoretical spectrum. The isotope structures are due to C, S, and H in the case of $Au_{25}(PET)_{18}$, while for $Ag_{25}(DMBT)_{18}$, all the elements contribute to the structure. Luo et al. were able to trace all the stable intermediate species from reduction of Au(I)thiolate to evolution of $Au_{25}(SR)_{18}$ clusters by high resolution electrospray ionization mass spectrometry.[311]

3.3.2. MS/MS and Related Studies.

Tandem mass spectrometry or MS/MS is the best analytical technique for understanding the fragmentation pattern of ions. Even though this technique has been used for a variety of biological samples, e.g. proteins of similar masses, it has not been explored much in the context of atomically precise clusters. Fields-Zinna et al.[312]

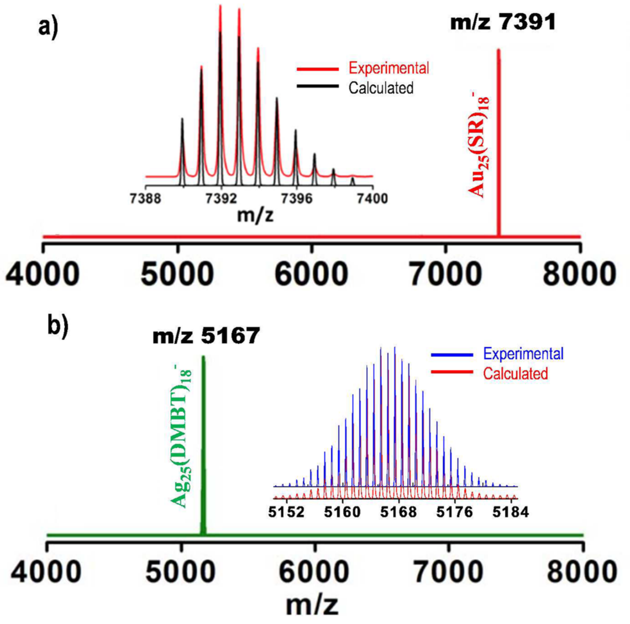

Figure 9. HR ESI mass spectra of $Au_{25}(PET)_{18}^{-}$ (a) and $Ag_{25}(DMBT)_{18}^{-}$ (b) clusters. Insets show the expanded views of the molecular peaks plotted with the corresponding calculated patterns. It may be noted from inset of (b) that intensity oscillations are reproduced exactly as predicted. Reprinted with permission from ref 310. Copyright 2016 Nature Publishing Group.

performed the very first tandem mass spectrometric analysis of $Au_{25}(SR)_{18}$ cluster. They conducted the low energy collision-induced dissociation tandem mass spectrometry (CID MS/MS) study of mixed ligand (phenylethanethiolate (−PET) and methoxy penta(ethylene glycol) thiolate (−SPEG)) protected Au_{25} clusters. The spectrum showed the generation of lower m/z fragment ions (Figure 10a) derived from $[Na_4Au_{25}(PET)_8(SPEG)_{10}]^{3+}$ (m/z 2929). Several fragments of the type AuL_2, Au_2L_3, etc., were observed along with the Au_4L_4 fragment, which confirmed the occurrence of the semi-ring rearrangements on the surface of the cluster. Analogous fragments have also been observed for bigger clusters such as $Au_{38}(SR)_{24}$, $Au_{144}(SR)_{60}$, etc., indicative of a similar surface structure in these systems.[313] Ghosh et al.[219] have shown a detailed fragmentation pattern of Au_{18} clusters protected with glutathione. $Au_{18}(SG)_{14}^{4-}$ was seen in the ESI MS as a main peak, which was selected for the MS/MS study (Figure 10b) for further fragmentation. Two types of losses were seen, mainly corresponding to m/z 32.5 and 4.5 (actually 32.5 × 4 = 130 and 4.5 × 4 = 18, respectively). The m/z 130 losses were due to fragmentation from the peptide ligand. Cleavage of the $C_{\text{glutamic acid}}{-}N_{\text{cysteine}}$ bond generated two subsequent fragments of masses m/z 130 ($C_5H_8O_3N$) and m/z 176 ($C_5H_8O_3N_2S$). The thiol containing fragment remained attached to the cluster core, and the other fragment left was assigned as SG_F.

Increase in collision energy leads to systematic fragmentation. Another type of loss corresponding to m/z 4.5 was due to water (with 4^{-} charge), which suggested the existence of glutathione as an anhydride on the cluster surface. Water loss was seen only after the initial fragmentation from $Au_{18}(SG)_{14}^{4-}$. Thereafter, with increase in collision energy, water loss occurred from a series of fragments. Interestingly, all the major ions formed in the gas phase contained eight electrons (including the ligand and the metal core) which are needed for a closed shell configuration. This report points to a high stability of these ions in the gas phase.

Ion mobility mass spectrometry (IMS) is an advanced technique for understanding the structural details. In general, IMS separates ions based on their size, and more accurately based on the collision cross section. Similar to liquid chromatography, here, too, smaller ions that undergo more collisions elute faster than larger ions. For nanosystems, it has been used mainly to understand several aspects of their fragmentation pattern and size distribution of gold nanoparticles. IMS also helps in understanding the fragments generated from them such as $Au_4(SR)_4$ which are often seen in the mass spectrum of $Au_{25}(SR)_{18}$. The same has also been found in the cases of $Au_{38}(PET)_{24}$ and $Au_{68}(PET)_{34}$ clusters. But, no such species has been found as a staple from the crystal structure, which suggests that this fragment is generated under the mass spectral conditions. Fields-Zinna et al. have shown the formation of such a tetrameric ion in tandem mass spectrometric conditions from $Au_{25}(SR)_{18}$ clusters.[312] Through this technique, it is possible to reduce such fragmentation

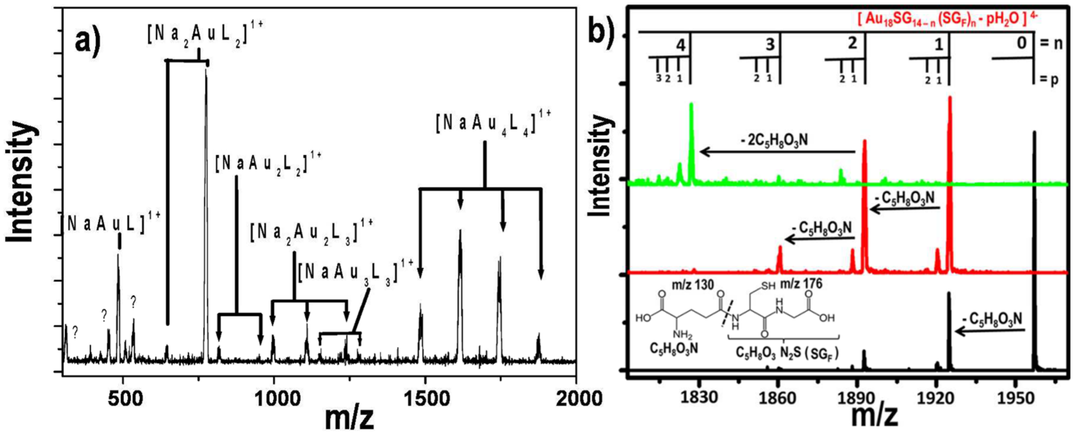

Figure 10. (a)ESI-QQQ-MS/MS spectrum of PEGylated Au_{25} sample (in methanol with excess NaOAc) after fragmentation under CID conditions. Brackets and arrows indicate Au_NL_M species, where L is the distribution of ligands (SC_2Ph and SPEG) in which SPEG is more prominent. Reprinted from ref 312. Copyright 2009 American Chemical Society. (b) MS/MS spectra of $[Au_{18}SG_{14}]^{4-}$ cluster with increasing collision energy (from bottom to up). The label n represents the number of glutathione ligands fragmented, and p represents the number of water losses. Inset at the bottom shows the characteristic cleavage of a bond in glutathione. Reprinted from ref 219. Copyright 2012 American Chemical Society.

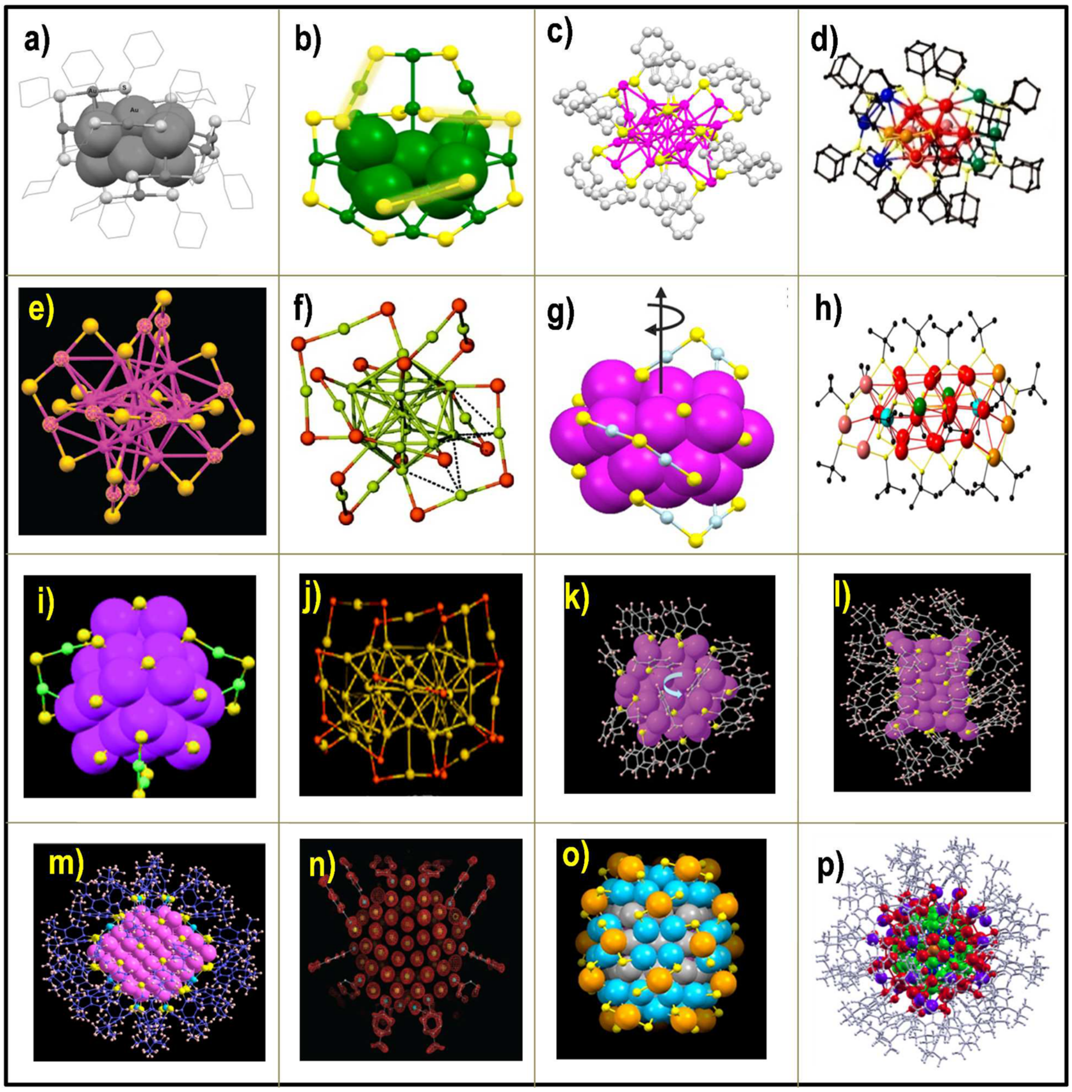

Figure 11. Crystal structures of $Au_{18}(SC_6H_{11})_{14}$ (a), $Au_{20}(TBBT)_{16}$ (b), $[Au_{23}(SC_6H_{11})_{16}]^-$ (c), $Au_{24}(SAdm)_{16}$ (d), $Au_{25}(PET)_{18}$ (e), $[N(C_8H_{17})_4][Au_{25}(PET)_{18}]$ (f), $Au_{28}(TBBT)_{20}$ (g), $Au_{30}S(S\text{-}t\text{-}Bu)_{18}$ (h), $Au_{36}(SPh\text{-}tBu)_{24}$ (i), $Au_{38}(PET)_{24}$ (j), $Au_{40}(o\text{-}MBT)_{24}$ (k), $Au_{52}(TBBT)_{32}$ (l), $Au_{92}(TBBT)_{44}$ (m), $Au_{102}(p\text{-}MBA)_{44}$ (n), $Au_{130}(p\text{-}MBT)_{50}$ (o), and $Au_{133}(SPh\text{-}tBu)_{52}$ (p) clusters, respectively. In some cases, the complete ligand structure is not shown. In such cases (b, e, f, g, i, j, n, o), only Au and S atoms are shown. Reprinted from refs 15, 41, 204, 317, 318, 320, 321, and 323−325. Copyright 2008, 2010, 2013, 2014, 2015, and 2016 American Chemical Society. Reprinted with permission from refs 43 and 316. Copyright 2012 and 2015 John Wiley & Sons. Reprinted with permission from refs 45 and 322. Copyright 2007 and 2015 American Association for the Advancement of Science.

which results in increase in intensity of the low intensity peak. Angel et al.[314] have shown ion mobility MS/MS studies of $Au_{25}(PET)_{18}$ cluster. From this IM-MS/MS study, it is possible to distinguish between the fragments of the outer protecting layer, made from six [−SR−Au−SR−Au−SR−] "staples", and the Au_{13} core. Several fragmentation patterns with predominant loss of $Au_4(SR)_4$ species were seen along with the other smaller fragments such as $Au(SR)_2^-$, $Au_2(SR)_3^-$, $Au_3(SR)_4^-$, and $Au_4(SR)_5^-$.

3.3.3. Single Crystal Studies. Even though there are a number of reports of atomically precise gold clusters based on mass spectrometry and other characterization techniques, only some are available with single crystal structure. Crystal structures of only 15 clusters, namely $Au_{18}(SR)_{14}$,[315,316] $Au_{20}(SR)_{16}$,[317] $Au_{23}(SR)_{16}$,[318] $Au_{24}(SR)_{16}$,[319] $Au_{25}(SR)_{18}$,[15,41] $Au_{28}(SR)_{20}$,[320] $Au_{30}S(SR)_{18}$,[321] $Au_{36}(SR)_{24}$,[43] $Au_{38}(SR)_{24}$,[204] $Au_{40}(SR)_{24}$,[322] $Au_{52}(SR)_{32}$,[322] $Au_{92}(SR)_{44}$,[323] $Au_{102}(SR)_{44}$,[45] $Au_{130}(SR)_{50}$,[324] and $Au_{133}(SR)_{52}$[325] with complete thiol protection (Figure 11) have been identified up to the end of October 2016. There are a few other reports of gold clusters with phosphine[326−328] or mixed ligands[42,47] (phosphine and thiols) protection, but in this section we will only discuss the complete thiol protected gold clusters. Unlike inorganic clusters,[329] obtaining a single crystal structure of protected noble metal clusters is very difficult primarily because of stability and sensitivity issues. The crystallization methodology and solvents also play important roles in forming diffractable crystals. For most cases, the vapor diffusion method works well, but concentrated cluster solutions are required for this case and the clusters must be highly pure.

The earliest report of a single crystal structure of a thiolate protected cluster is of $Au_{102}(p\text{-}MBA)_{44}$ made by Jadzinsky et al.[45] in 2007. The chiral nature of the cluster was also revealed by the crystal structure. In 2008, the Murray[15] and Jin[41] groups reported the crystal structure of $Au_{25}(PET)_{18}$ clusters which consisted of an icosahedral core, encapsulated with six

Table 2. Crystal Structures of Thiolated Gold Clusters[a]

	core		shell				M−M bond characteristics				
				characteristics							
cluster composition	composition	geometry	composition	no. $Au(SR)_2$ motifs	no. $Au_2(SR)_3$ motifs	others	bond type	bond dist (Å)	average bond dist (Å)	unit cell geometry	ref
$Au_{18}(SC_6H_{11})_{14}$	Au_9	bioctahedral	$Au_9(SC_6H_{11})_{14}$	3	1	four $Au_4(SR)_5$			3.09 ± 0.23	triclinic	315, 316
$Au_{20}(TBBT)_{16}$	Au_7	bitetrahedral	$Au_{13}(SR)_{16}$	2		$Au_8(SR)_8$ ring and $Au_3(SR)_4$ trimeric staple	5	2.88, 2.982, 2.72, 2.74, 3.03	–	orthorhombic	317
$[Au_{23}(SC_6H_{11})_{16}]TOA$	Au_{15}	cuboctahedron-based bipyramidal	$Au_8(SR)_{16}$	2	–	two $Au_3(SR)_4$ and four −SR	3	2.96 ± 0.28, ∼2.93, ∼2.7	2.96	orthorhombic	318
$Au_{24}(SAdm)_{16}$	Au_{15}	distorted cubocatahedral core	$Au_9(SR)_{16}$	1	1	$Au_3(SR)_4$	3	2.704−3.490, 2.92 ± 0.19, 3.03 ± 0.22	–	triclinic	319
$Au_{25}(PET)_{18}N(C_8H_{17})_4$	Au_{13}	icosahedral	$Au_{12}(SR)_{18}$	0	6	–	3	3.02−3.12, 3.14−3.27, 2.80−2.81	2.95	triclinic	41
$[N(C_8H_{17})_4][Au_{25}(PET)_{18}]$	Au_{13}	icosahedral	$Au_{12}(SR)_{18}$	0	6	–	3	2.79 ± 0.01, 2.93 ± 0.06	2.96	triclinic	15
$Au_{28}(TBBT)_{20}$	Au_{20}	rod-like kernel consisting of two interpenetrating cuboctahedral	$Au_8(SR)_{20}$	0	4	eight −SR	3	2.92, 2.87, 3.40	2.98	triclinic	320
$Au_{30}S(S\text{-}t\text{-}Bu)_{18}$	Au_{20}	bicuboctahedral	$Au_{10}S(SR)_{18}$	4		$Au_3(SR)_4$, SR, and μ_3 S	–	–	–	triclinic	321
$Au_{36}(SPh\text{-}tBu)_{24}$	$Au_4@Au_{24}(SR)_{12}$	face centered cubic	$Au_8(SR)_{12}$	0	4	–	2	2.81, 2.85	2.91	base-centered monoclinic	43
$Au_{38}(PET)_{24}$	Au_{23}	face fused bicosahedral	$Au_{15}(SR)_{12}$	3	6	–	–	–	3.0	triclinic	204
$Au_{40}(o\text{-}MBT)_{24}$	Au_{25}	snowflake-like Au_{25} kernel with tetrahedral units coiled up into a Kekulé-like superstructure	$Au_{15}(SR)_{24}$	6		three $Au_3(SR)_4$	5	2.78, 2.76, 2.90, 3.01, 3.16	–	triclinic	322
$Au_{52}(TBBT)_{32}$	Au_{32}	segregated into 10 tetrahedral units	$Au_{20}(SR)_{32}$	4	8		4	2.79 2.99 3.10, 3.62	–	triclinic	322
$Au_{102}(p\text{-}MBA)_{44}$	Au_{79}	icosahedral	$Au_{23}(SR)_{44}$	19	2	–	–	2.80−3.10	2.90	–	45
$Au_{130}(p\text{-}MBT)_{50}$	$Au_{13}@Au_{42}@Au_{50}$	ino-decahedral, ino-decahedral, pentagonal barrel	$Au_{25}(SR)_{50}$	25	0	–	–	–	–	monoclinic	324
$Au_{133}(SPh\text{-}tBu)_{52}$	$Au_{13}@Au_{42}@Au_{52}$	icosahedral, icosahedral, vacant rhombiicosidodecahedral	$Au_{26}(SR)_{26}$	26	0	–	–	–	–	monoclinic	325

[a] $Au_{92}(SR)_{44}$ has not been presented here as it has a self-assembled monolayer structure[323] which cannot be presented in this format.

$Au_2(SR)_3$ staples. Later in 2010, the total structure of $Au_{38}(PET)_{24}$ was solved by Qian et al.[204] It is composed of a bi-icosahedral core with three $Au(SR)_2$ staples and six $Au_2(SR)_3$ staples. The same structure had been predicted earlier in 2008 by Pei et al.[330] through DFT calculations using the "divide and protect" concept.[231] To construct the structure, the thiolate protected nanoclusters were divided in groups of $[Au]_{a+a'}[Au(SR)_2]_b[Au_2(SR)_3]_c$, where a, a', b, and c are integers. In this formulation, $[Au]_{a+a'}$ represents the gold core which satisfies the condition that the number of core "surface" Au atoms (a') equals the sum of end points of the staple motifs ($2b + 2c$); b and c are numbers of different types of staple motifs. That is, each of the core surface Au atoms is protected by one end point of the staple motif. This strategy was implemented based on the reported crystal structures of $[Au_{25}(SR)_{18}]^-$ and $Au_{102}(SR)_{44}$, which can be represented as $[Au]_{1+12}[Au_2(SR)_3]_6$ and $[Au]_{39+40}[Au(SR)_2]_{19}[Au_2(SR)_3]_2$, respectively. Therefore, for $Au_{38}(SR)_{24}$, the parameters a, a', b, and c must satisfy the following conditions: $(a + a' + b + 2c) = 38$, $(2b + 3c) = 24$, and $a' = (2b + 2c)$. Based on these, the possible combinations are (i) $[Au]_{2+24}[Au(SR)_2]_{12}$, (ii) $[Au]_{3+22}[Au(SR)_2]_9[Au_2(SR)_3]_2$, (iii) $[Au]_{4+20}[Au(SR)_2]_6[Au_2(SR)_3]_4$, (iv) $[Au]_{5+18}[Au(SR)_2]_3[Au_2(SR)_3]_6$, and (v) $[Au]_{6+16}[Au_2(SR)_3]_8$. Band gap analysis and a comparison of the calculated UV/vis spectra with experimental data predicted combination iv as the preferred structure for $Au_{38}(SR)_{24}$. The $Au_{38}(SR)_{24}$ cluster is also chiral because of the specific arrangement of the staples, which will be discussed later in greater detail.

In general, the single crystal data suggests that most of the nanoclusters have a core−shell structure (Figure 11). The core is composed of 15, 13, 20, 28, 23, and 79 atoms for Au_{23}, Au_{25}, Au_{28}, Au_{36}, Au_{38}, and Au_{102}, respectively (the structural information about the new clusters such as Au_{18}, Au_{20}, Au_{24}, Au_{30}, Au_{40}, Au_{52}, Au_{130}, and Au_{133} are described in Table 2). In each case, the core is surrounded by a shell, which is composed of two types of staple motifs: $Au(SR)_2$ and $Au_2(SR)_3$. In smaller clusters such as $Au_{25}(SR)_{18}$, the latter one is predominant, but in larger clusters, e.g. $Au_{102}(SR)_{44}$, the $Au(SR)_2$ motif dominates. In a few cases (e.g., Au_{23} and Au_{28} clusters) bridging −SR motifs are also present in their structure. Typically, the Au−Au bond distance average varies between 2.95 and 3.0 Å in these clusters. These structural illustrations help us understand atomically precise gold clusters in a much deeper way. More details are provided in Table 2. Recently, Azubel et al.[331] have determined the structure of Au_{68}NP at atomic resolution by a new approach employing aberration-corrected transmission electron microscopy with minimal electron dose and with electron density mapping. Li et al. have shown such a possibility for Au_{25} and Au_{39} clusters to understand their size and shape.[332] The structure obtained for the 68 atom cluster was correlated with DFT calculations. The 68 gold atoms are described as a 13-atom cuboctahedron (with an atom in the center) surrounded by 24 atoms extending the fcc-like framework and by an additional 31 atoms deviating from fcc packing. Unlike the case of Au_{102}, this cluster was found to be less symmetric. This technique opens up another way to look at the structures of clusters as structure determination through SXRD has not been an easy task so far. More detail structural analysis of various gold clusters can be found in the recent review article by Jin et al.[6]

3.3.4. NMR Spectroscopy. NMR spectroscopy has been used to investigate the structural stability of monolayer protected gold clusters. Parker et al.[333] have shown electron self-exchange dynamics of nanoparticle-coupled $[Au_{25}(PET)_{18}]^{0/1-}$ by NMR line broadening. From the crystal structure analysis, it has been observed that $Au_{25}(SR)_{18}$ cluster has $Au@Au_{12}@Au_{12}$ type structure,[41] where the first shell (shell 1) surrounds the central Au atom to form an Au_{13} kernel that is further encapsulated by another shell (shell 2) of Au_{12} atoms. In this cluster, two types of thiolate binding modes were identified: (I) 12-SR ligands which join the Au shells 1 and 2; (II) 6-SR ligands located on the Au_{12} shell 2. To determine which of these thiolate binding modes is more stable, Jin's group[334] performed an NMR study focusing on the oxidation resistance and thermal stability of the Au−S bond. In this experiment, $Au_{25}(SG)_{18}$ was systematically oxidized using $Ce(SO_4)_2$ and a time dependent NMR was measured. Assignments of all the peaks have been mentioned in another report.[335] Protons attached with C7 atom of the ligand split into two parts (because of chirality[335]) to form a doublet at 3.6 and 3.8 ppm corresponding to α-H of thiolate binding mode I and another doublet at 3.3 and 3.4 ppm corresponding to α-H of thiolate binding mode II. The ratio of mode I to mode II is 2:1. Upon addition of $Ce(SO_4)_2$, the doublet at 3.3/3.4 ppm was broadened and was almost lost after 6 h, which suggests that binding mode II is comparatively weak and is attacked first by the oxidant. In contrast, the doublet at 3.6/3.8 ppm remained unaffected even after 5 days, from which it can be concluded that binding mode I is much stronger than binding mode II. Thus, with an NMR study, one can correlate the structural stability in terms of Au−S bond strength under an oxidative atmosphere. The effect of charge state on NMR of $Au_{25}(SR)_{18}$ cluster has been demonstrated by Venzo et al.[182]

Although this review is focused on thiolated clusters, it is important to mention that ^{31}P NMR is also very useful in structural analysis of phosphinated gold clusters.[336,337] Clayden et al.[338] have shown the importance of high resolution solid and solution state ^{31}P NMR to understand the dynamics of phosphinated gold clusters. There are several such reports where ^{31}P NMR and ^{1}H NMR have been used as characterization tools, and many of them are tabulated in Table S1.

3.3.5. Other Spectroscopies. Among other spectroscopic techniques, infrared spectroscopy has mostly been used to understand the binding mode of the thiol group in metal nanoclusters and nanoparticles. The most common feature is the disappearance of S−H vibrational band to confirm that the binding of ligand occurs through the sulfur atom. In general, other features of IR spectra of the clusters tend to be identical with those of the corresponding free ligands. Farrag et al.[339] demonstrated that $Au_{25}(PET)_{18}$ showed a distinct shift of the aromatic C−H stretching band (appearing at 3000−3100 cm^{-1}) compared to the free PET ligand. This unusual shift of the C−H stretching band from 3030 to 3100 cm^{-1} to below 3000 cm^{-1} was attributed to an electronic interaction of the aromatic rings of the ligands with each other or with the gold core. But other PET protected Au_{38} and Au_{144} clusters showed the same features as seen for the PET ligand (except the S−H band). This was possibly due to an increase in the cluster size, which prohibited the close proximity of the ligands.

Dolamic et al.[340] carried out far-infrared spectroscopic studies of a few well-defined thiolate (2-phenylethanethiolate) protected gold clusters, such as Au_{25}, Au_{38}, Au_{40}, and Au_{144}. The spectra showed characteristic features for every individual cluster, but the differences were very small. Quantification of monomeric and dimeric staple units was not possible as there was no systematic variation, but the conformation of phenylethanthiolate could be predicted. The band at 490 cm^{-1} is associated with an out-of-plane vibrational mode of the phenyl moiety coupled to a C−C−S bending mode, which is an indication of the anti conformation of phenylethanethiolate. Crystal structures of $Au_{25}(PET)_{18}$ and $Au_{38}(PET)_{24}$ show the presence of 14:4 and 14:10 anti:gauche conformations, respectively. Mostly, anti conformation of the S−C−C phenyl unit has been observed for all the cases. Few units with gauche conformation were also noticed which lead to a shift of this band toward lower wavenumbers. Bands at 210−280 cm^{-1} region have been assigned to Au−S vibrations. Parker et al.[333] have found the Au−S vibrational band near 290 cm^{-1} for the $Au_{25}(PET)_{18}^{-}$ cluster from Raman spectroscopy. The band shows a lower energy shift by 24 cm^{-1} for the neutral Au_{25} cluster. Varnholt et al.[341] have investigated the influence of thiolate ligands on the Au−S vibrations and the effect of cluster size for a series of clusters such as $[Au_{25}(PET)_{18}]^{0/-}$, $Au_{25}(CamS)_{18}$ (CamS = 1*R*,4*S*-camphorthiol), $Au_{38}(PET)_{24}$, $Au_{40}(PET)_{24}$, and $Au_{144}(PET)_{60}$.

Considering the molecule-like nature of these atomically precise gold clusters, their electrochemical properties are interesting topics to explore, and voltammetry is a powerful technique to investigate the HOMO−LUMO gap or electron transfer in such systems.[1,342,343] The difference between the first oxidation and reduction potentials of a cluster is considered as the HOMO−LUMO gap.[1] Band gaps of several gold clusters such as $Au_{25}(SR)_{18}$ (∼1.65 V), $Au_{38}(SR)_{24}$ (1.2 V), and $Au_{75}(SR)_{40}$ (0.74 V) have been measured electrochemically.[250,252,344,345] The Murray group has studied these extensively starting from 2004.[1,250,252,344] From the square wave voltammetry analysis (SWV) of $Au_{25}(SR)_{18}$, four peaks at −2.09 V (R1), − 0.44 V (O1), − 0.08 V (O2), and 0.66 V (O3) [vs Ag/Ag^{+}] have been found which are due to $Au_{25}(SR)_{18}^{-/2-}$, $Au_{25}(SR)_{18}^{0/-}$, $Au_{25}(SR)_{18}^{+/0}$, and $Au_{25}(SR)_{18}^{2+/+}$ couples, respectively. R1, O1, O2, and O3 correspond to reversible reduction peak 1 and reversible oxidation peaks 1, 2, and 3, respectively. The Lee group has shown the electrochemical properties of Au_{25} clusters in which the water-soluble 3-mercaptopropylsulfonate protected Au_{25} clusters were phase transferred to different organic media and the solvent dependency was studied electrochemically.[346] Depending on solvent polarity, the HOMO−LUMO energy gap varies from 1.39 to 1.66 V. In another report, they made different mixed ligand protected (phosphine and thiols) bicosahedral Au_{25} clusters and found that the electrochemical and optical properties are drastically different from the complete thiol protected Au_{25} clusters.[347] Utilizing these electrochemical properties, this cluster has been made in ionic liquid form which shows effectiveness in glucose sensing.[348]

Several other spectroscopic techniques such as magnetic circular dichroism (MCD),[349−351] electron paramagnetic resonance (EPR),[352−354] extended X-ray absorption fine structure (EXAFS),[355−363] Mössbauer,[364−366] X-ray diffraction (XRD),[367] magnetophotoluminescence spectroscopy,[368] etc., have also been used for detailed understanding of the structure of atomically precise gold clusters, and a comprehensive list can be found in Table S1. A recent example of the power of EXAFS was shown by Yamazoe et al.,[369] where hierarchy in the bond stiffness in clusters such as $Au_{25}(PET)_{18}$, $Au_{38}(PET)_{24}$, and $Au_{144}(PET)_{60}$ has been measured successfully. They found that the Au−Au bonds have different stiffnesses depending on their lengths.

3.4. Other Gold Clusters

There are several reports of other gold clusters besides the well-defined clusters mentioned above, and in most of the cases, the composition was identified using mass spectrometry. It is important to mention here that as $Au_{25}(SR)_{18}$ cluster has been explored in much greater detail than any other one, it has been considered here as a representative of atomically precise clusters. Several clusters have been tabulated in Table S1 with a brief description. Along with thiol protection, protein protected nanoclusters[52,55,370−400] such as Au@BSA,[213] Au@lysozyme,[401] etc., are also known and most of them are highly luminescent in nature. For these systems, the number of metal atoms has been found from MALDI MS data after subtracting the protein mass (more details about protein protected cluster can found in section 7). There are a few clusters which do not have well-defined mass spectra, but they have step-like optical features.[402−405] Selenolate,[406−408] tellurolate,[409] DMF,[410] phosphine,[157,160,161,163,164,176,411−413] polymer,[414−417] alkyne,[418−421] mixed-ligand,[42,47] etc., protected clusters have also been reported by various research groups.

4. ATOMICALLY PRECISE SILVER CLUSTERS

Even though gold and silver belong to the same group of the periodic table, they show distinctly different properties in many cases. Compared to gold, silver in zerovalent state is much more reactive and easily oxidizable, making it difficult to explore its clusters in greater detail.[48] The Dickson group has studied extensively fluorescent silver clusters made under dendritic and DNA templates.[422−447] The Pradeep group has tried to examine the chemistry of silver clusters using mass spectrometry and other characterization tools.[11,14,16,37] Other groups such as those of Bigioni, Kitaev, Bakr, etc., are also working on silver clusters.[13,28,30,448,449] Crystal structures of a few mixed ligand protected silver clusters have been solved,[39,40] but well-defined mass spectra were missing for a few years. Crystal structures of the highly stable $Ag_{44}(SR)_{30}$ cluster (initially known as intensely and that of broadly absorbing nanoparticles (IBAN))[450] with diverse ligands and $Ag_{25}(SR)_{18}$[46] cluster have been determined, which has enhanced our understanding of Ag cluster systems.[44] It is to be noted that $Ag_{44}(SR)_{30}$ was initially synthesized by Bakr et al.[450] and $Ag_{25}(SR)_{18}$ was reported earlier by Cathcart et al.[451] and Chakraborty et al.[216]

4.1. Early Synthesis of Silver Clusters

Even though there were several attempts to make atomically precise silver clusters with the protection of different ligands,[179,450−454] in those early days none of them had detailed mass spectral data. Mrudula et al. measured the molecular mass of a 7 kDa cluster using MALDI MS, but it was not enough to identify the system precisely.[191] Wu et al.[455] have shown the very first ESI MS analysis of a monolayer protected silver cluster, whose precise composition was determined to be $Ag_7(DMSA)_4$. It was synthesized using $AgNO_3$ in a suitable solvent where ligand with an effective ratio (normally 1:*N* with respect to silver, where *N* = 2, 3, 4, 5, ..., 10) was added and the mixture was cooled in an ice bath (Figure 12). Then the required amount of $NaBH_4$ in an ice-cold solvent was added to reduce the metal, and the solution was stirred continuously for a few hours. Cluster formation was observed clearly by a color change, monitored with UV/vis

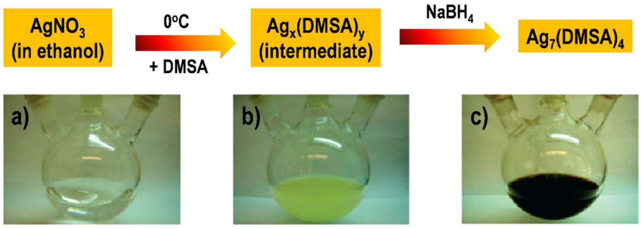

Figure 12. Photographs of $Ag_7(DMSA)_4$ cluster synthesis. From left to right: (a) ethanol solution of $AgNO_3$, (b) 4 h after the addition of DMSA, and (c) 12 h after addition of $NaBH_4$. Reprinted from ref 455. Copyright 2009 American Chemical Society.

spectroscopy. The cluster was purified by precipitation, and the precipitate was further extracted by a suitable solvent to get the purified cluster. Following this report several new methodologies have been developed to synthesize atomically precise silver clusters. Some of them will be discussed in section 4.2.

4.2. New Routes for Silver Clusters

Similar to gold clusters, various synthetic methodologies have been implemented for the synthesis of monolayer protected silver clusters and most of them have been discussed in the perspective article.[48] Recently, the Pradeep group developed two new routes for synthesizing atomically precise clusters. The first one is a solid state route,[37] where a solid silver precursor was taken in an agate mortar and ground well, then the corresponding thiol was added, and the mixture was ground for a few minutes (Figure 13). This results in a change in color that confirms the formation of thiolate. Then solid $NaBH_4$ was added and grinding was continued for a few minutes, which was followed by the addition of ethanol. Ethanol serves two important roles here: first, it helps to reduce the metal by providing a limited supply of water which controls the size of the cluster and, second, it washes out the excess ligands, as normally clusters are insoluble in ethanol. The mixture was then centrifuged well for a few minutes and the precipitate containing atomically precise clusters was extracted in appropriate solvents. Several clusters such as Ag_9,[37] Ag_{32},[35] Ag_{44},[36] and Ag_{152}[16] have been synthesized using this procedure.

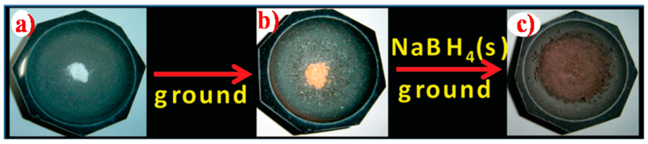

Figure 13. Photographs representing the changes during cluster synthesis (a−c) through a solid state route. (a) Silver nitrate taken in a mortar; (b) solid thiol was added and ground well followed by the addition of solid $NaBH_4$; (c) The mixture was stirred well and extracted in ethanol. Reprinted from ref 37. Copyright 2010 American Chemical Society.

The second synthetic procedure follows a high temperature route.[11] The corresponding silver precursor and ligand mixture were stirred for a few minutes at 70 °C, and then the required amount of formic acid was added. Here, formic acid was used instead of the traditional reducing agent, $NaBH_4$. The temperature was kept constant throughout the reaction. The color changes from light yellow to reddish brown in 3 h, which confirms the formation of the cluster. The slow reducing capacity of formic acid and high temperature control the cluster size. Similarly, Zheng et al. synthesized luminescent silver clusters under boiling water condition.[456] Chakraborty et al. have reported the synthesis of silver clusters using sunlight in a gel cavity.[21] Here, the gel cavity controls the size of the cluster formed by sunlight mediated reduction. Bakr et al.[450] synthesized intensely and broadly absorbing nanoparticles (IBANs), mentioned previously, which showed molecule-like optical absorption features. The cluster was formed using a solution phase route, in which a silver salt solution was reduced in the presence of the capping ligand, 4-fluorothiophenol (4FTP). Briefly, 4FTP was stirred with a silver precursor (4FTP:Ag = 2:1) in *N*,*N*-dimethylformamide (DMF) for 15 min. Then a solution of $NaBH_4$ in DMF ($NaBH_4$/Ag = 4:1) was added to the reaction mixture. The color of the solution changed to brown and darkened further with time. Initially, plasmonic nanoparticles were formed which showed an absorption band at 450 nm. Stirring was continued for 4 h, then a small volume of water was added, and the reaction mixture was left in the freezer (−4 °C) for several days. Under these conditions, the plasmonic feature changed to a new molecular peak with five intense and four broad bands. $Ag_{29}(BDT)_{12}$[457] and the “golden silver” nanoparticle, $Ag_{25}(DMBT)_{18}$,[46] have been synthesized through a one-step solution phase route using methanol−DCM solvent mixture. Several other methodologies are now available for synthesizing atomically precise silver clusters, and a brief description of each one is given in Table 1.

Box 3. Synthesis of $Ag_{44}(FTP)_{30}$ Cluster through the “Solid State” Route

About 20 mg of $AgNO_3$ and 12 mg of PPh_4Br were ground thoroughly in an agate mortar and pestle for 5 min. About 76 μL of 4-fluorothiophenol was added to it in one shot, and the mixture was ground for about 3 min more. Dry $NaBH_4$ (45 mg) was added and the mixture was ground until the pasty mass became brown in color. This was extracted with 7 mL of dichloromethane and kept undisturbed at room temperature until UV/vis spectra showed all the characteristic features of $Ag_{44}(SR)_{30}$ cluster. Then it was purified by repeated precipitation using methanol. Finally, the cluster was extracted in DCM. Using this technique, 4-FTP, 3-FTP, and 2-FTP protected clusters can be synthesized.

Purification is the key step for synthesizing atomically precise silver clusters. A convenient way to purify the material is to precipitate them using methanol (in aqueous or organic media). Similar is the case for the solid state route where washing with solvents such as ethanol/methanol serves the purpose of cleaning.[37] Kumar et al.[13] have shown the separation of glutathione protected silver clusters using PAGE, and 16 discrete bands were isolated with distinct UV/vis features. In a recent report on $Ag_{44}(MBA)_{30}$ cluster synthesis, protonation is identified to be important for purification, as MBA in thiolate form is not soluble in DMF.[44] Therefore, in order to extract the cluster in DMF in pure form, protonation is necessary. In another report on the Ag_{44}(4-FTP)$_{30}$ cluster, a two-phase (methanol−DCM) method has been used first to synthesize the cluster and, after the synthesis, the cluster then goes into the organic (DCM) layer.[222] Careful removal of the aqueous layer and subsequent washing generated the purified cluster.

4.3. Well-Defined Mass Spectral Characterization

As discussed in section 3.3, mass spectrometry is an ideal tool to identify the precise composition of quantum clusters. As

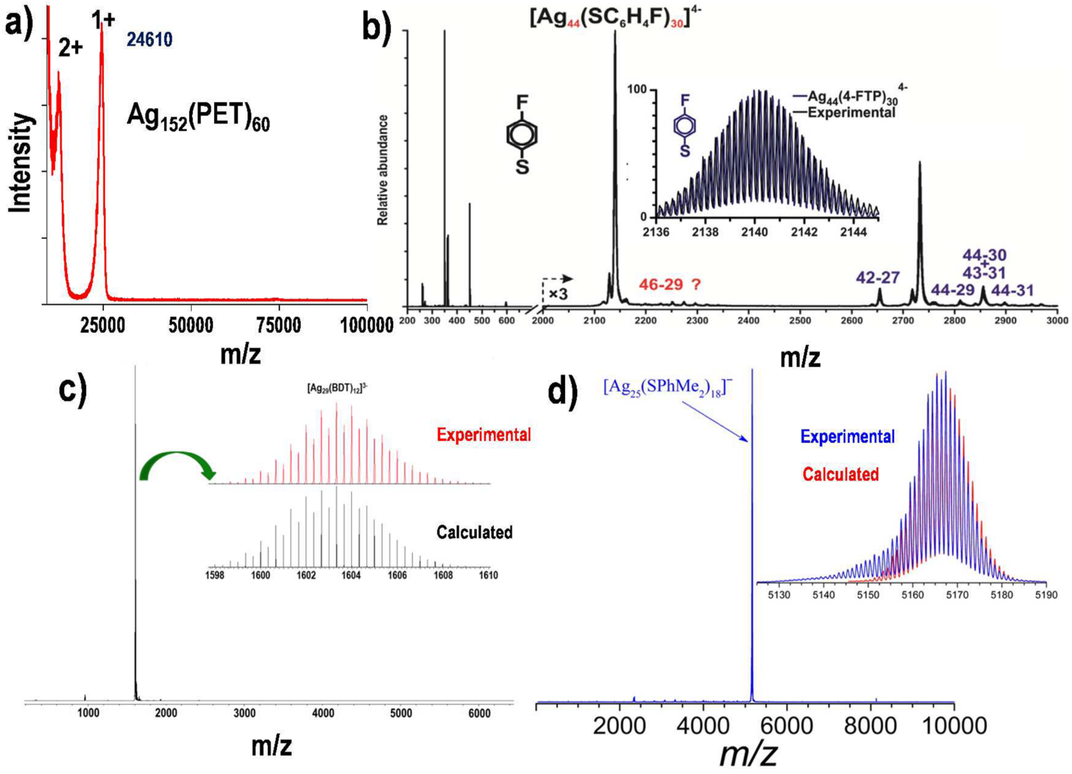

Figure 14. (a) MALDI MS spectra of $Ag_{152}(PET)_{60}$ cluster taken at threshold laser power. DCTB was used as the matrix. Reprinted from ref 16. Copyright 2012 American Chemical Society. (b) The HRESI MS of $Ag_{44}(SR)_{30}$ cluster (black trace) protected with *p*-fluorothiophenol. Blue trace is the calculated spectrum of the corresponding cluster. Reprinted with permission from ref 30. Copyright 2012 Royal Society of Chemistry. (c) and (d) represent the ESI mass spectral data of $Ag_{29}(BDT)_{12}$ and $Ag_{25}(DMBT)_{18}$ clusters. Insets in both show the expanded views of the molecular peaks along with the calculated patterns. Reprinted from refs 457 and ref 46. Copyright 2015 American Chemical Society.

silver has two isotopes, namely, 107 and 109 in a 50:50 ratio, we expect the MS peaks of silver clusters to be more complex and broader than the corresponding gold clusters (having one isotope ^{197}Au). Ag nanoclusters are highly fragile under the mass spectral conditions, so getting well-resolved mass spectra is a challenging task and most of the time only fragments are observed. As mentioned earlier, $Ag_7(DMSA)_4$ cluster is the earliest example of a Ag nanocluster whose composition was determined precisely via MS.[455] Several silver clusters have been identified by the Pradeep group using mass spectrometry.[11,14,16,37] MALDI MS can also be a good tool when used with a suitable matrix to identify the molecular peak, but the peak for Ag nanoclusters appears much broader than that for the corresponding gold clusters. As a result, it is difficult to predict the precise composition using MALDI MS. For this reason, the silver clusters reported by Mrudula et al.[191] showed a broad peak centered at *m/z* 7 kDa, but could not be assigned to a specific composition. The $Ag_{152}(SR)_{60}$ cluster[16] was found to have a sharp molecular peak at *m/z* 24 610 (Figure 14a) and a full width at half-maximum (fwhm) of 1.3 kDa in its MALDI MS spectrum. A dication at *m/z* 12 300 was also seen which further supported the composition. Varying the laser intensity led to systematic fragmentation of the cluster. Enhanced stability of the system can be attributed to the presence of the magic number of electrons (152 − 60 = 92) that results in a closed shell electronic structure. Rao et al.[37] reported the mass spectral identification of $Ag_9(H_2MSA)_7$ cluster synthesized through a solid state route. Guo et al.[28] have shown a series of multiply charged peaks for the $[Ag_{32}(SG)_{19}]^{q-}$ cluster with a well-defined isotopic distribution. The compositions of IBANs[450] were identified by Harkness et al.[30] in 2012. Based on isotopic distribution, the cluster was assigned as $Ag_{44}(4\text{-FTP})_{30}{}^{4-}$. The experimental MS spectrum (Figure 14b) matched exactly with that obtained from calculations, and its peak resolution was ∼0.25 mass unit. The extreme stability of this cluster is due to its closed shell configuration ((44 − 30) + 4 = 18 electrons). The corresponding selenolate analogue of Ag_{44} cluster also showed clear isotope distribution in its ESI mass spectrum, for the 2−, 3−, and 4− ions.[36] Recently discovered $Ag_{29}(BDT)_{12}$ and $Ag_{25}(DMBT)_{18}$ clusters show clean and high resolution mass spectra as presented in Figure 14, parts c and d, respectively.

Along with ESI MS, Wu et al.[455] performed MS/MS analysis of $Ag_7(DMSA)_4$, wherein they selected the dianion, $[Ag_7L_4 - 3H + 2Na]^{2-}$ (*m/z* 759.57) as the parent ion whose fragmentation was analyzed with increase in collision energy. At low voltage (10 V), the parent ion loses a neutral fragment through C−S bond cleavage. At high voltage (25−40 V), the rest of the ligands disintegrate, but one S atom from each ligand continues to be linked to the cluster core to form $Ag_7S_4^-$. At a still higher voltage, smaller fragments such as $Ag_6S_4^-$ and Ag_5S_4 were observed. The presence of four valence electrons was confirmed from this study, which explains the stability of such a cluster.

In order to fragment ions of such high masses and multiple chemical bonds, collision induced dissociation is inadequate. The energy imparted in collision with gas phase partners is not enough to cause fragmentation. In this context, surface induced dissociation has been found to be a useful method. Here, collision of the ions with a solid surface is used to impart the

DOI: 10.1021/acs.chemrev.6b00769
Chem. Rev. 2017, 117, 8208−8271

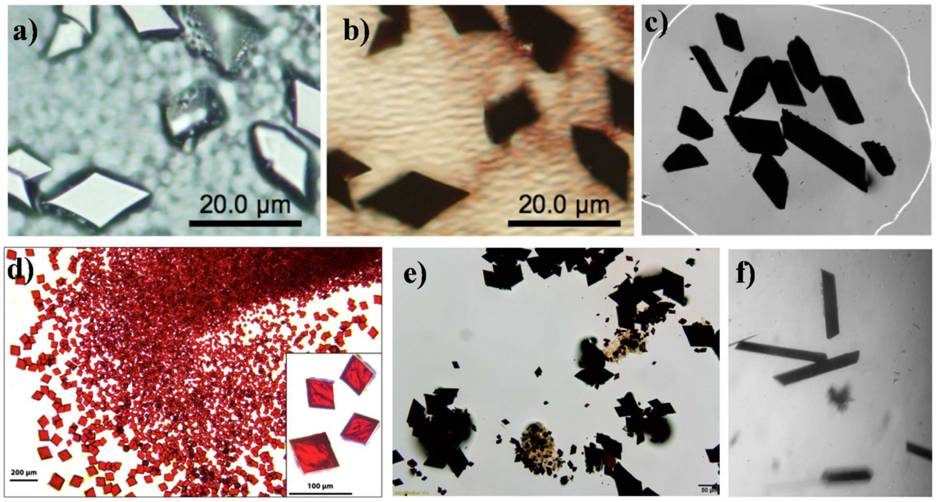

Figure 15. Optical micrographs of typical crystals of M_4Ag_{44}(p-MBA)$_{30}$ ((a) episcopic and (b) diascopic illumination), Ag_{44}(4-FTP)$_{30}$(PPh_4)$_4$ (c), Ag_{29}(BDT)$_{16}$TPP$_4$ (d), Ag_{25}(DMBT)$_{18}^-$(PPh_4)$^+$ (e) and [Ag_{67}($SPhMe_2$)$_{32}$(PPh_3)$_8$]$^{3+}$ (f) clusters, respectively. Reprinted with permission from refs 44 and 222. Copyright 2013 Nature Publishing Group (for (a), (b), and (c)). Reprinted from refs 457 and 46. Copyright 2015 American Chemical Society (for (c) and (d)). Reprinted from ref 459. Copyright 2016 American Chemical Society (for (f)).

required activation energy. An early example of this has been demonstrated recently for the $Ag_{11}(SG)_7Na_n^{3-}$ cluster.[458] Unprecedented charge stripping of the ion from −3 to −2 to even −1 was seen at 40 V laboratory collision energy. Several fragments due to AgSG, Ag, and SG losses were seen with increasing collision energy.

4.4. Single Crystal Studies

Because of the reduced stability, aerial oxidation, and less purity of silver clusters, formation of diffractable crystals is difficult for silver clusters. A few reports are known for mixed ligand (phosphine and thiol) and complete thiol protected silver clusters. Optical microscopic images of crystals of a few reported silver clusters are presented in Figure 15. More details about the unit cells and structural details are presented in Table 3. Yang et al.[39] reported the single crystal structure of a mixed ligand protected Ag_{14} cluster (Figure 16a) in 2012. In the subsequent year, the authors also resolved the structures of Ag_{16} and Ag_{32} clusters (Figures 16b,e) protected by mixed ligands.[40] As can be seen from Figure 16a, the $Ag_{14}(SC_6H_3F_2)_{12}(PPh_3)_8$ cluster contains an octahedral Ag_6^{4+} core which is encapsulated by eight cubically arranged $[Ag^+(SC_6H_3F_2^-)_2PPh_3]$ in a tetrahedral fashion that shares one corner (i.e., $SC_6H_3F_2^-$) between them. Another important characteristic of this cluster is that all the thiolate ligands bind to three Ag atoms and no staple motifs are found unlike in the case of gold clusters (i.e., $Au(SR)_2$ or $Au_2(SR)_3$). Crystal structures of Ag_{44} clusters protected with p-mercaptobenzoic acid and p-fluorothiophenol have also been solved (Figures 16f,g). Single crystal structures suggest the existence of a hollow cage core and completely different type of staples surrounding the core (different from other staples reported so far for both Au and Ag clusters).

Box 4. Crystallization of $Ag_{44}(MBA)_{30}$ Cluster

First, the cluster has to be purified by repeated protonation and precipitation steps using citric acid and toluene, respectively. Then the cluster is extracted in HPLC grade distilled DMF (without even traces of water). Note that the cluster concentration should be high (>50 mg/mL). This purified cluster is then kept under an argon atmosphere (should have an outlet) for solvent evaporation at low temperature (around 20 °C). After 2−3 days, crystals appear as dark brown diamond shaped objects, which can be seen by optical microscopy.

The hollow cage containing 12 silver atoms arranged in an icosahedral fashion is surrounded by 20 silver atoms to form a keplerate structure with a total of 32 silver atoms. The $Ag_{12}@Ag_{20}$ core is further encapsulated with six $Ag_2(SR)_5$ staples octahedrally. The average Ag−Ag bond distance in the core is much shorter than in the bulk, suggestive of strong Ag−Ag metal bonding in the cluster. The crystal structure of a dithiol protected silver cluster, $Ag_{29}(BDT)_{12}(TPP)_4$ [BDT, benzenedithiol; TPP, triphenylphosphine] has been solved (Figure 16d).[457] Interestingly, the cluster has an icosahedral core similar to $Au_{25}(SR)_{18}$, which is protected with a shell consisting of $Ag_{16}S_{24}P_4$. There are two types of silver atoms in the shell. Twelve silver atoms connected with the 12 surface silver atoms (as four Ag_3S_6 crowns) of the core giving rise to four tetrahedrally oriented trigonal prisms. The remaining four silver atoms face capped the core at four tetrahedral positions (as four $Ag_1S_3P_1$). The “golden silver” $Ag_{25}(DMBT)_{18}$ cluster has a structure similar to that of $Au_{25}(SR)_{18}$, i.e. an icosahedral core containing a central Ag which is then surrounded by six $Ag_2(SR)_3$ motifs (Figure 16c). Very recently, Alhilaly et al. have discovered an unusual box-shaped crystal structure of $[Ag_{67}(SPhMe_2)_{32}(PPh_3)_8]^{3+}$ cluster.[459] The nonspherical shape is because of its electronic instability as it is a 32 electron system which does not have a closed shell electronic structure. Yang et al. in their recent report solved crystal structures of plasmonic twinned silver nanoparticles with molecular formulas $[Ag_{136}(SR)_{64}Cl_3Ag_{0.45}]^-$ and $[Ag_{374}(SR)_{113}Br_2Cl_2]$, respectively.[460] These are the largest thiolated metal nanoparticles solved so far by single crystal studies.[460] Ag_{136} and Ag_{374} clusters can be described as 5-fold twinned cores enclosed within related structurally distinctive Ag−SR complex shells. The former one consists of a pentagonal bipyramidal core of 54 Ag atoms, whereas the latter one has an elongated pentagonal bipyramidal core (inodecahedron) with 207 Ag atoms.[460] Such 5-fold twinned metal cores have been seen for a few gold clusters such as Au_{102}[45] and

Table 3. Crystal Structures of Some Silver Clusters

			shell						
	core			characteristics		M−M bond characteristics			
cluster composition	composition	geometry	composition	no. $M(SR)_2$ and $M_2(SR)_3$ motifs	others	bond dist (Å)	average bond dist (Å)	unit cell geometry	ref
$Ag_{14}(SC_6H_3F_2)_{12}(PPh_3)_8$	Ag_6^{4+}	octahedral	$[Ag_8(SR)_{12}(PPh_3)_8]^{4-}$	–	$[Ag^+(SR)_2PPh_3]$	2.81–2.85	2.83	primitive	39
$Ag_{16}(DPPE)_4(SC_6H_3F_2)_{14}$	Ag_8^{6+}	nearly rhombus Ag_4 unit capped by two Ag_2 units above and below the rhombus	$[Ag_8(DPPE)_4(SC_6H_3F_2)_{14}]^{6-}$	–	$[Ag^+(SR)_2DPPE]$	2.694–3.040	2.845	–	40
$Ag_{25}(DMBT)_{18}PPH_4$	Ag_{13}	icosahedral	$Ag_{12}(DMBT)_{18}$	6 $Ag_2(DMBT)_3$	–	2.7486–2.7847, 2.8209–2.9975	–	triclinic	46
$Ag_{29}(BDT)_{12}(TPP)_4$	Ag_{13}	icosahedral	$Ag_{16}S_{24}P_4$	–	Ag_3S_6, $Ag_1S_3P_1$	2.77–2.92	2.77 and 2.92	cubic	457
$[Ag_{32}(DPPE)_5(SC_6H_3F_2)_{24}]^{2-}$	Ag_{22}^{12+}	pentagon face-sharing bi(pentagonal antiprism) Ag_{17} unit that is side-capped by one Ag atom and one near-square Ag_4 unit at the opposite direction	$[Ag_{10}(DPPE)_5(SC_6H_3F_2)_{24}]^{14-}$	–	$[Ag^+(SR)_2DPPE]$	2.657–3.089	2.917	–	40
$Ag_{44}(SR)_{30}^{4-}$	$Ag_{12}@Ag_{20}$	icosahedral, hollow cage	$Ag_{12}(SR)_{30}$	–	$Ag_2(SR)_5$	2.829, 2.846, 3.190	2.83	triclinic	44, 222
$[Ag_{67}(SPhMe_2)_{32}(PPh_3)_8]^{3+}$	Ag_{23}	Ag_{13} cuboctahedron sharing with Ag_8 crowns to form Ag_{21} metal core, which is again connected with two Ag atoms	$[Ag_{44}(SPhMe_2)_{32}(PPh_3)_8]$	4 $Ag(SR)_2$ connected to 2 Ag_{16} bowls	8 $Ag(SR)_3PPh_3$	2.846–3.048, 2.860, 2.806, 2.910	2.9195, 2.860	orthorhombic	459
$Ag_{136}(SR)_{64}Cl_3Ag_{0.45}^{-}$	Ag_{54}	pentagonal bipyramid of 54 Ag atoms	$Ag_{82}(SR)_{64}Ag_{0.45}$	–	–	–	2.870	triclinic	460
$Ag_{374}(SR)_{113}Br_2Cl_2$	Ag_{207}	elongated pentagonal bipyramid (ino- decahedron)	$Ag_{207}(SR)_{113}$	–	–	–	2.882	rhombohedral	460

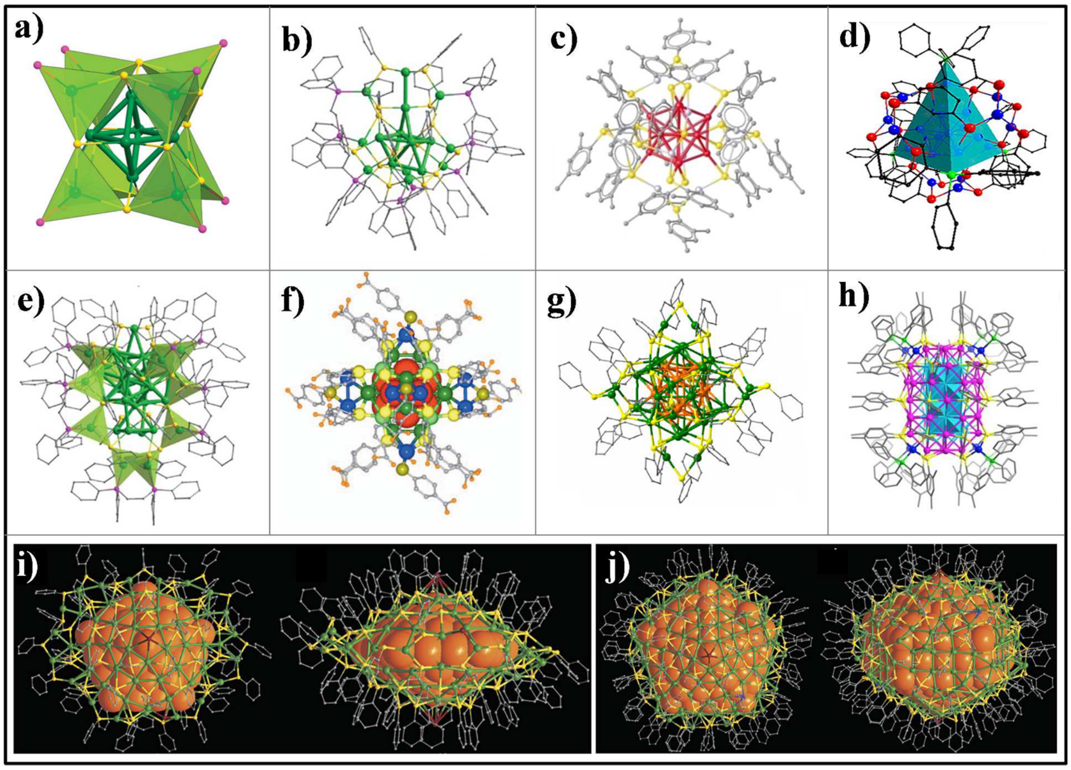

Figure 16. Crystal structures of $Ag_{14}(SC_6H_3F_2)_{12}(PPh_3)_8$ (a), $Ag_{16}(DPPE)_4(SC_6H_3F_2)_{14}$ (b), $Ag_{25}(DMBT)_{18}^-(PPh_4)^+$ (c), $[Ag_{29}(BDT)_{16}]TPP_4$ (d), $[Ag_{32}(DPPE)_5(SC_6H_3F_2)_{24}]^{2-}$ (e), $Na_4Ag_{44}(MBA)_{30}$ (f), $Ag_{44}(4\text{-}FTP)_{30}(PPh_4)_4$ (g), $[Ag_{67}(SPhMe_2)_{32}(PPh_3)_8]^{3+}$(h), $Ag_{136}(SR)_{64}Cl_3Ag_{0.45}^-$ (i), and $Ag_{374}(SR)_{113}Br_2Cl_2$ (j), respectively. In (a), only the Ag core and S atoms are shown. For (i) and (j), left and right sides represent the top and side views, respectively. Reprinted with permission from refs 39 and 40. Copyright 2012 and 2013 Royal Society of Chemistry (for (a), (b), and (e)). Reprinted with permission from refs 44 and 222. Copyright 2013 Nature Publishing Group (for (f) and (g)). Reprinted from refs 457 and 46. Copyright 2015 American Chemical Society (for (c) and (d)). Reprinted from ref 459. Copyright 2016 American Chemical Society (for (h)). Reprinted with permission from ref 460. Copyright 2016 Nature Publishing Group (for (f) and (g)).

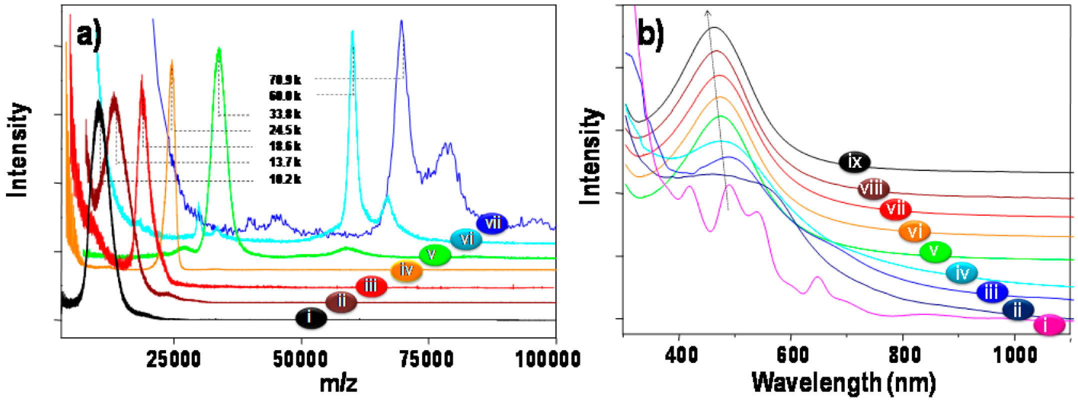

Figure 17. (a) MALDI MS spectra (collected in positive mode) of silver clusters prepared in solution. The spectra show a series of clusters with peak maxima ranging from 10.2k to 70.9k. Almost all of them (except [vi] and [vii], which have some other features with reduced intensity) show sharp single features which confirm the formation of one dominant cluster in each case. The fwhm varied from 1.5 to 5 kDa. The peaks (from bottom to top) were assigned as $Ag_{55}(PET)_{31}$ [i], $\sim Ag_{75}(PET)_{40}$ [ii], $\sim Ag_{114}(PET)_{46}$ [iii], $Ag_{152}(PET)_{60}$ [iv], $\sim Ag_{202}(BBS)_{70}$ [v], $\sim Ag_{423}(PET)_{105}$ [vi], and $\sim Ag_{530}(PET)_{100}$ [vii]. (b) UV/vis spectra of clusters with wavelength on the x-axis. From bottom to up: Ag_{44} [i], Ag_{55} [ii], $\sim Ag_{75}$ [iii], $\sim Ag_{114}$ [iv], Ag_{152} [v], $\sim Ag_{202}$ [vi], $\sim Ag_{423}$ [vii], $\sim Ag_{530}$ [viii], and AgNPs [ix]. The spectra show multiple features up to [iv] (namely, eight bands for Ag_{44}, two energy bands for Ag_{55} and $\sim Ag_{114}$, and three for $\sim Ag_{75}$). But from [v] to [ix], only a single plasmon-like feature was observed with a small blue shift (i.e., at higher energy). All the spectra have been shifted vertically for clarity. Reprinted with permission from ref 194. Copyright 2014 Royal Society of Chemistry.

Au_{130}.[324] More information about the crystal structures of silver clusters is presented in Table 3.

4.5. Thermal Stability of Silver Clusters

Thermal stability of monolayer protected clusters is an important property to explore. We have already discussed the temperature dependency of the $Au_{25}(SR)_{18}$ cluster in terms of its optical and photoluminescence properties. Thermal desorption of monolayer protected gold clusters results in the formation of alkyl disulfide in the gas phase and gold in the solid state.[461] The Au−S bond in several self-assembled

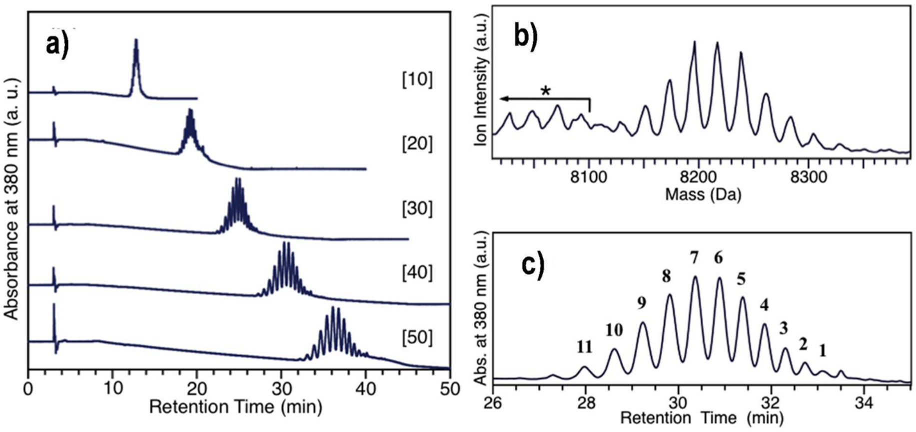

Figure 18. (a) Chromatograms of $PdAu_{24}(SC_{12}H_{25})_{18-n}(SBB)_n$ (n = 6−16) at different gradient programs. (b and c) Comparative MALDI mass spectra in negative mode (b) and chromatogram (c) of $PdAu_{24}(SC_{12}H_{25})_{18-n}(SBB)_n$ (n = 6−16) obtained using a gradient program [40], respectively. Reprinted from ref 12. Copyright 2013 American Chemical Society.

monolayers was seen to be stable even at temperatures in the range 100−150 °C.[462−465] This stability has also been observed for silver clusters.[466] Remya et al.[461] illustrated the thermal stability of atomically precise silver clusters protected with glutathione. With increase in temperature, the clusters underwent thiolate desorption as well as heterolytic bond cleavage, resulting in the formation of Ag_2S nanoparticles at 80 °C. The cluster initially dissociates into thiolates (AgSR) which can have the following two possible cleavage mechanisms.

$$2\mathrm{R{-}S{-}Ag} \rightarrow 2\mathrm{Ag} + \mathrm{R{-}S{-}S{-}R} \tag{8}$$

$$2\mathrm{R{-}S{-}Ag} \rightarrow 2\mathrm{Ag_2S} + \mathrm{R{-}S{-}R} \tag{9}$$

Out of these, reaction 9 was seen thermodynamically favorable as ΔH is more negative.[461] It is interesting to note that this is much lower than the temperature (~200 °C) needed for traditional Ag_2S nanoparticle synthesis. The mechanism of formation of Ag_2S nanoparticle by this route and its detailed characterization have been explored. The S−C bond cleavage, as revealed by mass spectrometry, in silver clusters is somewhat unusual because Ag−S cleavage is expected in view of its lower bond energy. In another study, Bakr et al.[450] have shown nonplasmonic to plasmonic transformation of monolayer protected silver clusters (IBANs) at ~90 °C. Several factors such as heat, light, etc., affect the stability of silver clusters, as silver is easily oxidized under these conditions. In view of this, thermal desorption of monolayers results in unprotected clusters, which have been used for catalysis. It is a standard practice to store such clusters in argon or nitrogen atmosphere in a refrigerator.

4.6. Emergence of Metallicity in Silver Clusters

The plasmon resonance which is defined as a strong collective oscillation of electrons[467] is responsible for the optical features and colors of noble metal nanoparticles. Several techniques such as photoelectron spectroscopy, conductivity, etc., are used to understand the emergence of metallicity in bare metal systems. Chakraborty et al. have demonstrated the emergence of metallicity in monolayer protected silver clusters through optical spectroscopy.[194] A systematic appearance of a plasmon-like optical absorption feature as a function of cluster size was observed in these systems. A wide range of clusters, namely $Ag_{44}(4\text{-FTP})_{30}$,[30] $Ag_{55}(PET)_{31}$, $\sim Ag_{75}(PET)_{40}$,[11] $\sim Ag_{114}(PET)_{46}$, $Ag_{152}(PET)_{60}$,[16] $\sim Ag_{202}(BBS)_{70}$, $\sim Ag_{423}(PET)_{105}$, and $\sim Ag_{530}(PET)_{100}$[468] were prepared and characterized using MALDI MS (Figure 17a).[194] Up to $\sim Ag_{114}$, multiple features were seen in the UV/vis spectra of the clusters. For Ag_{152} and clusters larger than that, the plasmonic feature corresponding to a single peak at ~460 nm evolved pointing to the emergence of metallicity in clusters composed of ~150 metal atoms (Figure 17b).[194] For silver clusters, metallicity has been seen at about 60 atoms (in unprotected clusters) in photoelectron spectroscopic studies, as mentioned by Taylor et al.[469] These photoelectron spectroscopic studies are generally discussed in the light of initial and final state effects.[469] Systematic shift of the 4f binding energy has been observed in supported gold clusters, but no such effect was observed in supported silver clusters.[469] The "spherical shell model"[104] suggests that the change in ionization energy as well as the increased width of the photoelectron spectra is proportional to $1/R$, where R is the radius of the cluster. However, naked clusters have been used in all of these photoelectron spectroscopic experiments, whereas this study has used monolayer protected clusters with distinct cores of smaller dimensions. Clusters with different ligands such as BBS also showed this, which implies that "the emergence of metallicity" is independent of the functionality of the thiol ligand.[194]

5. CHEMISTRY OF CLUSTERS

Additional functionalization of the shell (i.e., ligands) of the monolayer protected clusters can introduce new and diverse properties in such systems which may be important in different applications. Some of these aspects are described below.

5.1. Ligand Exchange

Ligand exchange is the most suitable and convenient way to incorporate desired properties such as FRET, chirality, etc., in a given monolayer protected noble metal cluster.[283,470−472] The sole idea of ligand exchange is to keep the cluster core intact while modifying the shell. This strategy was originally utilized by the Hutchison group[473,474] to replace the phosphine ligands of undecagold clusters by thiolate without changing the core size. The Pradeep group has also shown several exchange possibilities and incorporation of diverse properties in the Au_{25} cluster.[283,475,476] However, ligand exchange can result in an increase of the core size as was demonstrated by Shichibu et al.[477] for Au_{11} cluster; whose ligand exchange led to the

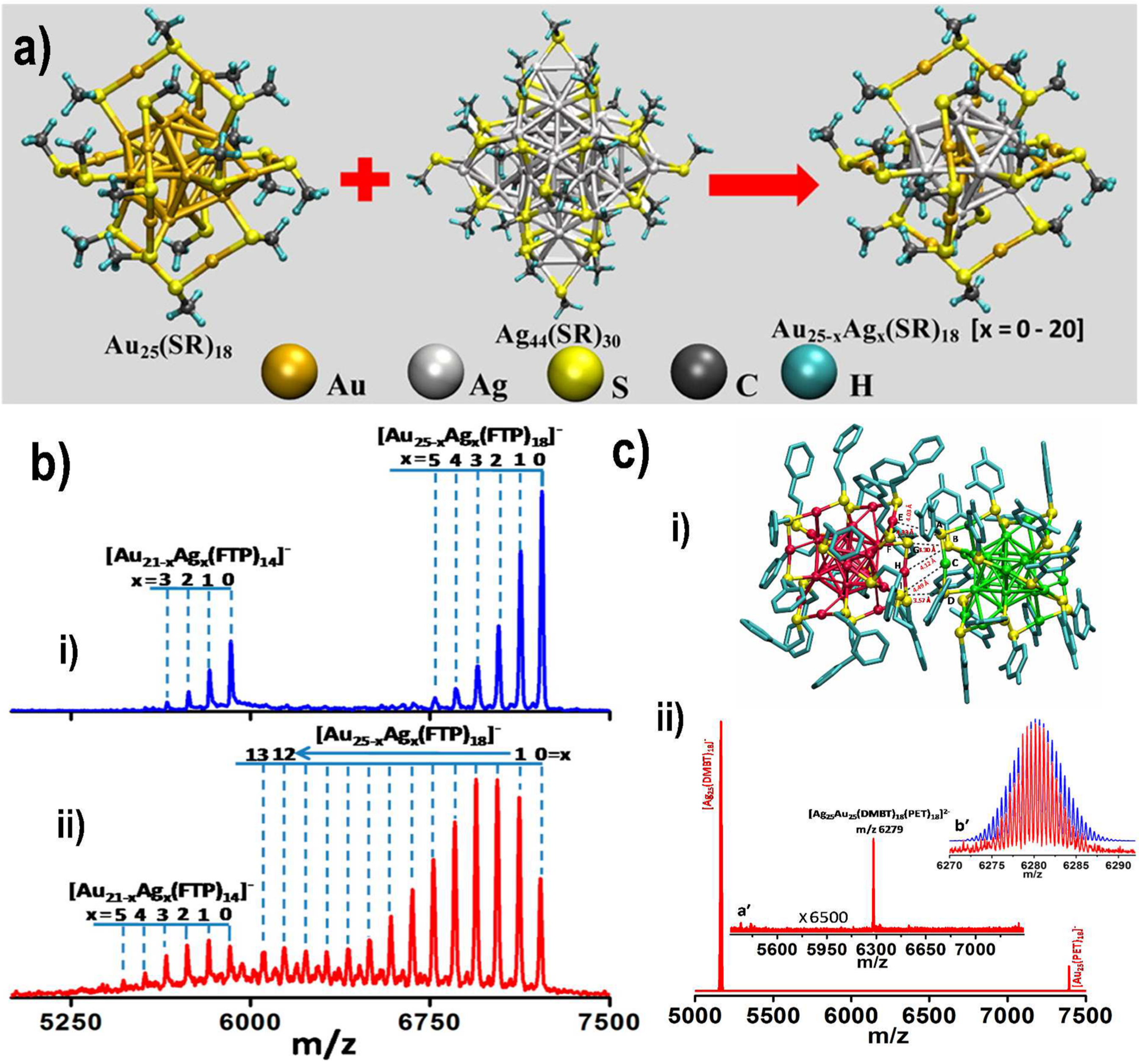

Figure 19. (a) Scheme of the intercluster reaction to yield alloy clusters. (b) Negative ion mode MALDI MS spectra showing time dependent changes in the reaction mixture of $Au_{25}(FTP)_{18}$ and $Ag_{44}(FTP)_{30}$ after 1 (i) and 3 h (ii) of the reaction. $[Au_{21-x}Ag_x(FTP)_{14}]$ are fragments from the alloy clusters due to the loss of $Au_4(FTP)_4$. Reprinted from ref 233. Copyright 2016 American Chemical Society. (c) (i) Minimum energy configuration of the adduct, $Au_{25}(PET)_{18}$−$Ag_{25}(DMBT)_{18}$ (**II**−**I**) upon intercluster reaction. Dashed lines show the shortest distances found between atoms in the staples of the two clusters which are marked with letters A−D on **I** and E−I on **II**. The hydrogen atoms are omitted from the ligands for clarity. Color code for the atoms: Au (red), Ag (green), S (yellow), and C (blue). (ii) Full range ESI MS spectrum of the mixture of $Ag_{25}(DMBT)_{18}$ (**I**) and $Au_{25}(PET)_{18}$ (**II**) at molar ratio (**I**:**II**) of 0.3:1.0 measured immediately after mixing. Inset a′ shows a feature due to the dianionic adduct, $[Ag_{25}Au_{25}(DMBT)_{18}(PET)_{18}]^{2-}$ formed between **I** and **II**. Theoretical (blue) and experimental (red) isotope patterns of the adduct features are given in the inset b′. Reprinted with permission from ref 310. Copyright 2016 Nature Publishing Group.

formation of the most stable Au_{25} cluster. Niihori et al.[12] have shown the precise isolation of ligand exchanged clusters taking $PdAu_{24}(SR)_{18}$ as an example. Each individual species of composition $PdAu_{24}(SR_1)_{18-n}(SR_2)_n$ (n = 0, 1, 2, ..., 18) was isolated using gradient HPLC. The corresponding chromatograms are displayed in Figure 18a. The mobile phase was systemically varied from pure MeOH to THF. The numbers 10, 20, 30, 40, and 50 in Figure 18a refer to the time (in minutes) taken for the mobile phase to become 100% THF, starting from pure MeOH. The corresponding mass spectral feature (Figure 18b) also shows an envelope similar to that of the HPLC chromatogram (Figure 18c). Each of these clusters was isolated and characterized using MALDI MS. Recently, the authors have carried out an extensive study of the separation and isolation of alloy clusters, such as $Au_{24}Pd(SR_1)_{18-x}(SR_2)_x$ and $Au_{24}Pd(SR_1)_{18-x}(SeR_2)_x$ (SR_1, SR_2 = thiolate; SeR_2 = selenolate).[256] Precise isolation after ligand exchange reaction opens up the possibility of individual structure analysis of clusters.

5.2. Ligand Conjugation

Ligand conjugation creates new properties such as fluorescence resonance energy transfer (FRET) in the cluster system. Muhammed et al.[478] incorporated the dansyl group in $Au_{25}(SG)_{18}$ cluster through ligand conjugation, which led to the observation of FRET in the conjugated cluster. $Au_{25}(SG)_{18}$ shows an emission at 585 nm (corresponding to an excitation of 535 nm), which overlaps with the emission band (peak maximum at 505 nm) of the dansyl chromophore. As a result, excitation of the dansyl group at 303 nm generates FRET. A systematic quenching of dansyl's emission and increase in emission intensity of $Au_{25}(SR)_{18}$ cluster suggests FRET, and it is generated through the energy transfer from the dansyl chromophore to the $Au_{25}(SR)_{18}$ cluster. A glutathione protected silver cluster has been functionalized with graphene through ligand conjugation.[54] This interesting behavior of ligand conjugation presents the probability of a new class of quantum cluster systems.

5.3. Intercluster Reactions

Krishnadas et al.[233] have shown mass spectrometric investigations of intercluster reaction between $Au_{25}(SR)_{18}$ and $Ag_{44}(SR)_{30}$ (a schematic of which is shown in Figure 19a) for the first time creating alloy clusters. Under ambient conditions, these clusters undergo spontaneous reactions in solution to form alloys, preserving the M_{25} and M_{44} nuclearity. The product peaks were distributed mainly in two regions: one near $Au_{25}(PET)_{18}$ peak regions (group I) and the other one near $Ag_{44}(FTP)_{30}$ peak regions (group II). HRESI MS of the reaction mixtures with different cluster ratios show (Figure 19b) different branches of peaks (in the group I regions). Two kinds of mass difference, corresponding to 89 and 99 Da, were seen which are due to exchange of Ag−Au and (Au−PET)−(Ag−FTP), respectively. Based on the HRESI MS data, the series of peaks in group I were assigned with the general formula, $Au_{25-x}Ag_x(PET)_{18-y}(FTP)_y$. With increase in the concentration of $Ag_{44}(FTP)_{30}$ in the reaction mixture, incorporation of more Ag and FTP ligands in $Au_{25}(PET)_{18}$ was noticed. Inclusion of Ag was seen from 1 to 13. Metal inclusion alone is noticeable when same ligands are used for both clusters. MALDI MS data of the reaction products between the FTP protected Au_{25} and Ag_{44} cluster are presented in Figure 19c, which clearly confirm the formation of $Au_{25-x}Ag_x(FTP)_{18}$ clusters. Silver inclusion of 1−5 atoms (Figure 19b,i) and 1−13 atoms (Figure 19b,ii) were seen after 1 and 3 h of reaction, respectively. Interestingly, after 24 h of reaction, Ag inclusion of up to 17 atoms was noticed. This report shows the role of metallic core and the surrounding monolayers in determining the chemistry of these clusters. Zhang et al.[479] have shown that Ag migration takes place between $Au_{38}(PET)_{24}$ and doped $Ag_xAu_{38-x}(PET)_{24}$ clusters in solution. Collisions between the reacting clusters are the reason for such a migration.

In a recent report, Krisnadas et al. have found that the reaction of $Au_{25}(SR)_{18}$ cluster with corresponding silver analogue, $Ag_{25}(SR)_{18}$, produced (Figure 19c,i) $Ag_mAu_n(SR)_{18}$ clusters ($n = 1–24$; $m + n = 25$), keeping the structure intact.[310] This is basically a substitution reaction where one cluster converts to another without changing the structure, as both $Au_{25}(SR)_{18}$ and $Ag_{25}(SR)_{18}$ have the same structure. A dianionic adduct, which was believed to be the earliest intermediate in such reactions, has been detected in electrospray ionization mass spectrometry (inset of Figure 19c,i). Formation of such an adduct is highly unlikely considering the negative charge of clusters, but in this case, the charge is well dispersed which does not create significant repulsion between each other. The van der Waals attractive forces between the alkyl/aryl groups in the staple motifs are responsible initially (Figure 19c,ii) for the formation of such adducts as confirmed form the molecular docking simulations. These two reports of intercluster reactions suggest that clusters can be treated exactly like molecules; they can exchange atoms without structural deformation. Baksi et al. discovered the gas phase dimer of $Au_{25}(SR)_{18}$ using ion mobility mass spectrometry.[480] Such transient species are shown to be important in explaining the chemical reactivity between clusters.

6. ALLOY CLUSTERS

Bimetallic nanostructures,[481] especially clusters, are of tremendous interest, particularly in the field of catalysis, because of their distinct properties from their corresponding monometallic counterparts.[482] Doping can also improve the cluster stability. The very first example of an atomically precise bimetallic cluster, $PdAu_{24}(SR)_{18}$, was synthesized by the Murray group,[303] which was further examined by the Negishi and Tsukuda groups[198,483] in greater detail. Negishi et al. performed the HPLC technique to isolate the cluster with high purity.[198] Figure 20a shows the MALDI MS of the isolated $PdAu_{24}(SR)_{18}$ cluster and its monometallic analogue $Au_{25}(SR)_{18}$, which differ by 91 mass units. From a detailed structural analysis, it was inferred that the Pd atom sits in the central position of the icosahedral core and that the alloy cluster has an enhanced stability compared to the $Au_{25}(SR)_{18}$ cluster. The position of Pd was further confirmed from the recent crystal structure of $Au_{24}Pd(SR)_{18}$ cluster (inset of Figure 20a).[484] Similarly, Ag,[485] Cu,[197,486] Pt,[199] Cd,[19] and Hg[19] doped Au_{25} and alloy clusters of three different metals, with the general formula $M_1Ag_xAu_{24-x}(SR)_{18}$[487] (where M = Cd, Hg), have also been reported by different research groups.[491] A few examples of alloys of other stable gold clusters, such as Au_{38}[492,493] and

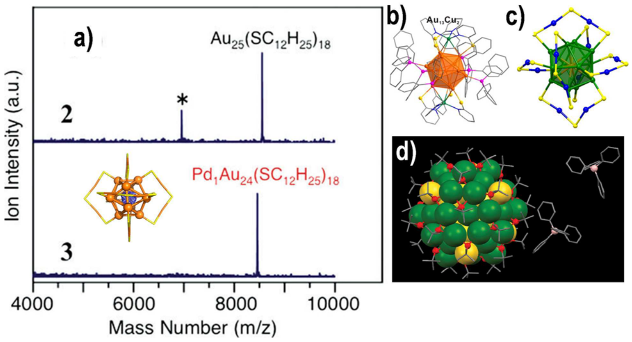

Figure 20. (a) Negative-ion MALDI mass spectra of fractions 2 (Au_{25} cluster) and 3 ($PdAu_{24}$ cluster) separated by HPLC. Reprinted with permission from ref 198. Copyright 2010 Royal Society of Chemistry. Inset shows the recent crystal structure of $Au_{24}Pd(PET)_{18}$. Reprinted from ref 484. Copyright 2016 American Chemical Society. On the right side, (b), (c), and (d) are the crystal structures $[Au_{13}Cu_2(PPh_3)_6(SPy)_6]^+$ (Py = 2-pyridyl), $PdAg_{24}(2,4\text{-}SPhCl_2)_{18}$, and $[Ag_{46}Au_{24}(SR)_{32}](BPh_4)_2$, respectively. (b) Reprinted from ref 488. Copyright 2013 American Chemical Society. (c) Reprinted from ref 489. Copyright 2015 American Chemical Society. Reprinted with permission from ref 490. Copyright 2015 American Association for the Advancement of Science.

Au_{144},[494] are also there in the literature. Udayabhaskararao et al.[17] synthesized the Ag_7Au_6 alloy cluster from $Ag_{7,8}$ clusters on successive addition of Au^{3+} solution. The alloy showed enhanced luminescence, both in the solution and in powder form. The excitation and emission features changed from 670 to 390 nm and from 770 to 650 nm, respectively relative to the monometallic clusters. Similarly, differences in the absorption features are also expected. Biltek et al. proposed a structure for the bimetallic $Ag_4Ni_2(DMSA)_4$ cluster using calculations.[495] Yang et al. reported the crystal structures of three alloy clusters, $Au_{13}Cu_x$ ($x = 2, 4, 8$), and for $x = 2$, the structure has been presented in Figure 20b.[488] The structure contains an Au_{13} icosahedron which is passivated by six PPh_3 and six 2-pyridinethiolates. Each Cu is coordinated by three pyridyl groups and they are face-capped. $Au_{12}Ag_{32}(SR)_{30}$ has a structure similar to the $Ag_{44}(SR)_{30}$ cluster with 12 gold atoms replacing the silver atoms in the hollow cage,[222] whereas the recently discovered Ag−Cu alloy cluster $[Ag_{28}Cu_{12}(SR)_{24}]^{4-}$ has a two-shell $Ag_4@Ag_{24}$ core protected by four nearly planar $Cu_3(SR)_6$ moieties.[496] Recently, crystal structures of alloys of $Ag_{25}(SR)_{18}$ with Au,[26] Pd (Figure 20c),[489] and Pt[489] have been revealed. These heteroatoms are present at the center of the icosahedra, forming a general $M@Ag_{12}@Ag_{12}(SR)_{18}$ structural configuration. Bootharaju et al. have shown unusual metal exchange pathways for $MAg_{24}(SR)_{18}$ clusters (where M = Pd, Pt).[497] The central Pd atom of $[PdAg_{24}(SR)_{18}]^{2-}$ cluster was replaced by Au during the metal exchange process to produce a bimetallic $[AuAg_{24}(SR)_{18}]^-$ cluster along with a minor product of $[Au_2Ag_{23}(SR)_{18}]^-$, whereas the central Pt atom remained intact in $[PtAg_{24}(SR)_{18}]^{2-}$ clusters.[497] In this case, the incoming gold replaced the noncentral Ag atoms to form trimetallic $[Au_xPtAg_{24-x}(SR)_{18}]^{2-}$ NCs, with $x = 1-2$. Wang et al. have reported the single crystal structure of $[Ag_{46}Au_{24}(SR)_{32}](BPh_4)_2$ (Figure 20d) which also shows enhanced catalytic activity.[490] The structure can be represented simply as $Ag_2@Au_{18}@Ag_{20}@Ag_{24}Au_6(SR)_{32}$. This is the very first alloy cluster with gold and silver coexisting on staples. Similarly, a recent report of $[Au_{80}Ag_{30}(C{\equiv}CPh)_{42}Cl_9]Cl$ cluster can be presented as $Au_6@Au_{35}@Ag_{30}Au_{18}@Au_{21}$.[498] More information about alloy clusters reported so far is given in Table 4.

7. PROTEIN PROTECTED CLUSTERS

Similar to several ligands, proteins can also act as stabilizers and a few proteins also have the added advantage of reducing power, using which they can reduce the precursor metal ions of Au, Ag, Cu, etc. Even though formation of nanoparticles through proteins was easy and efficient, controlling the size to make atomically precise nanoclusters with proteins was not attempted until 2009. Xie et al. have succeeded in synthesizing atomically precise Au_{25} cluster within the bovine serum albumin (BSA) template.[213] The synthetic methodology was very simple which involved the mixing of Au^{3+} ion precursor with the protein at alkaline pH.[213] Under basic conditions, aromatic amino acids present in the BSA donate electrons to reduce the gold ions while cysteine residue takes the place of the stabilizer to form the Au nanocluster. Comparing the mass of Au@BSA cluster and that of BSA protein alone through MALDI MS, the number of Au atoms in the cluster can be calculated. From the mass spectral analysis, the number of Au atoms inside a BSA protein was found to be 25.[213] Much higher QY (6%) was seen for this Au_{25}@BSA cluster in comparison to the thiolated Au_{25} cluster.[213] After the pioneering discovery of this green route, many reports with new synthetic routes started evolving.[389,396,398,503−506] Especially, using BSA, several atomically precise clusters such as Au_8@BSA,[371] Au_{16}@BSA,[504] Au_{38}@BSA,[507] Ag_8@BSA,[508] Ag_{15}@BSA,[32] Ag_{31}@BSA,[509] etc., have been made.[370,383,396,399,503−505] Different proteins such as lysozyme,[401,510−512] lactotransferrin,[214,371,513] insulin,[514,515] pepsin,[516] trypsin,[517] etc., have been used as scaffolds to synthesize a variety of metal and alloy nanoclusters. Chaudhari et al. have tried to understand the evolution and growth of nanoclusters inside protein templates using MALDI MS analysis.[371] They have also investigated the kinetics of the cluster growth by monitoring the fluorescence intensity.[518] Size evolution of protein protected clusters has also been investigated by small-angle X-ray scattering (SAXS).[519] Because of their biocompatibility, they have been used in several applications and many of them have been discussed in the application section.[378,379,390,504,505,520−522] Many review articles[50,52,55,523,524] and book chapters[525,526] including some from the present authors have covered this topic in detail.

8. OTHER PROPERTIES

Along with their unique optical and photoluminescence characteristics, monolayer protected clusters exhibit some other properties such as two-photon absorption, optical nonlinearity, magnetism, etc. These are briefly discussed in sections 8.1 and 8.2.

8.1. Two-Photon Absorption

Optical nonlinearity is a remarkable property[270,527−531] of noble metal clusters. The nonlinear optical (NLO) properties include two-photon absorption (TPA),[532,533] two-photon fluorescence (TPF), and second/third harmonic generation (SHG/THG).[528,529] The simultaneous absorption of two photons (of identical or different frequencies) in order to excite a molecule from the ground state to a higher energy electronic state is often known as TPA. Ramakrishna et al.[534] observed a similar phenomenon for $Au_{25}(SR)_{18}$ clusters. This cluster can be useful for two-photon imaging with infrared light as it has reasonable luminescence efficiency ($\sim 2.5 \times 10^{-4}$) in the NIR region. Figure 21a shows the corresponding optical spectrum of Au_{25} cluster protected with hexanethiol (taken in hexane solvent). As discussed earlier, it consists of several bands starting from the ultraviolet to the visible region with a maximum near 675 nm. Excitation at 1290 nm from the output of an optical parametric amplifier results in emission with a maximum at 830 nm (Figure 21a). Slope from the corresponding pump-power dependency plot (Figure 21b) gave a value of ∼2 which indicates that it is a two-photon excited emission. Using H_2TPP in toluene as standard, the TPA cross section for $Au_{25}(SR)_{18}$ cluster was measured to be 2700 GM, which is superior to many other NIR emitting organic chromophores. The study also revealed that emission in the visible region (maximum at 510 nm) is also a two-photon-absorption phenomenon (Figure 21c,d). Patel et al.[535] determined a large two-photon cross section value of ∼5000 GM for three water-soluble silver clusters emitting at 660, 680, and 710 nm, respectively. Two-photon excited fluorescence from a DNA-templated Ag nanocluster has been reported by Yau et al.[536] Upon excitation of 800 nm, the cluster exhibited an emission at 630 nm with a two-photon-absorption cross section of ∼3000 GM.

It is important to mention that, in most of the cases, the multiphoton absorption and emission of nanoclusters have been investigated at single wavelengths, which presents only a

Table 4. List of Selected Alloy Clusters

core	ligand	composition	focus	synthesis	physical state of the product	other measured properties	ref
Ag_7Au_6	mercaptosuccinic acid	$Ag_7Au_6(H_2MSA)_{10}$	characterization	three step solution phase	solid	ESI MS, TDDFT, XPS, SEM/EDAX, ^1H NMR, UV/vis	17
$Au_{25-n}Ag_n$	dodecanethiol	$Au_{25-n}Ag_n(SC_{12}H_{25})_{18}$	characterization	Brust method	solid	MALDI MS, LDI, XPS, UV/vis	485
$Au_{24}Pd$	phenylethanethiol	$PdAu_{24}(PET)_{18}$	characterization	Brust method	solid	ESI MS, ESI-FTICR-MS, MALDI MS, AAS	303
$Au_{24}Pd$	dodecanethiol	$Pd_1Au_{24}(SC_{12}H_{25})_{18}$	characterization	Brust method	solid	HPLC, TGA, MALDI MS, XPS, FT-IR, UV/vis	198
$Au_{24}Pt$	phenylethanethiol	$PtAu_{24}(PET)_{18}$	characterization	Brust method	solid	ESI-MS, UV/vis, SEC, ^1H NMR, COSY, XRD, MALDI MS	199
$Au_{24}Pt$	phenylethanethiol	$PtAu_{24}(PET)_{18}$	structure and electronic properties	Brust method	solid	EXAFS, MALDI MS, XPS, calculation	499
$Au_{24}Cd$, $Au_{24}Hg$	phenylethanethiol	$CdAu_{24}(PET)_{18}$, $HgAu_{24}(PET)_{18}$	crystal structure, properties	Brust method with modification	solid	ESI MS, UV/vis, TGA, MALDI MS, TDDFT	19
$Au_{25-n}Cu_n$	octaneselenol	$Cu_nAu_{25-n}(SeC_8H_{17})_{18}$ (n = 0−9)	characterization	modified Brust method	solid	MALDI MS, UV/vis, DPV, PL, XRD and TEM	197
$Au_{25}Ag_2$	phenylethanethiol	$Au_{25}Ag_2(PET)_{18}$	characterization	solution phase mixing	solid	UV/vis, ESI MS, DFT, XRD, catalysis	500
$Au_{24}Pd$, $Au_{37}Pd$, $Au_{36}Pd_2$	phenylethanethiol	$PdAu_{24}(PET)_{18}$, $PdAu_{37}(PET)_{24}$, $Pd_2Au_{36}(PET)_{24}$	characterization	modified Brust method	solid	MALDI MS, UV/vis, SEC, LDI	492
$Au_{36}Pd_2$	phenylethanethiol	$Pd_2Au_{36}(PET)_{24}$	characterization	modified Brust method	solid	HR ESI MS, MALDI MS, XPS	493
$(Au-Ag)_{144}$	phenylethanethiol	$(Au-Ag)_{144}(PET)_{60}$	characterization	modified Brust method	solid	UV/vis, ESI MS, MALDI MS,	494
Ag_4Ni_2	dimercaptosuccinic acid	$Ag_4Ni_2(DMSA)_4$	characterization	one step solution phase	solid	ESI MS, UV/vis, PAGE, calculation	495
$Au_{13}Cu_x$(x = 2, 4, 8)	pyridine-2-thiol, 4-*tert*-butylbenzenethiol, triphenylphosphine, pyridinediphenylphosphine	$[Au_{13}Cu_2(PPh_3)_6(SPy)_6]^+$, $[Au_{13}Cu_4(PPh_2Py)_4(SC_6H_4\text{-tert-}C_4H_9)_8]^+$, $[Au_{13}Cu_8(PPh_2Py)_{12}]^+$	crystal structure	two step solution phase	solid	UV/vis, computational calculation, TGA, ESI MS, and catalytic performance	488
$Au_{12}Ag_{32}$	*p*-fluorothiophenol, 3,4-difluorothiophenol, 4-(trifluoromethyl)thiophenol	$Au_{12}Ag_{32}(SR)_{30}$	crystal structure	one step solution phase	solid	UV/vis, PDOS, calculation	222
$Ag_{28}Cu_{12}$	2,4-dichlorobenzenethiol	$[Ag_{28}Cu_{12}(SR)_{24}]^{4-}$	crystal structure	one step solution phase	solid	UV/vis, ESI MS, CD, DFT	496
$Au_{24}Ag_{20}$	phenylalkynyl, 2-pyridylthiolate	$Au_{24}Ag_{20}(2\text{-}SPy)_4(PhC\equiv C)_{20}Cl_2$	crystal structure	two step solution phase	solid	UV/vis, TGA, TPD MS, PDOS	501
M_xAu_{25-x}	phenylethanethiol	$Cu_xAu_{25-x}(SR)_{18}$, $Ag_xAu_{25-x}(SR)_{18}$, $Cd_1Au_{24}(SR)_{18}$ and $Hg_1Au_{24}(SR)_{18}$	characterization and crystal structure	solution phase	solid	ESI MS, UV/vis, MALDI MS	502
$M_1Ag_xAu_{24-x}$	phenylethanethiol	$Cd_1Ag_xAu_{24-x}(SR)_{18}$, $Hg^1Ag_xAu_{24-x}(SR)_{18}$	characterization	solution phase	solid	ESI MS, UV/vis	487
$Ag_{24}Au$	dimethylbenzenethiol	$AuAg_{24}(SPhMe_2)_{18}{}^-$	crystal structure	solution phase then galvanic exchange	solid	ESI MS, UV/vis, transient absorption	26
$Ag_{24}Pd$, $Ag_{24}Pt$	3,5-dichlorobenzenethiol	$(PPh_4)_2[PdAg_{24}(SR)_{18}]$, $(PPh_4)_2[Pt_xAg_{25-x}(SR)_{18}]$ (x = 1, 2)	crystal structure	solution phase	solid	ESI MS, UV/vis, CD, TGA, DFT	489
$Ag_{46}Au_{24}$	*tert*-butylthiol	$[Ag_{46}Au_{24}(SR)_{32}](BPh_4)_2$	crystal structure	solution phase	solid	NMR, TEM, UV/vis	490
$Au_{80}Ag_{30}$	phenylalkyne	$[Au_{80}Ag_{30}(C\equiv CPh)_{42}Cl_9]Cl$	crystal structure	solution phase	solid	UV/vis	498

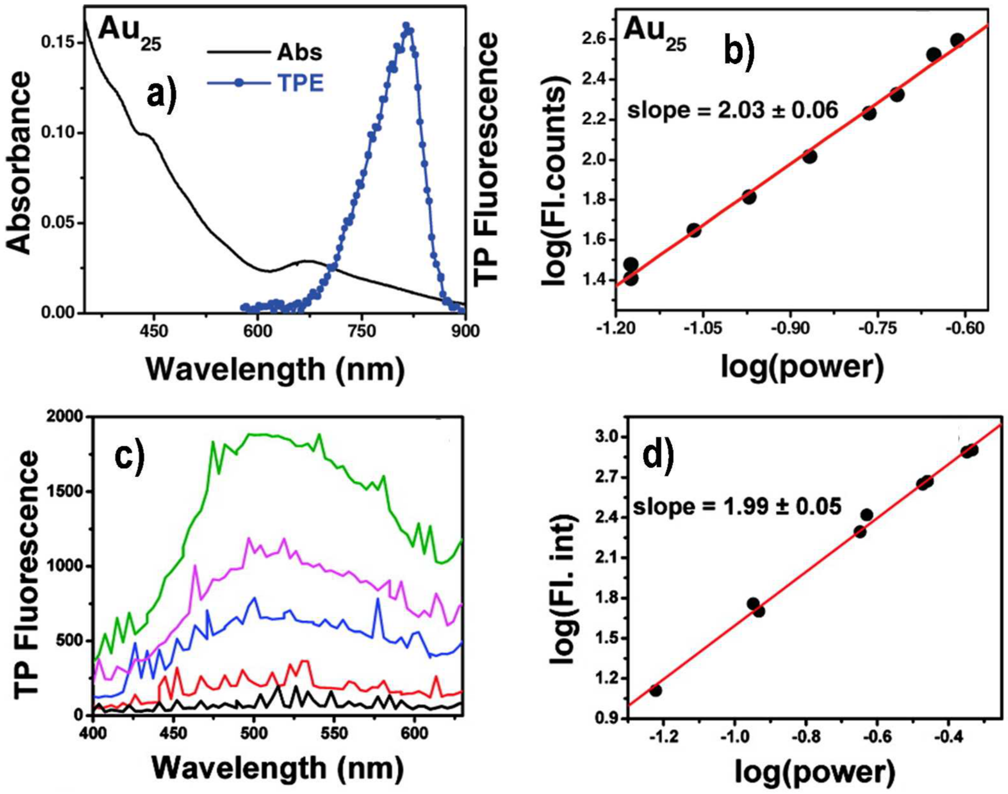

Figure 21. (a) Optical absorption of $Au_{25}(SR)_{18}$ cluster and two-photon emission spectrum after excitation at 1290 nm. (b) Power dependence of the fluorescence obtained at 1290 nm suggesting it to be a two-photon process. (c) Two-photon excited fluorescence spectra of $Au_{25}(SR)_{18}$ at different pump powers after excitation at 800 nm and (d) power dependence of the emission at 510 nm. Reprinted from ref 534. Copyright 2008 American Chemical Society.

fragmentary image of the NLO properties. Recently, Olesiak-Banska et al.[533] have investigated third-order NLO properties of $Au_{25}(Capt)_{18}$ clusters by the Z-scan technique with femtosecond laser excitation in a broad range of wavelengths. They have also listed a summary of NLO properties of gold nanoclusters reported so far.[533]

8.2. Magnetism

Single gold atoms (adsorbed on a support or in gas beams) are paramagnetic, whereas bulk gold is diamagnetic.[352] The paramagnetism is due to the unpaired 6s electron of gold. Such paramagnetism and its evolution from single gold atoms to metallic nanoparticles are of potential interest and importance in the understanding of the magnetic nature of gold. Hori et al.[537] reported size dependency of magnetism of gold nanoparticles; they claimed that thiol suppresses magnetization. In 2005, Crespo et al. showed the magnetism in thiolated nanoparticles of 1.4 nm.[538]

Similarly, the magnetic nature of gold clusters, especially when they are atomically precise, needs to be investigated. Zhu et al.[352] found reversible switching of magnetism in $Au_{25}(PET)_{18}$ cluster. The EPR spectra of microcrystalline and frozen solutions of $[Au_{25}(SR)_{18}]^0$ cluster showed an $S = 1/2$ signal, which suggests that each cluster has one unpaired spin. The EPR signal disappeared upon the reduction of the cluster to its negative charge state, $[Au_{25}(SR)_{18}]^-$. Interestingly, the signal could be switched back when the negatively charged cluster was oxidized using H_2O_2, to return back to the neutral cluster. Thus, paramagnetism could be switched on and off just by changing the charge state of the cluster (Figure 22). The origin of this magnetism was explained by DFT calculations, which revealed that the unpaired spin resides in the HOMO that has a distinct p-like character (Figure 22). This switching property of the $Au_{25}(SR)_{18}$ cluster can therefore be used as a paramagnetic probe. Negishi et al.[539] investigated a series of atomically precise clusters of general formula $Au_N(SG)_M$, where (N, M) = (10, 10), (15, 13), (22, 16), (22, 16), (25, 18), (29, 20), and (39, 24), by studying them via X-ray magnetic circular dichroism. The magnetic moment was found to increase with increase in the cluster core size. The hole created by Au−S bonding was more responsible than the quantum size effect of gold clusters, for the spin polarization phenomenon. McCoy et al.[540] have shown that chemical oxidation can lead to superatom paramagnetism in $Au_{102}(MBA)_{44}$ cluster. The superatom electron configuration of $Au_{102}(MBA)_{44}$ cluster is $(1S)^2$ $(1P)^6$ $(1D)^{10}$ $(2S)^2$ $(1F)^{14}$ $(2P)^6$ $(1G)^{18}$. Addition or removal of electrons from these superatomic orbitals can make the superatom a paramagnet.

9. APPLICATIONS

The unique optical and luminescence properties of noble metal nanoclusters make them highly appropriate for various applications such as sensing,[541,542] catalysis,[543,544] optics, imaging,[50] and biolabeling.[3,53,55,162,298,510,545−548] Mathew and Pradeep[51] have addressed the applications of noble metal nanoclusters in detail in their review article. Some specific examples are explained below.

9.1. Sensors

Sensing of different molecules or biomolecules or ions including hazardous ions (such as Hg^{2+}) using nanomaterials have now become an interesting topic in materials

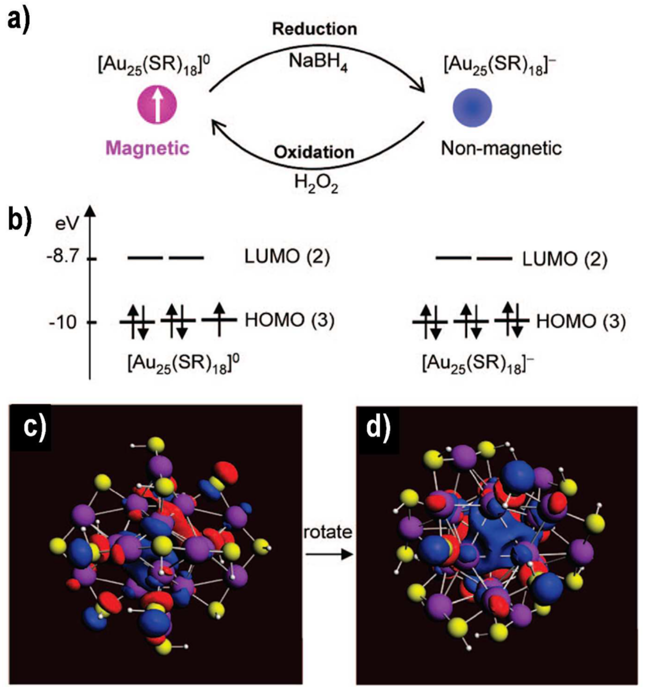

Figure 22. (a) Reversible conversion between neutral and anionic $Au_{25}(SR)_{18}$ nanoparticles. (b) DFT-calculated Kohn−Sham orbital energy level diagrams for neutral and anionic nanoparticles, respectively. (c, d) Views of the Kohn−Sham HOMO for $[Au_{25}(SH)_{18}]^0$ at LB94//XR/TZP level of theory. The HOMO possesses two lobes and exhibits distinct P-like character. Image d is rotated relative to (c) to show one of the lobes (contributed by three Au atoms in the icosahedral shell). Color code: purple, Au; yellow, S; white, H. Reprinted from ref 352. Copyright 2009 American Chemical Society.

science.[545,547,549−551] Noble metal nanoclusters have also begun to play an important role in this regard.[216,547,552,553] In most of the cases, luminescence quenching is primarily utilized. Mathew et al.[554] developed a novel sensor based on a hybrid material, composed of two systems, namely, gold mesoflowers and BSA protected Ag_{15} clusters. Here, too, the sensing indicator was the change in the color of luminescence. Initially, fluorescent isothiocyanate (FITC) was coated on the gold mesoflowers, which resulted in bright green luminescence. Further functionalization with Ag_{15}@BSA cluster on the Au@SiO_2−FITC mesoflowers produced red luminescence (Figure 23a). Upon exposure to Hg^{2+} or TNT (trinitrotoluene), the red luminescence was quenched and a green luminescence, characteristic of the underlying FITC, appeared. In some instances, sensing is based on fluorescence enhancement (details are given in Table 5). Most of the literature on sensors is focused on the detection of Hg^{2+} and Cu^{2+} ions. For example, gold clusters have a strong tendency to sense Cu^{2+}, as can be seen from the case of Au_{15} clusters reported by Shibu et al.[555] This cluster was fabricated with chitosan to make a composite whose intense red luminescence (Figures 23b,c) was quenched upon addition of Cu^{2+} or on dipping the composite in Cu^{2+} solution.[552] The composite film exhibited visual sensitivity to Cu^{2+}, up to 1 ppm (Figure 23d), below the permissible limit (1.3 ppm) in drinking water (by the Environmental Protection Agency (EPA)). Although the limit of detection for toxic metal ions reached below the parts per billion level in a few reports,[511,556] the underlying mechanism was not identified.

The luminescence and optical properties of noble metal nanoclusters are highly sensitive to the local environment and depend on the interaction with external analytes, which makes these clusters act as "turn-off" or "turn-on" sensors.[49] Since these clusters have a core−shell geometry, the analyte can interact with the metal atoms in the core as well as with the ligands forming the shell. There are three types of primary interactions between metallic core and analytes, namely (i) analyte induced metal core decomposition, (ii) deposition of analyte on the metal surface, and (iii) metallophilic interactions. Interaction with the shell can take place by (i) an enzymatic reaction, (ii) incorporation of recognition moieties, or (iii) analyte induced aggregation.[49] As an example, a mechanism has been outlined to describe the interaction of Hg^{2+} with luminescent silver clusters.[216] It was proposed that the interaction is induced by the ligands that contain thiol moieties. Because of the soft−soft interaction with S, Hg^{2+} initially gets attached to the ligand and then sits on the silver surface where

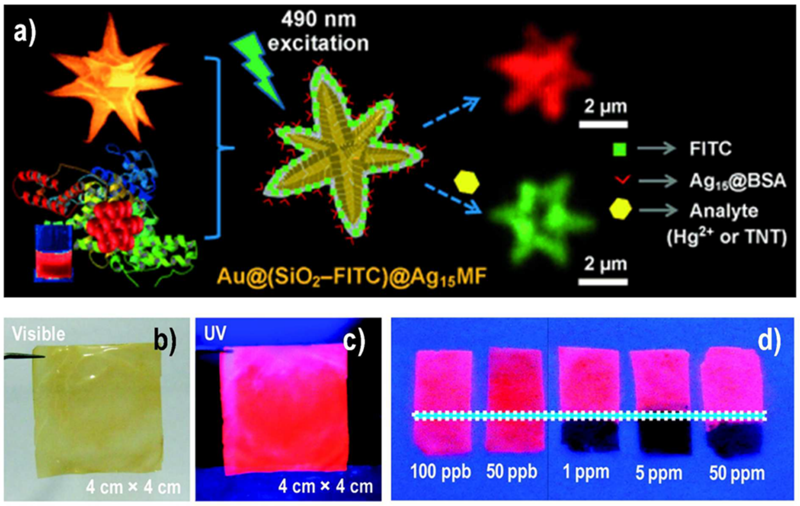

Figure 23. (a) Schematic of different analytes sensing by Ag_{15} cluster coated gold mesoflower. Reprinted with permission from ref 554. Copyright 2012 John Wiley & Sons. (b and c) Photographs of Au_{15} cluster incorporated film under white light and UV light, respectively. (d) Dependence of Cu^{2+} concentration on luminescence quenching. Reprinted from ref 552. Copyright 2012 American Chemical Society.

Table 5. Sensing Properties of Metal Clusters

sensor type	cluster core	protecting ligand	sensed metal ion/molecule	property with which sensing was done	sensing limit	ref
chemical sensor	Ag_n	glutathione	Hg^{2+}	absorption and fluorescence quenching	1 ppb	216
	$Ag_{4,5}$	lipoic acid	Hg^{2+}	fluorescence quenching	10^{-10} M	212
	Au_n	BSA	Cu^{2+}	fluorescence quenching	5×10^{-5} M	520
	Au_{15}	GSH and cyclodextrin	Cu^{2+}	fluorescence quenching	1.3 ppm	552
	Au_n	lipoic acid	Hg^{2+}	fluorescence quenching	5×10^{-10} M	294
	Ag_n	denatured BSA	Hg^{2+}	fluorescence quenching	1×10^{-8} M	557
	Au_{38}	BSA	Cu^{2+}	fluorescence quenching	1.5×10^{-8} M	507
	Au_{10-39}	glutathione	Cu^{2+}	fluorescence quenching	8.6×10^{-8} M	558
	Au_n	11-mercaptoundecanoic acid	Hg^{2+}	fluorescence quenching	5×10^{-9} M	559
	Au_n	lysozyme	Hg^{2+}	fluorescence quenching	3×10^{-12} M	511
	Au_n	thiolate α-cyclodextrin	Hg^{2+}	fluorescence quenching	4.9×10^{-11} M	556
	Au_n	lysozyme	Hg^{2+}	fluorescence quenching	1×10^{-8} M	510
	Au_n	BSA	Hg^{2+}	FRET	1×10^{-10} M	560
	Au_n	BSA	Hg^{2+}	fluorescence quenching	5×10^{-10} M	561
	Au_n	glutathione	Cu^{2+}	fluorescence quenching	3.6×10^{-9} M	562
	Ag_n	polymethacrylic acid	Cr^{3+}	fluorescence quenching	1×10^{-7} M	563
	Au_{16}	BSA	Ag^{+}	fluorescence enhancement	1×10^{-7} M	504
	Au_{25}	glutathione	Ag^{+}	fluorescence enhancement	2×10^{-7} M	504
	Au_n	BSA	CN^{-}	fluorescence quenching	2×10^{-7} M	564
	Ag_{14}	glutathione	S^{2-}	fluorescence quenching	2×10^{-9} M	302
	Au_n	oligonucleotide	Hg^{2+}	fluorescence quenching	5×10^{-9} M	565
	Au_n	BSA	Hg^{2+}	fluorescence quenching	80 nM	521
	Au_n	cysteine	As^{3+}	fluorescence quenching	53.7×10^{-9} M	566
	Cu_5 and Cu_{13}	BSA	Pb^{2+}	fluorescence quenching	>20 ppm	522
	Ag_n	polymethacrylic acid	Cu^{2+}	fluorescence quenching	8×10^{-9} M	567
	Au_n	Nlf	Cu^{2+}	fluorescence quenching	10 ppm	214
	AgAu	BSA	Al^{3+}	fluorescence quenching	0.8×10^{-6} M	568
biological sensor	Au_n	PAMAM	hIgG	turn-off fluorescence	mM to nM	569
	Ag_n	DNA	miRNA	turn-off fluorescence	0.5×10^{-6} M	570
	Au_n	MUA	PDGF AA	turn-on fluorescence	0.5×10^{-9} M	571
	Au_n	*S*-mannose	Con A	turn-off fluorescence	75×10^{-12} M	572
	Au_n	mannose	Tg	turn-on fluorescence	48×10^{-12} M	573
	Au_n	*S*-mannose	Tg	turn-on fluorescence	90×10^{-12} M	574
	Au_n and AuNPs	mannose, anti-Tg	Tg	turn-on fluorescence	$65 (\pm 16) \times 10^{-9}$ M	573
	Au_n	glutathione	GST-tagged proteiens	naked eye detection	750×10^{-9} M	575
	Au_n	protein A	hIgG	turn-on fluorescence	10×10^{-9} M	576
	Ag_n	DNA-Apt	thrombin	turn-off fluorescence	1×10^{-9} M	577
	Ag_n	DNA	human Braf oncogene	turn-on fluorescence	10×10^{-9} M	217
	$\sim Ag_{10}$	DNA	DNA	turn-on fluorescence	$<1 \times 10^{-6}$ M	578

it oxidizes Ag(0) to Ag^+ ion. In the process, Hg^{2+} gets reduced to its metallic state and forms an alloy with the silver core, which has been probed by TEM and PXRD. Details of the limits of sensing of several ions are listed in Table 5.

9.2. Biological Applications

Because of the nontoxicity of gold particles, they have been extensively used in various biological applications[579] such as biolabeling,[580] cancer treatment,[581,582] drug screening,[583] drug delivery,[580,584,585] etc.[55,505,547,585−587] Silver clusters are mostly toxic for biological applications, as silver ions leach into the cells and kill them completely above a threshold. Hence, they can only be used for limited imaging purposes and for their antibacterial activity. Below is a discussion of a few biological applications of gold and silver clusters.

9.2.1. Biolabels. Cysteine with its thiol functionality can easily coordinate with gold because of the strong binding between gold and sulfur. This strategy has been used for biolabeling as some proteins contain this amino acid residue and, therefore, can easily get attached to the cluster core. Many examples of this kind are reported in the literature. For a detailed discussion, the readers may refer to the book chapter by Ackerson et al.[588] Another property of gold nanoclusters that has been used for biolabeling as well as bioimaging is fluorescence. Liu et al. have shown that insulin encapsulated highly red luminescent Au nanoclusters can be used for fluorescence imaging (Figure 24a).[514] The initial target was to check the cytotoxicity, for which C2C12, a mouse myoblast cell line, was used as a test candidate. The uptake efficiency of insulin−Au nanoclusters for C2C12 cells served as a biomarker to distinguish the differentiated versus undifferentiated C2C12 myoblasts. The cells with suitable treatment were imaged under a confocal microscope to examine the uptake of the insulin−Au nanoclusters after 2 h of feeding. Color processing of the obtained image was further carried out to make each compartment more distinguishable. The corresponding image is shown in Figure 24a, which clearly shows that the intense red

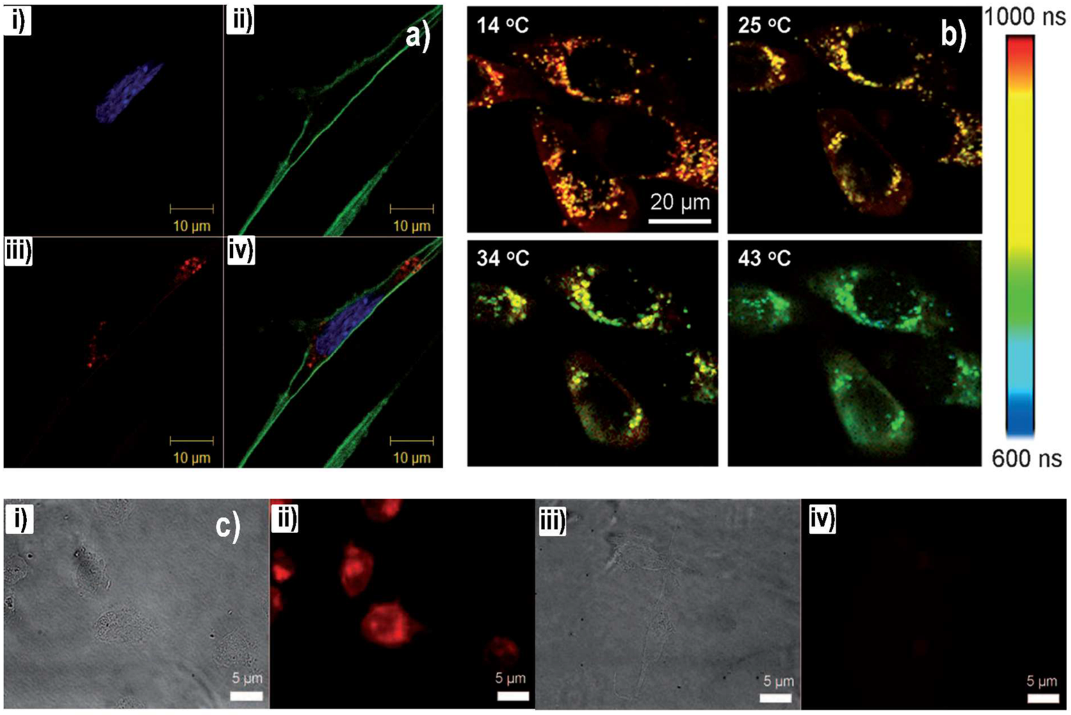

Figure 24. (a) Microscopic observation of internalization of insulin−Au nanoclusters. Differentiated C2C12 myoblasts were treated with insulin−Au nanoclusters for 2 h. (i) Cell nucleus stained with 4′,6-diamidino-2-phenylindole (DAPI, blue). (ii) Actin fiber stained with Alexa Fluor 488 phalloidin to confirm the cell boundary (green). (iii) Insulin−Au nanoclusters exhibit red luminescence. (iv) Fluorescence image overlay of the three images. Reprinted with permission from ref 514. Copyright 2011 John Wiley & Sons. (b) Typical FLIM images of HeLa cells with internalized Au nanoclusters at four different temperatures. Reprinted with permission from ref 589. Copyright 2013 John Wiley & Sons. (c) Bright-field (i, iii) and corresponding fluorescence microscopy (ii, iv) images showing the interaction of FA-conjugated Au nanocluster@BSA with different types of cell lines. Left panel (i and ii): images of folate-receptor-positive KB cells with FA-conjugated Au nanocluster@BSA incubated for 24 h; right panel (iii and iv): images of folate-receptor-negative mouse fibroblast L929 cells with FA-conjugated Au nanocluster@BSA incubated for 24 h. Reprinted with permission from ref 507. Copyright 2010 John Wiley & Sons.

fluorescence of insulin−Au nanoclusters overlap with that of the fully differentiated C2C12 mouse myoblasts in the cytoplasm.

Shang et al.[589] demonstrated gold nanoclusters as biomarkers for temperature sensing in human cancer cells. Incubation was done with Au nanoclusters in a serum-free cell culture medium for 2 h. Appreciable amounts of Au nanoclusters were observed inside HeLa cells. Then, using a temperature controlled sample stage, the temperature of the environment of the HeLa cells was varied. Lifetime maps were calculated and are shown in Figure 24b, which provides clear evidence that the long fluorescence lifetime components in the range of 600−1000 ns arise from the internalized Au nanoclusters rather than from the cellular autofluorescence. Muhammed et al.[22,507] have shown the biolabeling application effectively for BSA protected gold clusters and the thiolated Au_{23} cluster. This gold nanocluster (BSA protected) is highly luminescent in the pH range 2−12, which makes it a good staining agent for cell imaging. It has two advantages over quantum dots: low cytotoxicity and high photostability. As certain cancerous cells (such as oral, ovarian, and breast) are enriched with folic acid (FA) receptors and they can internalize FA conjugated molecules, gold clusters have been functionalized with FA by EDC coupling of FA and BSA.[590] This biolabeled nanocluster has been used for cancer cell imaging, and it has been found that it can be an effective tool to identify cancer cells as the bright red luminescence (Figure 24c) appears only for clusters treated with cancer cells.

9.2.2. Biomedical Targeting. Integrating biocompatibility, stability, low toxicity, and specificity of targeting desired organs and cells in a material or molecules is a great challenge in biology. Gold clusters have shown their effectiveness in this field, too.[548] Sun et al.[591] have shown a controlled assembly of paired gold clusters within an apoferritin reactor which can be used for in vivo kidney targeting. Gold clusters were assembled at the ferroxidase active sites of ferritin heavy chain. These assembled clusters did not lose their intrinsic fluorescence property, but rather underwent an enhancement. As a result, these assemblies can also be used for in vitro and in vivo imaging. Several other groups have used luminescent gold nanoclusters as an effective targeting tool in biological applications.[384,548,592]

9.2.3. Other Biological Applications. Noble metal nanoclusters have been used in several other biological applications such as gene delivery,[593] imaging,[514,594,595] antibacterial activity,[21,596] etc.[548] In most cases, gold clusters have been chosen because of their high biocompatibility and low cytotoxicity, but silver shows higher antibacterial property than gold.[21] Silver ion leaching is the main reason behind their antibacterial nature.

9.3. SERS

Surface enhanced Raman spectroscopy (SERS) of noble metal nanoparticles,[597−601] superlattices, or other nanostructures have been studied extensively and various reports exist in the literature, but such reports are rare for ultrasmall nanoclusters. Chakraborty et al. have shown SERS from an atomically precise

$Ag_{152}(SR)_{60}$ cluster.[602] Several analytes such as crystal violet (CV), R_6G, and adenine were used, and they exhibited effective SERS on $Ag_{152}(SR)_{60}$ substrate with an enhancement factor of the order 10^9. For CV, the lower detection limit was 10^{-9} M. The cluster was drop cast on a glass slide, which was then used as the SERS substrate. Plasmon-like optical features, crystalline nature (of the individual nanoclusters and their assembly), and the absence of visible luminescence are the main reasons for this enhancement. It is noteworthy that this cluster can also be coated on cotton and paper, and simultaneously its SERS can be measured. Unprecedented enhancement of $Ag_{152}(SR)_{60}$ suggests a significant cost-saving associated with the use of these materials in comparison to typical silver nanoparticle systems composed of thousands of atoms.

9.4. Catalysis

Because of their high surface area, nanomaterials have proved to be effective in the field of catalysis.[603−643] Additionally, noble metal nanoclusters have unique core−shell structures and nonmetallic electronic properties which make them even more attractive and promising in this area.[644,645] Nanoclusters of size 1−2 nm exhibit strong quantum confinement effects that are important for nanocatalysis. With precise composition and well-defined structures, it is indeed possible to correlate the structural properties of these atomically precise entities with their catalytic properties. It is also possible to determine the active sites for the catalytic activity, which is important to explore the chemistry of a catalyst. Among the noble metals, gold shows enormous catalytic activity. Following the work by Haruta et al.[646,647] on ultrafine gold particles smaller than 10 nm, several studies investigated the catalytic activity of gold.[648,649] The area has been reviewed previously.[259,644,650−654]

The novelty of such nanoparticles or nanoclusters lies in two major factors: (a) high enhancement in efficiency due to high surface to volume ratio and (b) extreme control over selectivity by specific active sites. In general, there are two kinds of noble metal particle catalysts: unsupported (Figure 25a) and supported (Figure 25b). We will describe them briefly here, although there are several review articles focusing on the catalytic activity of noble metal nanoclusters.[260,655−658] To design a novel nanocluster catalyst, it is important for the cluster to have an exposed metal surface. As these clusters are usually protected by ligands, choosing an appropriate ligand is the key factor; the ligands will protect the cluster while allowing the exposed metal surface to interact with smaller molecules. Tsukuda et al.[656] have shown that gold clusters stabilized with polyvinylpyrrolidone (PVP) have high catalytic activity. From a detailed structural analysis using FTIR, XPS, and XANES, it was found that these clusters were negatively charged. Thus, PVP not only acts as a stabilizer but also modulates the electronic structure that affects the catalytic activity. Several oxidation reactions have been studied using these PVP protected gold clusters[656] whose details are summarized in Table 6.

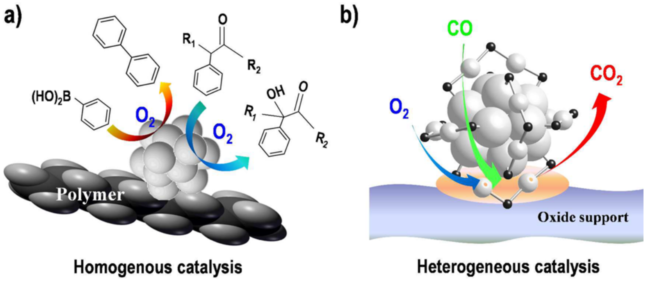

Figure 25. Schematic representation of homogeneous and heterogeneous catalysis by gold cluster. (a) Oxidation reactions catalyzed by Au@PVP clusters. (b) CO oxidation by Au_{25} cluster supported on a CeO_2 surface.

Supported heterogeneous catalysts have essentially two components: an active nanocluster and a support.[659] Usually, metal oxides or other powders are used as supports. Anchoring the cluster on its surface to prevent sintering during catalysis is the main role of the support. The preparation of such catalysts involves saturation of the metal oxide powder (support) in a cluster solution, followed by drying of the material and calcination at 350−1000 °C.[659] At this high temperature, the protecting ligands get removed from the cluster system and the bare clusters supported on the metal oxide are ready for catalysis reactions. Such supported catalysts have shown high catalytic activities for a range of oxidation and epoxidation reactions, as listed in Table 6.[659] Turner et al.[660] illustrated the catalytic activity of Au_{55} cluster for the selective oxidation of styrene by dioxygen. They proposed that initially the gold entities dissociatively chemisorb O_2 to yield O adatoms, which trigger the subsequent catalytic chemistry. Au_{11},[661] Au_{25},[361,662,663] $Ag_{7,8}$,[664] etc., also show catalytic activities under different conditions and for different reactions. Xie et al. developed Au_{25} and $PdAu_{24}$ cluster based catalysts supported on multiwalled carbon nanotubes (Figure 26).[663] Their study shows that single Pd atom doping can significantly improve the catalytic performance. Two possible mechanisms have been suggested for the Pd induced enhancement of catalytic performance. One could be the creation of highly active reaction sites by the Pd atom on the surface of Au_{24}, and the other is the activation of Au sites by Pd induced modulation of the electronic structure. Both of these mechanisms are well supported, with two other reports for the case of Pd incorporated gold particles[665] and Au incorporated Pd nanoparticles,[666] respectively. But here authors support the later one based on DFT structure analysis. As Pd atom was located inside the Au icosahedron, DFT study predicts[667] that electron transfer occurs from Pd to Au. Therefore, based on this structural model, Au sites in $PdAu_{24}$@CNT are more negative than Au_{25}@CNT.

Electron transfer from Pd for the case of $PdAu_{24}$@CNT helps to activate the oxygen more effectively, which results in increased catalytic performance compared to Au_{25}@CNT. Different groups[659,668−676] have addressed several such examples of catalytically active gold clusters in various articles and reviews, and a brief summary is listed in Table 6.

9.5. Solar Cells

Metal nanoclusters can also serve as effective photosensitizers that can be used for designing solar cells.[703] Chen et al.[24] named such solar cells as metal cluster sensitized solar cells (MCSCs). A glutathione protected gold cluster has been used as a sensitizer. The cluster shows bright orange luminescence (emitting at 600 nm), and it has an absorption feature near 400 nm. First, the mesoscopic films of TiO_2 were cast on fluorine-doped tin oxide (FTO) glass electrode, which was then immersed in the gold cluster solution for 48 h. Then the gold cluster modified TiO_2 electrode was sandwiched with a Pt-deposited FTO counter electrode. $Co(bpy)_3(PF_6)_2$/Co-

Table 6. Catalytic Performance of Selected Clusters[a]

cluster	average size	type of catalysis	support	type of catalytic reaction	ref
$Au_{25}(PET)_{18}$, $Au_{38}(PET)_{24}$, $Au_{144}(PET)_{60}$	1−2 nm	homogeneous	–	styrene oxidation, hydrogenation of aldehydes and ketones	655
Au@PVP	~1 nm	homogeneous	–	alcohol oxidation	414−416
Cu@(PAMAM−OH)	1.2 ± 0.3 nm	homogeneous	–	hydrogenation of carbonyl and olefin groups	677
$Au_{25}(PET)_{18}$	~1 nm	homogeneous	–	hydrogenation of cyclic ketone	678
$Au_{25}(PET)_{18}$	~1 nm	homogeneous	–	hydrogenation of aldehydes and ketones	645
AuAg@PVP	1.3−2.2 nm	homogeneous	–	alcohol oxidation	679
$Au_{11}Cl_3(PPh_3)_8$, $Au_{25}(PET)_{18}$, $Au_{55}(PPh_3)_{12}Cl_6$, $Au_{140}(S(CH_2)_5CH_3)_{53}$	0.8−1.7 nm	homogeneous	–	electroreduction of O_2	680
$Au_{25}(SG)_{18}$	~1 nm	homogeneous	–	electrooxidation of ascorbic acid	681
$Au_{25}(PET)_{18}$	~1 nm	homogeneous	–	electroreduction of CO_2 to CO	662
Au@PoPD	~3 nm	homogeneous	–	aerobic oxidation of alcohols	682
Au@THPC	2.0 ± 0.3 nm	homogeneous	–	aerobic oxidation of alcohols	683
Au@PS	1−2 nm	homogeneous	–	aerobic oxidation of alcohols	684
Au@PAA-1	2.4 ± 0.7 nm	homogeneous	–	aerobic oxidation of alcohols	685
Au@Poly(EOEOVE)	<4 nm	homogeneous	–	alcohol oxidation	686
Au@PNIPAM	2.6 ± 1.0 nm	homogeneous	–	aerobic oxidation of alcohols	687
Au@PVP	–	homogeneous	–	N-formylation of amines	688
Au@PVP	1.3 nm	homogeneous	–	oxygenation of benzylic ketones	689
Au@PVP	1.3 nm	homogeneous	–	oxidation of organoboron compounds	690
Au@PVP	1.3 nm	homogeneous	–	intramolecular addition of alcohols to alkenes	691
Au@PVP	1.3 nm	homogeneous	–	intramolecular addition of toluenesulfonamide	692
Au@PVP	1.3 nm	homogeneous	–	intramolecular addition reactions of primary amines	693
$Au_{38}(PET)_{24}$	1.1 nm	heterogeneous	CeO_2	CO oxidation	694
Au_n[b]	1−6 nm	heterogeneous	TiO_2	CO oxidation	695
$Au_{25}(SR)_{18}$[b]	~1 nm	heterogeneous	HAP	styrene oxidation	696
$Au_m(SG)_n$, (m, n) = (10, 10), (18, 14), (25, 18), and (39, 24)[b]	<2 nm	heterogeneous	HAP	cyclohexane oxidation	672
$Au_{38}(PET)_{24}$	~1.1 nm	heterogeneous	TiO_2, Fe_2O_3, and CeO_2	oxidation of sulfide to sulfoxide	697
$Au_{\sim 10}$[b]	~0.5 nm	heterogeneous	FeOOH	CO oxidation	698
$Au_{144}(PET)_{60}$[b]	1.67 ± 0.2 nm	heterogeneous	CuO−$mSiO_2$	CO oxidation	699
$Au_{25}(PET)_{18}$	~1 nm	heterogeneous	TiO_2, Fe_2O_3, and CeO_2	CO oxidation	23
$Pt_1Au_{24}(SC_2H_4)_{18}$	~1 nm	heterogeneous	TiO_2	styrene oxidation	199
$Pd_1Au_{24}(SC_2H_4)_{18}$[b]	~1 nm	heterogeneous	CNT	alcohol oxidation	663
Au_{11}@TPP[b]	0.8 ± 0.3 nm	heterogeneous	$mSiO_2$	alcohol oxidation	700
$Au_{55}(PPh_3)_{12}Cl_6$	~1.4 nm	heterogeneous	SiO_2	styrene oxidation	660
$Au_{25}(PET)_{18}$	~1 nm	heterogeneous	CeO_2	homocoupling of aryl iodides	701
$Au_{25}(SR)_{18}$	~1 nm	heterogeneous	TiO_2	photocatalytic degradation of methyl orange	702
$Ag_{7,8}(H_2MSA)_{7,8}$	<1 nm	heterogeneous	SiO_2, TiO_2, Fe_2O_3, and Al_2O_3	reduction of nitrophenol	664

[a] It is important to mention here that in many cases, the actual cluster is almost completely inactive. Only after removal of ligands shell, they will be active for catalysis. Such clusters where the ligand shell is removed are labeled with a. [b] The nature of the cluster core may be affected by ligand desorption.

$(bpy)_3(PF_6)_3$ was used as an electrolyte in the experiment. The photocurrent action spectrum shows the maximum incident photon to photocurrent efficiency (IPCE) of MCSC to be 70% (Figure 27) in the range 400−425 nm, which is relatively higher than the IPCE of glutathione protected Au_{25} cluster (5−15%) reported by the Tatsuma group.[704,705] The high IPCE value in the 400−425 nm region indicates the high efficiency of this system to convert the absorbed incident photons into electrical energy. Its quantum efficiency was closer to the IPCE value (80%) of a comparative quantum dot solar cell (QDSC) consisting of CdS/ZnS modified TiO_2 electrode (Figure 27).[706] The maximum power conversion efficiency (η) of MCSC was in the range 2.03−2.36%, similar to the value (2−3%) reported for QDSC.[707,708] The effectiveness of these MCSCs is because of the higher HOMO/LUMO energy gap and stronger interaction with TiO_2, which allows substantial electron injection. The role of Co(II)/Co(III) was to deliver a steady photocurrent. Recently, Abbas et al. have explored the cluster size effect on solar cell performance by selecting four differently sized gold clusters such as $Au_{10-12}(SR)_{10-12}$, $Au_{15}(SR)_{13}$,

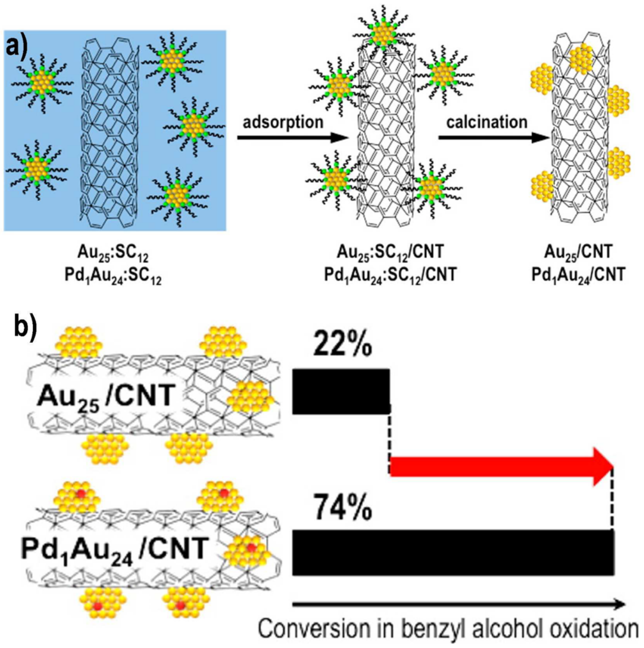

Figure 26. (a) Synthetic scheme of Au_{25}/CNT and $PdAu_{24}$/CNT catalyst. (b) Comparative conversion efficiency of two catalysts. Reprinted from ref 663. Copyright 2012 American Chemical Society.

$Au_{18}(SR)_{14}$, and $Au_{25}(SR)_{18}$, respectively. Among them, $Au_{18}(SR)_{14}$ shows a conversion efficiency of 3.8%.[709,710] This highlights the possibility of utilizing noble metal nanoclusters as sensitizers because of their wide range of photoabsorption capacity covering the entire visible window.

10. NEW MATERIALS

Nanomaterials in conjunction with other materials can give exotic properties. In this context, clusters embedded in soft and inorganic materials are a new addition. Attachment of clusters to nanoparticles has led to enhancement of the luminescence and associated properties of metals. Such properties in the context of mesostructures have enabled the development of fast-responding single particle sensors. Composite materials with graphene, gels, proteins, and oxides are known with varying properties from antimicrobial to catalytic effects. Current achievement in the area suggests the expansion of these materials into biological applications[711] and water purification.[712,713]

10.1. Graphene Composites

After C_{60} and nanotubes, graphene is perhaps the most exciting analogue of carbon, and it has been intensely explored in the recent past.[714−716] Creation of new materials using graphene is a fascinating area of research, and several nanocomposites have been made with graphene to incorporate diverse properties in a single system.[513] Chandrasekar and Pradeep[54] have illustrated the possibility of synthesizing a composite of graphene and silver clusters through covalent linkages (Figure 28a). Graphene, which contains carboxylic acid groups, was further functionalized to form thiolated graphene that was used in a ligand exchange reaction to generate the composite. The composite was purified by the phase transfer method. The optical properties of the composite exhibited the features of the cluster as well as graphene. Interestingly, the cluster fluorescence was only quenched when a high concentration of the thiolated graphene was used for the exchange process. A variety of nanocomposites can be generated by varying the functional groups, length, and properties of the linker molecules. Such composites can be used in several applications such as bioimaging,[717] biosensors,[718] antibacterial activity,[513] etc. Wang et al.[717] have shown the use of a transferrin functionalized gold cluster−graphene oxide nanocomposite for bioimaging of cancer cells (Figure 28b). In this system, transferrin acts as a reducing agent as well as a functional ligand for targeting the transferrin receptor. We believe that several such new materials can be developed in the future having implications in diverse fields.

10.2. Other Composites

Boron nitride sheets have drawn significant attention because of their graphene-like 2D layer structure. They also have high temperature stability, high mechanical strength, low dielectric

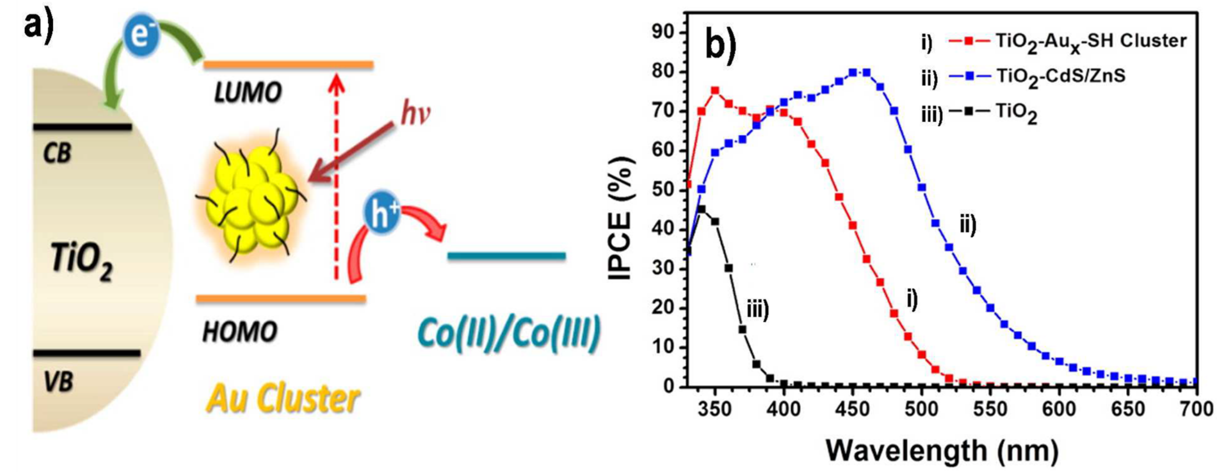

Figure 27. (a) Schematic view of the working principle of a metal cluster sensitized solar cell. (b) IPCE spectra (external quantum efficiency) of photoelectrochemical cell using photoanodes composed of (i) TiO_2-Au_x-SH cluster, (ii) TiO_2−CdS/ZnS, and (iii) TiO_2. Traces i and iii were recorded using 0.22 M $Co(bpy)_3(PF_6)_2$, 0.033 M $Co(bpy)_3(PF_6)_3$, 0.1 M $LiClO_4$, and 0.5 M 4-*tert*-butylpyridine in acetonitrile as electrolyte and Pt deposited on FTO as counter electrode. Trace ii was recorded using 2 M Na_2S and 2 M S in H_2O as electrolyte and Cu_2S-RGO film deposited on FTO as counter electrode. Reprinted from ref 24. Copyright 2013 American Chemical Society.

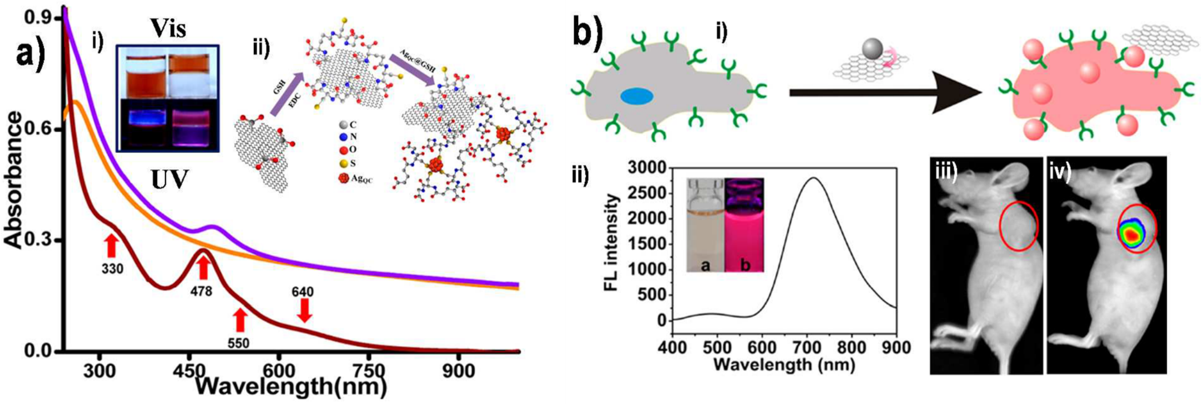

Figure 28. (a) UV/vis spectra of freshly prepared Ag nanoclusters in aqueous phase (brown trace), graphene−GSH (orange trace), and GRN−Ag nanocluster (violet trace). Inset i shows the photographs of the composite in water (left) and phase transfer to organic medium (right) under visible and UV light, respectively. Inset ii is the scheme of composite formation. Reprinted from ref 54. Copyright 2012 American Chemical Society. (b) Schematic of transferrin functionalized gold nanocluster−graphene oxide nanocomposite (i). Corresponding emission spectrum and photographs under visible and UV lights are given in (ii). Fluorescence imaging of HeLa tumor bearing mice (iv) and normal nude mice (iii). Reprinted from ref 717. Copyright 2013 American Chemical Society.

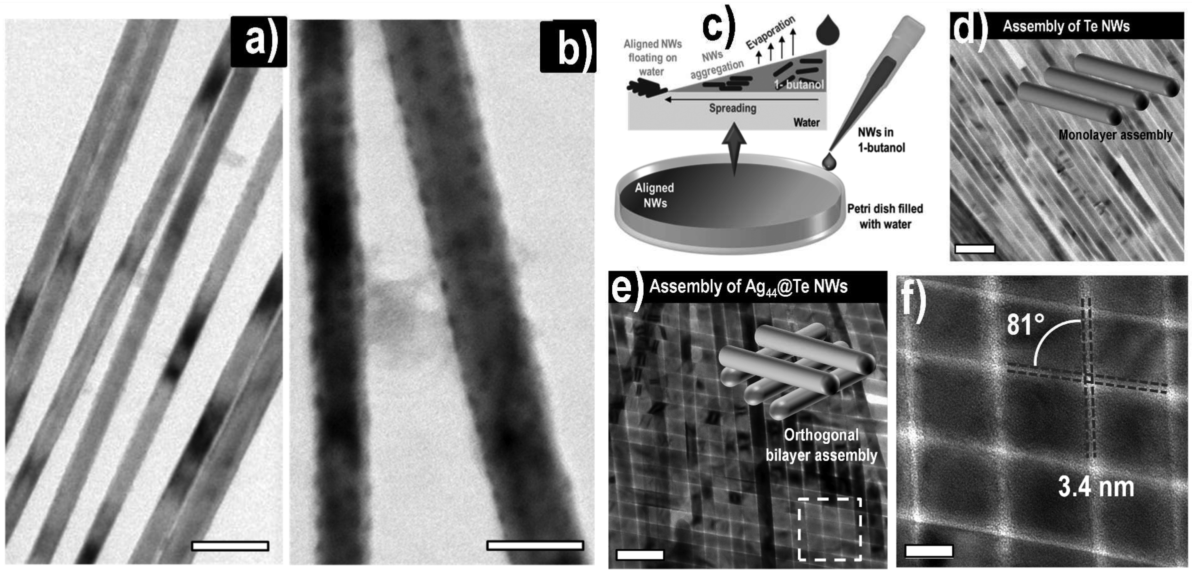

Figure 29. (a, b) TEM images of Ag_{44}@Te NWs at different magnifications. $Ag_{44}(SR)_{30}$ aggregates on the NW surface upon exposure to the electron beam are seen as nodules in (b). (c) Schematic illustration of the aligned NW assembly. Processes involved during the assembly formation are shown. (d) TEM image of the monolayer assembly formed at the air−water interface in the case of pristine Te NWs. A schematic of the oriented monolayer of Te NWs is shown in the inset. (e) TEM image of the crossed assembly formed with Ag_{44}@Te NWs for the same NW concentration as the pristine Te NWs. Schematic illustration of the crossed bilayer structure of the assembly, seen as a woven NW pattern in the TEM image, is shown in the inset. (f) Expanded view of the marked region in (e) showing uniform inter-NW distances (≈3.4 nm) for both the layers. Reprinted with permission from ref 721. Copyright 2016 John Wiley & Sons.

constant, and high thermal conductivity. Combining these properties of BN sheets with those of gold nanoclusters could lead to new composite systems with a potential for different applications. Yang et al.[719] prepared such composites by dispersing exfoliated BN sheets in poly diallyl-dimethylammonium chloride (PDDA) and then decorating the PDDA−BN sheets with orange luminescent gold nanoclusters (GNC). This composite was then used to immobilize antibody conjugates (Ab_2) to fabricate PDDA−BN−GNC−Ab2 bioconjugates used as fluorescence probes to detect interleukin-6 (IL-6). The PDDA−BN−GNC−Ab2 composite was then used as a biolabel for immunosensing using ITO chips. The limit of detection was found to be as low as 0.03 ng/mL.

Such composites can also be useful in drug delivery and diagnosis. George et al.[552] made a luminescent chitosan composite of gold cluster encapsulated in cyclodextrin for specific detection of Cu^{2+} ion. Mathew et al.[554] incorporated 15 atom BSA protected silver cluster on a silica coated gold mesoflower, which was then used as a fluorescence probe for sensing TNT. Details of these two systems have been discussed previously in section 9.1. Liu et al.[720] simultaneously determined ascorbic acid, dopamine, and uric acid via a graphene−multiwall carbon nanotube−gold nanocluster composite modified electrode.

In a recent report,[721] Som et al. have created Ag_{44}−Te nanowire (NW) composite materials which formed highly organized crossed bilayer assemblies at the air−water interface (Figure 29).[721]

Cluster attachment to the NWs was confirmed by electron microscopy studies of the Ag_{44}@Te NWs (Figure 29a,b). It is very difficult to identify individual $Ag_{44}(SR)_{30}$ clusters (as they do not produce enough contrast) in standard electron microscopy on a thick Te NW surface. However, existence of the cluster can be probed through TEM as high energy electron beam irradiation creates aggregation (Figure 29b). The cluster composite shows unusual orthogonal bilayer assembly at the air−water interface (Figure 29c,e). Note that only Te NWs show single layer assembly under the same condition (Figure 29d). This assembly has been directed through hydrogen bonding between the protecting ligand shells of $Ag_{44}(MBA)_{30}$ cluster anchored on NWs. Ag_{44} cluster layers remain sandwiched between two of the neighboring NWs at a constant distance which is dictated by the core size of the $Ag_{44}(SR)_{30}$ cluster (Figure 29f). On the other hand, orientation of the ligands in the space dictates the interlayer geometry. MBA protected Au_{102} cluster anchored on Te NWs also shows a similar assembly. Such bilayer assembly of the composite materials can be used for strain sensing.

11. OPTICAL CHIRALITY

Chirality has become an intensive research topic for nanoscale materials.[722−725] In clusters of the kind discussed here, chirality could arise because of the following four reasons: (i) ligands arrangement on the cluster surface, (ii) cis/trans isomerism in the bridged Au−S rings, (iii) inherent chirality of the cluster core, and (iv) chiral thiolate ligands.[722] Apart from the last one, which is investigated for several nanoparticles, others are important topics to explore and not many reports exist on them. Strong chiroptical properties of gold nanoclusters were observed first by Schaaff et al.[227] Since then several examples have been reported.[230,350,404,726−730] Optical chirality is typically probed with circular dichroism (CD)[230,404,727,729,731] and sometimes with vibrational circular dichroism (VCD),[726,732] along with NMR spectroscopy. Detection of the differential absorption of left- and right-circularly polarized light by a chiral sample is the basic principle of CD, whereas VCD is sensitive to the absolute configuration as well as the conformation of a chiral molecule in solution. Normally, achiral molecules or racemic mixtures do not show any VCD activity as, without a chiral environment, the two enantiomeric forms of the chiral conformation are equally abundant.[722] To explain the optical activity of these molecules, several models such as chiral footprint model,[727,733] intrinsic core chirality,[734,735] etc., have been proposed. Au_{34}^{-} and Au_{55} have been proposed to have inherent chiral cluster cores,[174,736−738] but it is very difficult to explore with CD as the structural distortion from symmetry is very small to be detected. X-ray diffraction and microscopic techniques[739−742] are very helpful in such cases; e.g. chiralities of $Au_{102}(SR)_{44}$[45] and $Au_{40}(SR)_{24}$[743] were seen through XRD. $Au_{38}(2\text{-PET})_{24}$ cluster is an example of clusters which show ligand arrangement induced chirality. $Au_{38}(SR)_{24}$[731] is a prolate shaped cluster containing a face fused bicosahedral Au_{23} core.[330] This core is further protected by six $Au_2(SR)_3$ and three $Au(SR)_2$ staple motifs. The bare core exists in D_{3h} symmetry, and the staples arrange in a chiral fashion to adopt D_3 symmetry which leads to chirality in the system because of their orientation.[20] The enantiomers can be separated through HPLC and examined by CD spectroscopy as seen in Figure 30.[20] Similar enantiomeric separation was reported for $Au_{40}(2\text{-PET})_{24}$[744] and $Au_{28}(TBBT)_{20}$ (TBBT = 4-*tert*-butylbenzenethiolate)[320] by chiral HPLC. For $Au_{102}(PMBA)_{44}$, the enantiomers were enriched during phase transfer with a chiral ammonium salt as phase transfer agent.[745] Chirality can also be induced to an achiral cluster through ligand exchange with chiral ligands.[746] Yao et al.[729,747] achieved chirality in monolayer protected silver clusters by introducing chiral thiols. Dolamic et al. have shown that an intrinsically chiral gold cluster, $Au_{38}(2\text{-PET})_{24}$ (2-PET = 2-phenylethylthiolate), can transfer its handedness to an achiral molecule (2-PET) adsorbed on its surface.[748] The cluster enantiomers show strong vibrational circular dichroism (VCD) signals in vibrations of the achiral adsorbate which could be due to the chirality transfer from the cluster to 2-PET.[748] The chirality in 2-PET arises because of the mirror symmetry breaking, which favors one enantiomer of a transiently chiral molecule. Such chirality transfer can play an important role in enantioselective chiral catalysis.

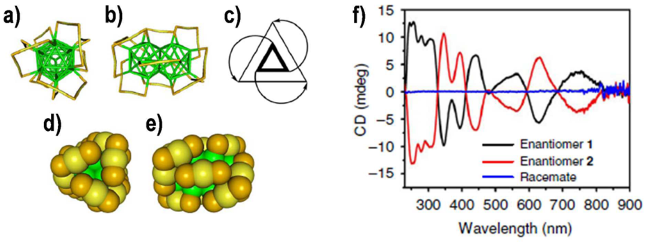

Figure 30. Crystal structure of the left-handed enantiomer of $Au_{38}(PET)_{24}$. (a) Top view of the cluster; (b) side view; (c) schematic representation highlighting the handedness of the cluster. The inner triangle represents the top three core atoms binding to the long staples. The arrows represent long staples, and the outer triangle represents the core Au atoms binding to the "end" of the staple. This representation is a top view along the C_3 axis, and the two triangles are not in one plane. (d) Top view in space-filling representation mode, (e) side view in space-filling representation mode. (f) CD spectra of isolated enantiomers 1 (black) and 2 (red) and the racemic $Au_{38}(PET)_{24}$ (blue), respectively. Reprinted with permission from ref 20. Copyright 2012 Nature Publishing Group.

12. SIMILAR STRUCTURES

Confinement in the subnanoscale occurs in several other systems. While similar structure exists in a range of materials such as zeolites, clathrates, metal organic frameworks (MOFs), etc., molecular clusters of similar nature exist in a few chemically similar systems. Metal hydrides are important analogues, hydrides can exist at the center of such metal clusters. A related category of materials exhibiting molecular cluster behavior is semiconductor quantum dots.

12.1. Hydride-Rich Silver Clusters

Generally these thiolated clusters are synthesized using a chemical reduction method in which the metal precursors, thiol, and $NaBH_4$ are mixed. It is important to see whether hydride ions can exist in the final clusters. To the best of our knowledge, there is no report in the literature on hydrido−gold clusters stabilized by thiol as it is extremely difficult to probe them with spectroscopy, but a few studies on Au(I)−hydrido complexes are known.[749,750] In the case of silver clusters, there are some reports of hydrido compounds stabilized by chalcogen donor ligands. These are believed to be intermediates in the formation of noble metal nanoclusters.

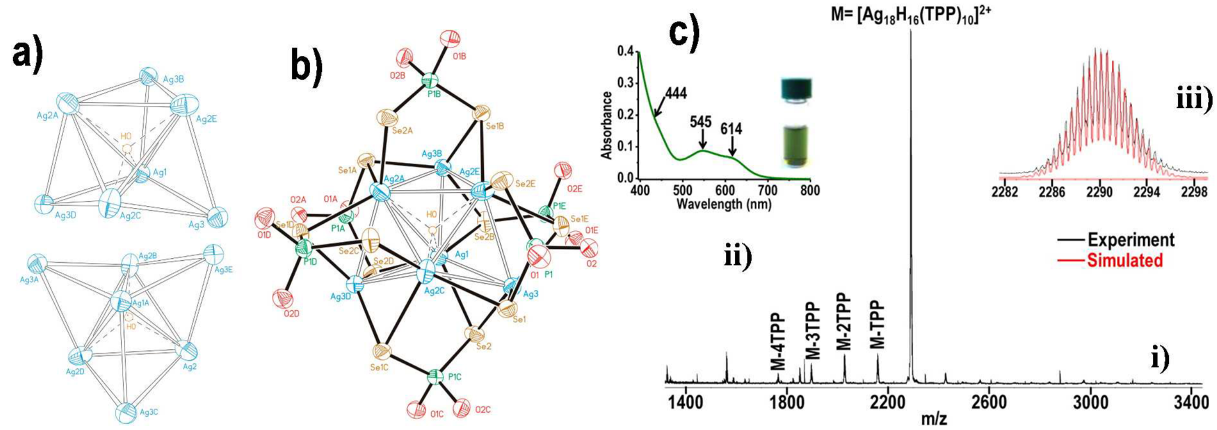

Figure 31. (a) Ag_7H core of the cluster disordered in two orientations (50% each). (b) Molecular structure of $[Ag_7(\mu_4{-}H)\ (Se_2P(O^iPr)_2)_6]$ (30% thermal ellipsoid) with isopropyl groups omitted for clarity. Reprinted from ref 751. Copyright 2013 American Chemical Society. (c) Characterization of $[Ag_{18}H_{16}(TPP)_{10}]^{2+}$ cluster. (i) Positive-mode ESI mass spectra of the cluster. Inset ii shows the corresponding UV/vis spectrum along with a photograph of the cluster in MeOH. Inset iii shows an expanded view of the molecular peak plotted with the corresponding simulated spectrum (red trace). Reprinted from ref 752. Copyright 2016 American Chemical Society.

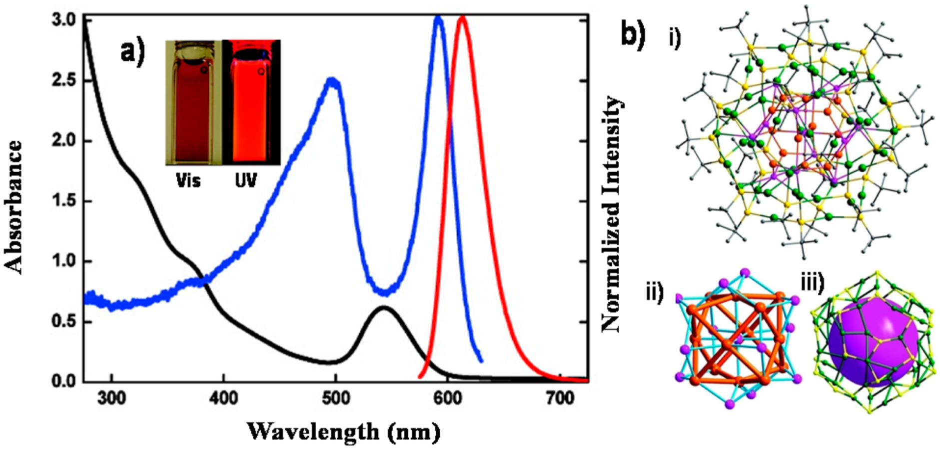

Figure 32. (a) Absorption (black trace), excitation (blue trace), and emission (red trace) spectra of the $[Ag_{62}S_{13}(SBu^t)_{32}](BF_4)_4$ cluster. Inset shows the corresponding photograph under visible and UV light. (b) Crystal structure of the silver sulfide cluster: (i) centrosymmetric structure of the cationic part of $[Ag_{62}S_{13}(SBu^t)_{32}](BF_4)_4$, (ii) $[Ag_{14}S_{13}]$ core configuration, and (iii) $Ag_{48}(SBu^t)_{32}$ shell structure. The $[Ag_{14}S_{13}]$ core and the *tert*-butyl groups have been omitted for clarity, and the artificial large purple sphere shows the inner space occupied by the $[Ag_{14}S_{13}]$ core. Color legend: orange, Ag (core); green, Ag (shell); purple, S^{2-}; yellow, S (thiolate); gray, C. Reprinted from ref 761. Copyright 2010 American Chemical Society.

Liu et al.[751] have shown an example of such intermediate silver clusters, $Ag_7(H)[E_2P(OR)_2]_6$, which can transform to nanoparticles later. Crystal structures of such hydride clusters have been solved with different ligands (E = S, Se and with different R). The cluster exhibits a tricapped tetrahedral Ag_7 skeleton, which is inscribed within an E_{12} icosahedron constituted by six dialkyl dichalcogenophosphate ligands in a tetrametallic-tetraconnective (μ_2, μ_2) bonding mode (Figure 31). In general such clusters are synthesized by the reduction of the precursor using $NaBH_4$.[753,754] The presence of a central hydride was probed by ^1H, ^2H, and ^{109}Ag NMR spectroscopies. Similar structures have also been found for Cu,[755−757] and they are used for H_2 production using solar energy.[758] Very recently, Bootharaju et al.[752] have synthesized three new hydride-rich silver clusters, namely $[Ag_{18}H_{16}(TPP)_{10}]^{2+}$, $[Ag_{25}H_{22}(DPPE)_8]^{3+}$, and $[Ag_{26}H_{22}(TFPP)_{13}]^{2+}$, using hydrides and different phosphines having single or multiple binding sites, such as triphenylphosphine (TPP), 1,2-bis-(diphenylphosphino)ethane [DPPE], and tris(4-fluorophenyl)-phosphine [TFPP], respectively. $NaBH_4$ was the source of hydride for all these clusters. The numbers of free electrons for these hydride-rich clusters have been calculated in the same way as mentioned in section 1. Hydrides are considered as electron withdrawing ligands (similar to thiols), and therefore, the numbers of free electrons for the above-mentioned three clusters ($[Ag_{18}H_{16}(TPP)_{10}]^{2+}$, $[Ag_{25}H_{22}(DPPE)_8]^{3+}$, and $[Ag_{26}H_{22}(TFPP)_{13}]^{2+}$) are 0 (18 − 16 − 2), 0 (25 − 22 − 3), and 2 (26 − 22 − 2), respectively (note that phosphines do not enter into the free electron count). The third one completes the electron-shell closing rule which explains its stability, whereas for the first two cases stability comes from the geometry. All of these clusters have distinct optical features (an example is given in Figure 31c, for the Ag_{18} cluster) and the first two cluster solutions have a unique green color similar to the "green gold" compound by Crasto et al.[759] The cluster assignments were done based on the HRESI MS data (Figure 31c) where the molecular peak comes with good isotropic distribution. Discovery of such hydride-rich metal clusters shows that smaller ligands can also act as protecting ligands, and many clusters can be revisited to see the existence of

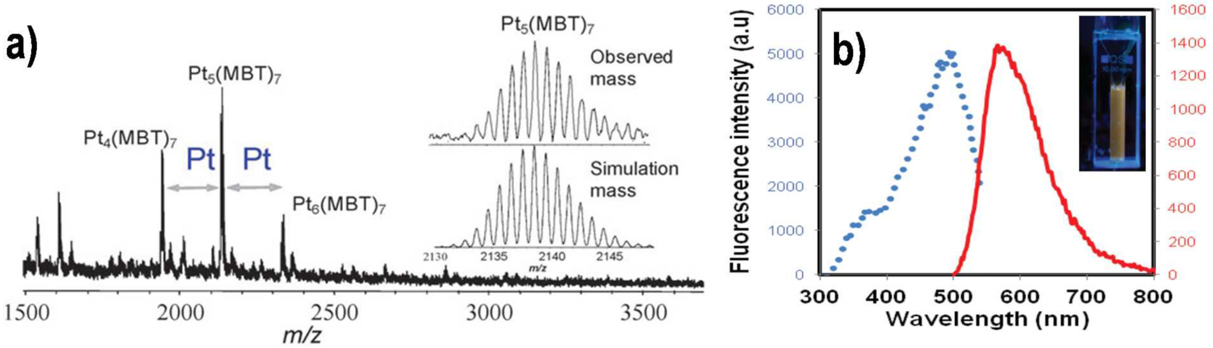

Figure 33. (a) MALDI mass spectrum of MBT-protected Pt nanoclusters in negative ion mode, obtained for DMF-protected Pt nanoclusters by ligand exchange with MBT. Inset shows the extended mass spectrum of $Pt_5(MBT)_7$ along with the corresponding calculated spectrum. Reprinted with permission from ref 775. Copyright 2010 Royal Society of Chemistry. (b) Excitation (dashed line) and emission (solid line) spectra of yellow-emitting Pt nanoclusters. Inset shows the photograph under UV irradiation (λ = 366 nm). Reprinted from ref 776. Copyright 2012 American Chemical Society.

hydride in the clusters, as in most of the cases $NaBH_4$ was used as the reducing agent. Buckart et al.[760] have shown an anomalous behavior of hydride in the case of gas phase gold clusters where hydride mimics gold. However, one should not get confused in making the electron count, considering the electrons of hydride, as chemistry in the solution phase and chemistry in the gas phase are completely different. Also, while dihydrogen was the source of hydrogen in the gas phase, borohydride was the only source of hydride in the solution.

12.2. Silver Sulfide Clusters

Monolayer protected silver sulfide clusters are another class of materials which have properties similar to those of the noble metal nanoclusters. Although very few articles are reported in the literature on this specific topic, these systems can give a deep insight into the metal sulfide chemistry. These materials are the smallest versions of quantum dots. They are atomically precise, while such characterization is usually not possible for quantum dots. Li et al.[761] deciphered the single crystal structure of an atomically precise silver sulfide nanocluster, $[Ag_{62}S_{13}(SBu^t)_{32}](BF_4)_4$, which also exhibited luminescence. The cluster was synthesized by heating three components: $AgBF_4$, H_2NNH_2, and $AgSBu^t$. The thiol acts not only as a protecting agent but also as a source of S^{2-} by the cleavage of the $-C-S$ bond.[761] The cluster displayed unique UV/vis features (bands in the UV regions and a low energy band at 543 nm) along with a sharp emission at 621 nm (when excited at 497 and 591 nm) (Figure 32a). The single crystal data suggested that the cluster possessed a core/shell geometry. It can be seen from Figure 32b that the core is made up of 14 Ag^+ ions and 13 sulfur ions. Eight of the 14 Ag^+ ions form a cubic structure, with the remaining six Ag^+ ions positioned at the center of the tetrasilver square faces (Figure 32b,ii). Out of the 13 sulfur atoms, one is at the center of the core and the remaining 12 are located on the 12 edges. This core is further surrounded by a $Ag_{48}(SBu^t)_{32}$ shell.[761] The Ag^+ in the shell can be classified into 36 surface ions and 12 subsurface ions. The thiolates can coordinate to three surface silver atoms or to one subsurface and two surface silver atoms. In another work, Li et al.[762] have reported a nest-like structure for the $[Ag_{33}S_3(SBu^t)_{16}(CF_3COO)_9(NO_3)(CH_3CN)_2](NO_3)$ cluster. Some of the other known examples of silver sulfide clusters are $Ag_{56}S_{12}(SBu^t)_{20}$],[763] $[Ag_{70}S_{20}(SPh)_{28}(dppm)_{10}](CF_3CO_2)_2$,[764] $[Ag_{123}S_{35}(SBu^t)_{50}]$,[765] $[Ag_{262}S_{100}(SBu^t)_{62}(dppp)_6]$,[764] $[Ag_{320}S_{130}(SBu^t)_{60}(dppp)_{12}]$,[766] $[Ag_{344}S_{124}(SBu^t)_{96}]$,[765] $[Ag_{352}S_{128}(S^tC_5H_{11})_{96}]$,[766] and $[Ag_{490}S_{188}(S^tC_5H_{11})_{114}]$.[766] Recently Manju et al. have reported a highly luminescent $Ag_{56}Se_{13}S_{15}$ cluster which shows Hg^{2+} detection at 1 ppb level.[767]

13. ATOMICALLY PRECISE Pt AND Pd CLUSTERS

So far, we have discussed mainly thiolated gold and silver clusters. In this section we will briefly describe nanoclusters of other noble metals such as Pd[768] and Pt.[193] Very few reports can be found for these metal nanoclusters. Their reduced stability (compared to gold) in the zero oxidation state makes it difficult to synthesize and characterize them. It is important to mention the early work of the Dahl group[769−771] on carbonyl protected Pd and Pt clusters, but in this section we are focusing largely on thiolated clusters. Apart from Pt and Pd clusters, only two reports exist for another noble metal, namely Ir.[772,773]

13.1. Platinum Clusters

Synthesis of monodispersed Pt nanoparticles began with the report of Kimura and Chen in 2001.[774] Kawasaki et al.[775] demonstrated the first surfactant-free solution phase synthesis of highly stable Pt nanoclusters. High temperature reduction in DMF was the key factor that led to the generation of this cluster. The assignment, $Pt_5(MBT)_7$, was made from the MALDI MS data of the ligand exchanged (with 2-mercaptobenzothiazole) cluster which showed an intense peak at m/z 2140. The experimental spectrum matched exactly with the corresponding calculated one (Figure 33a). Two other peaks seen on either side of the main peak were assigned as $Pt_6(MBT)_7$ and $Pt_4(MBT)_7$, respectively. Le Guével et al.[776] synthesized glutathione protected yellow emitting Pt nanoclusters, which showed emission at 570 nm (Figure 33b). Tanaka et al. used mercapto acetic acid protected blue emitting platinum nanoclusters for bioimaging of HeLa cells.[777] In the experiment, they labeled the cluster with chemokine receptors in living HeLa cells through a conjugated protein bound antibody. Yuan et al.[279] have demonstrated that reversible phase transfer can lead to blue emitting Pt nanoclusters. They also showed the effectiveness of this method for other metals such as Au, Ag, and Cu.[279] Chakraborty et al. have synthesized atomically precise blue emitting platinum clusters through the solid state route.[193] Mass spectral (both ESI and MALDI MS) characterization yielded an assignment of $Pt_{11}(BBS)_8$, where BBS refers to 4-*tert*-butylbenzyl mercaptan. The cluster was blue emitting with a QY of 3×10^{-3}, which is much smaller

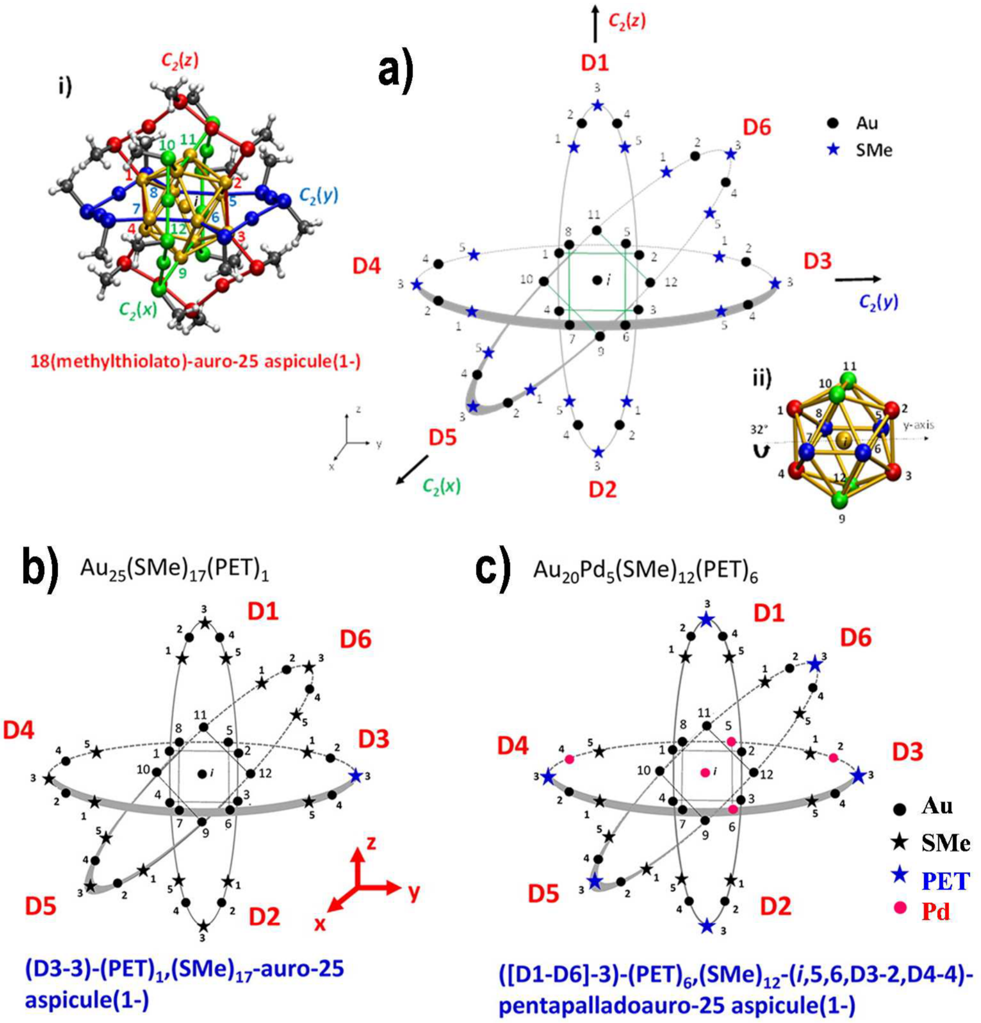

(D3-3)-(PET)$_1$,(SMe)$_{17}$-auro-25 aspicule(1-)

([D1-D6]-3)-(PET)$_6$,(SMe)$_{12}$-(*i*,5,6,D3-2,D4-4)-pentapalladoauro-25 aspicule(1-)

Figure 34. (a) Borromean rings diagram of $Au_{25}(SMe)_{18}$. The core Au atoms are numbered from 1 to 12, and the staple atoms are numbered clockwise from the end of the staple, from 1 to 5. The lines that join core Au atoms on opposite ends of the same staple are shown by the green lines. The staple directions are labeled by the six staple locants D1 to D6, marked in red. Inset i shows a 3D visualization of the ring structure of the core and staples of $Au_{25}(SR)_{18}$ aspicule, with each (Au_8S_6) ring consisting of two coplanar staples and the core atoms that are bonded to these staples. See that there are three distinct, interconnected Au_8S_6 rings in green (x axis), blue (y axis), and red (z axis). The R group used here is CH_3. Inset ii shows a close-up of the numbering scheme of the core atoms marked on the edge projection of the core icosahedron. Modifications of $Au_{25}(SMe)_{18}$ with ligand and metal atom substituents for the following cases: (b) a single bridging ligand (PET) exchange and (c) six bridging ligands and five metal (Pd) atoms exchanged (which is at present a hypothetical structure). Taken from ref 232. Copyright 2015 American Chemical Society.

than the cluster reported by Tanaka et al.[777] Besides the above-mentioned cases, there are also reports of other platinum nanoclusters.[778−784]

13.2. Palladium Clusters

For palladium, most of the reports are on nanoparticles, with TEM as the main characterization technique.[785−793] In many cases, the Pd nanoparticles were seen to have completely different structures than Au or Ag NPs.[794−796] An unusual sulfidized Pd layer was seen in between metallic core and thiolated shell. Corthey et al.[796] have explained the possible reason for such PdS layer formation in thiolated Pd nanoparticles. According to them, initial Pd(0) clusters, formed due to the reduction of Pd(II) species, are likely to be responsible for the S−C bond cleavage which leads to the formation of adsorbed sulfide. Once such a PdS layer formed, the clusters are still active for the adsorption of thiolate moieties but cannot decompose further, which results in the formation of Pd@PdS@SR type of nanoparticles. However, not many reports of Pd nanoclusters are there today to conclude the presence of such a PdS layer in between the metallic core and thiolate ligands. In 2001 Zamborini et al.[797] synthesized alkanethiolate protected Pd clusters and compared their reactivity, electrochemistry, and properties to those of the corresponding monolayer protected gold clusters. Their significant difference from Au MPCs drew the interest of other groups to work in this area. Negishi et al.[798] characterized thiolated Pd clusters via mass spectral analysis. Two major peaks corresponding to $Pd_5(SC_{18}H_{37})_{10}$ and $Pd_{10}(SC_{18}H_{37})_{12}$ were seen in the MALDI MS spectrum using anthracene as the matrix. The average cluster core diameter was found to be ~1 nm, consistent with the formula $Pd_n(SR)_m$, where $m = 0.6n$.[798] From the optical spectrum a band gap of ~2 eV was observed which showed the emergence of nonmetallic properties as a result of size reduction.[798]

14. NAMING AND STRUCTURAL UNDERSTANDING

The discussion presented suggests that cluster systems behave as (a) molecules with (b) constituent units such as ligands and cores retaining their limited individualities while (c) the integrated entity behaves as an independent molecular unit in properties and functions. The most important single aspect that comes out of these studies is that clusters of this type are molecules-in-molecules and each of the constituents is essential for the integrity of the whole. They may be regarded as molecules protected with molecules. A detailed analysis of clusters was made by Natarajan et al. to suggest the compound name *aspicule* for this class of systems which is derived by combining the Greek root word *aspis* meaning "shield" with *cule* of "molecule", meaning "shielded molecule", reflecting their chemical, physical, and material character.[232] This name is suggested with the realization that, without a proper name, the variety and complexity of chemistry being evolved cannot be captured. Imagine, for example, ligand exchange changing the composition of the cluster. With multiple ligands being exchanged at specific locations, there is a need to indicate the binding sites. Some of these clusters may be isomeric in terms of their positions. In order to name different isomeric structures uniquely, a systematic way of drawing these structures is needed. A set of rules for naming the clusters is essential. Such naming systems have been introduced already for fullerenes and boranes.

Aspicule nomenclature has been proposed for the three most common gold clusters, $Au_{25}(SR)_{18}$, $Au_{38}(SR)_{24}$, and $Au_{144}(SR)_{60}$, which may be extended further for other clusters. The structure of an aspicule may be represented as three concentric shells of atoms: (i) the protective shell of ligand R groups, (ii) an intermediate mantle, and (iii) the inner metal core. The most common geometry for the inner core is icosahedral due to its high stability. They have simplified the structural representation in the form of a diagram (Figure 34a) with unique positional labels (locants) for (i) the core atoms, (ii) the staples, (iii) the ligands, and (iv) the staple metal atoms. Among the several possible structural representations and labeling schemes for Au_{25}, a simple topological representation was found based on a projection of the three-ring structure of $Au_{25}(SR)_{18}$, with all of the essential atoms and the octahedral symmetry as depicted in Figure 35a.

For developing the aspicule nomenclature these four points were taken care of: (i) symmetry, (ii) universality and ability to describe the structure and/or modifications of any aspicule, (iii) resemblance to IUPAC nomenclature, and (iv) simplicity, enough to use and remember, even for such complex structures. The name for $Au_{25}(SMe)_{18}$ according to the "aspicule nomenclature" is 18(methylthiolato)-auro-25 aspicule(1−) or $(SMe)_{18}$-auro-25 aspicule(1−), in its condensed form. $Au_{25}(SMe)_{17}(PET)_1$, based on the locants of Figure 34b, which has the PET ligand exchanged at the bridging position 3 on the D3 staple, is (D3-3)-(2-phenylethanethiolato),17-(methylthiolato)-auro-25 aspicule(1−) or, in its condensed form, (D3-3)-$(PET)_1$,$(SMe)_{17}$-auro-25 aspicule(1−). Here D3-3 corresponds to the ligand exchanging position. Similarly, an alloy cluster such as $Au_{20}Pd_5(SMe)_{12}(PET)_6$ can have its aspicule name (Figure 34c) as ([D1−D6]-3)-hexa(2-phenylethanethiolato),dodeca(methylthiolato)-(*i*,5,6,D3-2,D4-4)-pentapalladoauro-25 aspicule(1−) or, in its shorter form, ([D1−D6]-3)-$(PET)_6$,$(SMe)_{12}$-(*i*,5,6,D3-2,D4-4)-pentapalladoauro-25 aspicule(1−). As can be seen, a variety of isomers for various ligand and metal positions are possible, and they can be presented and labeled. A recent report of Au_{25} dimer and its associated isomers[480] can easily be explained with this model structure.

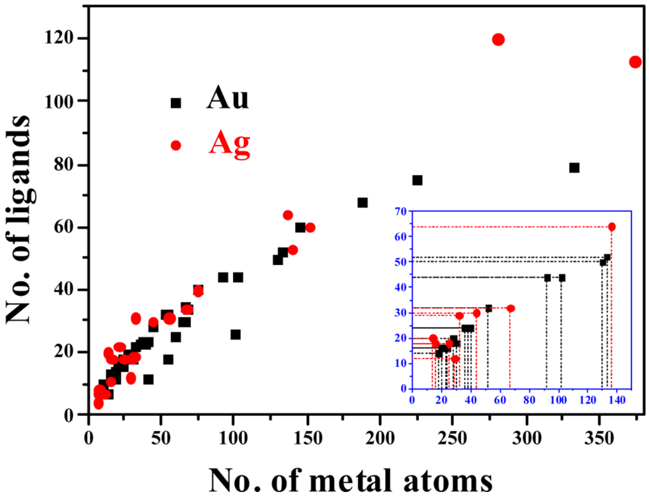

Figure 35. Plot of number of ligands with respect to the number of metal atoms for gold and silver clusters reported so far. Inset shows the same plot for clusters with crystal structures.

15. FUTURE PROSPECTS

The evolving interface of nanoparticles and clusters is being enriched by a large variety of molecular species with chemical diversity. Looking into the future, several avenues of unprecedented growth are evident. In the following, we attempt to capture some of these exciting areas.

15.1. New Synthetic Methodologies

Even though a wide series of gold clusters with different nuclearities have been synthesized so far (Figure 35), reports on silver clusters are limited and the list is just a handful for other noble metals. Significant improvement in synthetic methodology is needed in order to create variety in noble metal cluster science. It can also be extended to other metals such as Cu[211,758,799−801] and Fe.[802] Choice of ligands can solve the problem in many cases as can be seen in the recent reports. Tuning the thiol and phosphine ratios, use of carboxy and other oxy ligands for metals like Cu and Pd, use of hydride as ligand, etc., are important to consider.

15.2. Ligand Induced Properties

The metallic cores and the ligands, in part, add specific properties to the cluster system. Several of these properties are complementary, although integrated phenomena based on individual properties have not been explored adequately. The only phenomenon explored to some extent is FRET, which has been demonstrated in a few cases, in both ligand and protein protected clusters. Moving beyond, integration of other properties of the ligand and the core, enhancing electrical conductivity, magnetism, optical absorption, thermal conductivity, and catalysis may be explored.

15.3. Alloys

While early science of the complexity of the cluster core in terms of alloying is available, integration of cluster nuclei producing more complex multicluster systems is yet to evolve. One such possibility is cluster dimers and polymers which constitute new forms of architectures with unprecedented diversity. Such cluster building blocks may present new paradigms in materials science.

15.4. Hydride-Rich Clusters

Recently, isolation of several hydride-rich metal nanoclusters has shown that smaller ligands like H^- can also serve as protecting agents. In all of these cases, H^- comes from the very common reducing agent $NaBH_4$, which suggests a new direction of revisiting many of the clusters to check the existence of hydride in them. Such clusters may be possible with other metals, too. It will be interesting to have hydride-rich clusters as a potential candidate for hydrogen storage, although this appears to be an expensive and "heavy" proposition right now. Note that mass storage efficiency here is much lower than in materials such as magnesium hydrides.

15.5. Cluster Composites

The interface of inorganics and organics through clusters is another fascinating area. While there are many bioconjugates, the inherent advantages of clusters with luminescence, catalysis, and functionality, along with reduced sizes, provide new capabilities for chemical interactions, and the composites can access much smaller volumes than hitherto accessible by nanoparticles and can report on the events in the vicinity with better spatial accuracy. We hope that such new reports will change our understanding of biosystems significantly. In the case of inorganics, cluster conjugates with graphene and graphene analogues will be a new direction to pursue. Noble metal clusters can be conjugated with 2D chalcogenides and other quantum structures, using molecular linkers. These conjugate systems are likely to be novel ways of imparting properties to 2D sheets. The materials science of such conjugates will be a new direction forward. Some early directions in this context are available.[54]

15.6. Computational Approaches

The complex architecture being evolved will require new computational approaches. Early signs of such studies in cluster—virus interaction are seen in the recent past.[803] Precise understanding at still larger length scale may be feasible. Such studies are expected to point to newer interfaces in cluster science. Computations are essential to understand the events in clusters such as the early stages of intercluster reactions, which are impossible to capture today with the current level of instrumentation.

15.7. Stabilizing Cluster Luminescence

An important aspect of clusters is their luminescence. However, clusters have reduced stability. As a result, there is a need to protect them with appropriate shells with suitable functionality which allows their penetration into biological and other environments such as polymers, ceramics, etc. A possibility is silica protection, which has been examined some time ago.[804] However, such studies have not been continued. Properties get enhanced in confined environments, and this needs to be exploited.

15.8. Crystallization

Molecules of the kind described here have a distinct well-defined core with a precise number of ligands. There are plenty of clusters in terms of both gold and silver which have been reported recently. Among them, only a few have crystal structures. Therefore, it is important to develop new strategies to obtain crystals of most of the clusters. This is necessary for a detailed understanding of their structure, bonding, and properties. A comparison of the clusters reported so far and available crystal structures are presented in Figure 35. Gold and silver follow a similar trend, with a few exceptions. It is clear that there is ample room to discover new structures and the associated properties. One aspect requiring systematic investigation is the ease of forming crystals of the same core with chemically similar ligands. Multiple properties of ligands can be considered. Chemically constrained ligands such as calixarenes[805−807] have been considered with multiple thiols. Nonplanar thiols, dithiols, and such other systems will be of use in this context. New crystallization strategies such as electrocrystallization reported recently[808] may be extendable to other clusters.

Cluster crystals as materials have not been examined. While crystal structures have been looked at, studies have not gone beyond to determine the properties of crystals such as electrical conductivity, optical properties, temperature, pressure effects, etc. A rich area of cluster materials is yet to be explored.

15.9. Intercluster Reactions

Spontaneous reactions involving metal and ligand exchange and the new examples of isomorphous transformations[310] between clusters suggest that many new examples of this science are possible. In this process, it may be possible to create completely new clusters. Transformation of clusters from one to the other presents new examples of chemistry at the nanometer length scale. It is likely that these reactions produce new examples of nanochemistry.

15.10. Cluster Assembled Solids

Ligand protected clusters can be brought to the gas phase from solution, and they can be flown through in a gaseous stream. This suggests that protecting ligands can be removed, at least in some cases by thermal or photochemical processes. The resulting naked clusters could be new reagents as they are atomically precise and, in most cases, they will have only one type of cluster in comparison to many nuclearities that are formed in thermal or other evaporation processes. This naked cluster based synthesis of advanced materials would make the synthesis of cluster assembled porous solids possible. As clusters of this kind can be controlled by appropriate charges, their deposition can be controlled with electrical or magnetic means, allowing patterning. These cluster assembled films may be useful in creating photonic materials.

15.11. Clusters as New Molecules

The science of clusters is becoming analogous to that of molecules. Intercluster chemistry has shown several examples, and they suggest that the science of clusters is similar to that of simple molecules. Clusters with their cores and ligands act as single entities in these transformations. This new category of chemistry is distinctly different from that of the ligands and the cores which have been probed in more detail. Expansion of the area involving new clusters and reaction conditions will open up new areas of science. Ultimately these explorations could lead to new rules of cluster chemistry analogous to molecular science.

Applications of clusters in terms of sensors, solar cells, and bioimaging have appeared. However, potentially useful technologies which could impact industry have not come yet. These may happen, however, by combining properties of clusters with other novel materials such as 2D sheets, nanoparticles, and quantum dots.

In closing, it is clear that exploration of the science of clusters is expanding chemistry, materials science, and nanoscale phenomena. The properties of these systems will take their applications to biology, sensors, catalysis, and several areas of materials technology. Their emerging phenomena require new experimental and theoretical tools for detailed understanding. New synthetic chemistry is needed to discover unknown cluster systems. On the whole, a bright future is visible; some of the excitements on the horizon are likely to happen in the areas listed above, although we are aware that predictions are likely to reflect personal preferences.

ASSOCIATED CONTENT

Supporting Information

The Supporting Information is available free of charge on the ACS Publications website at DOI: 10.1021/acs.chemrev.6b00769.

> Table presenting summary of monolayer protected Au and Ag clusters, synthesized so far (PDF)

AUTHOR INFORMATION

Corresponding Author

*E-mail: pradeep@iitm.ac.in.

ORCID

Indranath Chakraborty: 0000-0003-4195-9384
Thalappil Pradeep: 0000-0003-3174-534X

Present Address

[†]I.C.: Department of Physics, Philipps University of Marburg, Marburg 35037, Germany.

Notes

The authors declare no competing financial interest.

Biographies

Indranath Chakraborty earned a Ph.D. in physical chemistry from the Indian Institute of Technology, Madras. He was an IIT Madras Institute Postdoctoral Fellow. Later, he was a postdoctoral research associate at the University of Illinois at Urbana−Champaign, IL, USA. Currently, he is an Alexander von Humboldt Postdoctoral Research Fellow at Philipps University of Marburg, Germany. His Ph.D. work has been on the formation, functionalization, and applications of atomically precise silver clusters. He has authored 28 scientific papers in journals and is an inventor in four patent applications. He is a recipient of the J. C. Bose Patent Award and the Malhotra Weikfield Foundation Nanoscience Fellowship Award.

Thalappil Pradeep is an institute professor at the Indian Institute of Technology Madras, Chennai, India. He is also the Deepak Parekh Institute Chair Professor and professor of chemistry. Besides the work on nanomaterials, he is involved in the development of affordable technologies for drinking water purification. His other interests are in ice chemistry, mass spectrometry, instrumentation, and business incubation. He is a fellow of all the science and engineering academies of India and is also a Fellow of the Royal Society of Chemistry. For more information, please see http://www.dstuns.iitm.ac.in/pradeep-research-group.php.

ACKNOWLEDGMENTS

Authors acknowledge funding from the Department of Science and Technology, Government of India. I.C. thanks IITM for research and a postdoctoral fellowship. I.C. thanks Sathi Roy for her help in formatting the references and suggestions.

ABBREVIATIONS

AAS	atomic absorption spectroscopy
AFM	atomic force microscopy
Apt-thrombin	27-Nt DNA aptamer
BSA	bovine serum albumin
CD	circular dichroism spectroscopy
Con A	concanavalin A
COSY	correlation spectroscopy
CV	cyclic voltammetry
DFT	density functional theory
DLS	dynamic light scattering
DNA-apt	DNA aptamer-templated
DPV	differential pulse voltammetry
DSC	differential scanning calorimetry
EIND-SH	1,1,3,3,5,5,7,7-octaethyl-*s*-hydrindacene-4-thio
ESI MS	electrospray ionization mass spectrometry
ET	energy transfer
EXAFS	extended X-ray absorption fine structure
FTIR	Fourier transform infrared spectroscopy
GST	glutathione *S*-transferase
HAADF	high angle annular dark field
hIgG	human immunoglobulin G
HPLC	high pressure liquid chromatography
MALDI MS	matrix assisted laser desorption ionization mass spectrometer
MUA	11-mercaptoundecanoic acid
NMR	nuclear magnetic resonance spectroscopy
OSWV	Osteryoung square wave voltammogram
PAGE	polyacrylamide gel electrophoresis
PAMAM	poly(amido) amine
PDGF AA	platelet-derived growth factor AA
PDOS	projected densities of states
PET	2-phenylethanethiol
PL	photoluminescence spectroscopy
SAXRD	small angle X-ray diffraction
SAXS	small angle X-ray scattering
SEC	size exclusion chromatography
SEM	scanning electron microscopy
STM	scanning tunneling microscopy
TDDFT	time dependent density-functional theory
TEM	transmission electron microscopy
Tg	thyroglobulin
TGA	thermogravimetric analysis
TOA	tetraoctylammonium bromide
UV/vis	ultraviolet−visible spectroscopy
XANES	X-ray near-edge absorption
XRD	X-ray diffraction

REFERENCES

(1) Murray, R. W. Nanoelectrochemistry: Metal Nanoparticles, Nanoelectrodes, and Nanopores. *Chem. Rev.* **2008**, *108*, 2688−720.

(2) Hühn, J.; Carrillo-Carrion, C.; Soliman, M. G.; Pfeiffer, C.; Valdeperez, D.; Masood, A.; Chakraborty, I.; Zhu, L.; Gallego, M.; Yue, Z.; et al. Selected Standard Protocols for the Synthesis, Phase Transfer, and Characterization of Inorganic Colloidal Nanoparticles. *Chem. Mater.* **2017**, *29*, 399−461.

(3) Daniel, M. C.; Astruc, D. Gold Nanoparticles: Assembly, Supramolecular Chemistry, Quantum-size-related Properties, and Applications Toward Biology, Catalysis, and Nanotechnology. *Chem. Rev.* **2004**, *104*, 293−346.

(4) Schmid, G. Large Clusters and Colloids. Metals in the Embryonic State. *Chem. Rev.* **1992**, *92*, 1709−1727.

(5) Aikens, C. M. Electronic Structure of Ligand-Passivated Gold and Silver Nanoclusters. *J. Phys. Chem. Lett.* **2011**, *2*, 99−104.

(6) Jin, R.; Zeng, C.; Zhou, M.; Chen, Y. Atomically Precise Colloidal Metal Nanoclusters and Nanoparticles: Fundamentals and Opportunities. *Chem. Rev.* **2016**, *116*, 10346−10413.

(7) Fernando, A.; Weerawardene, K. L. D. M.; Karimova, N. V.; Aikens, C. M. Quantum Mechanical Studies of Large Metal, Metal Oxide, and Metal Chalcogenide Nanoparticles and Clusters. *Chem. Rev.* **2015**, *115*, 6112−6216.

(8) Castleman, A. W.; Khanna, S. N. Clusters, Superatoms, and Building Blocks of New Materials. *J. Phys. Chem. C* **2009**, *113*, 2664−2675.

(9) Reveles, J. U.; Khanna, S. N.; Roach, P. J.; Castleman, A. W., Jr. Multiple Valence Superatoms. *Proc. Natl. Acad. Sci. U. S. A.* **2006**, *103*, 18405−18410.

(10) Walter, M.; Akola, J.; Lopez-Acevedo, O.; Jadzinsky, P. D.; Calero, G.; Ackerson, C. J.; Whetten, R. L.; Gronbeck, H.; Hakkinen, H. A Unified View of Ligand-Protected Gold Clusters as Superatom Complexes. *Proc. Natl. Acad. Sci. U. S. A.* **2008**, *105*, 9157−9162.

(11) Chakraborty, I.; Udayabhaskararao, T.; Pradeep, T. High Temperature Nucleation and Growth of Glutathione Protected ∼ Ag_{75} Clusters. *Chem. Commun.* **2012**, *48*, 6788−6790.

(12) Niihori, Y.; Matsuzaki, M.; Pradeep, T.; Negishi, Y. Separation of Precise Compositions of Noble Metal Clusters Protected with Mixed Ligands. *J. Am. Chem. Soc.* **2013**, *135*, 4946−4949.

(13) Kumar, S.; Bolan, M. D.; Bigioni, T. P. Glutathione-Stabilized Magic-Number Silver Cluster Compounds. *J. Am. Chem. Soc.* **2010**, *132*, 13141−13143.

(14) Udaya Bhaskara Rao, T.; Pradeep, T. Luminescent Ag_7 and Ag_8 Clusters by Interfacial Synthesis. *Angew. Chem., Int. Ed.* **2010**, *49*, 3925−3929.

(15) Heaven, M.; Dass, A.; White, P.; Holt, K.; Murray, R. Crystal Structure of the Gold Nanoparticle $[N(C_8H_{17})_4]$-$[Au_{25}(SCH_2CH_2Ph)_{18}]$. *J. Am. Chem. Soc.* **2008**, *130*, 3754−3755.

(16) Chakraborty, I.; Govindarajan, A.; Erusappan, J.; Ghosh, A.; Pradeep, T.; Yoon, B.; Whetten, R. L.; Landman, U. The Superstable 25 kDa Monolayer Protected Silver Nanoparticle: Measurements and Interpretation as an Icosahedral $Ag_{152}(SCH_2CH_2Ph)_{60}$ Cluster. *Nano Lett.* **2012**, *12*, 5861−5866.

(17) Udayabhaskararao, T.; Sun, Y.; Goswami, N.; Pal, S. K.; Balasubramanian, K.; Pradeep, T. Ag_7Au_6: A 13-Atom Alloy Quantum Cluster. *Angew. Chem., Int. Ed.* **2012**, *51*, 2155−2159.

(18) Nishigaki, J.-i.; Tsunoyama, R.; Tsunoyama, H.; Ichikuni, N.; Yamazoe, S.; Negishi, Y.; Ito, M.; Matsuo, T.; Tamao, K.; Tsukuda, T. A New Binding Motif of Sterically Demanding Thiolates on a Gold Cluster. *J. Am. Chem. Soc.* **2012**, *134*, 14295−14297.

(19) Yao, C.; Lin, Y.-j.; Yuan, J.; Liao, L.; Zhu, M.; Weng, L.-h.; Yang, J.; Wu, Z. Mono-cadmium vs Mono-mercury Doping of Au_{25} Nanoclusters. *J. Am. Chem. Soc.* **2015**, *137*, 15350−15353.

(20) Dolamic, I.; Knoppe, S.; Dass, A.; Bürgi, T. First Enantioseparation and Circular Dichroism Spectra of Au_{38} Clusters Protected by Achiral Ligands. *Nat. Commun.* **2012**, *3*, 798.

(21) Chakraborty, I.; Udayabhaskararao, T.; Deepesh, G. K.; Pradeep, T. Sunlight Mediated Synthesis and Antibacterial Properties of Monolayer Protected Silver Clusters. *J. Mater. Chem. B* **2013**, *1*, 4059−4064.

(22) Muhammed, M. A. H.; Verma, P. K.; Pal, S. K.; Kumar, R. C. A.; Paul, S.; Omkumar, R. V.; Pradeep, T. Bright, NIR-Emitting Au_{23} from Au_{25}: Characterization and Applications Including Biolabeling. *Chem. - Eur. J.* **2009**, *15*, 10110−10120.

(23) Nie, X.; Qian, H.; Ge, Q.; Xu, H.; Jin, R. CO Oxidation Catalyzed by Oxide-Supported $Au_{25}(SR)_{18}$ Nanoclusters and Identification of Perimeter Sites as Active Centers. *ACS Nano* **2012**, *6*, 6014−6022.

(24) Chen, Y.-S.; Choi, H.; Kamat, P. V. Metal-Cluster-Sensitized Solar Cells. A New Class of Thiolated Gold Sensitizers Delivering Efficiency Greater Than 2%. *J. Am. Chem. Soc.* **2013**, *135*, 8822−8825.

(25) Weissker, H. C.; Escobar, H. B.; Thanthirige, V. D.; Kwak, K.; Lee, D.; Ramakrishna, G.; Whetten, R. L.; López-Lozano, X. Information on Quantum States Pervades the Visible Spectrum of the Ubiquitous $Au_{144}(SR)_{60}$ Gold Nanocluster. *Nat. Commun.* **2014**, *5*, 3785.

(26) Bootharaju, M. S.; Joshi, C. P.; Parida, M. R.; Mohammed, O. F.; Bakr, O. M. Templated Atom-Precise Galvanic Synthesis and Structure Elucidation of a $[Ag_{24}Au(SR)_{18}]^-$ Nanocluster. *Angew. Chem.* **2016**, *128*, 934−938.

(27) Dass, A. Mass Spectrometric Identification of $Au_{68}(SR)_{34}$ Molecular Gold Nanoclusters with 34-Electron Shell Closing. *J. Am. Chem. Soc.* **2009**, *131*, 11666−11667.

(28) Guo, J.; Kumar, S.; Bolan, M.; Desireddy, A.; Bigioni, T. P.; Griffith, W. P. Mass Spectrometric Identification of Silver Nanoparticles: The Case of $Ag_{32}(SG)_{19}$. *Anal. Chem.* **2012**, *84*, 5304−5308.

(29) Harkness, K. M.; Cliffel, D. E.; McLean, J. A. Characterization of Thiolate-Protected Gold Nanoparticles by Mass Spectrometry. *Analyst* **2010**, *135*, 868−874.

(30) Harkness, K. M.; Tang, Y.; Dass, A.; Pan, J.; Kothalawala, N.; Reddy, V. J.; Cliffel, D. E.; Demeler, B.; Stellacci, F.; Bakr, O. M.; McLean, J. A. $Ag_{44}(SR)_{30}{}^{4-}$: a Silver-Thiolate Superatom Complex. *Nanoscale* **2012**, *4*, 4269−4274.

(31) Kumara, C.; Dass, A. AuAg Alloy Nanomolecules with 38 Metal Atoms. *Nanoscale* **2012**, *4*, 4084−4086.

(32) Mathew, A.; Sajanlal, P. R.; Pradeep, T. A Fifteen Atom Silver Cluster Confined in Bovine Serum Albumin. *J. Mater. Chem.* **2011**, *21*, 11205−11212.

(33) Qian, H.; Zhu, Y.; Jin, R. Atomically Precise Gold Nanocrystal Molecules with Surface Plasmon Resonance. *Proc. Natl. Acad. Sci. U. S. A.* **2012**, *109*, 696−700.

(34) Tsunoyama, R.; Tsunoyama, H.; Pannopard, P.; Limtrakul, J.; Tsukuda, T. MALDI Mass Analysis of 11 kDa Gold Clusters Protected by Octadecanethiolate Ligands. *J. Phys. Chem. C* **2010**, *114*, 16004−16009.

(35) Udayabhaskararao, T.; Bootharaju, M. S.; Pradeep, T. Thiolate-Protected Ag_{32} Clusters: Mass Spectral Studies of Composition and Insights into the Ag-Thiolate Structure from NMR. *Nanoscale* **2013**, *5*, 9404−9411.

(36) Chakraborty, I.; Kurashige, W.; Kanehira, K.; Gell, L.; Häkkinen, H.; Negishi, Y.; Pradeep, T. $Ag_{44}(SeR)_{30}$: A Hollow Cage Silver Cluster with Selenolate Protection. *J. Phys. Chem. Lett.* **2013**, *4*, 3351−3355.

(37) Rao, T. U. B.; Nataraju, B.; Pradeep, T. Ag_9 Quantum Cluster through a Solid-State Route. *J. Am. Chem. Soc.* **2010**, *132*, 16304−16307.

(38) Qian, H.; Zhu, M.; Wu, Z.; Jin, R. Quantum Sized Gold Nanoclusters with Atomic Precision. *Acc. Chem. Res.* **2012**, *45*, 1470−1479.

(39) Yang, H.; Lei, J.; Wu, B.; Wang, Y.; Zhou, M.; Xia, A.; Zheng, L.; Zheng, N. Crystal Structure of a Luminescent Thiolated Ag Nanocluster with an Octahedral $Ag_6{}^{4+}$ core. *Chem. Commun.* **2013**, *49*, 300−302.

(40) Yang, H.; Wang, Y.; Zheng, N. Stabilizing Subnanometer Ag(0) Nanoclusters by Thiolate and Diphosphine Ligands and their Crystal Structures. *Nanoscale* **2013**, *5*, 2674−2677.

(41) Zhu, M.; Aikens, C. M.; Hollander, F. J.; Schatz, G. C.; Jin, R. Correlating the Crystal Structure of A Thiol-Protected Au_{25} Cluster and Optical Properties. *J. Am. Chem. Soc.* **2008**, *130*, 5883−5885.

(42) Das, A.; Li, T.; Nobusada, K.; Zeng, Q.; Rosi, N. L.; Jin, R. Total Structure and Optical Properties of a Phosphine/Thiolate-Protected Au_{24} Nanocluster. *J. Am. Chem. Soc.* **2012**, *134*, 20286−20289.

(43) Zeng, C.; Qian, H.; Li, T.; Li, G.; Rosi, N. L.; Yoon, B.; Barnett, R. N.; Whetten, R. L.; Landman, U.; Jin, R. Total Structure and Electronic Properties of the Gold Nanocrystal $Au_{36}(SR)_{24}$. *Angew. Chem., Int. Ed.* **2012**, *51*, 13114−13118.

(44) Desireddy, A.; Conn, B. E.; Guo, J.; Yoon, B.; Barnett, R. N.; Monahan, B. M.; Kirschbaum, K.; Griffith, W. P.; Whetten, R. L.; Landman, U.; Bigioni, T. P. Ultrastable Silver Nanoparticles. *Nature* **2013**, *501*, 399−402.

(45) Jadzinsky, P. D.; Calero, G.; Ackerson, C. J.; Bushnell, D. A.; Kornberg, R. D. Structure of a Thiol Monolayer-Protected Gold Nanoparticle at 1.1 Å Resolution. *Science* **2007**, *318*, 430−433.

(46) Joshi, C. P.; Bootharaju, M. S.; Alhilaly, M. J.; Bakr, O. M. $[Ag_{25}(SR)_{18}]^-$: The "Golden" Silver Nanoparticle. *J. Am. Chem. Soc.* **2015**, *137*, 11578−11581.

(47) Shichibu, Y.; Negishi, Y.; Watanabe, T.; Chaki, N. K.; Kawaguchi, H.; Tsukuda, T. Biicosahedral Gold Clusters $[Au_{25}(PPh_3)_{10}(SC_nH_{2n+1})_5Cl_2]^{2+}$ (n = 2−18): A Stepping Stone to Cluster-Assembled Materials. *J. Phys. Chem. C* **2007**, *111*, 7845−7847.

(48) Udayabhaskararao, T.; Pradeep, T. New Protocols for the Synthesis of Stable Ag and Au Nanocluster Molecules. *J. Phys. Chem. Lett.* **2013**, *4*, 1553−1564.

(49) Yuan, X.; Luo, Z.; Yu, Y.; Yao, Q.; Xie, J. Luminescent Noble Metal Nanoclusters as an Emerging Optical Probe for Sensor Development. *Chem. - Asian J.* **2013**, *8*, 858−871.

(50) Goswami, N.; Zheng, K.; Xie, J. Bio-NCs - the Marriage of Ultrasmall Metal Nanoclusters with Biomolecules. *Nanoscale* **2014**, *6*, 13328−13347.

(51) Mathew, A.; Pradeep, T. Noble Metal Clusters: Applications in Energy, Environment, and Biology. *Part. Part. Sys. Charact.* **2014**, *31*, 1017−1053.

(52) Yang, X.; Wang, E. K. Synthesis and Applications of Silver Nanoclusters Protected by Polymers, Protein, Peptide and Short Molecules. *RSC Smart Mater.* **2014**, *7*, 100−130.

(53) Fang, J.; Zhang, B.; Yao, Q.; Yang, Y.; Xie, J.; Yan, N. Recent Advances in the Synthesis and Catalytic Applications of Ligand-Protected, Atomically Precise Metal Nanoclusters. *Coord. Chem. Rev.* **2016**, *322*, 1−29.

(54) Chandrasekar, A.; Pradeep, T. Luminescent Silver Clusters with Covalent Functionalization of Graphene. *J. Phys. Chem. C* **2012**, *116*, 14057−14061.

(55) Xavier, P. L.; Chaudhari, K.; Baksi, A.; Pradeep, T. Protein-Protected Luminescent Noble Metal Quantum Clusters: an Emerging Trend in Atomic Cluster Nanoscience. *Nano Rev.* **2012**, *3*, 14767−14782.

(56) Sankar, M. U.; Aigal, S.; Maliyekkal, S. M.; Chaudhary, A.; Anshup; Kumar, A. A.; Chaudhari, K.; Pradeep, T. Biopolymer-Reinforced Synthetic Granular Nanocomposites for Affordable Point-of-use Water Purification. *Proc. Natl. Acad. Sci. U. S. A.* **2013**, *110*, 8459−8464.

(57) Aikens, C. M. Modelling Small Gold and Silver Nanoparticles with Electronic Structure Methods. *Mol. Simul.* **2012**, *38*, 607−614.

(58) Arvizo, R. R.; Bhattacharyya, S.; Kudgus, R. A.; Giri, K.; Bhattacharya, R.; Mukherjee, P. Intrinsic Therapeutic Applications of Noble Metal Nanoparticles: Past, Present and Future. *Chem. Soc. Rev.* **2012**, *41*, 2943−2970.

(59) Azcarate, J. C.; Corthey, G.; Pensa, E.; Vericat, C.; Fonticelli, M. H.; Salvarezza, R. C.; Carro, P. Understanding the Surface Chemistry of Thiolate-Protected Metallic Nanoparticles. *J. Phys. Chem. Lett.* **2013**, *4*, 3127−3138.

(60) Bhattacharya, R.; Mukherjee, P. Biological Properties of "Naked" Metal Nanoparticles. *Adv. Drug Delivery Rev.* **2008**, *60*, 1289−1306.

(61) Chiu, T.-C.; Hu, C.-C. In *Biodetection Based on Resonance Light Scattering of Noble Metal Nanoparticles*; Pan Stanford Publishing Pte. Ltd.: 2012; pp 157−180.

(62) Eustis, S.; El-Sayed, M. A. Why Gold Nanoparticles are More Precious than Pretty Gold: Noble Metal Surface Plasmon Resonance and its Enhancement of the Radiative and nonradiative Properties of Nanocrystals of Different Shapes. *Chem. Soc. Rev.* **2006**, *35*, 209−217.

(63) Haes, A. J.; Stuart, D. A.; Nie, S.; Van Duyne, R. P. Using Solution-Phase Nanoparticles, Surface-Confined Nanoparticle Arrays and Single Nanoparticles as Biological Sensing Platforms. *J. Fluoresc.* **2004**, *14*, 355−367.

(64) Hough, R.; Reich, M.; Noble, R. In *Noble Metal Nanoparticles in Ore Systems*; Pan Stanford Publishing Pte. Ltd.: 2012; pp 141−167.

(65) Huang, X.; Jain, P. K.; El-Sayed, I. H.; El-Sayed, M. A. Gold Nanoparticles: Interesting Optical Properties and Recent Applications in Cancer Diagnostics and Therapy. *Nanomedicine* **2007**, *2*, 681−93.

(66) Huang, X.; Jain, P. K.; El-Sayed, I. H.; El-Sayed, M. A. Plasmonic Photothermal Therapy (PPTT) Using Gold Nanoparticles. *Lasers Med. Sci.* **2008**, *23*, 217−28.

(67) Jain, P. K.; Huang, X.; El-Sayed, I. H.; El-Sayed, M. A. Noble Metals on the Nanoscale: Optical and Photothermal Properties and Some Applications in Imaging, Sensing, Biology, and Medicine. *Acc. Chem. Res.* **2008**, *41*, 1578−1586.

(68) Jana, N. R. Gram-scale Synthesis of Soluble, Near-Monodisperse Gold Nanorods and Other Anisotropic Nanoparticles. *Small* **2005**, *1*, 875−882.

(69) Khlebtsov, N. G.; Dykman, L. A. Optical Properties and Biomedical Applications of Plasmonic Nanoparticles. *J. Quant. Spectrosc. Radiat. Transfer* **2010**, *111*, 1−35.

(70) Lin, H.-Y.; Huang, P.-J.; Huang, C.-H.; Wang, Y.-C.; Wang, C.-R. C. In *Synthesis and Optical Properties of Noble Metal Nanoparticles for Biodetection*; Pan Stanford Publishing Pte. Ltd.: 2012; pp 1−10.

(71) Liz-Marzan, L. M. Tailoring Surface Plasmons through the Morphology and Assembly of Metal Nanoparticles. *Langmuir* **2006**, *22*, 32−41.

(72) Nehl, C. L.; Hafner, J. H. Shape-Dependent Plasmon Resonances of Gold Nanoparticles. *J. Mater. Chem.* **2008**, *18*, 2415−2419.

(73) Long, N. V.; Yang, Y.; Teranishi, T.; Thi, C. M.; Cao, Y.; Nogami, M. Biomedical Applications of Advanced Multifunctional Magnetic Nanoparticles. *J. Nanosci. Nanotechnol.* **2015**, *15*, 10091−10107.

(74) Sarina, S.; Waclawik, E. R.; Zhu, H. Photocatalysis on Supported Gold and Silver Nanoparticles under Ultraviolet and Visible Light Irradiation. *Green Chem.* **2013**, *15*, 1814−1833.

(75) Shahbazali, E.; Hessel, V.; Noel, T.; Wang, Q. Metallic Nanoparticles Made in Flow and their Catalytic Applications in Organic Synthesis. *Nanotechnol. Rev.* **2014**, *3*, 65−86.

(76) Wu, L.; Reinhard, B. M. Probing Subdiffraction Limit Separations with Plasmon Coupling Microscopy: Concepts and Applications. *Chem. Soc. Rev.* **2014**, *43*, 3884−3897.

(77) Zhou, X.; Liu, G.; Yu, J.; Fan, W. Surface Plasmon Resonance-Mediated Photocatalysis by Noble Metal-Based Composites under Visible Light. *J. Mater. Chem.* **2012**, *22*, 21337−21354.

(78) Chiu-Lam, A.; Rinaldi, C. Nanoscale Thermal Phenomena in the Vicinity of Magnetic Nanoparticles in Alternating Magnetic Fields. *Adv. Funct. Mater.* **2016**, *26*, 3933−3941.

(79) Gao, Y.; Lim, J.; Teoh, S.-H.; Xu, C. Emerging Translational Research on Magnetic Nanoparticles for Regenerative Medicine. *Chem. Soc. Rev.* **2015**, *44*, 6306−6329.

(80) Kaewsaneha, C.; Tangboriboonrat, P.; Polpanich, D.; Elaissari, A. Multifunctional Fluorescent-Magnetic Polymeric Colloidal Particles: Preparations and Bioanalytical Applications. *ACS Appl. Mater. Interfaces* **2015**, *7*, 23373−23386.

(81) Lee, N.; Yoo, D.; Ling, D.; Cho, M. H.; Hyeon, T.; Cheon, J. Iron Oxide Based Nanoparticles for Multimodal Imaging and Magnetoresponsive Therapy. *Chem. Rev.* **2015**, *115*, 10637−10689.

(82) McNamara, K.; Tofail, S. A. M. Nanosystems: the Use of Nanoalloys, Metallic, Bimetallic, and Magnetic Nanoparticles in Biomedical Applications. *Phys. Chem. Chem. Phys.* **2015**, *17*, 27981−27995.

(83) Mendoza-Garcia, A.; Sun, S. Recent Advances in the High-Temperature Chemical Synthesis of Magnetic Nanoparticles. *Adv. Funct. Mater.* **2016**, *26*, 3809−3817.

(84) Moraes Silva, S.; Tavallaie, R.; Sandiford, L.; Tilley, R. D.; Gooding, J. J. Gold Coated Magnetic Nanoparticles: from Preparation to Surface Modification for Analytical and Biomedical Applications. *Chem. Commun.* **2016**, *52*, 7528−7540.

(85) Tokarev, A.; Yatvin, J.; Trotsenko, O.; Locklin, J.; Minko, S. Nanostructured Soft Matter with Magnetic Nanoparticles. *Adv. Funct. Mater.* **2016**, *26*, 3761−3782.

(86) Ulbrich, K.; Hola, K.; Subr, V.; Bakandritsos, A.; Tucek, J.; Zboril, R. Targeted Drug Delivery with Polymers and Magnetic Nanoparticles: Covalent and Noncovalent Approaches, Release Control, and Clinical Studies. *Chem. Rev.* **2016**, *116*, 5338−5431.

(87) Arvizo, R.; Bhattacharya, R.; Mukherjee, P. Gold Nanoparticles: Opportunities and Challenges in Nanomedicine. *Expert Opin. Drug Delivery* **2010**, *7*, 753−763.

(88) Dykman, L.; Khlebtsov, N. Gold Nanoparticles in Biomedical Applications: Recent Advances and Perspectives. *Chem. Soc. Rev.* **2012**, *41*, 2256−82.

(89) Sperling, R. A.; Rivera Gil, P.; Zhang, F.; Zanella, M.; Parak, W. J. Biological Applications of Gold Nanoparticles. *Chem. Soc. Rev.* **2008**, *37*, 1896−1908.

(90) Zeng, S.; Yong, K.-T.; Roy, I.; Dinh, X.-Q.; Yu, X.; Luan, F. A Review on Functionalized Gold Nanoparticles for Biosensing Applications. *Plasmonics* **2011**, *6*, 491−506.

(91) Hunt, L. B. The True Story of Purple of Cassius. *Gold Bull.* **1976**, *9*, 134−139.

(92) Sreeprasad, T.; Pradeep, T. Noble Metal Nanoparticles. In *Springer Handbook of Nanomaterials*; Vajtai, R., Ed.; Springer: Berlin, 2013; pp 303−388.

(93) Faraday, M. The Bakerian Lecture: Experimental Relations of Gold (and Other Metals) to Light. *Philosophical Transactions of the Royal Society of London* **1857**, *147*, 145−181.

(94) Pasteur, L. On the extension of the germ theory to the etiology of certain common diseases. *C. R. Acad. Sci. XC* **1880**, 1033−1044.

(95) Frens, G.; Overbeek, J. T. G. Carey Lea's Colloidal Silver. *Kolloid Z. Z. Polym.* **1969**, *233*, 922−929.

(96) Kim, J. S.; Kuk, E.; Yu, K. N.; Kim, J. H.; Park, S. J.; Lee, H. J.; Kim, S. H.; Park, Y. K.; Park, Y. H.; Hwang, C. Y.; Kim, Y. K.; Lee, Y. S.; Jeong, D. H.; Cho, M. H. Antimicrobial Effects of Silver Nanoparticles. *Nanomedicine* **2007**, *3*, 95−101.

(97) Pal, S.; Tak, Y. K.; Song, J. M. Does the Antibacterial Activity of Silver Nanoparticles Depend on the Shape of the Nanoparticle? A Study of the Gram-Negative Bacterium Escherichia coli. *Appl. Environ. Microbiol.* **2007**, *73*, 1712−1720.

(98) Shahverdi, A. R.; Fakhimi, A.; Shahverdi, H. R.; Minaian, S. Synthesis and Effect of Silver Nanoparticles on the Antibacterial Activity of Different Antibiotics Against Staphylococcus Aureus and Escherichia Coli. *Nanomedicine* **2007**, *3*, 168−171.

(99) Tolaymat, T. M.; El Badawy, A. M.; Genaidy, A.; Scheckel, K. G.; Luxton, T. P.; Suidan, M. An Evidence-based Environmental Perspective of Manufactured Silver Nanoparticle in SynthesIs and Applications: a Systematic Review and Critical Appraisal of Peer-reviewed Scientific Papers. *Sci. Total Environ.* **2010**, *408*, 999−1006.

(100) Corma, A.; Garcia, H. Supported Gold Nanoparticles as Catalysts for Organic Reactions. *Chem. Soc. Rev.* **2008**, *37*, 2096−2126.

(101) Stratakis, M.; Garcia, H. Catalysis by Supported Gold Nanoparticles: Beyond Aerobic Oxidative Processes. *Chem. Rev.* **2012**, *112*, 4469−4506.

(102) Pradeep, T. *Nano: The Essentials*; Tata McGraw-Hill Education: 2007.

(103) Kroto, H. W.; Heath, J. R.; O'Brien, S. C.; Curl, R. F.; Smalley, R. E. C_{60}: Buckminsterfullerene. *Nature* **1985**, *318*, 162−163.

(104) de Heer, W. A. The Physics of Simple Metal Clusters: Experimental Aspects and Simple Models. *Rev. Mod. Phys.* **1993**, *65*, 611−676.

(105) Cohen, M. L.; Chou, M. Y.; Knight, W. D.; De Heer, W. A. Physics of Metal Clusters. *J. Phys. Chem.* **1987**, *91*, 3141−3149.

(106) Castleman, A. W., Jr. *Studies of Gas-phase Clusters: Application to Nucleation and Aerosol Formation*; Pennsylvania State University: 1985; p 35.

(107) Castleman, A. W., Jr.; Keesee, R. G. Clusters: Properties and Formation. *Annu. Rev. Phys. Chem.* **1986**, *37*, 525−50.

(108) Chen, Z. Y.; Castleman, A. W., Jr. Growth of Titanium Nitride: from Clusters to Microcrystals. *J. Chem. Phys.* **1993**, *98*, 231−5.

(109) Kay, B. D.; Hermann, V.; Castleman, A. W., Jr. Studies of Gas Phase Clusters: the Solvation of Nitric Acid in Microscopic Aqueous Clusters. *Chem. Phys. Lett.* **1981**, *80*, 469−74.

(110) Kay, B. D.; Hofmann-Sievert, R.; Castleman, A. W., Jr. A Molecular Beam Clectric Deflection Study of Clusters: Acid and Salt Molecules in Microscopic Aqueous and Ammonia Clusters. *Chem. Phys.* **1986**, *102*, 407−15.

(111) Kimble, M. L.; Justes, D. R.; Moore, N. A.; Castleman, A. W., Jr. In *Elucidating Mechanistic Details of Catalytic Reactions Utilizing Gas Phase Clusters*; World Scientific Publishing Co. Pte. Ltd.: 2005; pp 127−134.

(112) Wisniewski, E. S.; Leskiw, B. D.; Hurley, S. M.; Dermota, T. E.; Hydutsky, D. P.; Knappenberger, K. L., Jr.; Hershberger, M. A.; Castleman, A. W., Jr. In *Dynamics of Gas Phase Clusters: Insights into Size and Solvation Effects on Electronic Relaxation and Hydrogen Transfer*; World Scientific Publishing Co. Pte. Ltd.: 2002; pp 21−41.

(113) Zemski, K. A.; Justes, D. R.; Castleman, A. W., Jr. Studies of Metal Oxide Clusters: Elucidating Reactive Sites Responsible for the Activity of Transition Metal Oxide Catalysts. *J. Phys. Chem. B* **2002**, *106*, 6136−6148.

(114) Ziemann, P. J.; Castleman, A. W., Jr. Stabilities and Structures of Gas-Phase Magnesium Oxide Clusters. *J. Chem. Phys.* **1991**, *94*, 718−28.

(115) Katakuse, I.; Ichihara, T.; Fujita, Y.; Matsuo, T.; Sakurai, T.; Matsuda, H. Mass Distributions of Copper, Silver and Gold Clusters and Electronic Shell Structure. *Int. J. Mass Spectrom. Ion Processes* **1985**, *67*, 229−236.

(116) Wurth, W.; Martins, M. Chapter 12 Electronic Structure and Magnetic Properties of Small Deposited Transition Metal Clusters. In *The Chemical Physics of Solid Surfaces*; Woodruff, D. P., Ed.; Elsevier: 2007; Vol. *12*, pp 471−485.

(117) Johnston, R. L. *Atomic and Molecular Clusters*; CRC Press: 2002. DOI: 10.1201/9781420055771.

(118) Baksi, A.; Pradeep, T.; Yoon, B.; Yannouleas, C.; Landman, U. Bare Clusters Derived from Protein Templates: $Au_{25}{}^{+}$, $Au_{38}{}^{+}$ and $Au_{102}{}^{+}$. *ChemPhysChem* **2013**, *14*, 1272−1282.

(119) Baksi, A.; Pradeep, T. Noble Metal Alloy Clusters in the Gas Phase Derived from Protein Templates: Unusual Recognition of Palladium by Gold. *Nanoscale* **2013**, *5*, 12245−12254.

(120) Häkkinen, H.; Abbet, S.; Sanchez, A.; Heiz, U.; Landman, U. Structural, Electronic, and Impurity-Doping Effects in Nanoscale Chemistry: Supported Gold Nanoclusters. *Angew. Chem., Int. Ed.* **2003**, *42*, 1297−1300.

(121) Arenz, M.; Landman, U.; Heiz, U. CO Combustion on Supported Gold Clusters. *ChemPhysChem* **2006**, *7*, 1871−1879.

(122) Harding, C.; Habibpour, V.; Kunz, S.; Farnbacher, A. N.-S.; Heiz, U.; Yoon, B.; Landman, U. Control and Manipulation of Gold Nanocatalysis: Effects of Metal Oxide Support Thickness and Composition. *J. Am. Chem. Soc.* **2009**, *131*, 538−548.

(123) Abbet, S.; Heiz, U.; Häkkinen, H.; Landman, U. CO Oxidation on a Single Pd Atom Supported on Magnesia. *Phys. Rev. Lett.* **2001**, *86*, 5950−5953.

(124) Liu, C.; Yang, B.; Tyo, E.; Seifert, S.; DeBartolo, J.; von Issendorff, B.; Zapol, P.; Vajda, S.; Curtiss, L. A. Carbon Dioxide Conversion to Methanol over Size-Selected Cu_4 Clusters at Low Pressures. *J. Am. Chem. Soc.* **2015**, *137*, 8676−8679.

(125) Tyo, E. C.; Vajda, S. Catalysis by Clusters with Precise Numbers of Atoms. *Nat. Nanotechnol.* **2015**, *10*, 577−588.

(126) Vajda, S.; White, M. G. Catalysis Applications of Size-Selected Cluster Deposition. *ACS Catal.* **2015**, *5*, 7152−7176.

(127) Lu, J.; Cheng, L.; Lau, K. C.; Tyo, E.; Luo, X.; Wen, J.; Miller, D.; Assary, R. S.; Wang, H.-H.; Redfern, P.; Wu, H.; Park, J.-B.; Sun, Y.-K.; Vajda, S.; Amine, K.; Curtiss, L. A. Effect of the Size-Selective Silver Clusters on Lithium Peroxide Morphology in Lithium−Oxygen batteries. *Nat. Commun.* **2014**, *5*, 4895.

(128) Turkevich, J.; Stevenson, P. C.; Hillier, J. A Study of the Nucleation and Growth Processes in the Synthesis of Colloidal Gold. *Discuss. Faraday Soc.* **1951**, *11*, 55−75.

(129) Albano, V. G.; Bellon, P. L.; Manassero, M.; Sansoni, M. Intermetallic Pattern in Metal-Atom Clusters. Structural Studies on $Au_{11}X_3(PR_3)_7$ Species. *J. Chem. Soc. D* **1970**, 1210−1211.

(130) Briant, C. E.; Theobald, B. R. C.; White, J. W.; Bell, L. K.; Mingos, D. M. P.; Welch, A. J. Synthesis and X-ray Structural Characterization of the Centred Icosahedral Gold Cluster Compound $[Au_{13}(PMe_2Ph)_{10}Cl_2](PF_6)_3$; the Realization of a Theoretical Prediction. *J. Chem. Soc., Chem. Commun.* **1981**, 201−202.

(131) Copley, R. C. B.; Mingos, D. M. P. Synthesis and Characterization of the Centred Icosahedral Cluster Series $[Au_9MIB_4Cl_4(PMePh_2)_8][C_2B_9H_{12}]$, where MIB= Au, Ag or Cu. *J. Chem. Soc., Dalton Trans.* **1996**, 491−500.

(132) Frens, G. Particle Size and Sol Stability in Metal Colloids. *Kolloid Z. Z. Polym.* **1972**, *250*, 736−741.

(133) McPartlin, M.; Mason, R.; Malatesta, L. Novel Cluster Complexes of Gold(0)-Gold(I). *J. Chem. Soc. D* **1969**, *0*, 334−334.

(134) Bellon, P.; Manassero, M.; Sansoni, M. Crystal and Molecular Structure of Tri-iodoheptakis(tri-p-fluorophenylphosphine)-undecagold. *J. Chem. Soc., Dalton Trans.* **1972**, 1481−1487.

(135) Briant, O. E.; Hall, K. P.; Mingos, D. M. P. Unusual Degradation Reaction of Icosahedral Cluster Compounds of Gold with Chelating Diphosphanes and the X-ray Structure of dis-(dephenylphosphino)methanido-digold(I), $\{Au(Ph_2P)_2CH\}_2$. *J. Organomet. Chem.* **1982**, *229*, C5−C8.

(136) Demartin, F.; Manassero, M.; Naldini, L.; Ruggeri, R.; Sansoni, M. Synthesis and X-ray Characterization of an Iodine-bridged Tetranuclear Gold Cluster, di-[small micro]-iodo-tetrakis-(triphenylphosphine)-tetrahedro-tetragold. *J. Chem. Soc., Chem. Commun.* **1981**, 222−223.

(137) van der Velden, J. W. A.; Bour, J. J.; Vollenbroek, F. A.; Beurskens, P. T.; Smits, J. M. M. Synthesis of a New Pentanuclear Gold cluster by Metal Evaporation. Preparation and X-ray structure Determination of [tris{bis(diphenylphosphino)methane}][bis-(diphenylphosphino)methanido]pentagold Dinitrate. *J. Chem. Soc., Chem. Commun.* **1979**, 1162−1163.

(138) Briant, C. E.; Hall, K. P.; Mingos, D. M. P. Synthesis and Structural Characterisation of $[Au_6(PPh_3)_6]^-$ $(NO_3)_2{\cdot}3CH_2Cl_2$; an Edge-shared Bitetrahedral Gold Cluster. *J. Organomet. Chem.* **1983**, *254*, C18−C20.

(139) Briant, C. E.; Hall, K. P.; Mingos, D. M. P.; Wheeler, A. C. Synthesis and Structural Characterisation of Hexakis(triphenyl phosphine)hexagold(2+) nitrate, $[Au_6(PPh_3)_6][NO_3]_2$, and Related Clusters with Edgesharing Bitetrahedral Geometries. *J. Chem. Soc., Dalton Trans.* **1986**, 687−692.

(140) Van der Velden, J. W. A.; Beurskens, P. T.; Bour, J. J.; Bosman, W. P.; Noordik, J. H.; Kolenbrander, M.; Buskes, J. A. K. M. Intermediates in the Formation of Gold Clusters. Preparation and X-ray Analysis of $[Au_7(PPh_3)_7]^+$ and Synthesis and Characterization of $[Au_8(PPh_3)_6I]PF_6$. *Inorg. Chem.* **1984**, *23*, 146−151.

(141) Weinberger, D. S.; Melaimi, M.; Moore, C. E.; Rheingold, A. L.; Frenking, G.; Jerabek, P.; Bertrand, G. Isolation of Neutral Mono- and Dinuclear Gold Complexes of Cyclic (Alkyl) (amino)carbenes. *Angew. Chem., Int. Ed.* **2013**, *52*, 8964−8967.

(142) Zeller, E.; Beruda, H.; Schmidbaur, H. Tetrahedral Gold Cluster $[Au_4]^{2+}$: Crystal structure of $[(tert\text{-}Bu)_3PAu]_4(BF_4^-)_2.2CHCl_3$. *Inorg. Chem.* **1993**, *32*, 3203−3204.

(143) van der Velden, J. W. A.; Bour, J. J.; Bosman, W. P.; Noordik, J. H. Synthesis and X-ray Crystal Structure Determination of the Cationic Gold Cluster Compound $[Au_8(PPh_3)_7](NO_3)_2$. *J. Chem. Soc., Chem. Commun.* **1981**, 1218−1219.

(144) Bellon, P. L.; Cariati, F.; Manassero, M.; Naldini, L.; Sansoni, M. Novel Gold clusters. Preparation, Properties, and X-ray Structure Determination of Salts of octakis(triarylphosphine)enneagold, $[Au_9L_8]X_3$. *J. Chem. Soc. D* **1971**, 1423−1424.

(145) Briant, C. E.; Hall, K. P.; Wheeler, A. C.; Mingos, D. M. P. Structural Characterisation of $[Au_{10}Cl_3(PCy_2Ph)_6](NO_3)$ (Cy = cyclohexyl) and the Development of a Structural Principle for High Nuclearity Gold Clusters. *J. Chem. Soc., Chem. Commun.* **1984**, 248−250.

(146) van der Velden, J. W. A.; Vollenbroek, F. A.; Bour, J. J.; Beurskens, P. T.; Smits, J. M. M.; Bosnian, W. P. Gold Clusters Containing Bidentate Phosphine Ligands. Preparation and X-Ray Structure Investigation of $[Au_5(dppmH)_3(dppm)](NO_3)_2$ and $[Au_{13}(dppmH)_6](NO_3)_n$. *Recueil des Travaux Chimiques des Pays-Bas* **1981**, *100*, 148−152.

(147) Arratia-Perez, R.; Hernandez-Acevedo, L. Relativistic Electronic Structure of an Icosahedral $Au_{12}Pd$ cluster. *Chem. Phys. Lett.* **1999**, *303*, 641−648.

(148) Li, J.; Wang, S.-G. Phosphane-Stabilized Gold Clusters: Investigation of the Stability of $[Au_{13}(PMe_2Ph)_{10}Cl_2]^{3+}$. *J. Mol. Model.* **2010**, *16*, 505−512.

(149) Shafai, G.; Hong, S.; Bertino, M.; Rahman, T. S. Effect of Ligands on the Geometric and Electronic Structure of Au_{13} Clusters. *J. Phys. Chem. C* **2009**, *113*, 12072−12078.

(150) Shichibu, Y.; Suzuki, K.; Konishi, K. Facile Synthesis and Optical Properties of Magic-Number Au_{13} Clusters. *Nanoscale* **2012**, *4*, 4125−4129.

(151) Shichibu, Y.; Konishi, K. HCl-Induced Nuclearity Convergence in Diphosphine-Protected Ultrasmall Gold Clusters: A Novel Synthetic Route to "Magic-Number" Au_{13} Clusters. *Small* **2010**, *6*, 1216−1220.

(152) Chen, J.; Zhang, Q.-F.; Williard, P. G.; Wang, L.-S. Synthesis and Structure Determination of a New Au_{20} Nanocluster Protected by Tripodal Tetraphosphine Ligands. *Inorg. Chem.* **2014**, *53*, 3932−3934.

(153) Teo, B. K.; Shi, X.; Zhang, H. Pure Gold Cluster of 1:9:9:1:9:9:1 Layered Structure: a Novel 39-Metal-Atom Cluster $[(Ph_3P)_{14}Au_{39}Cl_6]Cl_2$ with an Interstitial Gold Atom in a Hexagonal Antiprismatic Cage. *J. Am. Chem. Soc.* **1992**, *114*, 2743−2745.

(154) Teo, B. K.; Zhang, H.; Shi, X. Molecular Architecture of a Novel Vertex-Sharing Biicosahedral Cluster $[(p\text{-}Tol_3P)_{10}Au_{13}Ag_{12}Br_8]$-$(PF_6)$ Containing a Staggered-Staggered-Staggered Configuration for the 25-Atom Metal Framework. *Inorg. Chem.* **1990**, *29*, 2083−2091.

(155) Teo, B. K.; Zhang, H.; Shi, X. Cluster of Clusters: a Modular Approach to Large Metal Clusters. Structural Characterization of a 38-atom Cluster $[(p\text{-}Tol_3P)_{12}Au_{18}Ag_{20}Cl_{14}]$ Based on Vertex-sharing Triicosahedra. *J. Am. Chem. Soc.* **1990**, *112*, 8552−8562.

(156) Teo, B. K.; Zhang, H.; Shi, X. Site Preference in Vertex-Sharing Polyicosahedral Supraclusters Containing Groups 10 and 11 Metals and Their Bonding Implications: Syntheses and Structures of the First Au-Ag-M (M = Pt, Ni) Biicosahedral Clusters $[(Ph_3P)_{10}Au_{12}Ag_{12}PtC_{17}]Cl$ and $[(Ph_3P)_{10}Au_{12}Ag_{12}NiCl_7](SbF_6)$. *Inorg. Chem.* **1994**, *33*, 4086−4097.

(157) Schmid, G.; Pugin, R.; Meyer-Zaika, W.; Simon, U. Clusters on Clusters: closo-Dodecaborate as a Ligand for Au_{55} Clusters. *Eur. J. Inorg. Chem.* **1999**, *1999*, 2051−2055.

(158) Maoz, R.; Cohen, S. R.; Sagiv, J. Nanoelectrochemical Patterning of Monolayer Surfaces: Toward Spatially Defined Self-Assembly of Nanostructures. *Adv. Mater.* **1999**, *11*, 55−61.

(159) Vidoni, O.; Reuter, T.; Torma, V.; Meyer-Zaika, W.; Schmid, G. Quasi One-Dimensional Gold Cluster Arrangements. *J. Mater. Chem.* **2001**, *11*, 3188−3190.

(160) Schmid, G.; Bäumle, M.; Beyer, N. Ordered Two-Dimensional Monolayers of Au_{55} Clusters. *Angew. Chem., Int. Ed.* **2000**, *39*, 181−183.

(161) Schmid, G.; Pugin, R.; Sawitowski, T.; Simon, U.; Marler, B. Transmission Electron Microscopic and Small angle X-ray Diffraction Investigations of $Au_{55}(PPh_3)_{12}Cl_6$ Microcrystals[dagger]. *Chem. Commun.* **1999**, 1303−1304.

(162) Schmid, G.; Baumle, M.; Geerkens, M.; Heim, I.; Osemann, C.; Sawitowski, T. Current and Future Applications of Nanoclusters. *Chem. Soc. Rev.* **1999**, *28*, 179−185.

(163) Schmid, G.; Reuter, T.; Simon, U.; Noyong, M.; Blech, K.; Santhanam, V.; Jäger, D.; Slomka, H.; Lüth, H.; Lepsa, M. I. Generation and Electrical Contacting of Gold Quantum Dots. *Colloid Polym. Sci.* **2008**, *286*, 1029−1037.

(164) Schmid, G.; Simon, U. Gold Nanoparticles: Assembly and Electrical Properties in 1−3 dimensions. *Chem. Commun.* **2005**, 697−710.

(165) Simon, U.; Schön, G.; Schmid, G. The Application of Au_{55} Clusters as Quantum Dots. *Angew. Chem., Int. Ed. Engl.* **1993**, *32*, 250−254.

(166) Torma, V.; Reuter, T.; Vidoni, O.; Schumann, M.; Radehaus, C.; Schmid, G. The Diode Behavior of Asymmetrically Ordered Au_{55} Clusters. *ChemPhysChem* **2001**, *2*, 546−548.

(167) Torma, V.; Schmid, G.; Simon, U. Structure−Property Relations in Au_{55} Cluster Layers Studied by Temperature-Dependent Impedance Measurements. *ChemPhysChem* **2001**, *2*, 321−325.

(168) Zhang, H.; Hartmann, U.; Schmid, G. Energy-Level Splitting of Ligand-Stabilized Au_{55} Clusters Observed by Scanning Tunneling Spectroscopy. *Appl. Phys. Lett.* **2004**, *84*, 1543−1545.

(169) Qian, H.; Jin, R. Synthesis and Electrospray Mass Spectrometry Determination of Thiolate-Protected $Au_{55}(SR)_{31}$ Nanoclusters. *Chem. Commun.* **2011**, *47*, 11462−11464.

(170) Tsunoyama, H.; Negishi, Y.; Tsukuda, T. Chromatographic Isolation of "Missing" Au_{55} Clusters Protected by Alkanethiolates. *J. Am. Chem. Soc.* **2006**, *128*, 6036−6037.

(171) Vogel, W.; Rosner, B.; Tesche, B. Structural Investigations of Gold (Au_{55}) Organometallic Complexes by X-ray Powder Diffraction and Transmission Electron Microscopy. *J. Phys. Chem.* **1993**, *97*, 11611−11616.

(172) Rapoport, D. H.; Vogel, W.; Cölfen, H.; Schlögl, R. Ligand-Stabilized Metal Clusters: Reinvestigation of the Structure of "$Au_{55}[P(C_6H_5)_3]_{12}Cl_6$. *J. Phys. Chem. B* **1997**, *101*, 4175−4183.

(173) Wallenberg, L. R.; Bovin, J. O.; Schmid, G. On the Crystal Structure of Small Gold Crystals and Large Gold Clusters. *Surf. Sci.* **1985**, *156*, 256−264.

(174) Wang, Z. W.; Palmer, R. E. Experimental Evidence for Fluctuating, Chiral-Type Au_{55} Clusters by Direct Atomic Imaging. *Nano Lett.* **2012**, *12*, 5510−5514.

(175) Jian, N.; Stapelfeldt, C.; Hu, K.-J.; Froba, M.; Palmer, R. E. Hybrid Atomic Structure of the Schmid Cluster $Au_{55}(PPh_3)_{12}Cl_6$ Resolved by Aberration-Corrected STEM. *Nanoscale* **2015**, *7*, 885−888.

(176) Schmid, G.; Pfeil, R.; Boese, R.; Bandermann, F.; Meyer, S.; Calis, G. H. M.; van der Velden, J. W. A. $Au_{55}[P(C_6H_5)_3]_{12}Cl_6$ — ein Goldcluster ungewöhnlicher Grösse. *Chem. Ber.* **1981**, *114*, 3634−3642.

(177) Brust, M.; Walker, M.; Bethell, D.; Schiffrin, D. J.; Whyman, R. Synthesis of Thiol-Derivatised Gold Nanoparticles in a Two-phase Liquid-Liquid System. *J. Chem. Soc., Chem. Commun.* **1994**, *0*, 801−802.

(178) Perala, S. R. K.; Kumar, S. On the Mechanism of Metal Nanoparticle Synthesis in the Brust−Schiffrin Method. *Langmuir* **2013**, *29*, 9863−9873.

(179) Branham, M. R.; Douglas, A. D.; Mills, A. J.; Tracy, J. B.; White, P. S.; Murray, R. W. Arylthiolate-Protected Silver Quantum Dots. *Langmuir* **2006**, *22*, 11376−11383.

(180) Devadas, M. S.; Kwak, K.; Park, J.-W.; Choi, J.-H.; Jun, C.-H.; Sinn, E.; Ramakrishna, G.; Lee, D. Directional Electron Transfer in Chromophore-Labeled Quantum-Sized Au_{25} Clusters: Au_{25} as an Electron Donor. *J. Phys. Chem. Lett.* **2010**, *1*, 1497−1503.

(181) Song, Y.; Harper, A. S.; Murray, R. W. Ligand Heterogeneity on Monolayer-Protected Gold Clusters. *Langmuir* **2005**, *21*, 5492−5500.

(182) Venzo, A.; Antonello, S.; Gascón, J. A.; Guryanov, I.; Leapman, R. D.; Perera, N. V.; Sousa, A.; Zamuner, M.; Zanella, A.; Maran, F. Effect of the Charge State ($z = -1, 0, +1$) on the Nuclear Magnetic Resonance of Monodisperse $Au_{25}[S(CH_2)_2Ph]_{18}^{z}$ Clusters. *Anal. Chem.* **2011**, *83*, 6355−6362.

(183) Goulet, P. J. G.; Lennox, R. B. New Insights into Brust−Schriffin Metal Nanoparticle Synthesis. *J. Am. Chem. Soc.* **2010**, *132*, 9582−9584.

(184) Li, Y.; Zaluzhna, O.; Xu, B.; Gao, Y.; Modest, J. M.; Tong, Y. J. Mechanistic Insights into the Brust−Schiffrin Two-Phase Synthesis of Organo-Chalcogenate-Protected Metal Nanoparticles. *J. Am. Chem. Soc.* **2011**, *133*, 2092−2095.

(185) Zhu, M.; Lanni, E.; Garg, N.; Bier, M. E.; Jin, R. Kinetically Controlled, High-Yield Synthesis of Au_{25} Clusters. *J. Am. Chem. Soc.* **2008**, *130*, 1138−1139.

(186) Wu, Z.; Suhan, J.; Jin, R. One-pot Synthesis of Atomically Monodisperse, Thiol-Functionalized Au_{25} Nanoclusters. *J. Mater. Chem.* **2009**, *19*, 622−626.

(187) Maity, P.; Xie, S.; Yamauchi, M.; Tsukuda, T. Stabilized Gold Clusters: from Isolation Toward Controlled Synthesis. *Nanoscale* **2012**, *4*, 4027−4037.

(188) Duan, H.; Nie, S. Etching Colloidal Gold Nanocrystals with Hyperbranched and Multivalent Polymers: A New Route to Fluorescent and Water-Soluble Atomic Clusters. *J. Am. Chem. Soc.* **2007**, *129*, 2412−2413.

(189) Qian, H.; Zhu, M.; Lanni, E.; Zhu, Y.; Bier, M. E.; Jin, R. Conversion of Polydisperse Au Nanoparticles into Monodisperse Au_{25} Nanorods and Nanospheres. *J. Phys. Chem. C* **2009**, *113*, 17599−17603.

(190) Lin, C.-A. J.; Yang, T.-Y.; Lee, C.-H.; Huang, S. H.; Sperling, R. A.; Zanella, M.; Li, J. K.; Shen, J.-L.; Wang, H.-H.; Yeh, H.-I.; Parak, W. J.; Chang, W. H. Synthesis, Characterization, and Bioconjugation of Fluorescent Gold Nanoclusters toward Biological Labeling Applications. *ACS Nano* **2009**, *3*, 395−401.

(191) Mrudula, K. V.; Bhaskara Rao, T. U.; Pradeep, T. Interfacial synthesis of Luminescent 7 kDa Silver Clusters. *J. Mater. Chem.* **2009**, *19*, 4335−4342.

(192) Yu, Y.; Luo, Z.; Yu, Y.; Lee, J. Y.; Xie, J. Observation of Cluster Size Growth in CO-Directed Synthesis of $Au_{25}(SR)_{18}$ Nanoclusters. *ACS Nano* **2012**, *6*, 7920−7927.

(193) Chakraborty, I.; Bhuin, R. G.; Bhat, S.; Pradeep, T. Blue Emitting Undecaplatinum Cluster. *Nanoscale* **2014**, *6*, 8561−8564.

(194) Chakraborty, I.; Erusappan, J.; Govindarajan, A.; Sugi, K. S.; Udayabhaskararao, T.; Ghosh, A.; Pradeep, T. Emergence of Metallicity in Silver Clusters in the 150 Atom Regime: a Study of Differently Sized Silver Clusters. *Nanoscale* **2014**, *6*, 8024−8031.

(195) Ganguly, A.; Chakraborty, I.; Udayabhaskararao, T.; Pradeep, T. A Copper Cluster Protected with Phenylethanethiol. *J. Nanopart. Res.* **2013**, *15*, 1522.

(196) Sarkar, S.; Chakraborty, I.; Panwar, M. K.; Pradeep, T. Isolation and Tandem Mass Spectrometric Identification of a Stable Monolayer Protected Silver−Palladium Alloy Cluster. *J. Phys. Chem. Lett.* **2014**, *5*, 3757−3762.

(197) Kurashige, W.; Munakata, K.; Nobusada, K.; Negishi, Y. Synthesis of Stable Cu_nAu_{25-n} Nanoclusters ($n = 1-9$) using Selenolate Ligands. *Chem. Commun.* **2013**, *49*, 5447−5449.

(198) Negishi, Y.; Kurashige, W.; Niihori, Y.; Iwasa, T.; Nobusada, K. Isolation, Structure, and Stability of a Dodecanethiolate-Protected Pd_1Au_{24} Cluster. *Phys. Chem. Chem. Phys.* **2010**, *12*, 6219−6225.

(199) Qian, H.; Jiang, D.-e.; Li, G.; Gayathri, C.; Das, A.; Gil, R. R.; Jin, R. Monoplatinum Doping of Gold Nanoclusters and Catalytic Application. *J. Am. Chem. Soc.* **2012**, *134*, 16159−16162.

(200) Shichibu, Y.; Negishi, Y.; Tsunoyama, H.; Kanehara, M.; Teranishi, T.; Tsukuda, T. Extremely High Stability of Glutathionate-Protected Au_{25} Clusters Against Core Etching. *Small* **2007**, *3*, 835−839.

(201) Dhanalakshmi, L.; Udayabhaskararao, T.; Pradeep, T. Conversion of Double Layer Charge-Stabilized Ag@citrate Colloids to Thiol Passivated Luminescent Quantum Clusters. *Chem. Commun.* **2012**, *48*, 859−861.

(202) Shimizu, T.; Teranishi, T.; Hasegawa, S.; Miyake, M. Size Evolution of Alkanethiol-Protected Gold Nanoparticles by Heat Treatment in the Solid State. *J. Phys. Chem. B* **2003**, *107*, 2719−2724.

(203) Gaur, S.; Miller, J. T.; Stellwagen, D.; Sanampudi, A.; Kumar, C. S. S. R.; Spivey, J. J. Synthesis, Characterization, and Testing of Supported Au Catalysts Prepared from Atomically-Tailored $Au_{38}(SC_{12}H_{25})_{24}$ Clusters. *Phys. Chem. Chem. Phys.* **2012**, *14*, 1627−1634.

(204) Qian, H.; Eckenhoff, W. T.; Zhu, Y.; Pintauer, T.; Jin, R. Total Structure Determination of Thiolate-Protected Au_{38} Nanoparticles. *J. Am. Chem. Soc.* **2010**, *132*, 8280−8281.

(205) Zheng, J.; Dickson, R. M. Individual Water-Soluble Dendrimer-Encapsulated Silver Nanodot Fluorescence. *J. Am. Chem. Soc.* **2002**, *124*, 13982−13983.

(206) Liu, T.; Su, Y.; Song, H.; Lv, Y. Microwave-assisted Green Synthesis of Ultrasmall Fluorescent Water-soluble Silver Nanoclusters and its Application in Chiral Recognition of Amino Acids. *Analyst* **2013**, *138*, 6558−6564.

(207) Ershov, B. G.; Henglein, A. Time-Resolved Investigation of Early Processes in the Reduction of Ag^+ on Polyacrylate in Aqueous Solution. *J. Phys. Chem. B* **1998**, *102*, 10667−10671.

(208) Linnert, T.; Mulvaney, P.; Henglein, A.; Weller, H. Long-lived Nonmetallic Silver Clusters in Aqueous Solution: Preparation and Photolysis. *J. Am. Chem. Soc.* **1990**, *112*, 4657−4664.

(209) Ledo-Suárez, A.; Rivas, J.; Rodríguez-Abreu, C. F.; Rodríguez, M. J.; Pastor, E.; Hernández-Creus, A.; Oseroff, S. B.; López-Quintela, M. A. Facile Synthesis of Stable Subnanosized Silver Clusters in Microemulsions. *Angew. Chem., Int. Ed.* **2007**, *46*, 8823−8827.

(210) Xu, H.; Suslick, K. S. Sonochemical Synthesis of Highly Fluorescent Ag Nanoclusters. *ACS Nano* **2010**, *4*, 3209−3214.

(211) Vilar-Vidal, N.; Blanco, M. C.; López-Quintela, M. A.; Rivas, J.; Serra, C. Electrochemical Synthesis of Very Stable Photoluminescent Copper Clusters. *J. Phys. Chem. C* **2010**, *114*, 15924−15930.

(212) Adhikari, B.; Banerjee, A. Facile Synthesis of Water-Soluble Fluorescent Silver Nanoclusters and HgII Sensing. *Chem. Mater.* **2010**, *22*, 4364−4371.

(213) Xie, J.; Zheng, Y.; Ying, J. Y. Protein-Directed Synthesis of Highly Fluorescent Gold Nanoclusters. *J. Am. Chem. Soc.* **2009**, *131*, 888−889.

(214) Xavier, P. L.; Chaudhari, K.; Verma, P. K.; Pal, S. K.; Pradeep, T. Luminescent Quantum Clusters of Gold in Transferrin Family Protein, Lactoferrin Exhibiting FRET. *Nanoscale* **2010**, *2*, 2769−2776.

(215) Muhammed, M. A.; Aldeek, F.; Palui, G.; Trapiella-Alfonso, L.; Mattoussi, H. Growth of in situ Functionalized Luminescent Silver Nanoclusters by Direct Reduction and Size Focusing. *ACS Nano* **2012**, *6*, 8950−8961.

(216) Chakraborty, I.; Udayabhaskararao, T.; Pradeep, T. Luminescent Sub-nanometer Clusters for Metal Ion Sensing: A New Direction in Nanosensors. *J. Hazard. Mater.* **2012**, *211*−*212*, 396−403.

(217) Yeh, H.-C.; Sharma, J.; Han, J. J.; Martinez, J. S.; Werner, J. H. A DNA−Silver Nanocluster Probe That Fluoresces upon Hybridization. *Nano Lett.* **2010**, *10*, 3106−3110.

(218) Chakraborty, I.; Mahata, S.; Mitra, A.; De, G.; Pradeep, T. Controlled Synthesis and Characterization of the Elusive Thiolated Ag_{55} Cluster. *Dalton Trans.* **2014**, *43*, 17904−17907.

(219) Ghosh, A.; Udayabhaskararao, T.; Pradeep, T. One-Step Route to Luminescent $Au_{18}SG_{14}$ in the Condensed Phase and Its Closed Shell Molecular Ions in the Gas Phase. *J. Phys. Chem. Lett.* **2012**, *3*, 1997−2002.

(220) Chakraborty, I.; Pradeep, T. Reversible Formation of Ag_{44} from Selenolates. *Nanoscale* **2014**, *6*, 14190−14194.

(221) AbdulHalim, L. G.; Ashraf, S.; Katsiev, K.; Kirmani, A. R.; Kothalawala, N.; Anjum, D. H.; Abbas, S.; Amassian, A.; Stellacci, F.; Dass, A.; Hussain, I.; Bakr, O. M. A Scalable Synthesis of Highly Stable and Water Dispersible $Ag_{44}(SR)_{30}$ Nanoclusters. *J. Mater. Chem. A* **2013**, *1*, 10148−10154.

(222) Yang, H.; Wang, Y.; Huang, H.; Gell, L.; Lehtovaara, L.; Malola, S.; Hakkinen, H.; Zheng, N. All-thiol-stabilized Ag_{44} and $Au_{12}Ag_{32}$ Nanoparticles with Single-crystal Structures. *Nat. Commun.* **2013**, *4*, 2422.

(223) Whetten, R. L.; Khoury, J. T.; Alvarez, M. M.; Murthy, S.; Vezmar, I.; Wang, Z. L.; Stephens, P. W.; Cleveland, C. L.; Luedtke, W. D.; Landman, U. Nanocrystal Gold Molecules. *Adv. Mater.* **1996**, *8*, 428−433.

(224) Cleveland, C. L.; Landman, U.; Schaaff, T. G.; Shafigullin, M. N.; Stephens, P. W.; Whetten, R. L. Structural Evolution of Smaller Gold Nanocrystals: The Truncated Decahedral Motif. *Phys. Rev. Lett.* **1997**, *79*, 1873−1876.

(225) Yannouleas, C.; Landman, U. Electronic Entropy, Shell Structure, and Size-Evolutionary Patterns of Metal Clusters. *Phys. Rev. Lett.* **1997**, *78*, 1424−1427.

(226) Cleveland, C. L.; Landman, U.; Shafigullin, M. N.; Stephens, P. W.; Whetten, R. L. Structural Evolution of Larger Gold Clusters. *Z. Phys. D: At., Mol. Clusters* **1997**, *40*, 503−508.

(227) Schaaff, T. G.; Knight, G.; Shafigullin, M. N.; Borkman, R. F.; Whetten, R. L. Isolation and Selected Properties of a 10.4 kDa Gold:Glutathione Cluster Compound. *J. Phys. Chem. B* **1998**, *102*, 10643−10646.

(228) Ingram, R. S.; Hostetler, M. J.; Murray, R. W. Poly-hetero-ω-functionalized Alkanethiolate-Stabilized Gold Cluster Compounds. *J. Am. Chem. Soc.* **1997**, *119*, 9175−9178.

(229) Negishi, Y.; Nobusada, K.; Tsukuda, T. Glutathione-Protected Gold Clusters Revisited: Bridging the Gap between Gold(I) Thiolate Complexes and Thiolate-Protected Gold Nanocrystals. *J. Am. Chem. Soc.* **2005**, *127*, 5261−5270.

(230) Yao, H.; Miki, K.; Nishida, N.; Sasaki, A.; Kimura, K. Large Optical Activity of Gold Nanocluster Enantiomers Induced by a Pair of Optically Active Penicillamines. *J. Am. Chem. Soc.* **2005**, *127*, 15536−15543.

(231) Häkkinen, H.; Walter, M.; Grönbeck, H. Divide and Protect: Capping Gold Nanoclusters with Molecular Gold−Thiolate Rings. *J. Phys. Chem. B* **2006**, *110*, 9927−9931.

(232) Natarajan, G.; Mathew, A.; Negishi, Y.; Whetten, R. L.; Pradeep, T. A Unified Framework for Understanding the Structure and Modifications of Atomically Precise Monolayer Protected Gold Clusters. *J. Phys. Chem. C* **2015**, *119*, 27768−27785.

(233) Krishnadas, K. R.; Ghosh, A.; Baksi, A.; Chakraborty, I.; Natarajan, G.; Pradeep, T. Intercluster Reactions between $Au_{25}(SR)_{18}$ and $Ag_{44}(SR)_{30}$. *J. Am. Chem. Soc.* **2016**, *138*, 140−148.

(234) Gross, D. H. E.; Madjet, M. E. Fragmentation Phase Transition in Atomic Clusters. IV. Liquid-gas Transition in Finite Metal Clusters and in the Bulk. *Z. Phys. B: Condens. Matter* **1997**, *104*, 541−551.

(235) Knight, W. D.; Clemenger, K.; de Heer, W. A.; Saunders, W. A.; Chou, M. Y.; Cohen, M. L. Electronic Shell Structure and Abundances of Sodium Clusters. *Phys. Rev. Lett.* **1984**, *52*, 2141−2143.

(236) Morse, M. D. Clusters of transition-metal atoms. *Chem. Rev.* **1986**, *86*, 1049−1109.

(237) O'Hair, R. J.; Khairallah, G. Gas Phase Ion Chemistry of Transition Metal Clusters: Production, Reactivity, and Catalysis. *J. Cluster Sci.* **2004**, *15*, 331−363.

(238) Singh, D. M. D. J.; Pradeep, T.; Bhattacharjee, J.; Waghmare, U. V. Novel Cage Clusters of MoS2 in the Gas Phase. *J. Phys. Chem. A* **2005**, *109*, 7339−7342.

(239) Singh, D. M. D. J.; Pradeep, T.; Bhattacharjee, J.; Waghmare, U. V. Closed-Cage Clusters in the Gaseous and Condensed Phases Derived from Sonochemically Synthesized MoS_2 Nanoflakes. *J. Am. Soc. Mass Spectrom.* **2007**, *18*, 2191−2197.

(240) Bhat, S.; Chakraborty, I.; Baksi, A.; Narayanan, R. P.; Pradeep, T. Evolution of Atomically Precise Clusters through the Eye of Mass Spectrometry. *Nanoscience* **2016**, 3, 343−385.

(241) Ingram, R. S.; Hostetler, M. J.; Murray, R. W.; Schaaff, T. G.; Khoury, J. T.; Whetten, R. L.; Bigioni, T. P.; Guthrie, D. K.; First, P. N. 28 kDa Alkanethiolate-Protected Au Clusters Give Analogous Solution Electrochemistry and STM Coulomb Staircases. *J. Am. Chem. Soc.* **1997**, *119*, 9279−9280.

(242) Logunov, S. L.; Ahmadi, T. S.; El-Sayed, M. A.; Khoury, J. T.; Whetten, R. L. Electron Dynamics of Passivated Gold Nanocrystals Probed by Subpicosecond Transient Absorption Spectroscopy. *J. Phys. Chem. B* **1997**, *101*, 3713−3719.

(243) Schaaff, T. G.; Shafigullin, M. N.; Khoury, J. T.; Vezmar, I.; Whetten, R. L.; Cullen, W. G.; First, P. N.; Gutiérrez-Wing, C.; Ascensio, J.; Jose-Yacamán, M. J. Isolation of Smaller Nanocrystal Au Molecules: Robust Quantum Effects in Optical Spectra. *J. Phys. Chem. B* **1997**, *101*, 7885−7891.

(244) Schaaff, T. G.; Whetten, R. L. Giant Gold-Glutathione Cluster Compounds: Intense Optical Activity in Metal-Based Transitions. *J. Phys. Chem. B* **2000**, *104*, 2630−2641.

(245) Templeton, A. C.; Cliffel, D. E.; Murray, R. W. Redox and Fluorophore Functionalization of Water-Soluble, Tiopronin-Protected Gold Clusters. *J. Am. Chem. Soc.* **1999**, *121*, 7081−7089.

(246) Hicks, J. F.; Templeton, A. C.; Chen, S.; Sheran, K. M.; Jasti, R.; Murray, R. W.; Debord, J.; Schaaff, T. G.; Whetten, R. L. The Monolayer Thickness Dependence of Quantized Double-Layer Capacitances of Monolayer-Protected Gold Clusters. *Anal. Chem.* **1999**, *71*, 3703−3711.

(247) Ingram, R. S.; Murray, R. W. Electroactive Three-Dimensional Monolayers: Anthraquinone ω-Functionalized Alkanethiolate-Stabilized Gold Clusters. *Langmuir* **1998**, *14*, 4115−4121.

(248) Schaaff, T. G.; Shafigullin, M. N.; Khoury, J. T.; Vezmar, I.; Whetten, R. L. Properties of a Ubiquitous 29 kDa Au:SR Cluster Compounds. *J. Phys. Chem. B* **2001**, *105*, 8785−8796.

(249) Link, S.; Beeby, A.; FitzGerald, S.; El-Sayed, M. A.; Schaaff, T. G.; Whetten, R. L. Visible to Infrared Luminescence from a 28-Atom Gold Cluster. *J. Phys. Chem. B* **2002**, *106*, 3410−3415.

(250) Donkers, R. L.; Lee, D.; Murray, R. W. Synthesis and Isolation of the Molecule-like Cluster $Au_{38}(PhCH_2CH_2S)_{24}$. *Langmuir* **2004**, *20*, 1945−1952.

(251) Jimenez, V. L.; Georganopoulou, D. G.; White, R. J.; Harper, A. S.; Mills, A. J.; Lee, D.; Murray, R. W. Hexanethiolate Monolayer Protected 38 Gold Atom Cluster. *Langmuir* **2004**, *20*, 6864−6870.

(252) Lee, D.; Donkers, R. L.; Wang, G.; Harper, A. S.; Murray, R. W. Electrochemistry and Optical Absorbance and Luminescence of Molecule-like Au_{38} Nanoparticles. *J. Am. Chem. Soc.* **2004**, *126*, 6193−6199.

(253) Bigioni, T. P.; Whetten, R. L.; Dag, Ö. Near-Infrared Luminescence from Small Gold Nanocrystals. *J. Phys. Chem. B* **2000**, *104*, 6983−6986.

(254) Kimura, K.; Sugimoto, N.; Sato, S.; Yao, H.; Negishi, Y.; Tsukuda, T. Size Determination of Gold Clusters by Polyacrylamide Gel Electrophoresis in a Large Cluster Region. *J. Phys. Chem. C* **2009**, *113*, 14076−14082.

(255) Negishi, Y.; Nakazaki, T.; Malola, S.; Takano, S.; Niihori, Y.; Kurashige, W.; Yamazoe, S.; Tsukuda, T.; Häkkinen, H. A Critical Size for Emergence of Nonbulk Electronic and Geometric Structures in Dodecanethiolate-Protected Au Clusters. *J. Am. Chem. Soc.* **2015**, *137*, 1206−1212.

(256) Niihori, Y.; Matsuzaki, M.; Uchida, C.; Negishi, Y. Advanced Use of High-Performance Liquid Chromatography for Synthesis of Controlled Metal Clusters. *Nanoscale* **2014**, *6*, 7889−7896.

(257) Knoppe, S.; Boudon, J.; Dolamic, I.; Dass, A.; Burgi, T. Size Exclusion Chromatography for Semipreparative Scale Separation of $Au_{38}(SR)_{24}$ and $Au_{40}(SR)_{24}$ and Larger Clusters. *Anal. Chem.* **2011**, *83*, 5056−5061.

(258) Ghosh, A.; Hassinen, J.; Pulkkinen, P.; Tenhu, H.; Ras, R. H. A.; Pradeep, T. Simple and Efficient Separation of Atomically Precise Noble Metal Clusters. *Anal. Chem.* **2014**, *86*, 12185−12190.

(259) Zhu, Y.; Jin, R.; Sun, Y. Atomically Monodisperse Gold Nanoclusters Catalysts with Precise Core-shell Structure. *Catalysts* **2011**, *1*, 3−17.

(260) Jin, R.; Qian, H.; Wu, Z.; Zhu, Y.; Zhu, M.; Mohanty, A.; Garg, N. Size Focusing: A Methodology for Synthesizing Atomically Precise Gold Nanoclusters. *J. Phys. Chem. Lett.* **2010**, *1*, 2903−2910.

(261) Negishi, Y.; Takasugi, Y.; Sato, S.; Yao, H.; Kimura, K.; Tsukuda, T. Magic-Numbered Au_n Clusters Protected by Glutathione Monolayers (n = 18, 21, 25, 28, 32, 39): Isolation and Spectroscopic Characterization. *J. Am. Chem. Soc.* **2004**, *126*, 6518−6519.

(262) Yu, Y.; Chen, X.; Yao, Q.; Yu, Y.; Yan, N.; Xie, J. Scalable and Precise Synthesis of Thiolated Au_{10-12}, Au_{15}, Au_{18}, and Au_{25} Nanoclusters via pH Controlled CO Reduction. *Chem. Mater.* **2013**, *25*, 946−952.

(263) Yuan, X.; Zhang, B.; Luo, Z.; Yao, Q.; Leong, D. T.; Yan, N.; Xie, J. Balancing the Rate of Cluster Growth and Etching for Gram-Scale Synthesis of Thiolate-Protected Au_{25} Nanoclusters with Atomic Precision. *Angew. Chem., Int. Ed.* **2014**, *53*, 4623−4627.

(264) Yuan, X.; Yu, Y.; Yao, Q.; Zhang, Q.; Xie, J. Fast Synthesis of Thiolated Au_{25} Nanoclusters via Protection−Deprotection Method. *J. Phys. Chem. Lett.* **2012**, *3*, 2310−2314.

(265) Jin, R. Atomically Precise Metal Nanoclusters: Stable Sizes and Optical Properties. *Nanoscale* **2015**, *7*, 1549−1565.

(266) Varnavski, O.; Ramakrishna, G.; Kim, J.; Lee, D.; Goodson, T. Critical Size for the Observation of Quantum Confinement in Optically Excited Gold Clusters. *J. Am. Chem. Soc.* **2010**, *132*, 16−17.

(267) Alvarez, M. M.; Khoury, J. T.; Schaaff, T. G.; Shafigullin, M.; Vezmar, I.; Whetten, R. L. Critical Sizes in the Growth of Au Clusters. *Chem. Phys. Lett.* **1997**, *266*, 91−98.

(268) Hostetler, M. J.; Wingate, J. E.; Zhong, C.-J.; Harris, J. E.; Vachet, R. W.; Clark, M. R.; Londono, J. D.; Green, S. J.; Stokes, J. J.; Wignall, G. D.; Glish, G. L.; Porter, M. D.; Evans, N. D.; Murray, R. W. Alkanethiolate Gold Cluster Molecules with Core Diameters from 1.5 to 5.2 nm: Core and Monolayer Properties as a Function of Core Size. *Langmuir* **1998**, *14*, 17−30.

(269) Miller, S. A.; Womick, J. M.; Parker, J. F.; Murray, R. W.; Moran, A. M. Femtosecond Relaxation Dynamics of $Au_{25}L_{18}^-$ Monolayer-Protected Clusters. *J. Phys. Chem. C* **2009**, *113*, 9440−9444.

(270) Miller, S. A.; Fields-Zinna, C. A.; Murray, R. W.; Moran, A. M. Nonlinear Optical Signatures of Core and Ligand Electronic States in $Au_{24}PdL_{18}$. *J. Phys. Chem. Lett.* **2010**, *1*, 1383−1387.

(271) Qian, H.; Sfeir, M. Y.; Jin, R. Ultrafast Relaxation Dynamics of $[Au_{25}(SR)_{18}]^q$ Nanoclusters: Effects of Charge State. *J. Phys. Chem. C* **2010**, *114*, 19935−19940.

(272) Varnavski, O.; Ramakrishna, G.; Kim, J.; Lee, D.; Goodson, T. Optically Excited Acoustic Vibrations in Quantum-Sized Monolayer-Protected Gold Clusters. *ACS Nano* **2010**, *4*, 3406−3412.

(273) Devadas, M. S.; Kim, J.; Sinn, E.; Lee, D.; Goodson, T.; Ramakrishna, G. Unique Ultrafast Visible Luminescence in Monolayer-Protected Au_{25} Clusters. *J. Phys. Chem. C* **2010**, *114*, 22417−22423.

(274) Miles, D. T.; Murray, R. W. Temperature-Dependent Quantized Double Layer Charging of Monolayer-Protected Gold Clusters. *Anal. Chem.* **2003**, *75*, 1251−1257.

(275) Shibu, E. S.; Pradeep, T. Photoluminescence and Temperature-Dependent Emission Studies of Au_{25} Clusters In the Solid State. *Int. J. Nanosci.* **2009**, *08*, 223−226.

(276) Devadas, M. S.; Bairu, S.; Qian, H.; Sinn, E.; Jin, R.; Ramakrishna, G. Temperature-Dependent Optical Absorption Properties of Monolayer-Protected Au_{25} and Au_{38} Clusters. *J. Phys. Chem. Lett.* **2011**, *2*, 2752−2758.

(277) Mooney, J.; Kambhampati, P. Correction to "Get the Basics Right: Jacobian Conversion of Wavelength and Energy Scales for Quantitative Analysis of Emission Spectra. *J. Phys. Chem. Lett.* **2014**, *5*, 3497−3497.

(278) Luo, Z.; Yuan, X.; Yu, Y.; Zhang, Q.; Leong, D. T.; Lee, J. Y.; Xie, J. From Aggregation-Induced Emission of Au(I)−Thiolate Complexes to Ultrabright Au(0)@Au(I)−Thiolate Core−Shell Nanoclusters. *J. Am. Chem. Soc.* **2012**, *134*, 16662−16670.

(279) Yuan, X.; Luo, Z.; Zhang, Q.; Zhang, X.; Zheng, Y.; Lee, J. Y.; Xie, J. Synthesis of Highly Fluorescent Metal (Ag, Au, Pt, and Cu) Nanoclusters by Electrostatically Induced Reversible Phase Transfer. *ACS Nano* **2011**, *5*, 8800−8808.

(280) Weerawardene, K. L. D. M.; Aikens, C. M. Theoretical Insights into the Origin of Photoluminescence of $Au_{25}(SR)_{18}^-$ Nanoparticles. *J. Am. Chem. Soc.* **2016**, *138*, 11202−11210.

(281) Wu, Z.; Jin, R. On the Ligand's Role in the Fluorescence of Gold Nanoclusters. *Nano Lett.* **2010**, *10*, 2568−2573.

(282) Wang, S.; Zhu, X.; Cao, T.; Zhu, M. A Simple Model for Understanding the Fluorescence Behavior of Au_{25} Nanoclusters. *Nanoscale* **2014**, *6*, 5777−5781.

(283) Shibu, E. S.; Muhammed, M. A. H.; Tsukuda, T.; Pradeep, T. Ligand Exchange of $Au_{25}SG_{18}$ Leading to Functionalized Gold Clusters: Spectroscopy, Kinetics, and Luminescence. *J. Phys. Chem. C* **2008**, *112*, 12168−12176.

(284) van Wijngaarden, J. T.; Toikkanen, O.; Liljeroth, P.; Quinn, B. M.; Meijerink, A. Temperature-Dependent Emission of Monolayer-Protected Au_{38} Clusters. *J. Phys. Chem. C* **2010**, *114*, 16025−16028.

(285) Ciabatti, I.; Femoni, C.; Iapalucci, M. C.; Longoni, G.; Zacchini, S.; Zarra, S. Surface Decorated Platinum Carbonyl Clusters. *Nanoscale* **2012**, *4*, 4166−4177.

(286) Fresch, B.; Boyen, H. G.; Remacle, F. Magnetostructural Effects in Ligand Stabilized Pd_{13} Clusters: a Density Functional Theory Study. *Nanoscale* **2012**, *4*, 4138−4147.

(287) Green, T. D.; Knappenberger, K. L. Relaxation dynamics of $Au_{25}L_{18}$ Nanoclusters Studied by Femtosecond Time-resolved Near Infrared Transient Absorption Spectroscopy. *Nanoscale* **2012**, *4*, 4111−4118.

(288) Gronbeck, H. The Bonding in Thiolate Protected Gold Nanoparticles from Au4f Photoemission Core Level Shifts. *Nanoscale* **2012**, *4*, 4178−4182.

(289) Jin, R.; Eah, S.-K.; Pei, Y. Quantum-sized Metal Nanoclusters. *Nanoscale* **2012**, *4*, 4026−4026.

(290) Martin, M. N.; Li, D.; Dass, A.; Eah, S.-K. Ultrafast, 2 min Synthesis of Monolayer-Protected Gold Nanoclusters (d < 2 nm). *Nanoscale* **2012**, *4*, 4091−4094.

(291) Meng, X.; Xu, Q.; Wang, S.; Zhu, M. Ligand-exchange Synthesis of Selenophenolate-capped Au_{25} Nanoclusters. *Nanoscale* **2012**, *4*, 4161−4165.

(292) Nambiar, S. R.; Aneesh, P. K.; Sukumar, C.; Rao, T. P. Mixed Monolayer Protected Gold Atom-oxide Cluster Synthesis and Characterization. *Nanoscale* **2012**, *4*, 4130−4137.

(293) Pei, Y.; Zeng, X. C. Investigating the Structural Evolution of Thiolate Protected Gold Clusters from First-principles. *Nanoscale* **2012**, *4*, 4054−4072.

(294) Shang, L.; Yang, L.; Stockmar, F.; Popescu, R.; Trouillet, V.; Bruns, M.; Gerthsen, D.; Nienhaus, G. U. Microwave-assisted Rapid Synthesis of Luminescent Gold Nanoclusters for Sensing Hg^{2+} in Living Cells Using Fluorescence Imaging. *Nanoscale* **2012**, *4*, 4155−4160.

(295) Sharma, J.; Rocha, R. C.; Phipps, M. L.; Yeh, H.-C.; Balatsky, K. A.; Vu, D. M.; Shreve, A. P.; Werner, J. H.; Martinez, J. S. A DNA-templated Fluorescent Silver Nanocluster with Enhanced Stability. *Nanoscale* **2012**, *4*, 4107−4110.

(296) Tang, Z.; Ahuja, T.; Wang, S.; Wang, G. Near Infrared Luminescence of Gold Nanoclusters Affected by the Bonding of 1,4-dithiolate Durene and Monothiolate Phenylethanethiolate. *Nanoscale* **2012**, *4*, 4119−4124.

(297) Wang, L.-M.; Wang, L.-S. Probing the Electronic Properties and Structural Evolution of Anionic Gold Clusters in the Gas Phase. *Nanoscale* **2012**, *4*, 4038−4053.

(298) Wang, M.; Wu, Z.; Yang, J.; Wang, G.; Wang, H.; Cai, W. $Au_{25}(SG)_{18}$ as a Fluorescent Iodide Sensor. *Nanoscale* **2012**, *4*, 4087−4090.

(299) Wong, O. A.; Heinecke, C. L.; Simone, A. R.; Whetten, R. L.; Ackerson, C. J. Ligand Symmetry-equivalence on Thiolate Protected Gold Nanoclusters Determined by NMR Spectroscopy. *Nanoscale* **2012**, *4*, 4099−4102.

(300) Yamamoto, H.; Yano, H.; Kouchi, H.; Obora, Y.; Arakawa, R.; Kawasaki, H. N,N-Dimethylformamide-stabilized Gold Nanoclusters as a Catalyst for the Reduction of 4-Nitrophenol. *Nanoscale* **2012**, *4*, 4148−4154.

(301) Zheng, J.; Zhou, C.; Yu, M.; Liu, J. Different Sized Luminescent Gold Nanoparticles. *Nanoscale* **2012**, *4*, 4073−4083.

(302) Zhou, T.; Rong, M.; Cai, Z.; Yang, C. J.; Chen, X. Sonochemical Synthesis of Highly Fluorescent Glutathione-Stabilized Ag Nanoclusters and S^{2-} sensing. *Nanoscale* **2012**, *4*, 4103−4106.

(303) Fields-Zinna, C. A.; Crowe, M. C.; Dass, A.; Weaver, J. E. F.; Murray, R. W. Mass Spectrometry of Small Bimetal Monolayer-Protected Clusters. *Langmuir* **2009**, *25*, 7704−7710.

(304) Tracy, J. B.; Kalyuzhny, G.; Crowe, M. C.; Balasubramanian, R.; Choi, J.-P.; Murray, R. W. Poly(ethylene glycol) Ligands for High-Resolution Nanoparticle Mass Spectrometry. *J. Am. Chem. Soc.* **2007**, *129*, 6706−6707.

(305) Negishi, Y.; Chaki, N. K.; Shichibu, Y.; Whetten, R. L.; Tsukuda, T. Origin of Magic Stability of Thiolated Gold Clusters: A Case Study on $Au_{25}(SC_6H_{13})_{18}$. *J. Am. Chem. Soc.* **2007**, *129*, 11322−11323.

(306) Dass, A.; Stevenson, A.; Dubay, G. R.; Tracy, J. B.; Murray, R. W. Nanoparticle MALDI-TOF Mass Spectrometry without Fragmentation: $Au_{25}(SCH_2CH_2Ph)_{18}$ and Mixed Monolayer $Au_{25}(SCH_2CH_2Ph)_{18-x}(L)_x$. *J. Am. Chem. Soc.* **2008**, *130*, 5940−5946.

(307) Dass, A. Faradaurate Nanomolecules: A Superstable Plasmonic 76.3 kDa Cluster. *J. Am. Chem. Soc.* **2011**, *133*, 19259−19261.

(308) Dharmaratne, A. C.; Krick, T.; Dass, A. Nanocluster Size Evolution Studied by Mass Spectrometry in Room Temperature $Au_{25}(SR)_{18}$ Synthesis. *J. Am. Chem. Soc.* **2009**, *131*, 13604−13605.

(309) Nimmala, P. R.; Yoon, B.; Whetten, R. L.; Landman, U.; Dass, A. $Au_{67}(SR)_{35}$ Nanomolecules: Characteristic Size-Specific Optical, Electrochemical, Structural Properties and First-Principles Theoretical Analysis. *J. Phys. Chem. A* **2013**, *117*, 504−517.

(310) Krishnadas, K. R.; Baksi, A.; Ghosh, A.; Natarajan, G.; Pradeep, T. Structure-Conserving Spontaneous Transformations between Nanoparticles. *Nat. Commun.* **2016**, *7*, 13447.

(311) Luo, Z.; Nachammai, V.; Zhang, B.; Yan, N.; Leong, D. T.; Jiang, D.-e.; Xie, J. Toward Understanding the Growth Mechanism: Tracing All Stable Intermediate Species from Reduction of Au(I)−Thiolate Complexes to Evolution of Au_{25} Nanoclusters. *J. Am. Chem. Soc.* **2014**, *136*, 10577−10580.

(312) Fields-Zinna, C. A.; Sampson, J. S.; Crowe, M. C.; Tracy, J. B.; Parker, J. F.; deNey, A. M.; Muddiman, D. C.; Murray, R. W. Tandem Mass Spectrometry of Thiolate-Protected Au Nanoparticles $Na_xAu_{25}(SC_2H_4Ph)_{18-y}(S(C_2H_4O)_5CH_3)_y$. *J. Am. Chem. Soc.* **2009**, *131*, 13844−13851.

(313) Chaki, N. K.; Negishi, Y.; Tsunoyama, H.; Shichibu, Y.; Tsukuda, T. Ubiquitous 8 and 29 kDa Gold:Alkanethiolate Cluster Compounds: Mass-Spectrometric Determination of Molecular Formulas and Structural Implications. *J. Am. Chem. Soc.* **2008**, *130*, 8608−8610.

(314) Angel, L. A.; Majors, L. T.; Dharmaratne, A. C.; Dass, A. Ion Mobility Mass Spectrometry of $Au_{25}(SCH_2CH_2Ph)_{18}$ Nanoclusters. *ACS Nano* **2010**, *4*, 4691−4700.

(315) Chen, S.; Wang, S.; Zhong, J.; Song, Y.; Zhang, J.; Sheng, H.; Pei, Y.; Zhu, M. The Structure and Optical Properties of the $[Au_{18}(SR)_{14}]$ Nanocluster. *Angew. Chem., Int. Ed.* **2015**, *54*, 3145−3149.

(316) Das, A.; Liu, C.; Byun, H. Y.; Nobusada, K.; Zhao, S.; Rosi, N.; Jin, R. Structure Determination of $[Au_{18}(SR)_{14}]$. *Angew. Chem., Int. Ed.* **2015**, *54*, 3140−3144.

(317) Zeng, C.; Liu, C.; Chen, Y.; Rosi, N. L.; Jin, R. Gold−Thiolate Ring as a Protecting Motif in the $Au_{20}(SR)_{16}$ Nanocluster and Implications. *J. Am. Chem. Soc.* **2014**, *136*, 11922−11925.

(318) Das, A.; Li, T.; Nobusada, K.; Zeng, C.; Rosi, N. L.; Jin, R. Nonsuperatomic $[Au_{23}(SC_6H_{11})_{16}]^-$ Nanocluster Featuring Bipyramidal Au_{15} Kernel and Trimeric $Au_3(SR)_4$ Motif. *J. Am. Chem. Soc.* **2013**, *135*, 18264−18267.

(319) Crasto, D.; Barcaro, G.; Stener, M.; Sementa, L.; Fortunelli, A.; Dass, A. $Au_{24}(SAdm)_{16}$ Nanomolecules: X-ray Crystal Structure, Theoretical Analysis, Adaptability of Adamantane Ligands to Form $Au_{23}(SAdm)_{16}$ and $Au_{25}(SAdm)_{16}$, and Its Relation to $Au_{25}(SR)_{18}$. *J. Am. Chem. Soc.* **2014**, *136*, 14933−14940.

(320) Zeng, C.; Li, T.; Das, A.; Rosi, N. L.; Jin, R. Chiral Structure of Thiolate-Protected 28-Gold-Atom Nanocluster Determined by X-ray Crystallography. *J. Am. Chem. Soc.* **2013**, *135*, 10011−10013.

(321) Crasto, D.; Malola, S.; Brosofsky, G.; Dass, A.; Häkkinen, H. Single Crystal XRD Structure and Theoretical Analysis of the Chiral $Au_{30}S(S\text{-}t\text{-}Bu)_{18}$ Cluster. *J. Am. Chem. Soc.* **2014**, *136*, 5000−5005.

(322) Zeng, C.; Chen, Y.; Liu, C.; Nobusada, K.; Rosi, N. L.; Jin, R. Gold Tetrahedra Coil up: Kekulé-like and Double Helical Superstructures. *Sci. Adv.* **2015**, *1*, e1500425.

(323) Zeng, C.; Liu, C.; Chen, Y.; Rosi, N. L.; Jin, R. Atomic Structure of Self-Assembled Monolayer of Thiolates on a Tetragonal Au_{92} Nanocrystal. *J. Am. Chem. Soc.* **2016**, *138*, 8710−8713.

(324) Chen, Y.; Zeng, C.; Liu, C.; Kirschbaum, K.; Gayathri, C.; Gil, R. R.; Rosi, N. L.; Jin, R. Crystal Structure of Barrel-Shaped Chiral $Au_{130}(p\text{-MBT})_{50}$ Nanocluster. *J. Am. Chem. Soc.* **2015**, *137*, 10076−10079.

(325) Dass, A.; Theivendran, S.; Nimmala, P. R.; Kumara, C.; Jupally, V. R.; Fortunelli, A.; Sementa, L.; Barcaro, G.; Zuo, X.; Noll, B. C.

$Au_{133}(SPh\text{-}tBu)_{52}$ Nanomolecules: X-ray Crystallography, Optical, Electrochemical, and Theoretical Analysis. *J. Am. Chem. Soc.* **2015**, *137*, 4610−4613.

(326) Gutrath, B. S.; Oppel, I. M.; Presly, O.; Beljakov, I.; Meded, V.; Wenzel, W.; Simon, U. $[Au_{14}(PPh_3)_8(NO_3)_4]$: An Example of a New Class of $Au(NO_3)$-Ligated Superatom Complexes. *Angew. Chem., Int. Ed.* **2013**, *52*, 3529−3532.

(327) Wan, X. K.; Yuan, S. F.; Lin, Z. W.; Wang, Q. M. A Chiral Gold Nanocluster Au_{20} Protected byTtetradentate Phosphine Ligands. *Angew. Chem., Int. Ed.* **2014**, *53*, 2923−6.

(328) Chen, J.; Zhang, Q.-F.; Bonaccorso, T. A.; Williard, P. G.; Wang, L.-S. Controlling Gold Nanoclusters by Diphospine Ligands. *J. Am. Chem. Soc.* **2014**, *136*, 92−95.

(329) Schubert, U. Cluster-based Inorganic-Organic Hybrid Materials. *Chem. Soc. Rev.* **2011**, *40*, 575−582.

(330) Pei, Y.; Gao, Y.; Zeng, X. C. Structural Prediction of Thiolate-Protected Au_{38}: A Face-Fused Bi-icosahedral Au Core. *J. Am. Chem. Soc.* **2008**, *130*, 7830−7832.

(331) Azubel, M.; Koivisto, J.; Malola, S.; Bushnell, D.; Hura, G. L.; Koh, A. L.; Tsunoyama, H.; Tsukuda, T.; Pettersson, M.; Häkkinen, H.; Kornberg, R. D. Electron Microscopy of Gold Nanoparticles at Atomic Resolution. *Science* **2014**, *345*, 909−912.

(332) Han, Y.; He, D. S.; Liu, Y.; Xie, S.; Tsukuda, T.; Li, Z. Y. Size and Shape of Nanoclusters: Single-Shot Imaging Approach. *Small* **2012**, *8*, 2361−2364.

(333) Parker, J. F.; Choi, J.-P.; Wang, W.; Murray, R. W. Electron Self-exchange Dynamics of the Nanoparticle Couple $[Au_{25}(SC_2Ph)_{18}]^{0/1-}$ By Nuclear Magnetic Resonance Line-Broadening. *J. Phys. Chem. C* **2008**, *112*, 13976−13981.

(334) Wu, Z.; Jin, R. Stability of the Two Au-S Binding Modes in $Au_{25}(SG)_{18}$ Nanoclusters Probed by NMR and Optical Spectroscopy. *ACS Nano* **2009**, *3*, 2036−2042.

(335) Wu, Z.; Gayathri, C.; Gil, R. R.; Jin, R. Probing the Structure and Charge State of Glutathione-Capped $Au_{25}(SG)_{18}$ Clusters by NMR and Mass Spectrometry. *J. Am. Chem. Soc.* **2009**, *131*, 6535−6542.

(336) Stefanescu, D. M.; Glueck, D. S.; Siegel, R.; Wasylishen, R. E. Synthesis and Characterization of Phosphido-Monolayer-Protected Gold Nanoclusters. *Langmuir* **2004**, *20*, 10379−10381.

(337) Zhang, Q.-F.; Williard, P. G.; Wang, L.-S. Polymorphism of Phosphine-Protected Gold Nanoclusters: Synthesis and Characterization of a New 22-Gold-Atom Cluster. *Small* **2016**, *12*, 2518−2525.

(338) Clayden, N. J.; Dobson, C. M.; Hall, K. P.; Mingos, D. M. P.; Smith, D. J. Studies of Gold Cluster Compounds using High-resolution ^{31}P Solid-state Nuclear Magnetic Resonance Spectroscopy. *J. Chem. Soc., Dalton Trans.* **1985**, 1811−1814.

(339) Farrag, M.; Tschurl, M.; Dass, A.; Heiz, U. Infra-red Spectroscopy of Size Selected Au_{25}, Au_{38} and Au_{144} Ligand Protected Gold Clusters. *Phys. Chem. Chem. Phys.* **2013**, *15*, 12539−42.

(340) Dolamic, I.; Varnholt, B.; Burgi, T. Far-infrared Spectra of Well-defined Thiolate-Protected Gold Clusters. *Phys. Chem. Chem. Phys.* **2013**, *15*, 19561−19565.

(341) Varnholt, B.; Oulevey, P.; Luber, S.; Kumara, C.; Dass, A.; Bürgi, T. Structural Information on the Au−S Interface of Thiolate-Protected Gold Clusters: A Raman Spectroscopy Study. *J. Phys. Chem. C* **2014**, *118*, 9604−9611.

(342) Liu, Z.; Xu, Q.; Jin, S.; Wang, S.; Xu, G.; Zhu, M. Electron Transfer Reaction Between Au_{25} Nanocluster and Phenothiazine-tetrachloro-p-benzoquinone Complex. *Int. J. Hydrogen Energy* **2013**, *38*, 16722−16726.

(343) Song, Y.; Fu, F.; Zhang, J.; Chai, J.; Kang, X.; Li, P.; Li, S.; Zhou, H.; Zhu, M. The Magic Au_{60} Nanocluster: A New Cluster-Assembled Material with Five Au_{13} Building Blocks. *Angew. Chem., Int. Ed.* **2015**, *54*, 8430−8434.

(344) Balasubramanian, R.; Guo, R.; Mills, A. J.; Murray, R. W. Reaction of $Au_{55}(PPh_3)_{12}Cl_6$ with Thiols Yields Thiolate Monolayer Protected Au_{75} Clusters. *J. Am. Chem. Soc.* **2005**, *127*, 8126−8132.

(345) Matsuo, S.; Yamazoe, S.; Goh, J.-Q.; Akola, J.; Tsukuda, T. The Electrooxidation-Induced Structural Changes of Gold Di-superatomic Molecules: Au_{23} vs. Au_{25}. *Phys. Chem. Chem. Phys.* **2016**, *18*, 4822−4827.

(346) Kwak, K.; Lee, D. Electrochemical Characterization of Water-Soluble Au_{25} Nanoclusters Enabled by Phase-Transfer Reaction. *J. Phys. Chem. Lett.* **2012**, *3*, 2476−2481.

(347) Park, S.; Lee, D. Synthesis and Electrochemical and Spectroscopic Characterization of Biicosahedral Au_{25} Clusters. *Langmuir* **2012**, *28*, 7049−7054.

(348) Kwak, K.; Kumar, S. S.; Pyo, K.; Lee, D. Ionic Liquid of a Gold Nanocluster: A Versatile Matrix for Electrochemical Biosensors. *ACS Nano* **2014**, *8*, 671−679.

(349) Yao, H. On the Electronic Structures of $Au_{25}(SR)_{18}$ Clusters Studied by Magnetic Circular Dichroism Spectroscopy. *J. Phys. Chem. Lett.* **2012**, *3*, 1701−1706.

(350) Yao, H.; Iwatsu, M. Water-Soluble Phosphine-Protected $_{Au11}$ Clusters: Synthesis, Electronic Structure, and Chiral Phase Transfer in a Synergistic Fashion. *Langmuir* **2016**, *32*, 3284−3293.

(351) Jaw, H. R. C.; Mason, W. R. Magnetic Circular Dichroism Spectra for the octakis(triphenylphosphino)nonagold(3+) ion. *Inorg. Chem.* **1991**, *30*, 275−278.

(352) Zhu, M.; Aikens, C. M.; Hendrich, M. P.; Gupta, R.; Qian, H.; Schatz, G. C.; Jin, R. Reversible Switching of Magnetism in Thiolate-Protected Au_{25} Superatoms. *J. Am. Chem. Soc.* **2009**, *131*, 2490−2492.

(353) Akbari-Sharbaf, A.; Hesari, M.; Workentin, M. S.; Fanchini, G. Electron Paramagnetic Resonance in Positively Charged Au_{25} Molecular Nanoclusters. *J. Chem. Phys.* **2013**, *138*, 024305.

(354) Ionita, P.; Volkov, A.; Jeschke, G.; Chechik, V. Lateral Diffusion of Thiol Ligands on the Surface of Au Nanoparticles: An Electron Paramagnetic Resonance Study. *Anal. Chem.* **2008**, *80*, 95−106.

(355) MacDonald, M. A.; Chevrier, D. M.; Zhang, P.; Qian, H.; Jin, R. The Structure and Bonding of $Au_{25}(SR)_{18}$ Nanoclusters from EXAFS: The Interplay of Metallic and Molecular Behavior. *J. Phys. Chem. C* **2011**, *115*, 15282−15287.

(356) Cluskey, P. D.; Newport, R. J.; Benfield, R. E.; Gurman, S. J.; Schmid, G. An EXAFS Study of some Gold and Palladium Cluster compounds. *Z. Phys. D: At., Mol. Clusters* **1993**, *26*, 8−11.

(357) Shivhare, A.; Lee, K. E.; Hu, Y.; Scott, R. W. J. Following the Reactivity of $Au_{25}(SC_8H_9)_{18}{}^-$ Clusters with Pd^{2+} and Ag^+ Ions Using in Situ X-ray Absorption Spectroscopy: A Tale of Two Metals. *J. Phys. Chem. C* **2015**, *119*, 23279−23284.

(358) Zhang, P. X-ray Spectroscopy of Gold−Thiolate Nanoclusters. *J. Phys. Chem. C* **2014**, *118*, 25291−25299.

(359) Negishi, Y.; Kurashige, W.; Kobayashi, Y.; Yamazoe, S.; Kojima, N.; Seto, M.; Tsukuda, T. Formation of a $Pd@Au_{12}$ Superatomic Core in $Au_{24}Pd_1(SC_{12}H_{25})_{18}$ Probed by ^{197}Au Mössbauer and Pd K-Edge EXAFS Spectroscopy. *J. Phys. Chem. Lett.* **2013**, *4*, 3579−3583.

(360) Christensen, S. L.; Cho, P.; Chatt, A.; Zhang, P. A Site-specific Comparative Study of Au_{102} and Au_{25} Nanoclusters Using Theoretical EXAFS and l-DOS. *Can. J. Chem.* **2015**, *93*, 32−36.

(361) Shivhare, A.; Chevrier, D. M.; Purves, R. W.; Scott, R. W. J. Following the Thermal Activation of $Au_{25}(SR)_{18}$ Clusters for Catalysis by X-ray Absorption Spectroscopy. *J. Phys. Chem. C* **2013**, *117*, 20007−20016.

(362) Chevrier, D. M.; Yang, R.; Chatt, A.; Zhang, P. Bonding Properties of Thiolate-Protected Gold Nanoclusters and Structural Analogs from X-ray Absorption Apectroscopy. *Nanotechnol. Rev.* **2015**, *4*, 193−206.

(363) Bovenkamp-Langlois, L.; Schaefer, M. W. The Characterization of Atomically Precise Nanoclusters Using X-Ray Absorption Spectroscopy. In *X-ray and Neutron Techniques for Nanomaterials Characterization*; Kumar, C. S. S. R., Ed.; Springer: Berlin, 2016; pp 247−313.

(364) Kojima, N.; Kobayashi, Y.; Negishi, Y.; Seto, M.; Tsukuda, T. Structural Evolution of Glutathionate-protected Gold Clusters Studied by means of ^{197}Au Mössbauer Spectroscopy. *Hyperfine Interact.* **2013**, *217*, 91−98.

(365) Kojima, N.; Ikeda, K.; Kobayashi, Y.; Tsukuda, T.; Negishi, Y.; Harada, G.; Sugawara, T.; Seto, M. Study of the Structure and Electronic State of Thiolate-Protected Gold Clusters by means of ^{197}Au Mössbauer Spectroscopy. *Hyperfine Interact.* **2012**, *207*, 127−131.

(366) Tsukuda, T.; Negishi, Y.; Kobayashi, Y.; Kojima, N. ^{197}Au Mössbauer Spectroscopy of $Au_{25}(SG)_{18}^{-}$ Revisited. *Chem. Lett.* **2011**, *40*, 1292−1293.

(367) Tlahuice-Flores, A. New insight into the Structure of Thiolated Gold Clusters: a Structural Prediction of the $Au_{187}(SR)_{68}$ Cluster. *Phys. Chem. Chem. Phys.* **2015**, *17*, 5551−5555.

(368) Green, T. D.; Herbert, P. J.; Yi, C.; Zeng, C.; McGill, S.; Jin, R.; Knappenberger, K. L. Characterization of Emissive States for Structurally Precise $Au_{25}(SC_8H_9)_{180}$ Monolayer-Protected Gold Nanoclusters Using Magnetophotoluminescence Spectroscopy. *J. Phys. Chem. C* **2016**, *120*, 17784−17790.

(369) Yamazoe, S.; Takano, S.; Kurashige, W.; Yokoyama, T.; Nitta, K.; Negishi, Y.; Tsukuda, T. Hierarchy of bond stiffnesses within icosahedral-based gold clusters protected by thiolates. *Nat. Commun.* **2016**, *7*, 10414.

(370) Cao, X.-L.; Li, H.-W.; Yue, Y.; Wu, Y. pH-Induced Conformational Changes of BSA in Fluorescent AuNCs at BSA and its Effects on NCs Emission. *Vib. Spectrosc.* **2013**, *65*, 186−192.

(371) Chaudhari, K.; Xavier, P. L.; Pradeep, T. Understanding the Evolution of Luminescent Gold Quantum Clusters in Protein Templates. *ACS Nano* **2011**, *5*, 8816−8827.

(372) Chen, S.; Zhang, J.; Jiang, S.; Lin, G.; Luo, B.; Yao, H.; Lin, Y.; He, C.; Liu, G.; Lin, Z. Self-Assembled Superparamagnetic Iron Oxide Nanoclusters for Universal Cell Labeling and MRI. *Nanoscale Res. Lett.* **2016**, *11*, 263.

(373) Chen, X.; Essner, J. B.; Baker, G. A. Exploring Luminescence-based Temperature Sensing using Protein-passivated Gold Nanoclusters. *Nanoscale* **2014**, *6*, 9594−9598.

(374) Chib, R.; Butler, S.; Raut, S.; Shah, S.; Borejdo, J.; Gryczynski, Z.; Gryczynski, I. Effect of Quencher, Denaturants, Temperature and pH on the Fluorescent Properties of BSA Protected Gold Nanoclusters. *J. Lumin.* **2015**, *168*, 62−68.

(375) Das, T.; Maity, A.; Mondal, S.; Purkayastha, P. Modulation of Energy/electron Transfer in Gold Nanoclusters by Single Walled Carbon Nanotubes. *Spectrochim. Acta, Part A* **2015**, *141*, 144−148.

(376) Gerdon, A. E.; Wright, D. W.; Cliffel, D. E. Quartz Crystal Microbalance Detection of Glutathione-Protected Nanoclusters using Antibody Recognition. *Anal. Chem.* **2005**, *77*, 304−310.

(377) Gerdon, A. E.; Wright, D. W.; Cliffel, D. E. Epitope Mapping of the Protective Antigen of B. anthracis by using Nanoclusters Presenting Conformational Peptide Epitopes. *Angew. Chem., Int. Ed.* **2006**, *45*, 594−598.

(378) Li, H.; Guo, Y.; Xiao, L.; Chen, B. Selective and Sensitive Detection of acetylcholinesterase Activity using Denatured Protein-protected Gold Nanoclusters as a label-free probe. *Analyst* **2014**, *139*, 285−289.

(379) Liu, X.; Fu, C.; Ren, X.; Liu, H.; Li, L.; Meng, X. Fluorescence Switching Method for Cascade detection of Salicylaldehyde and Zinc(II) ion using Protein Protected Gold Nanoclusters. *Biosens. Bioelectron.* **2015**, *74*, 322−328.

(380) Loftus, A. F.; Reighard, K. P.; Kapourales, S. A.; Leopold, M. C. Monolayer-Protected Nanoparticle Film Assemblies as Platforms for Controlling Interfacial and Adsorption Properties in Protein Monolayer Electrochemistry. *J. Am. Chem. Soc.* **2008**, *130*, 1649−1661.

(381) Mitra, A.; Bhaumik, A. Nanoscale Silver Cluster Embedded in Artificial Heterogeneous Matrix Consisting of Protein and Sodium Polyacrylate. *Mater. Lett.* **2007**, *61*, 659−662.

(382) Raut, S.*Development of Novel Fluorescent Probe- Protein Protected Gold Nanoclusters for Biomedical Applications.* Ph.D. Thesis, University of North Texas Health Science Center at Fort Worth, 2013; 122 pp.

(383) Raut, S.; Chib, R.; Butler, S.; Borejdo, J.; Gryczynski, Z.; Gryczynski, I. Evidence of energy transfer from tryptophan to BSA/HSA protected gold nanoclusters. *Methods Appl. Fluoresc.* **2014**, *2*, 035004.

(384) Retnakumari, A.; Jayasimhan, J.; Chandran, P.; Menon, D.; Nair, S.; Mony, U.; Koyakutty, M. CD33 Monoclonal Antibody Conjugated Au Cluster Nano-bioprobe for Targeted flow-cytometric Detection of Acute Myeloid Leukaemia. *Nanotechnology* **2011**, *22*, 285102.

(385) Simms, G. A.; Padmos, J. D.; Zhang, P. Structural and Electronic Properties of Protein/thiolate-protected Gold nanocluster with "Staple" Motif: A XAS, L-DOS, and XPS study. *J. Chem. Phys.* **2009**, *131*, 214703.

(386) Song, G.-B.; Xu, J.; Zheng, H.; Feng, Y.; Zhang, W.-W.; Li, K.; Ge, S.-s.; Li, K.; Zhang, H. Novel Soluble Dietary Fiber-Tannin Self-Assembled Film: A Promising Protein Protective Material. *J. Agric. Food Chem.* **2015**, *63*, 5813−5820.

(387) Song, W.; Liang, R.-P.; Wang, Y.; Zhang, L.; Qiu, J.-D. Green Synthesis of Peptide-Templated Gold Nanoclusters as Novel Fluorescence Probes for Detecting Protein Kinase Activity. *Chem. Commun.* **2015**, *51*, 10006−10009.

(388) Su, L.; Shu, T.; Wang, J.; Zhang, Z.; Zhang, X. Hidden Dityrosine Residues in Protein-Protected Gold Nanoclusters. *J. Phys. Chem. C* **2015**, *119*, 12065−12070.

(389) Su, L.; Shu, T.; Wang, Z.; Cheng, J.; Xue, F.; Li, C.; Zhang, X. Immobilization of Bovine Serum Albumin-protected Gold Nanoclusters by using Polyelectrolytes of Opposite Charges for the Development of the Reusable Fluorescent Cu^{2+}-sensor. *Biosens. Bioelectron.* **2013**, *44*, 16−20.

(390) Tsai, C.-Y.; Li, C.-W.; Li, J.-R.; Jang, B.-H.; Chen, S.-H. Steroid Probes Conjugated with Protein-Protected Gold Nanocluster: Specific and Rapid Fluorescence Imaging of Steroid Receptors in Target Cells. *J. Fluoresc.* **2016**, *26*, 1239−1248.

(391) Zang, J.; Li, C.; Zhou, K.; Dong, H.; Chen, B.; Wang, F.; Zhao, G. Nanomolar Hg^{2+} Detection Using β-Lactoglobulin-Stabilized Fluorescent Gold Nanoclusters in Beverage and Biological Media. *Anal. Chem.* **2016**, *88*, 10275−10283.

(392) Wang, L.; Hess, A.; Chang, T. Z.; Wang, Y.-C.; Champion, J. A.; Compans, R. W.; Wang, B.-Z. Nanoclusters Self-assembled from Conformation-stabilized Influenza M2e as broadly Cross-protective Influenza Vaccines. *Nanomedicine* **2014**, *10*, 473−482.

(393) Wang, L.-L.; Qiao, J.; Qi, L.; Xu, X.-Z.; Li, D. Construction of OVA-stabilized Fluorescent Gold Nanoclusters for Sensing Glucose. *Sci. China: Chem.* **2015**, *58*, 1508−1514.

(394) Wang, Y.; Wang, Y.; Zhou, F.; Kim, P.; Xia, Y. Protein-Protected Au Clusters as a New Class of Nanoscale Biosensor for Label-Free Fluorescence Detection of Proteases. *Small* **2012**, *8*, 3769−3773.

(395) Xu, S.; Lu, X.; Yao, C.; Huang, F.; Jiang, H.; Hua, W.; Na, N.; Liu, H.; Ouyang, J. A Visual Sensor Array for Pattern Recognition Analysis of Proteins Using Novel Blue-Emitting Fluorescent Gold Nanoclusters. *Anal. Chem.* **2014**, *86*, 11634−11639.

(396) Yan, L.; Cai, Y.; Zheng, B.; Yuan, H.; Guo, Y.; Xiao, D.; Choi, M. M. F. Microwave-assisted Synthesis of BSA-Stabilized and HSA-Protected Gold Nanoclusters with Red emission. *J. Mater. Chem.* **2012**, *22*, 1000−1005.

(397) Yoshimoto, J.; Sangsuwan, A.; Osaka, I.; Yamashita, K.; Iwasaki, Y.; Inada, M.; Arakawa, R.; Kawasaki, H. Optical Properties of 2-Methacryloyloxyethyl Phosphorylcholine-Protected Au_4 Nanoclusters and Their Fluorescence Sensing of C-Reactive Protein. *J. Phys. Chem. C* **2015**, *119*, 14319−14325.

(398) Yue, Y.; Li, H.-W.; Liu, T.-Y.; Wu, Y. Exploring the role of Ligand-BSA in the Response of BSA-protected Gold-nanoclusters to Silver (I) Ions by FT-IR and Circular dichroism Spectra. *Vib. Spectrosc.* **2014**, *74*, 137−141.

(399) Zhang, M.; Dang, Y.-Q.; Liu, T.-Y.; Li, H.-W.; Wu, Y.; Li, Q.; Wang, K.; Zou, B. Pressure-Induced Fluorescence Enhancement of the BSA-Protected Gold Nanoclusters and the Corresponding Conformational Changes of Protein. *J. Phys. Chem. C* **2013**, *117*, 639−647.

(400) Zhang, X.-D.; Luo, Z.; Chen, J.; Song, S.; Yuan, X.; Shen, X.; Wang, H.; Sun, Y.; Gao, K.; Zhang, L.; Fan, S.; Leong, D. T.; Guo, M.; Xie, J. Ultrasmall Glutathione-Protected Gold Nanoclusters as Next

Generation Radiotherapy Sensitizers with High Tumor Uptake and High Renal Clearance. *Sci. Rep.* **2015**, *5*, 8669.

(401) Baksi, A.; Xavier, P. L.; Chaudhari, K.; Goswami, N.; Pal, S. K.; Pradeep, T. Protein-Encapsulated Gold Cluster Aggregates: the Case of Lysozyme. *Nanoscale* **2013**, *5*, 2009−2016.

(402) Mukhopadhyay, R.; Mitra, S.; Johnson, M.; Rajeev Kumar, V. R.; Pradeep, T. Evolution of the Alkyl-chain Dynamics in Monolayer-protected Gold Clusters. *Phys. Rev. B: Condens. Matter Mater. Phys.* **2007**, *75*, 075414.

(403) Resmi, M. R.; Sandhyarani, N.; Unnikrishnan, R.; Ma, S.; Pradeep, T. Charge-Transfer Complexation of C_{60} with Diphenyltetrathiafulvalene (DPTTF) Capped Gold Clusters. *J. Colloid Interface Sci.* **1999**, *217*, 395−402.

(404) Gautier, C.; Taras, R.; Gladiali, S.; Burgi, T. Chiral 1,1′-binaphthyl-2,2′-dithiol-Stabilized Gold Clusters: Size Separation and Optical Activity in the UV-vis. *Chirality* **2008**, *20*, 486−493.

(405) Wolfe, R. L.; Balasubramanian, R.; Tracy, J. B.; Murray, R. W. Fully Ferrocenated Hexanethiolate Monolayer-Protected Gold Clusters. *Langmuir* **2007**, *23*, 2247−2254.

(406) Kurashige, W.; Yamaguchi, M.; Nobusada, K.; Negishi, Y. Ligand-Induced Stability of Gold Nanoclusters: Thiolate versus Selenolate. *J. Phys. Chem. Lett.* **2012**, *3*, 2649−2652.

(407) Negishi, Y.; Arai, R.; Niihori, Y.; Tsukuda, T. Isolation and Structural Characterization of Magic Silver Clusters Protected by 4-(tert-butyl)benzyl Mercaptan. *Chem. Commun.* **2011**, *47*, 5693−5695.

(408) Kurashige, W.; Yamazoe, S.; Kanehira, K.; Tsukuda, T.; Negishi, Y. Selenolate-Protected Au_{38} Nanoclusters: Isolation and Structural Characterization. *J. Phys. Chem. Lett.* **2013**, *4*, 3181−3185.

(409) Kurashige, W.; Yamazoe, S.; Yamaguchi, M.; Nishido, K.; Nobusada, K.; Tsukuda, T.; Negishi, Y. Au_{25} Clusters Containing Unoxidized Tellurolates in the Ligand Shell. *J. Phys. Chem. Lett.* **2014**, *5*, 2072−2076.

(410) Kawasaki, H.; Yamamoto, H.; Fujimori, H.; Arakawa, R.; Iwasaki, Y.; Inada, M. Stability of the DMF-Protected Au Nanoclusters: Photochemical, Dispersion, and Thermal Properties. *Langmuir* **2010**, *26*, 5926−5933.

(411) Schmid, G.; Beyer, N. A New Approach to Well-Ordered Quantum Dots. *Eur. J. Inorg. Chem.* **2000**, *2000*, 835−837.

(412) Schmid, G.; Meyer-Zaika, W.; Pugin, R.; Sawitowski, T.; Majoral, J.-P.; Caminade, A.-M.; Turrin, C.-O. Naked Au_{55} Clusters: Dramatic Effect of a Thiol-Terminated Dendrimer. *Chem. - Eur. J.* **2000**, *6*, 1693−1697.

(413) Schmid, G. n.; Liu, Y.-P.; Schumann, M.; Raschke, T.; Radehaus, C. Quasi One-Dimensional Arrangements of $Au_{55}(PPh_3)_{12}Cl_6$ Clusters and Their Electrical Properties at Room Temperature. *Nano Lett.* **2001**, *1*, 405−407.

(414) Tsunoyama, H.; Ichikuni, N.; Sakurai, H.; Tsukuda, T. Effect of Electronic Structures of Au Clusters Stabilized by Poly(N-vinyl-2-pyrrolidone) on Aerobic Oxidation Catalysis. *J. Am. Chem. Soc.* **2009**, *131*, 7086−7093.

(415) Tsunoyama, H.; Ichikuni, N.; Tsukuda, T. Microfluidic Synthesis and Catalytic Application of PVP-Stabilized, ∼ 1 nm Gold Clusters. *Langmuir* **2008**, *24*, 11327−11330.

(416) Tsunoyama, H.; Sakurai, H.; Negishi, Y.; Tsukuda, T. Size-Specific Catalytic Activity of Polymer-Stabilized Gold Nanoclusters for Aerobic Alcohol Oxidation in Water. *J. Am. Chem. Soc.* **2005**, *127*, 9374−9375.

(417) Tsunoyama, H.; Tsukuda, T. Magic Numbers of Gold Clusters Stabilized by PVP. *J. Am. Chem. Soc.* **2009**, *131*, 18216−18217.

(418) Maity, P.; Takano, S.; Yamazoe, S.; Wakabayashi, T.; Tsukuda, T. Binding Motif of Terminal Alkynes on Gold Clusters. *J. Am. Chem. Soc.* **2013**, *135*, 9450−9457.

(419) Maity, P.; Tsunoyama, H.; Yamauchi, M.; Xie, S.; Tsukuda, T. Organogold Clusters Protected by Phenylacetylene. *J. Am. Chem. Soc.* **2011**, *133*, 20123−20125.

(420) Maity, P.; Wakabayashi, T.; Ichikuni, N.; Tsunoyama, H.; Xie, S.; Yamauchi, M.; Tsukuda, T. Selective Synthesis of Organogold Magic Clusters $Au_{54}(CCPh)_{26}$. *Chem. Commun.* **2012**, *48*, 6085−6087.

(421) Sugiuchi, M.; Shichibu, Y.; Nakanishi, T.; Hasegawa, Y.; Konishi, K. Cluster-[small pi] Electronic Interaction in a Superatomic Au_{13} Cluster Bearing [sigma]-bonded Acetylide Ligands. *Chem. Commun.* **2015**, *51*, 13519−13522.

(422) Antoku, Y.; Hotta, J.-I.; Mizuno, H.; Dickson, R. M.; Hofkens, J.; Vosch, T. Transfection of Living HeLa Cells with Fluorescent Poly-cytosine Encapsulated Ag Nanoclusters. *Photochem. Photobiol. Sci.* **2010**, *9*, 716−721.

(423) Peyser-Capadona, L.; Zheng, J.; Gonzalez, J. I.; Lee, T.-H.; Patel, S. A.; Dickson, R. M. Nanoparticle-free single molecule anti-Stokes Raman spectroscopy. *Phys. Rev. Lett.* **2005**, *94*, 058301.

(424) Choi, S.; Dickson, R. M.; Yu, J. Developing Luminescent Silver Nanodots for Biological Applications. *Chem. Soc. Rev.* **2012**, *41*, 1867−1891.

(425) Choi, S.; Yu, J.; Patel, S. A.; Tzeng, Y.-L.; Dickson, R. M. Tailoring Silver Nanodots for Intracellular Staining. *Photochem. Photobiol. Sci.* **2011**, *10*, 109−115.

(426) Dickson, R. M.; Lee, T.-H. Harnessing Ag Nanocluster Dynamics for Nanotechnology. Presented at the National Meeting of the American Chemical Society, 2003; Paper PHYS 238.

(427) Dickson, R. M.; Lyon, L. A. Apparatus and Method of Optical Transfer and Control in Plasmon Supporting Metal Nanostructures. U.S. Patent US6539156B1, 2003.

(428) Lee, T.-H.; Dickson, R. M. Single-Molecule LEDs from Nanoscale Electroluminescent Junctions. *J. Phys. Chem. B* **2003**, *107*, 7387−7390.

(429) Lee, T.-H.; Dickson, R. M. Nanocomputing with Nanoclusters. *Opt. Photonics News* **2004**, *15*, 22−27.

(430) Lee, T.-H.; Gonzalez, J. I.; Dickson, R. M. Strongly Enhanced field-dependent Single-Molecule Electroluminescence. *Proc. Natl. Acad. Sci. U. S. A.* **2002**, *99*, 10272−5.

(431) Lee, T.-H.; Gonzalez, J. I.; Zheng, J.; Dickson, R. M. Single-Molecule Optoelectronics. *Acc. Chem. Res.* **2005**, *38*, 534−541.

(432) Patel, S. A.; Cozzuol, M.; Hales, J. M.; Richards, C. I.; Sartin, M.; Hsiang, J.-C.; Vosch, T.; Perry, J. W.; Dickson, R. M. Electron Transfer-Induced Blinking in Ag Nanodot Fluorescence. *J. Phys. Chem. C* **2009**, *113*, 20264−20270.

(433) Patel, S. A.; Richards, C. I.; Hsiang, J.-C.; Dickson, R. M. Water-Soluble Ag Nanoclusters Exhibit Strong Two-Photon-Induced Fluorescence. *J. Am. Chem. Soc.* **2008**, *130*, 11602−11603.

(434) Petty, J. T.; Fan, C.; Story, S. P.; Sengupta, B.; St. John Iyer, A.; Prudowsky, Z.; Dickson, R. M. DNA Encapsulation of 10 Silver Atoms Producing a Bright, Modulatable, Near-Infrared-Emitting Cluster. *J. Phys. Chem. Lett.* **2010**, *1*, 2524−2529.

(435) Petty, J. T.; Fan, C.-Y.; Story, S. P.; Sengupta, B.; Sartin, M.; Hsiang, J.-C.; Perry, J. W.; Dickson, R. M. Optically Enhanced, Near-IR, Silver Cluster Emission Altered by Single Base Changes in the DNA Template. *J. Phys. Chem. B* **2011**, *115*, 7996−8003.

(436) Petty, J. T.; Story, S. P.; Hsiang, J.-C.; Dickson, R. M. DNA-Templated Molecular Silver Fluorophores. *J. Phys. Chem. Lett.* **2013**, *4*, 1148−1155.

(437) Petty, J. T.; Zheng, J.; Hud, N. V.; Dickson, R. M. DNA-templated Ag Nanocluster formation. *J. Am. Chem. Soc.* **2004**, *126*, 5207−5212.

(438) Peyser, L. A.; Vinson, A. E.; Bartko, A. P.; Dickson, R. M. Photoactivated Fluorescence from Individual Silver Nanoclusters. *Science* **2001**, *291*, 103−106.

(439) Richards, C. I.; Choi, S.; Hsiang, J.-C.; Antoku, Y.; Vosch, T.; Bongiorno, A.; Tzeng, Y.-L.; Dickson, R. M. Oligonucleotide-Stabilized Ag Nanocluster Fluorophores. *J. Am. Chem. Soc.* **2008**, *130*, 5038−5039.

(440) Richards, C. I.; Hsiang, J.-C.; Senapati, D.; Patel, S.; Yu, J.; Vosch, T.; Dickson, R. M. Optically Modulated Fluorophores for Selective Fluorescence Signal Recovery. *J. Am. Chem. Soc.* **2009**, *131*, 4619−4621.

(441) Ritchie, C. M.; Johnsen, K. R.; Kiser, J. R.; Antoku, Y.; Dickson, R. M.; Petty, J. T. Ag Nanocluster formation using a Cytosine Oligonucleotide Template. *J. Phys. Chem. C* **2007**, *111*, 175−181.

(442) Vosch, T.; Antoku, Y.; Hsiang, J.-C.; Richards, C. I.; Gonzalez, J. I.; Dickson, R. M. Strongly Emissive Individual DNA-encapsulated Ag Nanoclusters as Single-molecule fluorophores. *Proc. Natl. Acad. Sci. U. S. A.* **2007**, *104*, 12616−12621.

(443) Yu, J.; Choi, S.; Dickson, R. M. Shuttle-based Fluorogenic Silver-cluster Biolabels. *Angew. Chem., Int. Ed.* **2009**, *48*, 318−320.

(444) Yu, J.; Choi, S.; Richards, C. I.; Antoku, Y.; Dickson, R. M. Live Cell Surface Labeling with Fluorescent Ag Nanocluster Conjugates. *Photochem. Photobiol.* **2008**, *84*, 1435−1439.

(445) Yu, J.; Patel, S. A.; Dickson, R. M. In vitro and Intracellular Production of Peptide-Encapsulated Fluorescent Silver Nanoclusters. *Angew. Chem., Int. Ed.* **2007**, *46*, 2028−2030.

(446) Zheng, J.; Capadona, L. A.; Petty, J. T.; Zhang, C.; Tzeng, Y.-L.; Dickson, R. M. Highly Fluorescent, Size-tunable, Water-soluble Au and Ag Nanodots for Single Molecule Biophysics in Living Systems. Presented at the National Meeting of the American Chemical Society, 2004; Paper PHYS-072.

(447) Zheng, J.; Dickson, R. M. Individual Water-Soluble Dendrimer-Encapsulated Silver Nanodot Fluorescence. *J. Am. Chem. Soc.* **2002**, *124*, 13982−13983.

(448) Cathcart, N.; Kitaev, V. Silver Nanoclusters: Single-Stage Scaleable Synthesis of Monodisperse Species and Their Chirooptical Properties. *J. Phys. Chem. C* **2010**, *114*, 16010−16017.

(449) AbdulHalim, L. G.; Hooshmand, Z.; Parida, M. R.; Aly, S. M.; Le, D.; Zhang, X.; Rahman, T. S.; Pelton, M.; Losovyj, Y.; Dowben, P. A.; Bakr, O. M.; Mohammed, O. F.; Katsiev, K. pH-Induced Surface Modification of Atomically Precise Silver Nanoclusters: An Approach for Tunable Optical and Electronic Properties. *Inorg. Chem.* **2016**, *55*, 11522−11528.

(450) Bakr, O. M.; Amendola, V.; Aikens, C. M.; Wenseleers, W.; Li, R.; Dal Negro, L.; Schatz, G. C.; Stellacci, F. Silver Nanoparticles with Broad Multiband Linear Optical Absorption. *Angew. Chem.* **2009**, *121*, 6035−6040.

(451) Cathcart, N.; Mistry, P.; Makra, C.; Pietrobon, B.; Coombs, N.; Jelokhani-Niaraki, M.; Kitaev, V. Chiral Thiol-Stabilized Silver Nanoclusters with Well-Resolved Optical Transitions Synthesized by a Facile Etching Procedure in Aqueous Solutions. *Langmuir* **2009**, *25*, 5840−5846.

(452) Díez, I.; Pusa, M.; Kulmala, S.; Jiang, H.; Walther, A.; Goldmann, A. S.; Müller, A. H. E.; Ikkala, O.; Ras, R. H. A. Color Tunability and Electrochemiluminescence of Silver Nanoclusters. *Angew. Chem., Int. Ed.* **2009**, *48*, 2122−2125.

(453) Nishida, N.; Yao, H.; Kimura, K. Chiral Functionalization of Optically Inactive Monolayer-Protected Silver Nanoclusters by Chiral Ligand-Exchange Reactions. *Langmuir* **2008**, *24*, 2759−2766.

(454) Ritchie, C. M.; Johnsen, K. R.; Kiser, J. R.; Antoku, Y.; Dickson, R. M.; Petty, J. T. Ag Nanocluster Formation Using a Cytosine Oligonucleotide Template. *J. Phys. Chem. C* **2007**, *111*, 175−181.

(455) Wu, Z.; Lanni, E.; Chen, W.; Bier, M. E.; Ly, D.; Jin, R. High Yield, Large Scale Synthesis of Thiolate-Protected Ag_7 Clusters. *J. Am. Chem. Soc.* **2009**, *131*, 16672−16674.

(456) Zheng, K.; Yuan, X.; Kuah, K.; Luo, Z.; Yao, Q.; Zhang, Q.; Xie, J. Boiling Water Synthesis of Ultrastable Thiolated Silver Nanoclusters with Aggregation-induced Emission. *Chem. Commun.* **2015**, *51*, 15165−15168.

(457) AbdulHalim, L. G.; Bootharaju, M. S.; Tang, Q.; Del Gobbo, S.; AbdulHalim, R. G.; Eddaoudi, M.; Jiang, D.-e.; Bakr, O. M. $Ag_{29}(BDT)_{12}(TPP)_4$: A Tetravalent Nanocluster. *J. Am. Chem. Soc.* **2015**, *137*, 11970−11975.

(458) Baksi, A.; Harvey, S. R.; Natarajan, G.; Wysocki, V. H.; Pradeep, T. Possible Isomers in Ligand Protected Ag_{11} Cluster Ions Identified by Ion Mobility Mass Spectrometry and Fragmented by Surface Induced Dissociation. *Chem. Commun.* **2016**, *52*, 3805−3808.

(459) Alhilaly, M. J.; Bootharaju, M. S.; Joshi, C. P.; Besong, T. M. D.; Emwas, A.-H.; Juarez Mosqueda, R.; Kaappa, S.; Malola, S.; Adil, K.; Shkurenko, A.; Häkkinen, H.; Eddaoudi, M.; Bakr, O. M. $[Ag_{67}(SPhMe_2)_{32}(PPh_3)_8]^{3+}$: Synthesis, Total Structure, and Optical Properties of a Large Box-Shaped Silver Nanocluster. *J. Am. Chem. Soc.* **2016**, *138*, 14727−14732.

(460) Yang, H.; Wang, Y.; Chen, X.; Zhao, X.; Gu, L.; Huang, H.; Yan, J.; Xu, C.; Li, G.; Wu, J.; Edwards, A. J.; Dittrich, B.; Tang, Z.; Wang, D.; Lehtovaara, L.; Hakkinen, H.; Zheng, N. Plasmonic Twinned Silver Nanoparticles with Molecular Precision. *Nat. Commun.* **2016**, *7*, 12809.

(461) Remya, K. P.; Udayabhaskararao, T.; Pradeep, T. Low-Temperature Thermal Dissociation of Ag Quantum Clusters in Solution and Formation of Monodisperse Ag_2S Nanoparticles. *J. Phys. Chem. C* **2012**, *116*, 26019−26026.

(462) Delamarche, E.; Michel, B.; Kang, H.; Gerber, C. Thermal Stability of Self-Assembled Monolayers. *Langmuir* **1994**, *10*, 4103−4108.

(463) Terrill, R. H.; Postlethwaite, T. A.; Chen, C.-h.; Poon, C.-D.; Terzis, A.; Chen, A.; Hutchison, J. E.; Clark, M. R.; Wignall, G. Monolayers in Three Dimensions: NMR, SAXS, Thermal, and Electron Hopping Studies of Alkanethiol Stabilized Gold Clusters. *J. Am. Chem. Soc.* **1995**, *117*, 12537−12548.

(464) Nuzzo, R.; Korenic, E.; Dubois, L. Studies of the Temperature-Dependent Phase Behavior of Long Chain n-alkyl Thiol Monolayers on Gold. *J. Chem. Phys.* **1990**, *93*, 767−773.

(465) Buttner, M.; Belser, T.; Oelhafen, P. Stability of Thiol-passivated Gold Particles at Elevated Temperatures Studied by X-ray Photoelectron Spectroscopy. *J. Phys. Chem. B* **2005**, *109*, 5464−5467.

(466) Murty, K. V. G. K.; Venkataramanan, M.; Pradeep, T. Self-assembled Monolayers of 1,4-Benzenedimethanethiol on Polycrystalline Silver and Gold Films: An Investigation of Structure, Stability, Dynamics, and Reactivity. *Langmuir* **1998**, *14*, 5446−5456.

(467) Mie, G. Beiträge zur Optik trüber Medien, speziell kolloidaler Metallösungen. *Ann. Phys.* **1908**, *330*, 377−445.

(468) Sugi, K. S.; Chakraborty, I.; Udayabhaskararao, T.; Mohanty, J. S.; Pradeep, T. Evolution of Atomically Precise Silver Clusters to Superlattice Crystals. *Part. Part. Sys. Charact.* **2013**, *30*, 241−243.

(469) Taylor, K. J.; Pettiette-Hall, C. L.; Cheshnovsky, O.; Smalley, R. E. Ultraviolet Photoelectron Spectra of Coinage Metal Clusters. *J. Chem. Phys.* **1992**, *96*, 3319−3329.

(470) Si, S.; Gautier, C.; Boudon, J.; Taras, R.; Gladiali, S.; Bürgi, T. Ligand Exchange on Au_{25} Cluster with Chiral Thiols. *J. Phys. Chem. C* **2009**, *113*, 12966−12969.

(471) Reyes, E. n.; Madueño, R.; Blázquez, M.; Pineda, T. Facile Exchange of Ligands on the 6-Mercaptopurine-Monolayer Protected Gold Clusters Surface. *J. Phys. Chem. C* **2010**, *114*, 15955−15962.

(472) Knoppe, S.; Dharmaratne, A. C.; Schreiner, E.; Dass, A.; Bürgi, T. Ligand Exchange Reactions on Au_{38} and Au_{40} Clusters: A Combined Circular Dichroism and Mass Spectrometry Study. *J. Am. Chem. Soc.* **2010**, *132*, 16783−16789.

(473) Grant, C. D.; Schwartzberg, A. M.; Yang, Y.; Chen, S.; Zhang, J. Z. Ultrafast Study of Electronic Relaxation Dynamics in Au_{11} Nanoclusters. *Chem. Phys. Lett.* **2004**, *383*, 31−34.

(474) Woehrle, G. H.; Warner, M. G.; Hutchison, J. E. Ligand Exchange Reactions Yield Subnanometer, Thiol-Stabilized Gold Particles with Defined Optical Transitions. *J. Phys. Chem. B* **2002**, *106*, 9979−9981.

(475) Habeeb Muhammed, M.; Ramesh, S.; Sinha, S.; Pal, S.; Pradeep, T. Two Distinct Fluorescent Quantum Clusters of Gold Starting from Metallic Nanoparticles by pH-dependent Ligand Etching. *Nano Res.* **2008**, *1*, 333−340.

(476) Habeeb Muhammed, M. A.; Pradeep, T. Aqueous to Organic Phase Transfer of Au_{25} Clusters. *J. Cluster Sci.* **2009**, *20*, 365−373.

(477) Shichibu, Y.; Negishi, Y.; Tsukuda, T.; Teranishi, T. Large-Scale Synthesis of Thiolated Au_{25} Clusters via Ligand Exchange Reactions of Phosphine-Stabilized Au_{11} Clusters. *J. Am. Chem. Soc.* **2005**, *127*, 13464−13465.

(478) Muhammed, M. A. H.; Shaw, A. K.; Pal, S. K.; Pradeep, T. Quantum Clusters of Gold Exhibiting FRET. *J. Phys. Chem. C* **2008**, *112*, 14324−14330.

(479) Zhang, B.; Salassa, G.; Burgi, T. Silver Migration between $Au_{38}(SC_2H_4Ph)_{24}$ and Doped $Ag_xAu_{38-x}(SC_2H_4Ph)_{24}$ Nanoclusters. *Chem. Commun.* **2016**, *52*, 9205−9207.

(480) Baksi, A.; Chakraborty, P.; Bhat, S.; Natarajan, G.; Pradeep, T. $[Au_{25}(SR)_{18}]_{22}^{-}$: A Noble Metal Cluster Dimer in the Gas Phase. *Chem. Commun.* **2016**, *52*, 8397−8400.

(481) Smith, J. G.; Chakraborty, I.; Jain, P. K. In Situ Single-Nanoparticle Spectroscopy Study of Bimetallic Nanostructure Formation. *Angew. Chem., Int. Ed.* **2016**, *55*, 9979−9983.

(482) Jin, R.; Zhao, S.; Xing, Y.; Jin, R. All-thiolate-protected Silver and Silver-rich Alloy Nanoclusters with Atomic Precision: Stable Sizes, Structural Characterization and Optical Properties. *CrystEngComm* **2016**, *18*, 3996−4005.

(483) Bruma, A.; Negreiros, F. R.; Xie, S.; Tsukuda, T.; Johnston, R. L.; Fortunelli, A.; Li, Z. Y. Direct Atomic Imaging and Density Functional Theory Study of the $Au_{24}Pd_1$ Cluster Catalyst. *Nanoscale* **2013**, *5*, 9620−9625.

(484) Tofanelli, M. A.; Ni, T. W.; Phillips, B. D.; Ackerson, C. J. Crystal Structure of the $PdAu_{24}(SR)_{180}$ Superatom. *Inorg. Chem.* **2016**, *55*, 999−1001.

(485) Negishi, Y.; Iwai, T.; Ide, M. Continuous Modulation of Electronic Structure of Stable Thiolate-protected Au_{25} Cluster by Ag doping. *Chem. Commun.* **2010**, *46*, 4713−4715.

(486) Yamazoe, S.; Kurashige, W.; Nobusada, K.; Negishi, Y.; Tsukuda, T. Preferential Location of Coinage Metal Dopants (M = Ag or Cu) in $[Au_{25-x}M_x(SC_2H_4Ph)_{18}]^-$ (x ∼ 1) As Determined by Extended X-ray Absorption Fine Structure and Density Functional Theory Calculations. *J. Phys. Chem. C* **2014**, *118*, 25284−25290.

(487) Yang, S.; Wang, S.; Jin, S.; Chen, S.; Sheng, H.; Zhu, M. A metal Exchange Method for Thiolate-protected Tri-metal $M_1Ag_xAu_{24-x}(SR)_{180}$ (M = Cd/Hg) Nanoclusters. *Nanoscale* **2015**, *7*, 10005−10007.

(488) Yang, H.; Wang, Y.; Lei, J.; Shi, L.; Wu, X.; Mäkinen, V.; Lin, S.; Tang, Z.; He, J.; Häkkinen, H.; Zheng, L.; Zheng, N. Ligand-Stabilized $Au_{13}Cu_x$ (x = 2, 4, 8) Bimetallic Nanoclusters: Ligand Engineering to Control the Exposure of Metal Sites. *J. Am. Chem. Soc.* **2013**, *135*, 9568−9571.

(489) Yan, J.; Su, H.; Yang, H.; Malola, S.; Lin, S.; Häkkinen, H.; Zheng, N. Total Structure and Electronic Structure Analysis of Doped Thiolated Silver $[MAg_{24}(SR)_{18}]^{2-}$ (M = Pd, Pt) Clusters. *J. Am. Chem. Soc.* **2015**, *137*, 11880−11883.

(490) Wang, S.; Jin, S.; Yang, S.; Chen, S.; Song, Y.; Zhang, J.; Zhu, M. Total Structure Determination of Surface Doping $[Ag_{46}Au_{24}(SR)_{32}](BPh_4)_2$ Nanocluster and its Structure-Related Catalytic Property. *Sci. Adv.* **2015**, *1*, e1500441.

(491) Yan, N.; Liao, L.; Yuan, J.; Lin, Y.-J.; Weng, L.-H.; Yang, J.; Wu, Z. Bi-metal Doping in Nanoclusters: Synergistic or Counteractive? *Chem. Mater.* **2016**, *28*, 8240−8247.

(492) Qian, H.; Barry, E.; Zhu, Y.; Jin, R. Doping 25-Atom and 38-Atom Gold Nanoclusters with Palladium. *Acta Phys.-Chim. Sin.* **2011**, *27*, 513−519.

(493) Negishi, Y.; Igarashi, K.; Munakata, K.; Ohgake, W.; Nobusada, K. Palladium Doping of Magic Gold Cluster $Au_{38}(SC_2H_4Ph)_{24}$: Formation of $Pd_2Au_{36}(SC_2H_4Ph)_{24}$ with Higher Stability than $Au_{38}(SC_2H_4Ph)_{24}$. *Chem. Commun.* **2012**, *48*, 660−662.

(494) Kumara, C.; Dass, A. $(AuAg)_{144}(SR)_{60}$ Alloy Nanomolecules. *Nanoscale* **2011**, *3*, 3064−3067.

(495) Biltek, S. R.; Mandal, S.; Sen, A.; Reber, A. C.; Pedicini, A. F.; Khanna, S. N. Synthesis and Structural Characterization of an Atom-Precise Bimetallic Nanocluster, $Ag_4Ni_2(DMSA)_4$. *J. Am. Chem. Soc.* **2013**, *135*, 26−29.

(496) Yan, J.; Su, H.; Yang, H.; Hu, C.; Malola, S.; Lin, S.; Teo, B. K.; Häkkinen, H.; Zheng, N. Asymmetric Synthesis of Chiral Bimetallic $[Ag_{28}Cu_{12}(SR)_{24}]^{4-}$ Nanoclusters via Ion Pairing. *J. Am. Chem. Soc.* **2016**, *138*, 12751−12754.

(497) Bootharaju, M. S.; Sinatra, L.; Bakr, O. M. Distinct Metal-Exchange Pathways of Doped Ag_{25} nanoclusters. *Nanoscale* **2016**, *8*, 17333−17339.

(498) Zeng, J.-L.; Guan, Z.-J.; Du, Y.; Nan, Z.-A.; Lin, Y.-M.; Wang, Q.-M. Chloride-Promoted Formation of a Bimetallic Nanocluster $Au_{80}Ag_{30}$ and the Total Structure Determination. *J. Am. Chem. Soc.* **2016**, *138*, 7848−7851.

(499) Christensen, S. L.; MacDonald, M. A.; Chatt, A.; Zhang, P.; Qian, H.; Jin, R. Dopant Location, Local Structure, and Electronic Properties of $Au_{24}Pt(SR)_{18}$ Nanoclusters. *J. Phys. Chem. C* **2012**, *116*, 26932−26937.

(500) Yao, C.; Chen, J.; Li, M.-B.; Liu, L.; Yang, J.; Wu, Z. Adding Two Active Silver Atoms on Au_{25} Nanoparticle. *Nano Lett.* **2015**, *15*, 1281−1287.

(501) Wang, Y.; Su, H.; Xu, C.; Li, G.; Gell, L.; Lin, S.; Tang, Z.; Häkkinen, H.; Zheng, N. An Intermetallic $Au_{24}Ag_{20}$ Superatom Nanocluster Stabilized by Labile Ligands. *J. Am. Chem. Soc.* **2015**, *137*, 4324−4327.

(502) Wang, S.; Song, Y.; Jin, S.; Liu, X.; Zhang, J.; Pei, Y.; Meng, X.; Chen, M.; Li, P.; Zhu, M. Metal Exchange Method Using Au_{25} Nanoclusters as Templates for Alloy Nanoclusters with Atomic Precision. *J. Am. Chem. Soc.* **2015**, *137*, 4018−4021.

(503) Wen, X.; Yu, P.; Toh, Y.-R.; Tang, J. Structure-Correlated Dual Fluorescent Bands in BSA-Protected Au_{25} Nanoclusters. *J. Phys. Chem. C* **2012**, *116*, 11830−11836.

(504) Yue, Y.; Liu, T.-Y.; Li, H.-W.; Liu, Z.; Wu, Y. Microwave-assisted Synthesis of BSA-Protected Small Gold Nanoclusters and their Fluorescence-enhanced Sensing of silver(i) ions. *Nanoscale* **2012**, *4*, 2251−2254.

(505) Zhou, W.; Cao, Y.; Sui, D.; Guan, W.; Lu, C.; Xie, J. Ultrastable BSA-capped Gold Nanoclusters with a Polymer-like Shielding Layer Against Reactive Oxygen Species in Living Cells. *Nanoscale* **2016**, *8*, 9614−9620.

(506) Mohanty, J. S.; Baksi, A.; Lee, H.; Pradeep, T. Noble Metal Clusters Protected with Mixed Proteins Exhibit Intense Photoluminescence. *RSC Adv.* **2015**, *5*, 48039−48045.

(507) Habeeb Muhammed, M. A.; Verma, P. K.; Pal, S. K.; Retnakumari, A.; Koyakutty, M.; Nair, S.; Pradeep, T. Luminescent Quantum Clusters of Gold in Bulk by Albumin-Induced Core Etching of Nanoparticles: Metal Ion Sensing, Metal-Enhanced Luminescence, and Biolabeling. *Chem. - Eur. J.* **2010**, *16*, 10103−10112.

(508) Le Guével, X.; Hötzer, B.; Jung, G.; Hollemeyer, K.; Trouillet, V.; Schneider, M. Formation of Fluorescent Metal (Au, Ag) Nanoclusters Capped in Bovine Serum Albumin Followed by Fluorescence and Spectroscopy. *J. Phys. Chem. C* **2011**, *115*, 10955−10963.

(509) Mohanty, J. S.; Xavier, P. L.; Chaudhari, K.; Bootharaju, M.; Goswami, N.; Pal, S.; Pradeep, T. Luminescent, Bimetallic AuAg Alloy Quantum Clusters in Protein Templates. *Nanoscale* **2012**, *4*, 4255−4262.

(510) Wei, H.; Wang, Z.; Yang, L.; Tian, S.; Hou, C.; Lu, Y. Lysozyme-stabilized Gold Fluorescent Cluster: Synthesis and Application as Hg^{2+} sensor. *Analyst* **2010**, *135*, 1406−1410.

(511) Lin, Y.-H.; Tseng, W.-L. Ultrasensitive Sensing of Hg^{2+} and CH_3Hg^+ Based on the Fluorescence Quenching of Lysozyme Type VI-Stabilized Gold Nanoclusters. *Anal. Chem.* **2010**, *82*, 9194−9200.

(512) Chen, W. Y.; Lin, J.-Y.; Chen, W.-J.; Luo, L.; Wei-Guang Diau, E.; Chen, Y.-C. Functional Gold Nanoclusters as Antimicrobial Agents for Antibiotic-resistant Aacteria. *Nanomedicine* **2010**, *5*, 755−764.

(513) Sreeprasad, T. S.; Maliyekkal, M. S.; Deepti, K.; Chaudhari, K.; Xavier, P. L.; Pradeep, T. Transparent, Luminescent, Antibacterial and Patternable Film Forming Composites of Graphene Oxide/Reduced Graphene Oxide. *ACS Appl. Mater. Interfaces* **2011**, *3*, 2643−2654.

(514) Liu, C.-L.; Wu, H.-T.; Hsiao, Y.-H.; Lai, C.-W.; Shih, C.-W.; Peng, Y.-K.; Tang, K.-C.; Chang, H.-W.; Chien, Y.-C.; Hsiao, J.-K.; Cheng, J.-T.; Chou, P.-T. Insulin-Directed Synthesis of Fluorescent Gold Nanoclusters: Preservation of Insulin Bioactivity and Versatility in Cell Imaging. *Angew. Chem.* **2011**, *123*, 7194−7198.

(515) Garcia, A. R.; Rahn, I.; Johnson, S.; Patel, R.; Guo, J.; Orbulescu, J.; Micic, M.; Whyte, J. D.; Blackwelder, P.; Leblanc, R. M. Human Insulin Fibril-assisted Synthesis of Fluorescent Gold Nano-

clusters in Alkaline Media under Physiological Temperature. *Colloids Surf., B* **2013**, *105*, 167−172.

(516) Kawasaki, H.; Hamaguchi, K.; Osaka, I.; Arakawa, R. pH-Dependent Synthesis of Pepsin-Mediated Gold Nanoclusters with Blue Green and Red Fluorescent Emission. *Adv. Funct. Mater.* **2011**, *21*, 3508−3515.

(517) Kawasaki, H.; Yoshimura, K.; Hamaguchi, K.; Arakawa, R. Trypsin-stabilized Fluorescent Gold Nanocluster for Sensitive and Selective Hg^{2+} Detection. *Anal. Sci.* **2011**, *27*, 591−596.

(518) Chaudhari, K.; Pradeep, T. Initial Growth Kinetics of Luminescent Quantum Clusters of Silver within Albumin Family Protein Templates. *J. Phys. Chem. C* **2015**, *119*, 9988−9994.

(519) Baksi, A.; Mitra, A.; Mohanty, J. S.; Lee, H.; De, G.; Pradeep, T. Size Evolution of Protein-Protected Gold Clusters in Solution: A Combined SAXS−MS Investigation. *J. Phys. Chem. C* **2015**, *119*, 2148−2157.

(520) Durgadas, C. V.; Sharma, C. P.; Sreenivasan, K. Fluorescent Gold Clusters as Nanosensors for Copper Ions in Live Cells. *Analyst* **2011**, *136*, 933−940.

(521) Hu, D.; Sheng, Z.; Gong, P.; Zhang, P.; Cai, L. Highly Selective Fluorescent Sensors for Hg^{2+} based on Bovine Serum Albumin-capped Gold Nanoclusters. *Analyst* **2010**, *135*, 1411−1416.

(522) Goswami, N.; Giri, A.; Bootharaju, M. S.; Xavier, P. L.; Pradeep, T.; Pal, S. K. Copper Quantum Clusters in Protein Matrix: Potential Sensor of Pb^{2+} ion. *Anal. Chem.* **2011**, *83*, 9676−9680.

(523) Song, X.-R.; Goswami, N.; Yang, H.-H.; Xie, J. Functionalization of Metal Nanoclusters for Biomedical Applications. *Analyst* **2016**, *141*, 3126−3140.

(524) Yang, X.; Wang, E. K. CHAPTER 5 Synthesis and Applications of Silver Nanoclusters Protected by Polymers, Protein, Peptide and Short Molecules. In *Functional Nanometer-Sized Clusters of Transition Metals: Synthesis, Properties and Applications*; The Royal Society of Chemistry: 2014; pp 100−130.

(525) Goswami, N.; Li, J.; Xie, J. Chapter 11 - Functionalization and Application. In *Frontiers of Nanoscience*; Tatsuya, T., Hannu, H., Eds.; Elsevier: 2015; Vol. *9*, pp 297−345.

(526) Pradeep, T.; Baksi, A.; Xavier, P. L. CHAPTER 7 Noble Metal Clusters in Protein Templates. In *Functional Nanometer-Sized Clusters of Transition Metals: Synthesis, Properties and Applications*; The Royal Society of Chemistry: 2014; pp 169−225.

(527) Philip, R.; Chantharasupawong, P.; Qian, H.; Jin, R.; Thomas, J. Evolution of Nonlinear Optical Properties: From Gold Atomic Clusters to Plasmonic Nanocrystals. *Nano Lett.* **2012**, *12*, 4661−4667.

(528) Knoppe, S.; Vanbel, M.; van Cleuvenbergen, S.; Vanpraet, L.; Bürgi, T.; Verbiest, T. Nonlinear Optical Properties of Thiolate-Protected Gold Clusters. *J. Phys. Chem. C* **2015**, *119*, 6221−6226.

(529) Knoppe, S.; Häkkinen, H.; Verbiest, T. Nonlinear Optical Properties of Thiolate-Protected Gold Clusters: A Theoretical Survey of the First Hyperpolarizabilities. *J. Phys. Chem. C* **2015**, *119*, 27676−27682.

(530) Russier-Antoine, I.; Bertorelle, F.; Vojkovic, M.; Rayane, D.; Salmon, E.; Jonin, C.; Dugourd, P.; Antoine, R.; Brevet, P.-F. Non-linear Optical Properties of Gold Quantum Clusters. The smaller the better. *Nanoscale* **2014**, *6*, 13572−13578.

(531) Day, P. N.; Pachter, R.; Nguyen, K. A.; Bigioni, T. P. Linear and Nonlinear Optical Response in Silver Nanoclusters: Insight from a Computational Investigation. *J. Phys. Chem. A* **2016**, *120*, 507−518.

(532) Polavarapu, L.; Manna, M.; Xu, Q.-H. Biocompatible Glutathione Capped Gold Clusters as one- and two-photon Excitation Fluorescence Contrast Agents for Live Cells Imaging. *Nanoscale* **2011**, *3*, 429−434.

(533) Olesiak-Banska, J.; Waszkielewicz, M.; Matczyszyn, K.; Samoc, M. A Closer Look at two-photon Absorption, Absorption Saturation and Nonlinear Refraction in Gold Nanoclusters. *RSC Adv.* **2016**, *6*, 98748−98752.

(534) Ramakrishna, G.; Varnavski, O.; Kim, J.; Lee, D.; Goodson, T. Quantum-Sized Gold Clusters as Efficient Two-Photon Absorbers. *J. Am. Chem. Soc.* **2008**, *130*, 5032−5033.

(535) Patel, S. A.; Richards, C. I.; Hsiang, J.-C.; Dickson, R. M. Water-Soluble Ag Nanoclusters Exhibit Strong Two-Photon-Induced Fluorescence. *J. Am. Chem. Soc.* **2008**, *130*, 11602−11603.

(536) Yau, S. H.; Abeyasinghe, N.; Orr, M.; Upton, L.; Varnavski, O.; Werner, J. H.; Yeh, H.-C.; Sharma, J.; Shreve, A. P.; Martinez, J. S.; Goodson Iii, T. Bright Two-photon Emission and ultra-fast Relaxation Dynamics in a DNA-templated Nanocluster Investigated by ultra-fast Spectroscopy. *Nanoscale* **2012**, *4*, 4247−4254.

(537) Hori, H.; Yamamoto, Y.; Iwamoto, T.; Miura, T.; Teranishi, T.; Miyake, M. Diameter Dependence of Ferromagnetic Spin Moment in Au Nanocrystals. *Phys. Rev. B: Condens. Matter Mater. Phys.* **2004**, *69*, 174411.

(538) Crespo, P.; Litrán, R.; Rojas, T. C.; Multigner, M.; de la Fuente, J. M.; Sánchez-López, J. C.; García, M. A.; Hernando, A.; Penadés, S.; Fernández, A. Permanent Magnetism, Magnetic Anisotropy, and Hysteresis of Thiol-Capped Gold Nanoparticles. *Phys. Rev. Lett.* **2004**, *93*, 087204.

(539) Negishi, Y.; Tsunoyama, H.; Suzuki, M.; Kawamura, N.; Matsushita, M. M.; Maruyama, K.; Sugawara, T.; Yokoyama, T.; Tsukuda, T. X-ray Magnetic Circular Dichroism of Size-Selected, Thiolated Gold Clusters. *J. Am. Chem. Soc.* **2006**, *128*, 12034−12035.

(540) McCoy, R. S.; Choi, S.; Collins, G.; Ackerson, B. J.; Ackerson, C. J. Superatom Paramagnetism Enables Gold Nanocluster Heating in Applied Radiofrequency Fields. *ACS Nano* **2013**, *7*, 2610−2616.

(541) Yuan, X.; Tay, Y.; Dou, X.; Luo, Z.; Leong, D. T.; Xie, J. Glutathione-Protected Silver Nanoclusters as Cysteine-Selective Fluorometric and Colorimetric Probe. *Anal. Chem.* **2013**, *85*, 1913−1919.

(542) Yuan, X.; Yeow, T. J.; Zhang, Q.; Lee, J. Y.; Xie, J. Highly Luminescent Ag^{+} Nanoclusters for Hg^{2+} ion Detection. *Nanoscale* **2012**, *4*, 1968−1971.

(543) Fang, J.; Li, J.; Zhang, B.; Yuan, X.; Asakura, H.; Tanaka, T.; Teramura, K.; Xie, J.; Yan, N. The Support Effect on the Size and Catalytic Activity of Thiolated Au_{25} Nanoclusters as Precatalysts. *Nanoscale* **2015**, *7*, 6325−6333.

(544) Yoskamtorn, T.; Yamazoe, S.; Takahata, R.; Nishigaki, J.-i.; Thivasasith, A.; Limtrakul, J.; Tsukuda, T. Thiolate-Mediated Selectivity Control in Aerobic Alcohol Oxidation by Porous Carbon-Supported Au_{25} Clusters. *ACS Catal.* **2014**, *4*, 3696−3700.

(545) Choi, S.; Dickson, R. M.; Yu, J. Developing Luminescent Silver Nanodots for Biological Applications. *Chem. Soc. Rev.* **2012**, *41*, 1867−1891.

(546) Schmid, G. The Relevance of Shape and Size of Au_{55} Clusters. *Chem. Soc. Rev.* **2008**, *37*, 1909−1930.

(547) Shang, L.; Dong, S.; Nienhaus, G. U. Ultra-small Fluorescent Metal Nanoclusters: Synthesis and Biological Applications. *Nano Today* **2011**, *6*, 401−418.

(548) Tan, X.; Jin, R. Ultrasmall Metal Nanoclusters for Bio-related Applications. *Wiley Interdisciplinary Reviews: Nanomed. Nanobiotech.* **2013**, *5*, 569−581.

(549) Chen, X.; Zhou, Y.; Peng, X.; Yoon, J. Fluorescent and Colorimetric Probes for Detection of thiols. *Chem. Soc. Rev.* **2010**, *39*, 2120−2135.

(550) Saha, K.; Agasti, S. S.; Kim, C.; Li, X.; Rotello, V. M. Gold Nanoparticles in Chemical and Biological sensing. *Chem. Rev.* **2012**, *112*, 2739−2779.

(551) Guan, G.; Zhang, S.-Y.; Cai, Y.; Liu, S.; Bharathi, M. S.; Low, M.; Yu, Y.; Xie, J.; Zheng, Y.; Zhang, Y.-W.; Han, M.-Y. Convenient Purification of Gold Clusters by Co-precipitation for Improved Sensing of Hydrogen Peroxide, Mercury ions and Pesticides. *Chem. Commun.* **2014**, *50*, 5703−5705.

(552) George, A.; Shibu, E. S.; Maliyekkal, S. M.; Bootharaju, M. S.; Pradeep, T. Luminescent, Freestanding Composite Films of Au_{15} for Specific Metal Ion Sensing. *ACS Appl. Mater. Interfaces* **2012**, *4*, 639−644.

(553) Kobayashi, N.; Kamei, Y.; Shichibu, Y.; Konishi, K. Protonation-Induced Chromism of Pyridylethynyl-Appended [core+exo]-Type Au_8 Clusters. Resonance-Coupled Electronic Perturbation

through π-Conjugated Group. *J. Am. Chem. Soc.* **2013**, *135*, 16078−16081.

(554) Mathew, A.; Sajanlal, P. R.; Pradeep, T. Selective Visual Detection of TNT at the Sub-Zeptomole Level. *Angew. Chem., Int. Ed.* **2012**, *51*, 9596−9600.

(555) Shibu, E. S.; Pradeep, T. Quantum Clusters in Cavities: Trapped Au_{15} in Cyclodextrins. *Chem. Mater.* **2011**, *23*, 989−999.

(556) Paau, M. C.; Lo, C. K.; Yang, X.; Choi, M. M. F. Synthesis of 1.4 nm α-Cyclodextrin-Protected Gold Nanoparticles for Luminescence Sensing of Mercury(II) with Picomolar Detection Limit. *J. Phys. Chem. C* **2010**, *114*, 15995−16003.

(557) Guo, C.; Irudayaraj, J. Fluorescent Ag Clusters via a Protein-Directed Approach as a Hg(II) Ion Sensor. *Anal. Chem.* **2011**, *83*, 2883−2889.

(558) Zhang, G.; Li, Y.; Xu, J.; Zhang, C.; Shuang, S.; Dong, C.; Choi, M. M. F. Glutathione-protected Fluorescent Gold Nanoclusters for Sensitive and Selective Detection of Cu^{2+}. *Sens. Actuators, B* **2013**, *183*, 583−588.

(559) Huang, C.-C.; Yang, Z.; Lee, K.-H.; Chang, H.-T. Synthesis of Highly Fluorescent Gold Nanoparticles for Sensing Mercury(II). *Angew. Chem., Int. Ed.* **2007**, *46*, 6824−6828.

(560) Pu, K.-Y.; Luo, Z.; Li, K.; Xie, J.; Liu, B. Energy Transfer between Conjugated-Oligoelectrolyte-Substituted POSS and Gold Nanocluster for Multicolor Intracellular Detection of Mercury Ion. *J. Phys. Chem. C* **2011**, *115*, 13069−13075.

(561) Xie, J.; Zheng, Y.; Ying, J. Y. Highly Selective and Ultrasensitive Detection of Hg^{2+} based on Fluorescence Quenching of Au Nanoclusters by Hg^{2+}-Au^{+} interactions. *Chem. Commun.* **2010**, *46*, 961−963.

(562) Chen, W.; Tu, X.; Guo, X. Fluorescent Gold Nanoparticles-based Fluorescence Sensor for Cu^{2+} ions. *Chem. Commun.* **2009**, 1736−1738.

(563) Liu, S.; Lu, F.; Zhu, J.-J. Highly Fluorescent Ag Nanoclusters: Microwave-assisted Green Synthesis and Cr^{3+} Sensing. *Chem. Commun.* **2011**, *47*, 2661−2663.

(564) Liu, Y.; Ai, K.; Cheng, X.; Huo, L.; Lu, L. Gold-Nanocluster-Based Fluorescent Sensors for Highly Sensitive and Selective Detection of Cyanide in Water. *Adv. Funct. Mater.* **2010**, *20*, 951−956.

(565) Guo, W.; Yuan, J.; Wang, E. Oligonucleotide-stabilized Ag Nanoclusters as Novel Fluorescence Probes for the Highly Selective and Sensitive Detection of the Hg^{2+} ion. *Chem. Commun.* **2009**, 3395−3397.

(566) Roy, S.; Palui, G.; Banerjee, A. The as-prepared Gold Cluster-based Fluorescent Sensor for the Selective Detection of As (III) Ions in Aqueous Solution. *Nanoscale* **2012**, *4*, 2734−2740.

(567) Shang, L.; Dong, S. Silver Nanocluster-based Fluorescent Sensors for Sensitive Detection of Cu(II). *J. Mater. Chem.* **2008**, *18*, 4636−4640.

(568) Zhou, T.-y.; Lin, L.-p.; Rong, M.-c.; Jiang, Y.-q.; Chen, X. Silver−Gold Alloy Nanoclusters as a Fluorescence-Enhanced Probe for Aluminum Ion Sensing. *Anal. Chem.* **2013**, *85*, 9839−9844.

(569) Triulzi, R. C.; Micic, M.; Giordani, S.; Serry, M.; Chiou, W.-A.; Leblanc, R. M. Immunoasssay based on the Antibody-conjugated PAMAM-dendrimer-gold Quantum dot Complex. *Chem. Commun.* **2006**, 5068−5070.

(570) Yang, S. W.; Vosch, T. Rapid Detection of MicroRNA by a Silver Nanocluster DNA Probe. *Anal. Chem.* **2011**, *83*, 6935−6939.

(571) Huang, C.-C.; Chiang, C.-K.; Lin, Z.-H.; Lee, K.-H.; Chang, H.-T. Bioconjugated Gold Nanodots and Nanoparticles for Protein Assays Based on Photoluminescence Quenching. *Anal. Chem.* **2008**, *80*, 1497−1504.

(572) Huang, C.-C.; Chen, C.-T.; Shiang, Y.-C.; Lin, Z.-H.; Chang, H.-T. Synthesis of Fluorescent Carbohydrate-Protected Au Nanodots for Detection of Concanavalin A and Escherichia coli. *Anal. Chem.* **2009**, *81*, 875−882.

(573) Huang, C.-C.; Hung, Y.-L.; Shiang, Y.-C.; Lin, T.-Y.; Lin, Y.-S.; Chen, C.-T.; Chang, H.-T. Photoassisted Synthesis of Luminescent Mannose−Au Nanodots for the Detection of Thyroglobulin in Serum. *Chem. - Asian J.* **2010**, *5*, 334−341.

(574) Huang, C.-C.; Lin, T.-Y.; Yu, W.-S.; Chen, C.-T.; Chang, H.-T. Time-Resolved Luminescence-Based Assay for Thyroglobulin. *J. Biomed. Nanotechnol.* **2009**, *5*, 579−585.

(575) Chen, C.-T.; Chen, W.-J.; Liu, C.-Z.; Chang, L.-Y.; Chen, Y.-C. Glutathione-bound Gold Nanoclusters for Selective-binding and Detection of Glutathione S-transferase-fusion Proteins from Cell Lysates. *Chem. Commun.* **2009**, 7515−7517.

(576) Shiang, Y.-C.; Lin, C.-A.; Huang, C.-C.; Chang, H.-T. Protein A-conjugated Luminescent Gold Nanodots as a label-free Assay for Immunoglobulin G in plasma. *Analyst* **2011**, *136*, 1177−1182.

(577) Sharma, J.; Yeh, H.-C.; Yoo, H.; Werner, J. H.; Martinez, J. S. Silver Nanocluster Aptamers: in situ Generation of Intrinsically Fluorescent Recognition Ligands for Protein Detection. *Chem. Commun.* **2011**, *47*, 2294−2296.

(578) Petty, J. T.; Sengupta, B.; Story, S. P.; Degtyareva, N. N. DNA Sensing by Amplifying the Number of Near-Infrared Emitting, Oligonucleotide-Encapsulated Silver Clusters. *Anal. Chem.* **2011**, *83*, 5957−5964.

(579) Luo, Z.; Zheng, K.; Xie, J. Engineering Ultrasmall Water-soluble Gold and Silver Nanoclusters for Biomedical Applications. *Chem. Commun.* **2014**, *50*, 5143−5155.

(580) Chen, D.; Luo, Z.; Li, N.; Lee, J. Y.; Xie, J.; Lu, J. Amphiphilic Polymeric Nanocarriers with Luminescent Gold Nanoclusters for Concurrent Bioimaging and Controlled Drug Release. *Adv. Funct. Mater.* **2013**, *23*, 4324−4331.

(581) Zhang, X.-D.; Chen, J.; Luo, Z.; Wu, D.; Shen, X.; Song, S.-S.; Sun, Y.-M.; Liu, P.-X.; Zhao, J.; Huo, S.; Fan, S.; Fan, F.; Liang, X.-J.; Xie, J. Enhanced Tumor Accumulation of Sub-2 nm Gold Nanoclusters for Cancer Radiation Therapy. *Adv. Healthcare Mater.* **2014**, *3*, 133−141.

(582) Zhang, X.-D.; Luo, Z.; Chen, J.; Shen, X.; Song, S.; Sun, Y.; Fan, S.; Fan, F.; Leong, D. T.; Xie, J. Ultrasmall $Au_{10-12}(SG)_{10-12}$ Nanomolecules for High Tumor Specificity and Cancer Radiotherapy. *Adv. Mater.* **2014**, *26*, 4565−4568.

(583) Yu, Y.; New, S. Y.; Xie, J.; Su, X.; Tan, Y. N. Protein-based Fluorescent Metal Nanoclusters for Small Molecular Drug Screening. *Chem. Commun.* **2014**, *50*, 13805−13808.

(584) Muthu, M. S.; Kutty, R. V.; Luo, Z.; Xie, J.; Feng, S.-S. Theranostic vitamin E TPGS Micelles of Transferrin Conjugation for Targeted Co-delivery of Docetaxel and Ultra Bright Gold Nanoclusters. *Biomaterials* **2015**, *39*, 234−248.

(585) Zhang, X.-D.; Luo, Z.; Chen, J.; Song, S.; Yuan, X.; Shen, X.; Wang, H.; Sun, Y.; Gao, K.; Zhang, L.; Fan, S.; Leong, D. T.; Guo, M.; Xie, J. Ultrasmall Glutathione-Protected Gold Nanoclusters as Next Generation Radiotherapy Sensitizers with High Tumor Uptake and High Renal Clearance. *Sci. Rep.* **2015**, *5*, 8669.

(586) Yuan, X.; Setyawati, M. I.; Tan, A. S.; Ong, C. N.; Leong, D. T.; Xie, J. Highly Luminescent Silver Nanoclusters with Tunable Emissions: Cyclic Reduction-decomposition Synthesis and Antimicrobial Properties. *NPG Asia Mater.* **2013**, *5*, e39.

(587) Zhang, X.-D.; Luo, Z.; Chen, J.; Wang, H.; Song, S.-S.; Shen, X.; Long, W.; Sun, Y.-M.; Fan, S.; Zheng, K.; Leong, D. T.; Xie, J. Storage of Gold Nanoclusters in Muscle Leads to their Biphasic in Vivo Clearance. *Small* **2015**, *11*, 1683−1690.

(588) Ackerson, C. J.; Powell, R. D.; Hainfeld, J. F. Site-specific Biomolecule Labeling with Gold Clusters. *Methods Enzymol.* **2010**, *481*, 195−230.

(589) Shang, L.; Stockmar, F.; Azadfar, N.; Nienhaus, G. U. Intracellular Thermometry by Using Fluorescent Gold Nanoclusters. *Angew. Chem., Int. Ed.* **2013**, *52*, 11154−11157.

(590) Lee, R. J.; Wang, S.; Low, P. S. Measurement of Endosome pH Following Folate Receptor-Mediated Endocytosis. *Biochim. Biophys. Acta, Mol. Cell Res.* **1996**, *1312*, 237−242.

(591) Sun, C.; Yang, H.; Yuan, Y.; Tian, X.; Wang, L.; Guo, Y.; Xu, L.; Lei, J.; Gao, N.; Anderson, G. J.; Liang, X.-J.; Chen, C.; Zhao, Y.; Nie, G. Controlling Assembly of Paired Gold Clusters within Apoferritin Nanoreactor for in Vivo Kidney Targeting and Biomedical Imaging. *J. Am. Chem. Soc.* **2011**, *133*, 8617−8624.

(592) Yamamura, T.; Ariyasu, S.; Sakamoto, R. Affinity Clusters: An Adenine-Coated Gold Cluster Binds to Thymine Loops in DNA. *Chem. - Asian J.* **2011**, *6*, 1761−1765.

(593) Tao, Y.; Li, Z.; Ju, E.; Ren, J.; Qu, X. Polycations-functionalized Water-soluble Gold Nanoclusters: a Potential Platform for Simultaneous Enhanced Gene Delivery and Cell Imaging. *Nanoscale* **2013**, *5*, 6154−6160.

(594) Shang, L.; Nienhaus, G. U. Gold Nanoclusters as Novel Optical Probes for in vitro and in vivo Fluorescence Imaging. *Biophys. Rev.* **2012**, *4*, 313−322.

(595) Palmal, S.; Jana, N. R. Gold Nanoclusters with Enhanced Tunable Fluorescence as Bioimaging probes. *Wiley Interdiscipl. Rev: Nanomed. Nanobiotech.* **2014**, *6*, 102−110.

(596) Chen, W.-Y.; Lin, J.-Y.; Chen, W.-J.; Luo, L.; Wei-Guang Diau, E.; Chen, Y.-C. Functional Gold Nanoclusters as Antimicrobial agents for Antibiotic-resistant Bacteria. *Nanomedicine* **2010**, *5*, 755−764.

(597) Anema, J. R.; Li, J.-F.; Yang, Z.-L.; Ren, B.; Tian, Z.-Q. Shell-Isolated Nanoparticle-Enhanced Raman Spectroscopy: Expanding the Versatility of Surface-Enhanced Raman Scattering. *Annu. Rev. Anal. Chem.* **2011**, *4*, 129−150.

(598) He, J.; Lin, X.-M.; Divan, R.; Jaeger, H. M. In-Situ Partial Sintering of Gold-Nanoparticle Sheets for SERS Applications. *Small* **2011**, *7*, 3487−3492.

(599) Kumar, G. V. P.; Shruthi, S.; Vibha, B.; Reddy, B. A. A.; Kundu, T. K.; Narayana, C. Hot Spots in Ag Core−Au Shell Nanoparticles Potent for Surface-Enhanced Raman Scattering Studies of Biomolecules. *J. Phys. Chem. C* **2007**, *111*, 4388−4392.

(600) Wang, Y.; Yan, B.; Chen, L. SERS Tags: Novel Optical Nanoprobes for Bioanalysis. *Chem. Rev.* **2013**, *113*, 1391−1428.

(601) Leng, W.; Vikesland, P. J. Nanoclustered Gold Honeycombs for Surface-Enhanced Raman Scattering. *Anal. Chem.* **2013**, *85*, 1342−1349.

(602) Chakraborty, I.; Bag, S.; Landman, U.; Pradeep, T. Atomically Precise Silver Clusters as New SERS Substrates. *J. Phys. Chem. Lett.* **2013**, *4*, 2769−2773.

(603) Bisson, L.; Boissiere, C.; Sanchez, C.; Thomazeau, C.; Uzio, D. New Palladium Nanomaterials for Catalysis: Mechanisms Controlling Formation and Evolution of Nanostructures in a Seed-mediated Synthesis. *MRS Online Proc. Libr.* **2007**, *1017*, 1017-DD16-26.

(604) Louis, B.; Begin, D.; Ledoux, M.-J.; Pham-Huu, C. In *Advances in the Use of Carbon Nanomaterials in Catalysis*; Elsevier Ltd.: 2009; pp 621−649.

(605) Viswanathan, B. The Science of Nanomaterials in Catalysis. *Chem. Ind. Dig.* **2009**, *22*, 69−77.

(606) Wu, Y.; Yu, J.; Liu, H.-M.; Xu, B.-Q. One-dimensional TiO_2 Nanomaterials: Preparation and Catalytic Applications. *J. Nanosci. Nanotechnol.* **2010**, *10*, 6707−6719.

(607) Banares, M. A. Operando Spectroscopy: the Knowledge Bridge to Assessing Structure-Performance Relationships in Catalyst Nanoparticles. *Adv. Mater.* **2011**, *23*, 5293−5301.

(608) Li, Y.; Yang, X.-Y.; Feng, Y.; Yuan, Z.-Y.; Su, B.-L. One-Dimensional Metal Oxide Nanotubes, Nanowires, Nanoribbons, and Nanorods: Synthesis, Characterizations, Properties and Applications. *Crit. Rev. Solid State Mater. Sci.* **2012**, *37*, 1−74.

(609) Smiljanic, M.; Srejic, I.; Grgur, B.; Rakocevic, Z.; Strbac, S. Catalysis of Hydrogen Evolution on Au(111) Modified by Spontaneously Deposited Pd Nanoislands. *Electrocatalysis* **2012**, *3*, 369−375.

(610) Bhatia, S. K.; Nicholson, D. Friction between Solids and Adsorbed Fluids is Spatially Distributed at the Nanoscale. *Langmuir* **2013**, *29*, 14519−14526.

(611) Polshettiwar, V. Nanomaterials in Catalysis. Edited by Philippe Serp and Karine Philippot. *Angew. Chem., Int. Ed.* **2013**, *52*, 11199.

(612) Zhu, J.; Holmen, A.; Chen, D. Carbon Nanomaterials in Catalysis: Proton Affinity, Chemical and Electronic Properties, and their Catalytic Consequences. *ChemCatChem* **2013**, *5*, 378−401.

(613) Dong, S. Research on Nanomaterials in the Chemical Aspects. *Appl. Mech. Mater.* **2014**, *484*−*485*, 118−121.

(614) Jia, Q.; Zhao, D.; Tang, B.; Zhao, N.; Li, H.; Sang, Y.; Bao, N.; Zhang, X.; Xu, X.; Liu, H. Synergistic catalysis of Au-Cu/TiO_2-NB Nanopaper in Aerobic Oxidation of Benzyl Alcohol. *J. Mater. Chem. A* **2014**, *2*, 16292−16298.

(615) Larsen, S. C. Applications of Zeolite and Mesoporous Silica Nanomaterials in Catalysis, Adsorption of Environmental Contaminants and Drug Delivery. Presented at the National Meeting of the American Chemical Society, 2014; Paper MWRM-243.

(616) Lehman, S. E.; Larsen, S. C. Zeolite and Mesoporous Silica Nanomaterials: Greener Syntheses, Environmental Applications and Biological Toxicity. *Environ. Sci.: Nano* **2014**, *1*, 200−213.

(617) Liu, H.; Ye, F.; Yao, Q.; Cao, H.; Xie, J.; Lee, J. Y.; Yang, J. Stellated Ag-Pt Bimetallic Nanoparticles: An Effective Platform for Catalytic Activity Tuning. *Sci. Rep.* **2015**, *4*, 3969.

(618) Majdalawieh, A.; Kanan, M. C.; El-Kadri, O.; Kanan, S. M. Recent Advances in Gold and Silver nanoparticles: Synthesis and Applications. *J. Nanosci. Nanotechnol.* **2014**, *14*, 4757−4780.

(619) Morsy, S. M. I.; Shaban, S. A. Investigation of Ionic Liquid with and without Suspension of Nanomaterials as Satalysis for Sulfur Removal from Gas Oil at Room Temperature. *Int. J. Curr. Microbiol. Appl. Sci.* **2014**, *3*, 167−180.

(620) Rossi, L. M.; Costa, N. J. S.; Silva, F. P.; Wojcieszak, R. Magnetic Nanomaterials in Catalysis: Advanced Catalysts for Magnetic Separation and Beyond. *Green Chem.* **2014**, *16*, 2906−2933.

(621) Varma, R. S. Magnetically Retrievable Nano-catalysts in Benign Media. Presented at the National Meeting of the American Chemical Society, 2014; Paper COLL-689.

(622) Zhang, Q.; Yin, Y. Nanomaterials Engineering and Applications in catalysis. *Pure Appl. Chem.* **2014**, *86*, 53−69.

(623) Han, H.-L.; Melaet, G.; Alayoglu, S.; Somorjai, G. A. In Situ Microscopy and Spectroscopy Applied to Surfaces at Work. *ChemCatChem* **2015**, *7*, 3625−3638.

(624) Merrill, N. A.; McKee, E. M.; Merino, K. C.; Drummy, L. F.; Lee, S.; Reinhart, B.; Ren, Y.; Frenkel, A. I.; Naik, R. R.; Bedford, N. M.; Knecht, M. R. Identifying the Atomic-Level Effects of Metal Composition on the Structure and Catalytic Activity of Peptide-Templated Materials. *ACS Nano* **2015**, *9*, 11968−11979.

(625) Mori, K.; Tanaka, H.; Dojo, M.; Yoshizawa, K.; Yamashita, H. Synergic Catalysis of PdCu Alloy Nanoparticles within a Macroreticular Basic Resin for Hydrogen Production from Formic Acid. *Chem. - Eur. J.* **2015**, *21*, 12085−12092.

(626) Philippot, K.; Lignier, P.; Chaudret, B. Organometallic Ruthenium Nanoparticles and Catalysis. *Top. Organomet. Chem.* **2014**, *48*, 319−370.

(627) Whitby, R. Nanomaterials in Catalysis edited by Philippe Serp and Karine Philippot. *Appl. Organomet. Chem.* **2015**, *29*, 59.

(628) Yao, Q.; Lu, Z.-H.; Wang, Y.; Chen, X.; Feng, G. Synergetic Catalysis of Non-noble Bimetallic Cu-Co Nanoparticles Embedded in SiO_2 Nanospheres in Hydrolytic Dehydrogenation of Ammonia Borane. *J. Phys. Chem. C* **2015**, *119*, 14167−14174.

(629) Zhang, D.-X.; Liu, J.; Zhang, H.-X.; Wen, T.; Zhang, J. A Rational Strategy To Construct a Neutral Boron Imidazolate Framework with Encapsulated Small-Size Au-Pd Nanoparticles for Catalysis. *Inorg. Chem.* **2015**, *54*, 6069−6071.

(630) Zhang, L.; Anderson, R. M.; Crooks, R. M.; Henkelman, G. Correlating Structure and Function of Metal Nanoparticles for Catalysis. *Surf. Sci.* **2015**, *640*, 65−72.

(631) Zhang, S.; Nguyen, L.; Liang, J.-X.; Shan, J.; Liu, J.; Frenkel, A. I.; Patlolla, A.; Huang, W.; Li, J.; Tao, F. Catalysis on Singly Dispersed bimetallic sites. *Nat. Commun.* **2015**, *6*, 7938.

(632) Zhong, L.; Anand, C.; Lakhi, K. S.; Lawrence, G.; Vinu, A. Bifunctional Mesoporous Carbon Nitride: Highly Efficient Enzyme-like Catalyst for One-pot Deacetalization-Knoevenagel Reaction. *Sci. Rep.* **2015**, *5*, 12901.

(633) Ansar, S. M.; Kitchens, C. L. The Impact of Gold Nanoparticle Stabilizing Ligand on Colloidal Catalytic Reduction of 4-Nitrophenol. *ACS Catal.* **2016**, *6*, 5553−5560.

(634) Bhosale, M. A.; Bhanage, B. M. A Simple Approach for Sonochemical Synthesis of Cu_2O Nanoparticles with high Catalytic Properties. *Adv. Powder Technol.* **2016**, *27*, 238−244.

(635) Huang, T.; Li, H.; Huang, L.; Li, S.; Li, K.; Zhou, Y. Hybrid Vesicles with Alterable Fully Covered Armors of Nanoparticles: Fabrication, Catalysis, and Surface-Enhanced Raman Scattering. *Langmuir* **2016**, *32*, 991−996.

(636) Kudaibergenov, S. E.; Tatykhanova, G. S.; Selenova, B. S. Polymer Protected and Gel Immobilized Gold and Silver Nanoparticles in Catalysis. *J. Inorg. Organomet. Polym. Mater.* **2016**, *26*, 1198−1211.

(637) Livingston, C.; Metz, K. Developing a Sustainable Catalyst: Synthesis, Characterization, and Catalytic Application of Palladium Nanoparticles in Carbon Microsphere Composites. Presented at the National Meeting of the American Chemical Society, 2016; Paper CHED-1177.

(638) Lu, Y.; Ballauff, M. Spherical Polyelectrolyte Brushes as Nanoreactors for the Generation of Metallic and Oxidic Nanoparticles: Synthesis and Application in Catalysis. *Prog. Polym. Sci.* **2016**, *59*, 86−104.

(639) Sakthikumar, K.; Ede, S. R.; Mishra, S.; Kundu, S. Shape-selective Synthesis of $Sn(MoO_4)_2$ Nanomaterials for Catalysis and Supercapacitor Applications. *Dalton Trans.* **2016**, *45*, 8897−8915.

(640) Walker, J. M.; Zaleski, J. M. A Simple Route to Diverse Noble Metal-decorated Iron Oxide Nanoparticles for Catalysis. *Nanoscale* **2016**, *8*, 1535−1544.

(641) Yang, L.; Liu, X.; Lu, Q.; Huang, N.; Liu, M.; Zhang, Y.; Yao, S. Catalytic and Peroxidase-like Activity of Carbon based-AuPd Bimetallic Nanocomposite Produced using Carbon Dots as the Reductant. *Anal. Chim. Acta* **2016**, *930*, 23−30.

(642) Ye, L.; Wen, G.; Ouyang, H.; Liu, Q.; Liang, A.; Jiang, Z. A Novel and Highly Sensitive Nanocatalytic Surface Plasmon Resonance-scattering Analytical Platform for Detection of Trace Pb Ions. *Sci. Rep.* **2016**, *6*, 24150.

(643) Ye, R.; Hurlburt, T. J.; Sabyrov, K.; Alayoglu, S.; Somorjai, G. A. Molecular Catalysis science: Perspective on Unifying the Fields of Catalysis. *Proc. Natl. Acad. Sci. U. S. A.* **2016**, *113*, 5159−5166.

(644) Yamazoe, S.; Koyasu, K.; Tsukuda, T. Nonscalable Oxidation Catalysis of Gold Clusters. *Acc. Chem. Res.* **2014**, *47*, 816−824.

(645) Zhu, Y.; Qian, H.; Drake, B. A.; Jin, R. Atomically Precise $Au_{25}(SR)_{18}$ Nanoparticles as Catalysts for the Selective Hydrogenation of α,β-Unsaturated Ketones and Aldehydes. *Angew. Chem., Int. Ed.* **2010**, *49*, 1295−1298.

(646) Haruta, M.; Kobayashi, T.; Sano, H.; Yamada, N. Novel Gold Catalysts for the Oxidation of Carbon Monoxide at a Temperature far Below 0° C. *Chem. Lett.* **1987**, *16*, 405−408.

(647) Haruta, M.; Yamada, N.; Kobayashi, T.; Iijima, S. Gold Catalysts Prepared by Coprecipitation for Low-temperature Oxidation of Hydrogen and of Carbon Monoxide. *J. Catal.* **1989**, *115*, 301−309.

(648) Hashmi, A. S. K.; Hutchings, G. J. Gold Catalysis. *Angew. Chem., Int. Ed.* **2006**, *45*, 7896−7936.

(649) Mallat, T.; Baiker, A. Oxidation of Alcohols with Molecular Oxygen on Solid Catalysts. *Chem. Rev.* **2004**, *104*, 3037−3058.

(650) Jin, R. The Impacts of Nanotechnology on Catalysis by Precious Metal Nanoparticles. *Nanotechnol. Rev.* **2012**, *1*, 31−56.

(651) Li, G.; Jin, R. Atomically Precise Gold Nanoclusters as New Model Catalysts. *Acc. Chem. Res.* **2013**, *46*, 1749−1758.

(652) Li, G.; Jin, R. Well-defined Gold Nanoclusters for Catalytic Applications. *RSC Catal. Ser.* **2014**, *18*, 27−46.

(653) Huang, J.; Haruta, M. Heterogeneous Catalysis by Gold Clusters. In *Bridging Heterogeneous and Homogeneous Catalysis*; Wiley-VCH Verlag GmbH & Co. KGaA: 2014; pp 397−424.

(654) Yamazoe, S.; Tsukuda, T. Metal Clusters in Catalysis. *RSC Smart Mater.* **2014**, *7*, 291−322.

(655) Zhu, Y.; Qian, H.; Zhu, M.; Jin, R. Thiolate-Protected Aun Nanoclusters as Catalysts for Selective Oxidation and Hydrogenation Processes. *Adv. Mater.* **2010**, *22*, 1915−1920.

(656) Tsukuda, T.; Tsunoyama, H.; Sakurai, H. Aerobic Oxidations Catalyzed by Colloidal Nanogold. *Chem. - Asian J.* **2011**, *6*, 736−748.

(657) Zhu, Y.; Qian, H.; Jin, R. Catalysis opportunities of Atomically Precise Gold Nanoclusters. *J. Mater. Chem.* **2011**, *21*, 6793−6799.

(658) Lewis, L. N. Chemical Catalysis by Colloids and Clusters. *Chem. Rev.* **1993**, *93*, 2693−2730.

(659) Yamazoe, S.; Koyasu, K.; Tsukuda, T. Nonscalable Oxidation Catalysis of Gold Clusters. *Acc. Chem. Res.* **2014**, *47*, 816−824.

(660) Turner, M.; Golovko, V. B.; Vaughan, O. P. H.; Abdulkin, P.; Berenguer-Murcia, A.; Tikhov, M. S.; Johnson, B. F. G.; Lambert, R. M. Selective Oxidation with Dioxygen by Gold Nanoparticle Catalysts Derived from 55-atom Clusters. *Nature* **2008**, *454*, 981−983.

(661) Andreiadis, E. S.; Vitale, M. R.; Mezailles, N.; Le Goff, X.; Le Floch, P.; Toullec, P. Y.; Michelet, V. Chiral Undecagold Clusters: Synthesis, Characterization and Investigation in Catalysis. *Dalton Trans.* **2010**, *39*, 10608−10616.

(662) Kauffman, D. R.; Alfonso, D.; Matranga, C.; Qian, H.; Jin, R. Experimental and Computational Investigation of Au_{25} Clusters and CO_2: A Unique Interaction and Enhanced Electrocatalytic Activity. *J. Am. Chem. Soc.* **2012**, *134*, 10237−10243.

(663) Xie, S.; Tsunoyama, H.; Kurashige, W.; Negishi, Y.; Tsukuda, T. Enhancement in Aerobic Alcohol Oxidation Catalysis of Au_{25} Clusters by Single Pd Atom Doping. *ACS Catal.* **2012**, *2*, 1519−1523.

(664) Leelavathi, A.; Bhaskara Rao, T.; Pradeep, T. Supported Quantum Clusters of Silver as Enhanced Catalysts for Reduction. *Nanoscale Res. Lett.* **2011**, *6*, 123.

(665) Jirkovský, J. S.; Panas, I.; Ahlberg, E.; Halasa, M.; Romani, S.; Schiffrin, D. J. Single Atom Hot-Spots at Au−Pd Nanoalloys for Electrocatalytic H_2O_2 Production. *J. Am. Chem. Soc.* **2011**, *133*, 19432−19441.

(666) Zhang, H.; Watanabe, T.; Okumura, M.; Haruta, M.; Toshima, N. Catalytically Highly Active top Gold atom on Palladium Nanocluster. *Nat. Mater.* **2012**, *11*, 49−52.

(667) Yuan, D.; Gong, X.; Wu, R. Atomic Configurations of Pd Atoms in PdAu(111) Bimetallic Surfaces Investigated using the First-principles Pseudopotential Plane Wave Approach. *Phys. Rev. B: Condens. Matter Mater. Phys.* **2007**, *75*, 085428.

(668) Bi, X.; Wang, R.; Ding, Y. Boosting the Performance of Pt Electro-catalysts toward formic acid Electro-oxidation by Depositing sub-monolayer Au Clusters. *Electrochim. Acta* **2011**, *56*, 10039−10043.

(669) Gao, Y.; Shao, N.; Pei, Y.; Chen, Z.; Zeng, X. C. Catalytic Activities of Subnanometer Gold Clusters (Au_{16}−Au_{18}, Au_{20}, and Au_{27}−Au_{35}) for CO Oxidation. *ACS Nano* **2011**, *5*, 7818−7829.

(670) Jena, N. K.; Chandrakumar, K. R. S.; Ghosh, S. K. Beyond the Gold−Hydrogen Analogy: Doping Gold Cluster with H-atom−O_2 Activation and Reduction of the Reaction Barrier for CO Oxidation. *J. Phys. Chem. Lett.* **2011**, *2*, 1476−1480.

(671) Jena, N. K.; Chandrakumar, K. R. S.; Ghosh, S. K. DNA Base−Gold Nanocluster Complex as a Potential Catalyzing Agent: An Attractive Route for CO Oxidation Process. *J. Phys. Chem. C* **2012**, *116*, 17063−17069.

(672) Liu, Y.; Tsunoyama, H.; Akita, T.; Xie, S.; Tsukuda, T. Aerobic Oxidation of Cyclohexane Catalyzed by Size-Controlled Au Clusters on Hydroxyapatite: Size Effect in the Sub-2 nm Regime. *ACS Catal.* **2011**, *1*, 2−6.

(673) Tenney, S. A.; Cagg, B. A.; Levine, M. S.; He, W.; Manandhar, K.; Chen, D. A. Enhanced activity for supported Au clusters: Methanol oxidation on Au/TiO_2(110). *Surf. Sci.* **2012**, *606*, 1233−1243.

(674) Veith, G. M.; Lupini, A. R.; Pennycook, S. J.; Dudney, N. J. Influence of Support Hydroxides on the Catalytic Activity of Oxidized Gold Clusters. *ChemCatChem* **2010**, *2*, 281−286.

(675) Gao, W.; Chen, X. F.; Li, J. C.; Jiang, Q. Is Au_{55} or Au_{38} Cluster a Threshold Catalyst for Styrene Epoxidation? *J. Phys. Chem. C* **2010**, *114*, 1148−1153.

(676) Li, G.; Abroshan, H.; Liu, C.; Zhuo, S.; Li, Z.; Xie, Y.; Kim, H. J.; Rosi, N. L.; Jin, R. Tailoring the Electronic and Catalytic Properties of Au_{25} Nanoclusters via Ligand Engineering. *ACS Nano* **2016**, *10*, 7998−8005.

(677) Maity, P.; Yamazoe, S.; Tsukuda, T. Dendrimer-Encapsulated Copper Cluster as a Chemoselective and Regenerable Hydrogenation Catalyst. *ACS Catal.* **2013**, *3*, 182−185.

(678) Zhu, Y.; Wu, Z.; Gayathri, C.; Qian, H.; Gil, R. R.; Jin, R. Exploring Stereoselectivity of Au_{25} Nanoparticle Catalyst for Hydrogenation of Cyclic ketone. *J. Catal.* **2010**, *271*, 155−160.

(679) Chaki, N. K.; Tsunoyama, H.; Negishi, Y.; Sakurai, H.; Tsukuda, T. Effect of Ag-Doping on the Catalytic Activity of Polymer-Stabilized Au Clusters in Aerobic Oxidation of Alcohol. *J. Phys. Chem. C* **2007**, *111*, 4885−4888.

(680) Chen, W.; Chen, S. Oxygen Electroreduction Catalyzed by Gold Nanoclusters: Strong Core Size Effects. *Angew. Chem., Int. Ed.* **2009**, *48*, 4386−4389.

(681) Kumar, S. S.; Kwak, K.; Lee, D. Amperometric Sensing Based on Glutathione Protected Au_{25} Nanoparticles and Their pH Dependent Electrocatalytic Activity. *Electroanalysis* **2011**, *23*, 2116−2124.

(682) Han, J.; Liu, Y.; Guo, R. Reactive Template Method to Synthesize Gold Nanoparticles with Controllable Size and Morphology Supported on Shells of Polymer Hollow Microspheres and Their Application for Aerobic Alcohol Oxidation in Water. *Adv. Funct. Mater.* **2009**, *19*, 1112−1117.

(683) Villa, A.; Wang, D.; Su, D. S.; Prati, L. Gold Sols as Catalysts for Glycerol Oxidation: The Role of Stabilizer. *ChemCatChem* **2009**, *1*, 510−514.

(684) Miyamura, H.; Yasukawa, T.; Kobayashi, S. Aerobic Oxidative Esterification of Alcohols Catalyzed by Polymer-incarcerated Gold Nanoclusters under Ambient Conditions. *Green Chem.* **2010**, *12*, 776−778.

(685) Biffis, A.; Cunial, S.; Spontoni, P.; Prati, L. Microgel-stabilized Gold Nanoclusters: Powerful "quasi-homogeneous" Catalysts for the Aerobic Oxidation of Alcohols in Water. *J. Catal.* **2007**, *251*, 1−6.

(686) Kanaoka, S.; Yagi, N.; Fukuyama, Y.; Aoshima, S.; Tsunoyama, H.; Tsukuda, T.; Sakurai, H. Thermosensitive Gold Nanoclusters Stabilized by Well-Defined Vinyl Ether Star Polymers: Reusable and Durable Catalysts for Aerobic Alcohol Oxidation. *J. Am. Chem. Soc.* **2007**, *129*, 12060−12061.

(687) Wang, Y.; Yan, R.; Zhang, J.; Zhang, W. Synthesis of Efficient and Reusable Catalyst of Size-controlled Au Nanoparticles within a Porous, Chelating and Intelligent Hydrogel for Aerobic Alcohol Oxidation. *J. Mol. Catal. A: Chem.* **2010**, *317*, 81−88.

(688) Ishida, T.; Haruta, M. N-Formylation of Amines via the Aerobic Oxidation of Methanol over Supported Gold Nanoparticles. *ChemSusChem* **2009**, *2*, 538−541.

(689) Sakurai, H.; Kamiya, I.; Kitahara, H.; Tsunoyama, H.; Tsukuda, T. Aerobic Oxygenation of Benzylic Ketones Promoted by a Gold Nanocluster Catalyst. *Synlett* **2009**, *2009*, 245−248.

(690) Sakurai, H.; Tsunoyama, H.; Tsukuda, T. *Trans. Mater. Res. Soc. Jpn.* **2006**, *31*, 521−524.

(691) Kamiya, I.; Tsunoyama, H.; Tsukuda, T.; Sakurai, H. Lewis Acid Character of Zero-valent Gold Nanoclusters under Aerobic Conditions: Intramolecular Hydroalkoxylation of Alkenes. *Chem. Lett.* **2007**, *36*, 646−647.

(692) Kitahara, H.; Kamiya, I.; Sakurai, H. Intramolecular Addition of Toluenesulfonamide to Unactivated Alkenes Catalyzed by Gold Nanoclusters under Aerobic Conditions. *Chem. Lett.* **2009**, *38*, 908−909.

(693) Kitahara, H.; Sakurai, H. Gold Nanoclusters as a Catalyst for Intramolecular Addition of Primary Amines to Unactivated Alkenes under Aerobic Conditions. *Chem. Lett.* **2010**, *39*, 46−48.

(694) Nie, X.; Zeng, C.; Ma, X.; Qian, H.; Ge, Q.; Xu, H.; Jin, R. CeO_2-supported $Au_{38}(SR)_{24}$ Nanocluster Catalysts for CO Oxidation: a Comparison of Ligand-on and -off Catalysts. *Nanoscale* **2013**, *5*, 5912−5918.

(695) Valden, M.; Lai, X.; Goodman, D. W. Onset of Catalytic Activity of Gold Clusters on Titania with the Appearance of Nonmetallic Properties. *Science* **1998**, *281*, 1647−1650.

(696) Liu, Y.; Tsunoyama, H.; Akita, T.; Tsukuda, T. Efficient and Selective Epoxidation of Styrene with TBHP Catalyzed by Au_{25} Clusters on Hydroxyapatite. *Chem. Commun.* **2010**, *46*, 550−552.

(697) Li, G.; Qian, H.; Jin, R. Gold Nanocluster-Catalyzed Selective Oxidation of Sulfide to Sulfoxide. *Nanoscale* **2012**, *4*, 6714−6717.

(698) Herzing, A. A.; Kiely, C. J.; Carley, A. F.; Landon, P.; Hutchings, G. J. Identification of Active Gold Nanoclusters on Iron Oxide Supports for CO Oxidation. *Science* **2008**, *321*, 1331−1335.

(699) Ma, G.; Binder, A.; Chi, M.; Liu, C.; Jin, R.; Jiang, D.-e.; Fan, J.; Dai, S. Stabilizing Gold Clusters by Heterostructured Transition-metal Oxide-mesoporous Silica Supports for Enhanced Catalytic Activities for CO Oxidation. *Chem. Commun.* **2012**, *48*, 11413−11415.

(700) Liu, Y.; Tsunoyama, H.; Akita, T.; Tsukuda, T. Preparation of ∼ 1 nm Gold Clusters Confined within Mesoporous Silica and Microwave-Assisted Catalytic Application for Alcohol Oxidation. *J. Phys. Chem. C* **2009**, *113*, 13457−13461.

(701) Li, G.; Liu, C.; Lei, Y.; Jin, R. Au_{25} Nanocluster-catalyzed Ullmann-type Homocoupling Reaction of Aryl Iodides. *Chem. Commun.* **2012**, *48*, 12005−12007.

(702) Yu, C.; Li, G.; Kumar, S.; Kawasaki, H.; Jin, R. Stable $Au_{25}(SR)_{18}/TiO_2$ Composite Nanostructure with Enhanced Visible Light Photocatalytic Activity. *J. Phys. Chem. Lett.* **2013**, *4*, 2847−2852.

(703) Jeseentharani, V.; Pugazhenthiran, N.; Mathew, A.; Chakraborty, I.; Baksi, A.; Ghosh, J.; Jash, M.; Anjusree, G. S.; Deepak, T. G.; Nair, A. S.; Pradeep, T. Atomically Precise Noble Metal Clusters Harvest Visible Light to Produce Energy. *ChemistrySelect* **2017**, *2*, 1454−1463.

(704) Kogo, A.; Sakai, N.; Tatsuma, T. Photoelectrochemical Analysis of Size-dependent Electronic Structures of Gold Clusters Supported on TiO_2. *Nanoscale* **2012**, *4*, 4217−4221.

(705) Sakai, N.; Tatsuma, T. Photovoltaic Properties of Glutathione-Protected Gold Clusters Adsorbed on TiO_2 Electrodes. *Adv. Mater.* **2010**, *22*, 3185−3188.

(706) Radich, J. G.; Dwyer, R.; Kamat, P. V. Cu_2S Reduced Graphene Oxide Composite for High-Efficiency Quantum Dot Solar Cells. Overcoming the Redox Limitations of S_2^{-}/S_n^{2-} at the Counter Electrode. *J. Phys. Chem. Lett.* **2011**, *2*, 2453−2460.

(707) Li, L.; Yang, X.; Gao, J.; Tian, H.; Zhao, J.; Hagfeldt, A.; Sun, L. Highly Efficient CdS Quantum Dot-Sensitized Solar Cells Based on a Modified Polysulfide Electrolyte. *J. Am. Chem. Soc.* **2011**, *133*, 8458−8460.

(708) Santra, P. K.; Nair, P. V.; George Thomas, K.; Kamat, P. V. $CuInS_2$-Sensitized Quantum Dot Solar Cell. Electrophoretic Deposition, Excited-State Dynamics, and Photovoltaic Performance. *J. Phys. Chem. Lett.* **2013**, *4*, 722−729.

(709) Abbas, M. A.; Kim, T.-Y.; Lee, S. U.; Kang, Y. S.; Bang, J. H. Exploring Interfacial Events in Gold-Nanocluster-Sensitized Solar Cells: Insights into the Effects of the Cluster Size and Electrolyte on Solar Cell Performance. *J. Am. Chem. Soc.* **2016**, *138*, 390−401.

(710) Kim, M. S.; Abbas, M. A.; Bang, J. H. $Ag_{16}(SG)_9$ Nanoclusters as a Light Harvester for Metal-Cluster-Sensitized Solar Cells. *Bull. Korean Chem. Soc.* **2016**, *37*, 791−792.

(711) Li, M.; Liu, Q.; Jia, Z.; Xu, X.; Cheng, Y.; Zheng, Y.; Xi, T.; Wei, S. Graphene oxide/hydroxyapatite composite coatings fabricated by electrophoretic nanotechnology for biological applications. *Carbon* **2014**, *67*, 185−197.

(712) Gupta, S. S.; Sreeprasad, T. S.; Maliyekkal, S. M.; Das, S. K.; Pradeep, T. Graphene from Sugar and its Application in Water Purification. *ACS Appl. Mater. Interfaces* **2012**, *4*, 4156−4163.

(713) Sen Gupta, S.; Chakraborty, I.; Maliyekkal, S. M.; Adit Mark, T.; Pandey, D. K.; Das, S. K.; Pradeep, T. Simultaneous Dehalogenation and Removal of Persistent Halocarbon Pesticides from Water Using Graphene Nanocomposites: A Case Study of Lindane. *ACS Sustainable Chem. Eng.* **2015**, *3*, 1155−1163.

(714) Allen, M. J.; Tung, V. C.; Kaner, R. B. Honeycomb Carbon: a Review of Graphene. *Chem. Rev.* **2010**, *110*, 132−145.

(715) Castro Neto, A. H.; Guinea, F.; Peres, N. M. R.; Novoselov, K. S.; Geim, A. K. The Electronic Properties of Graphene. *Rev. Mod. Phys.* **2009**, *81*, 109−162.

(716) Geim, A. K.; Novoselov, K. S. The Rise of Graphene. *Nat. Mater.* **2007**, *6*, 183−191.

(717) Wang, Y.; Chen, J. T.; Yan, X. P. Fabrication of Transferrin Functionalized Gold Nanoclusters/graphene Oxide Nanocomposite

for Turn-on Near-infrared Fluorescent Bioimaging of Cancer Cells and Small Animals. *Anal. Chem.* **2013**, *85*, 2529−2535.

(718) Ge, S.; Yan, M.; Lu, J.; Zhang, M.; Yu, F.; Yu, J.; Song, X.; Yu, S. Electrochemical Biosensor Based on Graphene Oxide−Au Nanoclusters Composites for L-cysteine Analysis. *Biosens. Bioelectron.* **2012**, *31*, 49−54.

(719) Yang, G.-H.; Shi, J.-J.; Wang, S.; Xiong, W.-W.; Jiang, L.-P.; Burda, C.; Zhu, J.-J. Fabrication of a Boron Nitride-gold Nanocluster Composite and its Versatile Application for Immunoassays. *Chem. Commun.* **2013**, *49*, 10757−10759.

(720) Liu, X.; Wei, S.; Chen, S.; Yuan, D.; Zhang, W. Graphene-multiwall Carbon Nanotube-Gold Nanocluster Composites Modified Electrode for the Simultaneous Determination of Ascorbic acid, Dopamine, and Uric acid. *Appl. Biochem. Biotechnol.* **2014**, *173*, 1717−1726.

(721) Som, A.; Chakraborty, I.; Maark, T. A.; Bhat, S.; Pradeep, T. Cluster-Mediated Crossed Bilayer Precision Assemblies of 1D Nanowires. *Adv. Mater.* **2016**, *28*, 2827−2833.

(722) Knoppe, S.; Bürgi, T. Chirality in Thiolate-Protected Gold Clusters. *Acc. Chem. Res.* **2014**, *47*, 1318−1326.

(723) He, X.; Wang, Y.; Jiang, H.; Zhao, L. Structurally Well-Defined Sigmoidal Gold Clusters: Probing the Correlation between Metal Atom Arrangement and Chiroptical Response. *J. Am. Chem. Soc.* **2016**, *138*, 5634−5643.

(724) Pelayo, J. J.; Whetten, R. L.; Garzón, I. L. Geometric Quantification of Chirality in Ligand-Protected Metal Clusters. *J. Phys. Chem. C* **2015**, *119*, 28666−28678.

(725) Aikens, C. M. Chapter 9 - Optical Properties and Chirality. In *Frontiers of Nanoscience*; Tatsuya, T.; Hannu, H., Eds.; Elsevier: 2015; Vol. *9*, pp 223−261.

(726) Gautier, C.; Burgi, T. Vibrational Circular Dichroism of N-acetyl-l-cysteine protected gold nanoparticles. *Chem. Commun.* **2005**, 5393−5395.

(727) Gautier, C.; Burgi, T. Chiral N-isobutyryl-cysteine Protected Gold Nanoparticles: Preparation, Size Selection, and Optical Activity in the UV-vis and Infrared. *J. Am. Chem. Soc.* **2006**, *128*, 11079−11087.

(728) Gautier, C.; Burgi, T. Chiral gold Nanoparticles. *ChemPhysChem* **2009**, *10*, 483−492.

(729) Yao, H.; Fukui, T.; Kimura, K. Chiroptical Responses of d-/l-Penicillamine-Capped Gold Clusters under Perturbations of Temperature Change and Phase Transfer. *J. Phys. Chem. C* **2007**, *111*, 14968−14976.

(730) Takano, S.; Tsukuda, T. Amplification of the Optical Activity of Gold Clusters by the Proximity of BINAP. *J. Phys. Chem. Lett.* **2016**, *7*, 4509−4513.

(731) Lopez-Acevedo, O.; Tsunoyama, H.; Tsukuda, T.; Häkkinen, H.; Aikens, C. M. Chirality and Electronic Structure of the Thiolate-Protected Au$_{38}$ Nanocluster. *J. Am. Chem. Soc.* **2010**, *132*, 8210−8218.

(732) Gautier, C.; Bürgi, T. Vibrational Circular Dichroism of Adsorbed Molecules: BINAS on Gold Nanoparticles. *J. Phys. Chem. C* **2010**, *114*, 15897−15902.

(733) Humblot, V.; Haq, S.; Muryn, C.; Hofer, W. A.; Raval, R. From Local Adsorption Stresses to Chiral surfaces: (R,R)-tartaric acid on Ni(110). *J. Am. Chem. Soc.* **2002**, *124*, 503−510.

(734) Garzón, I. L.; Beltrán, M. R.; González, G.; Gutıerrez-González, I.; Michaelian, K.; Reyes-Nava, J. A.; Rodrıguez-Hernández, J. I. Chirality, Defects, and Disorder in Gold Clusters. *Eur. Phys. J. D* **2003**, *24*, 105−109.

(735) Garzón, I. L.; Reyes-Nava, J. A.; Rodríguez-Hernández, J. I.; Sigal, I.; Beltrán, M. R.; Michaelian, K. Chirality in Bare and Passivated Gold Nanoclusters. *Phys. Rev. B: Condens. Matter Mater. Phys.* **2002**, *66*, 073403.

(736) Santizo, I. E.; Hidalgo, F.; Perez, L. A.; Noguez, C.; Garzon, I. L. Intrinsic Chirality in Bare Gold Nanoclusters: The Au$_{34}^-$ Case. *J. Phys. Chem. C* **2008**, *112*, 17533−17539.

(737) Lechtken, A.; Schooss, D.; Stairs, J. R.; Blom, M. N.; Furche, F.; Morgner, N.; Kostko, O.; von Issendorff, B.; Kappes, M. M. Au$_{34}^-$: a chiral gold cluster. *Angew. Chem., Int. Ed.* **2007**, *46*, 2944−2948.

(738) Hakkinen, H.; Moseler, M.; Kostko, O.; Morgner, N.; Hoffmann, M. A.; von Issendorff, B. Symmetry and Electronic Structure of Noble-Metal Nanoparticles and the Role of Relativity. *Phys. Rev. Lett.* **2004**, *93*, 093401.

(739) Böhringer, M.; Morgenstern, K.; Schneider, W.-D.; Berndt, R. Separation of a Racemic Mixture of Two-Dimensional Molecular Clusters by Scanning Tunneling Microscopy. *Angew. Chem., Int. Ed.* **1999**, *38*, 821−823.

(740) Chen, Q.; Frankel, D. J.; Richardson, N. V. Chemisorption Induced Chirality: Glycine on Cu. *Surf. Sci.* **2002**, *497*, 37−46.

(741) Ortega Lorenzo, M. O.; Baddeley, C. J.; Muryn, C.; Raval, R. Extended Surface Chirality from Supramolecular Assemblies of Adsorbed Chiral Molecules. *Nature* **2000**, *404*, 376−379.

(742) Parschau, M.; Romer, S.; Ernst, K.-H. Induction of Homochirality in Achiral Enantiomorphous Monolayers. *J. Am. Chem. Soc.* **2004**, *126*, 15398−15399.

(743) Varnholt, B.; Dolamic, I.; Knoppe, S.; Burgi, T. On the Flexibility of the Gold-thiolate Interface: Racemization of the Au$_{40}$(SR)$_{24}$ Cluster. *Nanoscale* **2013**, *5*, 9568−9571.

(744) Knoppe, S.; Dolamic, I.; Dass, A.; Bürgi, T. Separation of Enantiomers and CD Spectra of Au$_{40}$(SCH$_2$CH$_2$Ph)$_{24}$: Spectroscopic Evidence for Intrinsic Chirality. *Angew. Chem., Int. Ed.* **2012**, *51*, 7589−7591.

(745) Knoppe, S.; Wong, O. A.; Malola, S.; Hakkinen, H.; Burgi, T.; Verbiest, T.; Ackerson, C. J. Chiral Phase Transfer and Enantioenrichment of Thiolate-Protected Au$_{102}$ Clusters. *J. Am. Chem. Soc.* **2014**, *136*, 4129−4132.

(746) Knoppe, S.; Kothalawala, N.; Jupally, V. R.; Dass, A.; Burgi, T. Ligand Dependence of the Synthetic Approach and Chiroptical Properties of a Magic Cluster Protected with a Bicyclic Chiral Thiolate. *Chem. Commun.* **2012**, *48*, 4630−4632.

(747) Yao, H.; Saeki, M.; Kimura, K. Induced Optical Activity in Boronic-Acid-Protected Silver Nanoclusters by Complexation with Chiral Fructose. *J. Phys. Chem. C* **2010**, *114*, 15909−15915.

(748) Dolamic, I.; Varnholt, B.; Burgi, T. Chirality Transfer from Gold Nanocluster to Ndsorbate Evidenced by Vibrational Circular Dichroism. *Nat. Commun.* **2015**, *6*, 7117.

(749) Escalle, A. l.; Mora, G.; Gagosz, F.; Mézailles, N.; Le Goff, X. F.; Jean, Y.; Le Floch, P. Cationic Dimetallic Gold Hydride Complex Stabilized by a Xantphos-Phosphole ligand: Synthesis, X-ray Crystal Structure, and Density Functional Theory Study. *Inorg. Chem.* **2009**, *48*, 8415−8422.

(750) Tsui, E. Y.; Müller, P.; Sadighi, J. P. Reactions of a Stable Monomeric Gold(I) Hydride Complex. *Angew. Chem., Int. Ed.* **2008**, *47*, 8937−8940.

(751) Liu, C. W.; Lin, Y.-R.; Fang, C.-S.; Latouche, C.; Kahlal, S.; Saillard, J.-Y. [Ag$_7$(H){E$_2$P(OR)$_2$}$_6$] (E = Se, S): Precursors for the Fabrication of Silver Nanoparticles. *Inorg. Chem.* **2013**, *52*, 2070−2077.

(752) Bootharaju, M. S.; Dey, R.; Gevers, L. E.; Hedhili, M. N.; Basset, J.-M.; Bakr, O. M. A New Class of Atomically Precise, Hydride-Rich Silver Nanoclusters Co-Protected by Phosphines. *J. Am. Chem. Soc.* **2016**, *138*, 13770−13773.

(753) Zavras, A.; Khairallah, G. N.; Connell, T. U.; White, J. M.; Edwards, A. J.; Mulder, R. J.; Donnelly, P. S.; O'Hair, R. A. J. Synthesis, Structural Characterization, and Gas-Phase Unimolecular Reactivity of the Silver Hydride Nanocluster [Ag$_3$((PPh$_2$)$_2$CH$_2$)$_3$(μ_3-H)](BF$_4$)$_2$. *Inorg. Chem.* **2014**, *53*, 7429−7437.

(754) Zavras, A.; Ariafard, A.; Khairallah, G. N.; White, J. M.; Mulder, R. J.; Canty, A. J.; O'Hair, R. A. J. Synthesis, Structure and Gas-phase Reactivity of the Mixed Silver Hydride Borohydride Nanocluster [Ag$_3$(μ_3-H)(μ_3-BH$_4$)LPh$_3$]BF$_4$ (LPh = bis(diphenylphosphino)-methane). *Nanoscale* **2015**, *7*, 18129−18137.

(755) Liao, P. K.; Fang, C. S.; Edwards, A. J.; Kahlal, S.; Saillard, J. Y.; Liu, C. W. Hydrido Copper Clusters Supported by Dithiocarbamates: Oxidative Hydride Removal and Neutron Diffraction Analysis of [Cu$_7$(H){S$_2$C(aza-15-crown-5)}$_6$]. *Inorg. Chem.* **2012**, *51*, 6577−6591.

(756) Latouche, C.; Kahlal, S.; Lin, Y.-R.; Liao, J.-H.; Furet, E.; Liu, C. W.; Saillard, J.-Y. Anion Encapsulation and Geometric Changes in

Hepta- and Hexanuclear Copper(I) Dichalcogeno Clusters: A Theoretical and Experimental Investigation. *Inorg. Chem.* **2013**, *52*, 13253−13262.

(757) Liao, P.-K.; Liu, K.-G.; Fang, C.-S.; Liu, C. W.; Fackler, J. P.; Wu, Y.-Y. A Copper(I) Homocubane Collapses to a Tetracapped Tetrahedron Upon Hydride Insertion. *Inorg. Chem.* **2011**, *50*, 8410−8417.

(758) Dhayal, R. S.; Liao, J. H.; Lin, Y. R.; Liao, P. K.; Kahlal, S.; Saillard, J. Y.; Liu, C. W. A Nanospheric Polyhydrido Copper Cluster of Elongated Triangular Orthobicupola Array: Liberation of H_2 from Solar Energy. *J. Am. Chem. Soc.* **2013**, *135*, 4704−4707.

(759) Crasto, D.; Dass, A. Green Gold: $Au_{30}(S\text{-}t\text{-}C_4H_9)_{18}$ Molecules. *J. Phys. Chem. C* **2013**, *117*, 22094−22097.

(760) Buckart, S.; Ganteför, G.; Kim, Y. D.; Jena, P. Anomalous Behavior of Atomic Hydrogen Interacting with Gold Clusters. *J. Am. Chem. Soc.* **2003**, *125*, 14205−14209.

(761) Li, G.; Lei, Z.; Wang, Q.-M. Luminescent Molecular Ag−S Nanocluster $[Ag_{62}S_{13}(SBut)_{32}](BF_4)_4$. *J. Am. Chem. Soc.* **2010**, *132*, 17678−17679.

(762) Li, B.; Huang, R.-W.; Qin, J.-H.; Zang, S.-Q.; Gao, G.-G.; Hou, H.-W.; Mak, T. C. W. Thermochromic Luminescent Nest-Like Silver Thiolate Cluster. *Chem. - Eur. J.* **2014**, *20*, 12416−12420.

(763) Sun, D.; Wang, H.; Lu, H.-F.; Feng, S.-Y.; Zhang, Z.-W.; Sun, G.-X.; Sun, D.-F. Two Birds with One Stone: Anion Templated Ball-shaped Ag_{56} and Disc-like Ag_{20} Clusters. *Dalton Transac.* **2013**, *42*, 6281−6284.

(764) Fenske, D.; Persau, C.; Dehnen, S.; Anson, C. E. Syntheses and Crystal Structures of the Ag-S Cluster Compounds $[Ag_{70}S_{20}(SPh)_{28}(dppm)_{10}]$ $(CF_3CO_2)_2$ and $[Ag_{262}S_{100}(StBu)_{62}(dppb)_6]$. *Angew. Chem., Int. Ed.* **2004**, *43*, 305−309.

(765) Fenske, D.; Anson, C. E.; Eichhöfer, A.; Fuhr, O.; Ingendoh, A.; Persau, C.; Richert, C. Syntheses and Crystal Structures of $[Ag_{123}S_{35}(StBu)_{50}]$ and $[Ag_{344}S_{124}(StBu)_{96}]$. *Angew. Chem., Int. Ed.* **2005**, *44*, 5242−5246.

(766) Anson, C. E.; Eichhöfer, A.; Issac, I.; Fenske, D.; Fuhr, O.; Sevillano, P.; Persau, C.; Stalke, D.; Zhang, J. Synthesis and Crystal Structures of the Ligand-Stabilized Silver Chalcogenide Clusters $[Ag_{154}Se_{77}(dppxy)_{18}]$, $[Ag_{320}(StBu)_{60}S_{130}(dppp)_{12}]$, $[Ag_{352}S_{128}(StC_5H_{11})_{96}]$, and $[Ag_{490}S_{188}(StC_5H_{11})_{114}]$. *Angew. Chem., Int. Ed.* **2008**, *47*, 1326−1331.

(767) Manju, C. K.; Chakraborty, I.; Pradeep, T. Highly Luminescent Monolayer Protected $Ag_{56}Se_{13}S_{15}$ clusters. *J. Mater. Chem. C* **2016**, *4*, 5572−5577.

(768) Li, X.; Guo, Z.; Xiao, C.; Goh, T. W.; Tesfagaber, D.; Huang, W. Tandem Catalysis by Palladium Nanoclusters Encapsulated in Metal−Organic Frameworks. *ACS Catal.* **2014**, *4*, 3490−3497.

(769) Mednikov, E. G.; Jewell, M. C.; Dahl, L. F. Nanosized $(\mu_{12}\text{-}Pt)Pd_{164\text{-}x}Pt_x(CO)_{72}(PPh_3)_{20}$ $(x \approx 7)$ Containing Pt-Centered Four-Shell 165-Atom Pd−Pt Core with Unprecedented Intershell Bridging Carbonyl Ligands: Comparative Analysis of Icosahedral Shell-Growth Patterns with Geometrically Related $Pd_{145}(CO)_x(PEt_3)_{30}$ $(x \approx 60)$ Containing Capped Three-Shell Pd_{145} Core. *J. Am. Chem. Soc.* **2007**, *129*, 11619−11630.

(770) Mednikov, E. G.; Dahl, L. F. Syntheses, Structures and Properties of Primarily Nanosized Homo/heterometallic Palladium CO/PR_3 Ligated Ligands. *Philos. Trans. R. Soc., A* **2010**, *368*, 1301.

(771) Erickson, J. D.; Mednikov, E. G.; Ivanov, S. A.; Dahl, L. F. Isolation and Structural Characterization of a Mackay 55-Metal-Atom Two-Shell Icosahedron of Pseudo-Ih Symmetry, $Pd_{55}L_{12}(\mu_3\text{-}CO)_{20}$ (L = PR_3, R = Isopropyl): Comparative Analysis with Interior Two-Shell Icosahedral Geometries in Capped Three-Shell Pd_{145}, Pt-Centered Four-Shell Pd−Pt M_{165}, and Four-Shell Au_{133} Nanoclusters. *J. Am. Chem. Soc.* **2016**, *138*, 1502−1505.

(772) Bhat, S.; Chakraborty, I.; Maark, T. A.; Mitra, A.; De, G.; Pradeep, T. Atomically Precise and Monolayer Protected Iridium Clusters in solution. *RSC Adv.* **2016**, *6*, 26679−26688.

(773) Higaki, T.; Kitazawa, H.; Yamazoe, S.; Tsukuda, T. Partially Oxidized Iridium Clusters within Dendrimers: Size-Controlled Synthesis and Selective Hydrogenation of 2-nitrobenzaldehyde. *Nanoscale* **2016**, *8*, 11371−11374.

(774) Chen, S.; Kimura, K. Synthesis of Thiolate-Stabilized Platinum Nanoparticles in Protolytic Solvents as Isolable Colloids. *J. Phys. Chem. B* **2001**, *105*, 5397−5403.

(775) Kawasaki, H.; Yamamoto, H.; Fujimori, H.; Arakawa, R.; Inada, M.; Iwasaki, Y. Surfactant-free Solution Synthesis of Fluorescent Platinum Subnanoclusters. *Chem. Commun.* **2010**, *46*, 3759−3761.

(776) Le Guével, X.; Trouillet, V.; Spies, C.; Jung, G.; Schneider, M. Synthesis of Yellow-Emitting Platinum Nanoclusters by Ligand Etching. *J. Phys. Chem. C* **2012**, *116*, 6047−6051.

(777) Tanaka, S.-I.; Miyazaki, J.; Tiwari, D. K.; Jin, T.; Inouye, Y. Fluorescent Platinum Nanoclusters: Synthesis, Purification, Characterization, and Application to Bioimaging. *Angew. Chem., Int. Ed.* **2011**, *50*, 431−435.

(778) Duchesne, P. N.; Zhang, P. Local Structure of Fluorescent Platinum Nanoclusters. *Nanoscale* **2012**, *4*, 4199−4205.

(779) Huang, X.; Ishitobi, H.; Inouye, Y. Formation of Fluorescent Platinum Nanoclusters using Hyper-branched Polyethylenimine and their Conjugation to Antibodies for Bio-imaging. *RSC Adv.* **2016**, *6*, 9709−9716.

(780) Chen, D.; Zhao, C.; Ye, J.; Li, Q.; Liu, X.; Su, M.; Jiang, H.; Amatore, C.; Selke, M.; Wang, X. In Situ Biosynthesis of Fluorescent Platinum Nanoclusters: Toward Self-Bioimaging-Guided Cancer Theranostics. *ACS Appl. Mater. Interfaces* **2015**, *7*, 18163−18169.

(781) Hackendorn, R. A.; Virkar, A. V. Synthesis of Platinum Nanoclusters and Electrochemical Investigation of their stability. *J. Power Sources* **2013**, *240*, 618−629.

(782) Takahashi, M.; Imaoka, T.; Hongo, Y.; Yamamoto, K. Formation of a Pt_{12} Cluster by Single-Atom Control That Leads to Enhanced Reactivity: Hydrogenation of Unreactive Olefins. *Angew. Chem., Int. Ed.* **2013**, *52*, 7419−7421.

(783) Imaoka, T.; Kitazawa, H.; Chun, W.-J.; Yamamoto, K. Finding the Most Catalytically Active Platinum Clusters With Low Atomicity. *Angew. Chem., Int. Ed.* **2015**, *54*, 9810−9815.

(784) Yamamoto, K.; Imaoka, T.; Chun, W.-J.; Enoki, O.; Katoh, H.; Takenaga, M.; Sonoi, A. Size-specific Catalytic Activity of Platinum Clusters Enhances Oxygen Reduction Reactions. *Nat. Chem.* **2009**, *1*, 397−402.

(785) Chen, S.; Huang, K.; Stearns, J. A. Alkanethiolate-Protected Palladium Nanoparticles. *Chem. Mater.* **2000**, *12*, 540−547.

(786) Clergeaud, G.; Genç, R.; Ortiz, M.; O'Sullivan, C. K. Liposomal Nanoreactors for the Synthesis of Monodisperse Palladium Nanoparticles Using Glycerol. *Langmuir* **2013**, *29*, 15405−15413.

(787) Corthey, G.; Olmos-Asar, J. A.; Casillas, G.; Mariscal, M. M.; Mejía-Rosales, S.; Azcárate, J. C.; Larios, E.; José-Yacamán, M.; Salvarezza, R. C.; Fonticelli, M. H. Influence of Capping on the Atomistic Arrangement in Palladium Nanoparticles at Room Temperature. *J. Phys. Chem. C* **2014**, *118*, 24641−24647.

(788) Corthey, G.; Rubert, A. A.; Picone, A. L.; Casillas, G.; Giovanetti, L. J.; Ramallo-López, J. M.; Zelaya, E.; Benitez, G. A.; Requejo, F. G.; José-Yacamán, M.; Salvarezza, R. C.; Fonticelli, M. H. New Insights into the Chemistry of Thiolate-Protected Palladium Nanoparticles. *J. Phys. Chem. C* **2012**, *116*, 9830−9837.

(789) Liu, Y.; Sun, C.; Bolin, T.; Wu, T.; Liu, Y.; Sternberg, M.; Sun, S.; Lin, X.-M. Kinetic Pathway of Palladium Nanoparticle Sulfidation Process at High Temperatures. *Nano Lett.* **2013**, *13*, 4893−4901.

(790) Quiros, I.; Yamada, M.; Kubo, K.; Mizutani, J.; Kurihara, M.; Nishihara, H. Preparation of Alkanethiolate-Protected Palladium Nanoparticles and Their Size Dependence on Synthetic Conditions. *Langmuir* **2002**, *18*, 1413−1418.

(791) Sadeghmoghaddam, E.; Gu, H.; Shon, Y.-S. Pd Nanoparticle-Catalyzed Isomerization vs Hydrogenation of Allyl Alcohol: Solvent-Dependent Regioselectivity. *ACS Catal.* **2012**, *2*, 1838−1845.

(792) Sharma, S.; Kim, B.; Lee, D. Water-Soluble Pd Nanoparticles Capped with Glutathione: Synthesis, Characterization, and Magnetic Properties. *Langmuir* **2012**, *28*, 15958−15965.

(793) Yee, C. K.; Jordan, R.; Ulman, A.; White, H.; King, A.; Rafailovich, M.; Sokolov, J. Novel One-Phase Synthesis of Thiol-

Functionalized Gold, Palladium, and Iridium Nanoparticles Using Superhydride. *Langmuir* **1999**, *15*, 3486−3491.

(794) Ramallo-López, J. M.; Giovanetti, L.; Craievich, A. F.; Vicentin, F. C.; Marín-Almazo, M.; José-Yacaman, M.; Requejo, F. G. XAFS, SAXS and HREM Characterization of Pd Nanoparticles Capped with n-alkyl Thiol Molecules. *Phys. B* **2007**, *389*, 150−154.

(795) Zelakiewicz, B. S.; Lica, G. C.; Deacon, M. L.; Tong, Y. 13C NMR and Infrared Evidence of a Dioctyl-disulfide Structure on Octanethiol-protected Palladium Nanoparticle Surfaces. *J. Am. Chem. Soc.* **2004**, *126*, 10053−10058.

(796) Corthey, G.; Rubert, A. A.; Picone, A. L.; Casillas, G.; Giovanetti, L. J.; Ramallo-Lopez, J. M.; Zelaya, E.; Benitez, G. A.; Requejo, F. G.; Jose-Yacaman, M.; Salvarezza, R. C.; Fonticelli, M. H. New Insights into the Chemistry of Thiolate-Protected Palladium Nanoparticles. *J. Phys. Chem. C* **2012**, *116*, 9830−9837.

(797) Zamborini, F. P.; Gross, S. M.; Murray, R. W. Synthesis, Characterization, Reactivity, and Electrochemistry of Palladium Monolayer Protected Clusters. *Langmuir* **2001**, *17*, 481−488.

(798) Negishi, Y.; Murayama, H.; Tsukuda, T. Formation of $Pd_n(SR)_m$ Clusters ($n < 60$) in the Reactions of $PdCl_2$ and RSH (R = n-$C_{18}H_{37}$, n-$C_{12}H_{25}$). *Chem. Phys. Lett.* **2002**, *366*, 561−566.

(799) Jia, X.; Li, J.; Wang, E. Cu Nanoclusters with Aggregation Induced Emission Enhancement. *Small* **2013**, *9*, 3873−3879.

(800) Wu, Z.; Liu, J.; Gao, Y.; Liu, H.; Li, T.; Zou, H.; Wang, Z.; Zhang, K.; Wang, Y.; Zhang, H.; Yang, B. Assembly-Induced Enhancement of Cu Nanoclusters Luminescence with Mechanochromic Property. *J. Am. Chem. Soc.* **2015**, *137*, 12906−12913.

(801) Salorinne, K.; Chen, X.; Troff, R. W.; Nissinen, M.; Hakkinen, H. One-pot Synthesis and Characterization of Subnanometre-size Benzotriazolate Protected Copper Clusters. *Nanoscale* **2012**, *4*, 4095−4098.

(802) Goswami, N.; Baksi, A.; Giri, A.; Xavier, P. L.; Basu, G.; Pradeep, T.; Pal, S. K. Luminescent Iron Clusters in Solution. *Nanoscale* **2014**, *6*, 1848−1854.

(803) Marjomäki, V.; Lahtinen, T.; Martikainen, M.; Koivisto, J.; Malola, S.; Salorinne, K.; Pettersson, M.; Häkkinen, H. Site-specific Targeting of Enterovirus Capsid by Functionalized Monodisperse Gold Nanoclusters. *Proc. Natl. Acad. Sci. U. S. A.* **2014**, *111*, 1277−1281.

(804) Habeeb Muhammed, M. A.; Pradeep, T. $Au_{25}@SiO_2$: Quantum Clusters of Gold Embedded in Silica. *Small* **2011**, *7*, 204−208.

(805) Hassinen, J.; Pulkkinen, P.; Kalenius, E.; Pradeep, T.; Tenhu, H.; Häkkinen, H.; Ras, R. H. A. Mixed-Monolayer-Protected Au_{25} Clusters with Bulky Calix[4]arene Functionalities. *J. Phys. Chem. Lett.* **2014**, *5*, 585−589.

(806) Chen, X.; Häkkinen, H. Protected but Accessible: Oxygen Activation by a Calixarene-Stabilized Undecagold Cluster. *J. Am. Chem. Soc.* **2013**, *135*, 12944−12947.

(807) de Silva, N.; Ha, J.-M.; Solovyov, A.; Nigra, M. M.; Ogino, I.; Yeh, S. W.; Durkin, K. A.; Katz, A. A Bioinspired Approach for Controlling Accessibility in Calix[4]arene-bound Metal Cluster Catalysts. *Nat. Chem.* **2010**, *2*, 1062−1068.

(808) Antonello, S.; Dainese, T.; Pan, F.; Rissanen, K.; Maran, F. Electrocrystallization of Monolayer-Protected Gold Clusters: Opening the Door to Quality, Quantity, and New Structures. *J. Am. Chem. Soc.* **2017**, *139*, 4168−4174.

NOTE ADDED IN PROOF

Literature through December 2016 has been considered. Certain new developments of 2017 are also mentioned. As our review was getting ready for submission, a new review appeared (ref 6). We direct the readers to this review for a discussion of gold clusters, their structures, and additional discussion on future possibilities in this field.

DOI: 10.1021/acs.chemrev.6b00769
Chem. Rev. 2017, 117, 8208−8271